

1. REPORT NUMBER CA21-3114-2	2. GOVERNMENT ASSOCIATION NUMBER	3. RECIPIENT'S CATALOG NUMBER
4. TITLE AND SUBTITLE Evaluation of Steel Pin and Pin Plate Strengths	5. REPORT DATE April, 2021	
6. PERFORMING ORGANIZATION CODE		7. AUTHOR(S) Hooseok Lee, Mathew Reynolds, Chia-Ming Uang
8. PERFORMING ORGANIZATION REPORT NO. SSRP-21/04		9. PERFORMING ORGANIZATION NAME AND ADDRESS Department of Structural Engineering University of California, San Diego La Jolla, California 92093
10. WORK UNIT NUMBER		11. CONTRACT OR GRANT NUMBER 65A0687
12. SPONSORING AGENCY AND ADDRESS California Department of Transportation Division of Engineering Services 1801 30th St., MS-9-2/5i Sacramento, California 95816		13. TYPE OF REPORT AND PERIOD COVERED Final Report May 2018 - April 2021
14. SPONSORING AGENCY CODE		15. SUPPLEMENTARY NOTES Prepared in cooperation with the State of California Department of Transportation.

16. ABSTRACT

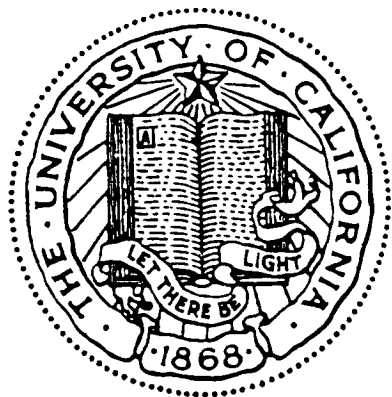
For evaluation of steel bridges, designers use the AASHTO Specifications to compute the capacities of steel pins and pin plates. The steel pin is treated as a beam, and a moment-shear interaction equation is used to define the capacity. The Specifications define the nominal bearing capacity as $1.5tDF_y$ for the pins, but reduce the capacity by one-thirds to tDF_y for the pin plates. Twelve 2-in. diameter steel pins with two steel grades were tested. Finite element analyses using ABAQUS were then conducted to correlate and to generalize the test results to 1 in. and 4 in. pins. It was found that the pins did not behave like a beam, and the pin capacity defined by the moment-shear interaction equation was exceeded by a large margin. A regression analysis was performed on the available test data to establish an equation for predicting the ultimate strength of the pins. The predictive equation is a function of the tensile strength of the pin material and two non-dimensional parameters, ratios of clear span and the loaded length to pin diameter. An equation for predicting the pin capacity for a severability limit state was also proposed. To evaluate the bearing capacity of pin plates, eight specimens with two steel grades were tested to failure. In addition, five pin specimens were tested to evaluate the bearing capacity of pins; three parameters (thickness of loading plate, steel grade of pin, and pin diameter) were considered. Test results showed that the approach used in the AASHTO LRFD Specifications is significantly conservative. The test data supports the inclusion of the 1.5 factor for pin plates, and the same equation as that for pin bearing capacity can be used. However, an alternate equation which achieves a better correlation with the test results was proposed. In addition, an equation for serviceability considerations was proposed. Test results also showed that the AASHTO LRFD Specifications underestimate the bearing strength of the pin by a large margin.

17. KEY WORDS Bridge, Steel, Pin, Pin Plate, Shear, Flexure, Bearing, Capacity	18. DISTRIBUTION STATEMENT No Restrictions	
19. SECURITY CLASSIFICATION (of this report) unclassified	20. NUMBER OF PAGES 184	21. COST OF REPORT CHARGED

DISCLAIMER STATEMENT

This document is disseminated in the interest of information exchange. The contents of this report reflect the views of the authors who are responsible for the facts and accuracy of the data presented herein. The contents do not necessarily reflect the official views or policies of the State of California or the Federal Highway Administration. This publication does not constitute a standard, specification or regulation. This report does not constitute an endorsement by the Department of any product described herein.

For individuals with sensory disabilities, this document is available in alternate formats. For information, call (916) 654-8899, TTY 711, or write to California Department of Transportation, Division of Research, Innovation and System Information, MS-83, P.O. Box 942873, Sacramento, CA 94273-0001.



**STRUCTURAL SYSTEMS
RESEARCH PROJECT**

Report No.
SSRP-21/04

Evaluation of Steel Pin and Pin Plate Strengths

by

Hooseok Lee

Mathew Reynolds

Chia-Ming Uang

Final Report Submitted to California Department of Transportation

April 2021

Department of Structural Engineering
University of California, San Diego
La Jolla, California 92093

University of California, San Diego
Department of Structural Engineering
Structural Systems Research Project

Report No. SSRP-21/04

Evaluations of Steel Pin and Pin Plate Strengths

by

Hooseok Lee

Graduate Student Researcher

Mathew Reynolds

Former Graduate Student Researcher

Chia-Ming Uang

Professor of Structural Engineering

Final Report Submitted to California Department of Transportation

Department of Structural Engineering
University of California, San Diego
La Jolla, California 92093

DISCLAIMER

This document is disseminated in the interest of information exchange. The contents of this report reflect the views of the authors who are responsible for the facts and accuracy of the data presented herein. The contents do not necessarily reflect the official views or policies of the State of California. This publication does not constitute a standard, specification or regulation. This report does not constitute an endorsement by the California Department of Transportation of any product described herein.

For individuals with sensory disabilities, this document is available in Braille, large print, audiocassette, or compact disk. To obtain a copy of this document in one of these alternate formats, please contact: Division of Research and Innovation, MS-83, California Department of Transportation, P.O. Box 942873, Sacramento, CA 94273-0001.

ACKNOWLEDGEMENTS

The California Department of Transportation (Caltrans) funded this work under Contract #65A0687. We would like to thank Dr. George Huang (project manager) for his guidance and advice.

The author would like to thank Mr. Martin Anderson for developing the initial test plan. The testing was conducted in the Charles Lee Powell Structures Laboratories at the University of California, San Diego; help from laboratory staff in conducting the tests was much appreciated.

ABSTRACT

For evaluation of steel bridges, designers use the AASHTO LRFD Specifications to compute the capacities of steel pins and pin plates. For steel pins, it is a common practice to treat the pin as a beam, and a moment-shear interaction equation in the Specifications is used to define the capacity. The Specifications define the nominal bearing capacity as $1.5tDF_y$ for the pins but reduce the capacity by one-third to tDF_y for the pin plates.

To evaluate the capacity of pins, twelve 2-in. diameter steel pins with two steel grades (A108 Grade 1018 and A668 Class F) were tested. Finite element analyses using ABAQUS were then conducted to correlate and to generalize the test results to 1 in. and 4 in. pins. It was found that the pins did not behave like a beam, and the pin capacity defined by the moment-shear interaction equation was exceeded by a large margin. A regression analysis was performed on the available test data to establish an equation for predicting the ultimate strength of the pins. The predictive equation is a function of the tensile strength of the pin material and two non-dimensional length parameters, the first being the clear span and the second being the loaded length of the pin normalized by the pin diameter. Based on the measured initial yield at the midspan of the pin, an equation for predicting the pin capacity for a severability limit state was also proposed.

To evaluate the bearing capacity of pin plates, eight specimens with both A36 steel and A572 Gr. 50 steel were tested to failure. In addition, five pin specimens were tested to evaluate the bearing capacity of pins; three parameters (thickness of loading plate, steel grade of pin, and pin diameter) were considered. Test results showed that the approach used in the AASHTO LRFD Specifications, which do not include the 1.5 factor for calculating the bearing capacity of pin plates, is significantly conservative. Conversely, the test data supports the inclusion of the 1.5 factor for pin plates, i.e., the same equation as that for pin bearing capacity can be used. However, an alternate equation which achieves a better correlation with the test results was proposed. In addition, an equation for serviceability considerations was proposed. Test results also showed that the AASHTO LRFD Specifications underestimate the bearing strength of the pin by a large margin.

TABLE OF CONTENTS

DISCLAIMER	ii
ACKNOWLEDGEMENTS	iii
ABSTRACT	iv
TABLE OF CONTENTS	v
LIST OF FIGURES	viii
LIST OF TABLES	xii
1 INTRODUCTION	1
1.1 Statement of Problem	1
2 STEEL PIN STRENGTHS	2
2.1 Introduction.....	2
2.1.1 Statement of Problem.....	2
2.1.2 Research Objective	3
2.2 Test Program.....	6
2.2.1 General.....	6
2.2.2 Test Setup.....	6
2.2.3 Specimen Design	6
2.2.4 Material Properties.....	7
2.2.5 Instrumentation	7
2.3 Test Results.....	17
2.3.1 Series A Specimens (A108 Gr. 1018 Steel).....	17
2.3.2 Series B Specimens (A668 Class F Steel)	19
2.4 Analysis of Test Results	44
2.4.1 Comparison of Test Results	44
2.4.2 Comparison of Test Results for Serviceability	45
2.4.3 Comparison of Test Results with AASHTO Specifications	45
2.5 FINITE ELEMENT ANALISYS	56
2.5.1 General.....	56
2.5.2 Finite Element Models	56

2.5.3	Material Stress-Strain Characteristics.....	57
2.5.4	Calibration of Finite Element Models.....	57
2.5.5	Correlation between Test Results and FEA.....	57
2.5.6	Simulated Results to Supplement Test Database ($D = 2$ in.).....	58
2.5.7	Simulated Results of Pins with $D = 1$ in. and $D = 4$ in.....	59
2.6	DEVELOPMENT OF PIN STRENGTH PREDICTIVE EQUATIONS	84
2.6.1	General.....	84
2.6.2	Proposed Model	84
2.6.3	Strength Limit State	85
2.6.4	Service Limit State.....	86
2.7	Summary and Concluding Remarks	94
2.7.1	Summary	94
2.7.2	Concluding Remarks.....	94
3	BEARING STRENGTH OF STEEL PIN PLATES.....	96
3.1	Introduction.....	96
3.1.1	Statement of Problem.....	96
3.1.2	Research Objective	98
3.2	Test Program.....	100
3.2.1	General.....	100
3.2.2	Material Properties.....	100
3.2.3	Specimen Design	100
3.2.4	Instrumentation	101
3.3	Test Results.....	110
3.3.1	Series C Specimens (A36 Steel)	110
3.3.2	Series D Specimens (A572 Gr. 50 Steel).....	110
3.4	Analysis of Test Results and FEM Correlation	128
3.4.1	Summary of Test Results	128
3.4.2	Comparison of Test and Code-Predicted Strengths	128
3.4.3	Response Correlation with Finite Element Analysis	130
3.5	Summary and Concluding Remarks	140
3.5.1	Summary.....	140

3.5.2	Concluding Remarks.....	140
4	BEARING STRENGTH OF STEEL PINS.....	141
4.1	Introduction.....	141
4.1.1	Statement of Problem.....	141
4.1.2	Research Objective	142
4.2	Test Program.....	142
4.2.1	General.....	142
4.2.2	Material Properties.....	142
4.2.3	Specimen Design	142
4.2.4	Instrumentation	143
4.3	Test Results.....	150
4.3.1	Series E Specimens ($D = 3.0$ in.).....	150
4.3.2	Series F Specimens ($D = 2.0$ in.)	150
4.4	Analysis of Test Results	150
4.5	Correlation between Test Results and FEA.....	151
4.6	Summary and Concluding Remarks	152
5	SUMMARY AND CONCLUSIONS	168
5.1	Pin Capacity of Combined Flexure and Shear.....	168
5.2	Bearing Capacity of Pin Plates	168
5.3	Pin Bearing Capacity	169
	REFERENCES.....	170

LIST OF FIGURES

Figure 2.1 AASHTO LRFD Pin Moment-Shear Interaction Curve	4
Figure 2.2 Interaction Curves for Pins Subjected to Shear and Moment (Kulicki 1983) ...	4
Figure 2.3 Moment in a Pin (Bresler et al. 1968)	5
Figure 2.4 Pin Test Setup.....	10
Figure 2.5 Pin with Loading and Support Cradles.....	11
Figure 2.6 Dimensions of Loading and Support Cradles for Pin Tests	12
Figure 2.7 Assuming Loading Pattern for Pin Design	13
Figure 2.8 Sample Pin Moment-Shear Interaction Check	13
Figure 2.9 Distribution of Pin Specimens in Moment-Shear Domain.....	14
Figure 2.10 Stress-strain Responses from Tensile Coupon Testing (Pin Tests).....	15
Figure 2.11 Instrumentation for Pin Tests	16
Figure 2.12 Displacement Transducer Layout for Pin Tests	16
Figure 2.13 Specimen A1: Deformed Shape	20
Figure 2.14 Specimen A1: Global Response	21
Figure 2.15 Specimen A2: Deformed Shape	22
Figure 2.16 Specimen A2: Global Response	23
Figure 2.17 Specimen A3: Deformed Shape	24
Figure 2.18 Specimen A3: Global Response	25
Figure 2.19 Specimen A4: Deformed Shape	26
Figure 2.20 Specimen A4: Global Response	27
Figure 2.21 Specimen A5: Deformed Shape	28
Figure 2.22 Specimen A5: Global Response	29
Figure 2.23 Specimen A6: Deformed Shape	30
Figure 2.24 Specimen A6: Global Response	31
Figure 2.25 Specimen A7: Deformed Shape	32
Figure 2.26 Specimen A7: Global Response	33
Figure 2.27 Specimen B1: Deformed Shape.....	34
Figure 2.28 Specimen B1: Global Response	35
Figure 2.29 Specimen B2: Deformed Shape.....	36
Figure 2.30 Specimen B2: Global Response	37

Figure 2.31 Specimen B3: Deformed Shape.....	38
Figure 2.32 Specimen B3: Global Response	39
Figure 2.33 Specimen B4: Deformed Shape.....	40
Figure 2.34 Specimen B4: Global Response	41
Figure 2.35 Specimen B5: Deformed Shape.....	42
Figure 2.36 Specimen B5: Global Response	43
Figure 2.37 Failure Mode	47
Figure 2.38 Summary of Global Response	48
Figure 2.39 Summary of Normalized Shear versus Midspan Deflection Relationship ...	49
Figure 2.40 Summary of Normalized Shear versus Midspan Deflection Relationship ...	50
Figure 2.41 Summary of Normalized Moment versus Midspan Deflection Relationship	51
Figure 2.42 Summary of Normalized Moment versus Midspan Deflection Relationship	52
Figure 2.43 Normalized Shear versus Midspan Deflection with Events at ϵ_y , $2\epsilon_y$ and $3\epsilon_y$	53
Figure 2.44 Summary of Pin Shear Strength at Different Limit States	54
Figure 2.45 Comparison of Pin Test Data with AASHTO Moment-Shear Interaction Curve.....	55
Figure 2.46 Typical Finite Element Model of Pin Test	63
Figure 2.47 True and Engineering Stress-Strain Relationships	64
Figure 2.48 Sensitive Study	65
Figure 2.49 Correlation between Test Results and FEM Analyses	66
Figure 2.50 Comparison of Deformed Shape	72
Figure 2.51 Deformed Shape of Selected Series C Models ($D = 2.0$ in.).....	78
Figure 2.52 Results of Test and Simulated Series C Pin Models in Moment-Shear Domain ($D = 2.0$ in.).....	79
Figure 2.53 Deformed Shape of Selected Series D Models ($D = 1.0$ in.).....	80
Figure 2.54 Results of Simulated Series D Models in the Moment-Shear Domain ($D =$ 1.0 in.).....	81
Figure 2.55 Deformed Shape of Selected Series E Models ($D = 4.0$ in.)	82

Figure 2.56 Results of Simulated Series D Models in the Moment-Shear Domain ($D = 4.0$ in.).....	83
Figure 2.57 Definition of α and β for Pin Strength Prediction.....	89
Figure 2.58 Comparison of Measured and Predicted Pin Ultimate Shear Strengths	90
Figure 2.59 Comparison of Measured and Bridge et al. (2001) Predicted Pin Ultimate Shear Strength.....	91
Figure 2.60 Global Response with Service Shear Strength	92
Figure 2.61 Comparison of Measured and Predicted Pin Service Shear Strengths	93
Figure 3.1 Notation and Location of Limit State Sections	99
Figure 3.2 Pin Plate Test Assembly.....	106
Figure 3.3 Pin Plate Test Setup.....	107
Figure 3.4 Stress-strain Responses from Tensile Coupon Testing (Pin Plate Tests).....	107
Figure 3.5 Instrumentation for Pin Plate Tests	109
Figure 3.6 Specimen C1-1: Deformed Shape	112
Figure 3.7 Specimen C1-2: Deformed Shape	113
Figure 3.8 Specimen C1: Global Response	114
Figure 3.9 Specimen C1: Strain Response.....	115
Figure 3.10 Specimen C2-1: Deformed Shape	116
Figure 3.11 Specimen C2-2: Deformed Shape	117
Figure 3.12 Specimen C2: Global Response	118
Figure 3.13 Specimen C2: Strain Response.....	119
Figure 3.14 Specimen D1-1: Deformed Shape	120
Figure 3.15 Specimen D1-2: Deformed Shape.....	121
Figure 3.16 Specimen D1: Global Response	122
Figure 3.17 Specimen D1: Strain Response	123
Figure 3.18 Specimen D2-1: Deformed Shape	124
Figure 3.19 Specimen D2-2: Deformed Shape	125
Figure 3.20 Specimen D2: Global Response	126
Figure 3.21 Specimen D2: Strain Response	127
Figure 3.22 Summary of Failure Pattern (Pin Plate Tests)	132
Figure 3.23 Summary of Global Responses (Pin Plate Tests)	133

Figure 3.24 Normalized Response for Comparison with Bearing Limit State (Pin Plate Tests).....	134
Figure 3.25 Proposed Projected Width for Plate Bearing Strength Prediction	135
Figure 3.26 Normalized Response for Comparison with Net Section Rupture Limit State (Pin Plate Tests).....	135
Figure 3.27 FEM Correlation of Specimen C1	136
Figure 3.28 FEM Correlation of Specimen C2	137
Figure 3.29 FEM Correlation of Specimen D1	138
Figure 3.30 FEM Correlation of Specimen D2.....	139
Figure 4.1 Test Assembly (Pin Bearing Tests)	147
Figure 4.2 Test Setup (Pin Bearing Tests)	147
Figure 4.3 Stress-strain Responses from Tensile Coupon Testing (Pin Bearing Tests).	148
Figure 4.4 Instrumentation (Pin Bearing Tests).....	149
Figure 4.5 Specimen E1: Deformed Shape and Global Response.....	154
Figure 4.6 Specimen E2: Deformed Shape and Global Response.....	155
Figure 4.7 Specimen E3: Deformed Shape and Global Response.....	156
Figure 4.8 Specimen F1: Deformed Shape and Global Response	157
Figure 4.9 Specimen F2: Deformed Shape and Global Response	158
Figure 4.10 Summary of Global Response (Pin Bearing Tests).....	159
Figure 4.11 Effect of Plate Thickness on Pin Bearing Response.....	159
Figure 4.12 Effect of Steel Grade on Pin Bearing Response	160
Figure 4.13 Effect of Pin Diameter on Pin Bearing Response.....	161
Figure 4.14 FEM Correlation of Specimen E1	162
Figure 4.15 FEM Correlation of Specimen E2	163
Figure 4.16 FEM Correlation of Specimen E3	164
Figure 4.17 FEM Correlation of Specimen F1	165
Figure 4.18 FEM Correlation of Specimen F2	166
Figure 4.19 FEA Simulated Pin Bearing Responses.....	167

LIST OF TABLES

Table 2.1 Pin Test Matrix	8
Table 2.2 Pin Mechanical Characteristics.....	8
Table 2.3 Chemical Compositions from Mill Certificates	9
Table 2.4 Summary of Test Results at Ultimate Strength.....	46
Table 2.5 Strengths at ϵ_y , $2\epsilon_y$, and $3\epsilon_y$	46
Table 2.6 Contact Parameters for Finite Element Analysis	60
Table 2.7 Ultimate Strength Comparison between FEM and Tests.....	60
Table 2.8 Matrix of Additional Data of Finite Element Modeling	61
Table 2.9 Matrix of Additional Data of FEM Series D Models ($D = 1.0$ in.).....	62
Table 2.10 Matrix of Additional Data of FEM Series E Models ($D = 4.0$ in.).....	62
Table 2.11 Summary of UCSD Test Data	88
Table 2.12 Summary of Test Data by Bridge et al. (2001).....	88
Table 3.1 Plate Bearing Test Matrix	102
Table 3.2 Plate Mechanical Characteristics	102
Table 3.3 Chemical Compositions from Mill Certificates	103
Table 3.4 Tensile Strength of Pin-Connected Plates Based on AASHTO Specifications	104
Table 3.5 Tensile Strengths of Pin-Connected Plates Based on AISC Specification	105
Table 3.6 Summary of Peak Strengths (Pin Plate Tests)	131
Table 4.1 Pin Bearing Test Matrix.....	144
Table 4.2 Plate Mechanical Characteristics (Pin Bearing Tests).....	144
Table 4.3 Chemical Compositions from Mill Certificates (Pin Bearing Tests).....	145
Table 4.4 Bearing Strength of Pin Based on AASHTO Specifications	146
Table 4.5 Contact Parameters for Finite Element Analysis (Pin Bearing Tests).....	153

1 INTRODUCTION

1.1 Statement of Problem

As part of a research project entitled “The Effect of End Eccentricity in Steel TRUSS Bridge for Load Rating Analysis,” experimental testing of steel pins and pin plates was conducted in the Powell Structural System Laboratory at the University of California, San Diego (UCSD) to evaluate their strengths. The following three test programs were conducted:

- Flexural/shear strength of steel pins,
- Bearing strength of steel pin plates, and
- Bearing strength of steel pins.

A description of each of the above three test programs is provided in Chapter 2, Chapter 3, and Chapter 4, respectively, in this report. Chapter 5 provides a summary and conclusions of this research.

2 STEEL PIN STRENGTHS

2.1 Introduction

2.1.1 Statement of Problem

Montgomery et al. (2018) provided a thorough literature review of the development of pin design since the 1930s. The AASHTO LRFD Bridge Design Specifications (AASHTO 2020) since the 2014 edition specify the resistance of pins subject to both shear and moment is expressed in the form of an interaction equation

$$\frac{6.0M_u}{\phi_f D^3 F_y} + \left(\frac{2.2V_u}{\phi_v D^2 F_y} \right)^3 \leq 0.95 \quad (2.1)$$

where the resistance factors, ϕ_f and ϕ_v , are equal to 1.00. For a circular section with a diameter D , the plastic flexural and shear strengths are

$$V_p = \frac{\pi D^2}{4} (0.58 F_y) \quad (2.2a)$$

$$M_p = \frac{D^3}{6} (F_y) \quad (2.2b)$$

Eq. (2.1) then can be re-written as

$$\frac{M_u}{\phi_f M_p} + \left(\frac{V_u}{\phi_v V_p} \right)^3 \leq 0.95 \quad (2.3)$$

See Figure 2.1 for the moment-shear interaction curve of this equation. The basis of Eq. (2.3) is presented below.

In designing the truss members of Greater New Orleans Bridge No. 2, Kulicki (1983) evaluated the moment-shear interaction of circular and rectangular cross section members (see Figure 2.2) for eyebar pin design. Marked points in the figure were derived from either lower-bound solutions using plastic theory or computer analysis for a yield criterion (either von Mises or Tresca yield criterion). The radial line in the figure represents the division between ratios of shear and moment for which first yield occurs in shear or bending. Above the radial line, first yield results from bending; below it, first yield results from shear. Two interaction curves for rectangular cross sections proposed by Drucker (1956) and Hodge (1957) were also shown in the figure. Drucker developed a simple

expression after considering a number of upper and lower bound solutions that used the Tresca yield criterion:

$$\frac{M_u}{M_p} + \left(\frac{V_u}{V_p}\right)^4 \leq 1.0 \quad (2.4)$$

Kulicki replaced the exponent of 4 in the above equation by 3 for a somewhat conservative solution. Furthermore, since neither Drucker or Hodge provided experimental verification, and considering the importance of eyebars, he suggested that the factor 1.0 on the right-hand side of the equation be reduced to 0.95:

$$\frac{M_u}{M_p} + \left(\frac{V_u}{V_p}\right)^3 \leq 0.95 \quad (2.5)$$

which is the basis of Eq. (2.3). This review of the development of pin capacity indicates that pins are treated as beams.

Design engineers usually proportion pins for the maximum shear and bending moment produced by the members connected. *Assuming* that the pin behaves like a beam, the bending moment and shear can be evaluated by assuming that the loading in each plate is either concentrated as shown in Figure 2.3(b) or distributed as shown in Figure 2.3(c). Whether both the internal forces and capacity of a pin can be determined by treating it as a beam will be evaluated by test results in this research.

2.1.2 Research Objective

While numerous studies have investigated the behavior of pin plates, much less research has been conducted on pins. In particular, experimental data on pins is very limited. The first objective of this test program was to validate Eq. (2.1) experimentally and, if needed, develop an alternate equation to predict the pin strength. For this purpose, both the strength limit state and service limit state were considered. The second objective was to evaluate if the beam-analogy design procedure is appropriate for pin design.

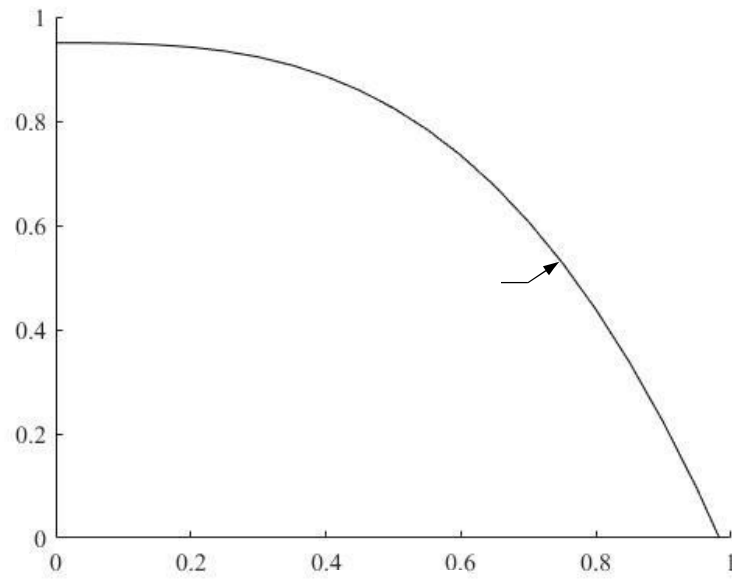


Figure 2.1 AASHTO LRFD Pin Moment-Shear Interaction Curve

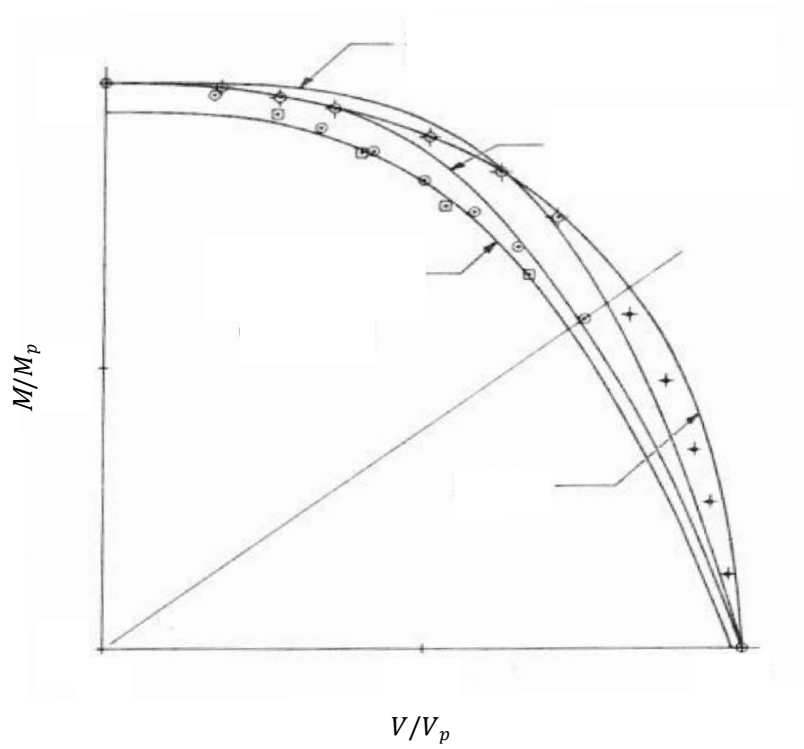
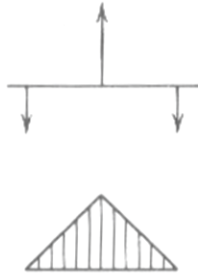
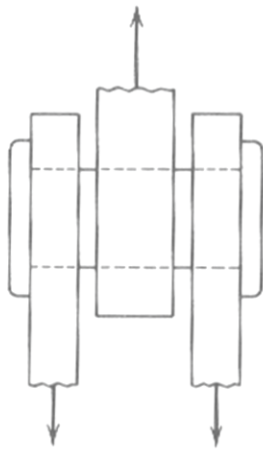
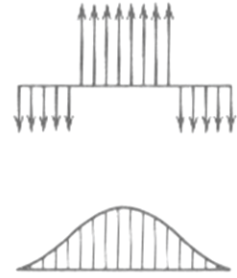


Figure 2.2 Interaction Curves for Pins Subjected to Shear and Moment (Kulicki 1983)



Concentrated Loads



Distributed Loads

Figure 2.3 Moment in a Pin (Bresler et al. 1968)

2.2 Test Program

2.2.1 General

Two grades of steel pin were tested: ASTM A108 Gr. 1018 to represent the steel in many existing bridges, and ASTM A668 Class F (previously A235 Class G) to represent modern pins. Pins of 2-in. diameter with various spans were tested to provide different shear and moment proportions such that various data points along the moment-shear interaction curve in Eq. (2.1) would be generated.

2.2.2 Test Setup

Pins were tested with a 600-kip Instron SATEC hydraulic test system at the UCSD's Powell Structures Laboratory. The test setup is shown in Figure 2.4. The pin sat in a semi-circular cradle comprised of a 1-in. thick base and two support plates. Pins were tested with different span lengths by adjusting the spacing of the support cradles. The pin was loaded by a loading cradle comprised of a single loading plate attached to a base [Figure 2.5].

2.2.3 Specimen Design

A total of 12 pin specimens, designated as A1 to A7 for pins of A1018 steel and B1 to B5 for A668 steel for tested (see Table 2.1). For specimen design, the specified minimum yield stresses (F_y) of the A108 and A668 pins were taken to be 40 ksi, and 50 ksi, respectively, per Section Table 6.4.2-1 of the AASHTO Specifications.

The span of the pins varied from 1.25 in. to 4.0 in. Variable spans were achieved by adjusting the spacing between two vertical plates of the support cradles (see Figure 2.6). Following the current design practice to treat the pin as a simply supported beam with the assumed loading shown in Figure 2.7, the demand-capacity ratios (DCR) along the span were computed from the moment and shear diagrams; see Figure 2.8 for a sample example (A4 Specimen) of the calculation. As shown in Figure 2.7, Section A corresponds to the midspan, where the moment is maximum but with no shear. Section B is located on the edge of the loading plate and has the highest combination of shear and moment. Table 2.1 summarizes the DCR values at Sections A and B; the larger value defines the critical location and governs the design per the AASHTO moment-shear interaction equation. The predicted pin capacity, P , is also listed for each test specimen. Figure 2.9 shows the distribution of the test specimens in the moment-shear interaction domain. It is noted that

the presence of two critical locations for concurrent effects creates a jump on the moment-shear interaction between the group of specimens dominated with moment to the group of specimens with a moment-shear interaction. This jump makes the practicality of designing specimens to fill the gap difficult. Conversely, the finite size of the plates means achieving a condition of pure shear impossible.

Figure 2.6 shows the dimensions of the loading and support cradles. A total of four loading cradles were fabricated for testing all pin specimens (see Figure 2.6 (a)). A514 steel with a specified yield stress of 100 ksi was used for the fabrication of all cradles.

2.2.4 Material Properties

Three steel grades, two for pins and one for cradles, were used in this test program. Figure 2.10 shows the stress-strain relationships obtained from tensile coupon testing conducted at UCSD (two coupons were tested for each steel grade.) Table 2.2 summarizes the mechanical properties of the steel materials. Table 2.3 shows the chemical composition of the materials obtained from Certified Mill Test Reports.

2.2.5 Instrumentation

A combination of linear transducers, strain gauge rosettes, and uniaxial strain gauges were used to measure the global and local responses. Figure 2.11 (a) and Figure 2.12 show the location of displacement transducers. L1 and L2 measured the vertical displacement of the top cradle relative to the base. L3 measured the vertical displacement of the top of the pin at a location 1.0 in. from the loading plate. L4 measured the vertical displacement of the bottom of the pin at midspan. Pin end rotation was measured by L5 and L6.

Figure 2.11 also shows the location of strain gauge rosette and uniaxial strain gauges. Uniaxial strain gage S5 measured flexural strain at the midspan of the pin. A 3-gage rosette strain R1 was installed at midspan; see Figure 2.11 (b) for the orientation. One leg of the support cradle was also instrumented with four uniaxial strain gages (S1 to S4).

Table 2.1 Pin Test Matrix

Steel Grade	A108 Grade 1018							A668 Class F					
Specimen No.	A1	A2	A3	A4	A5	A6	A7	B1	B2	B3	B4	B5	
Length of Pin (in.)	4.5	4.5	5	5.5	6	6.5	7	5	5.25	5.5	7.5	6	
Loading Plate ^a , t_{LC} (in.)	0.8	0.83	0.87	1	1	1	0.8	0.91	0.91	0.8	1	1	
Support Plate ^a , t_{BC} (in.)	0.5	0.75	1	1	1	1	1	0.77	1	1	1	1	
Gap ^b (in.)	0.100	0.085	0.065	0.125	0.250	0.375	1.350	0.125	0.045	0.163	0.500	1.000	
Span ^b , l (in.)	1.5	1.75	2	2.25	2.5	2.75	4.5	1.77	2	2.125	3	4	
Pin Resistance ^c , P (kips)	120	113	106	102	95	88	49	144	134	125	101	72	
$V_u/\phi_v V_p$	0.82	0.78	0.73	0.71	0.66	0.61	0.00	0.79	0.74	0.69	0.00	0.00	
$M_u/\phi_f M_p$	0.39	0.49	0.56	0.60	0.67	0.73	0.95	0.45	0.55	0.62	0.95	0.95	
DCR^c	at Section A	0.62	0.70	0.78	0.84	0.89	0.93	0.95	0.70	0.78	0.62	0.95	0.95
	at Section B	0.95	0.95	0.95	0.95	0.95	0.95	0.90	0.95	0.95	0.95	0.93	0.88

^a Measured thickness.

^b See Figure 2.5 for definition.

^c per Eq. (2.1).

Table 2.2 Pin Mechanical Characteristics

Specimen No.	Steel Grade (Heat No.)	Yield Stress ^a (ksi)	Tensile Strength (ksi)	Elong. (%)
Pins A1, A2, A3, A4, A5, A6, A7	A108 Gr. 1018 (100797419)	82.7, 81.1 (81.9) ^b	87.5, 88.9 (88.2) ^b	19.5, 22.4 (21.0) ^b
Pins B1, B2, B3, B4, B5	A668 Class F (A113014)	76.2, 76.2 (76.2) ^b [75.0] ^c	116.0, 117.0 (116.5) ^b [114.0] ^c	26.4, 26.7 (26.5) ^b [26.4] ^c
Cradles	A514 (LE0250)	111.8, 113.8 (112.8) ^b [114.5] ^c	120.1, 121.5 (120.8) ^b [122.0] ^c	27.1, 26.4 (26.7) ^b [40.0] ^c

^a Yield strength determined by the 0.2% strain offset method.

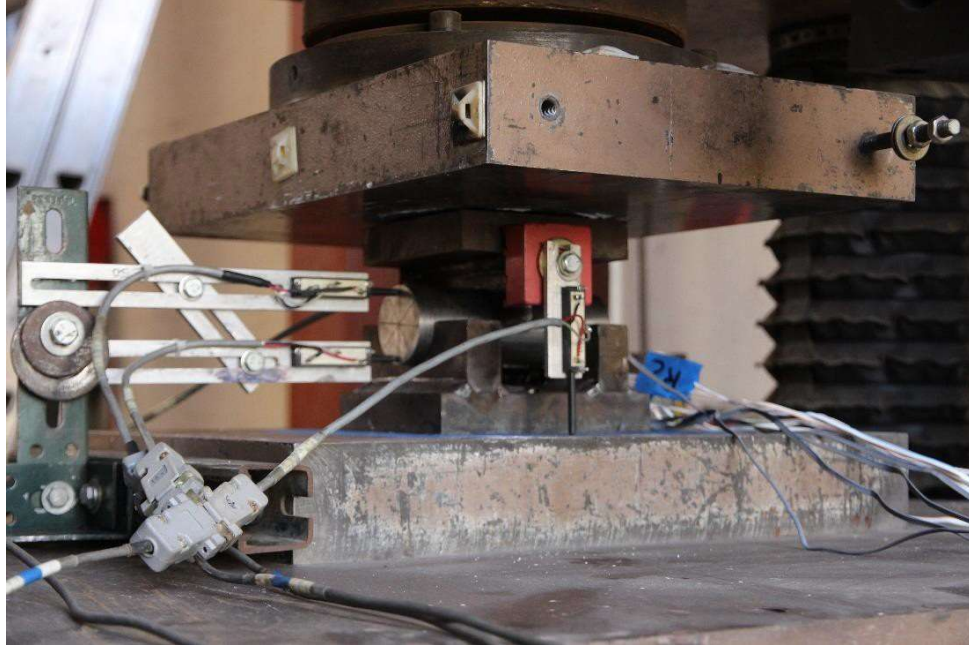
^b Mean value from two coupons.

^c From Certified Mill Test Reports.

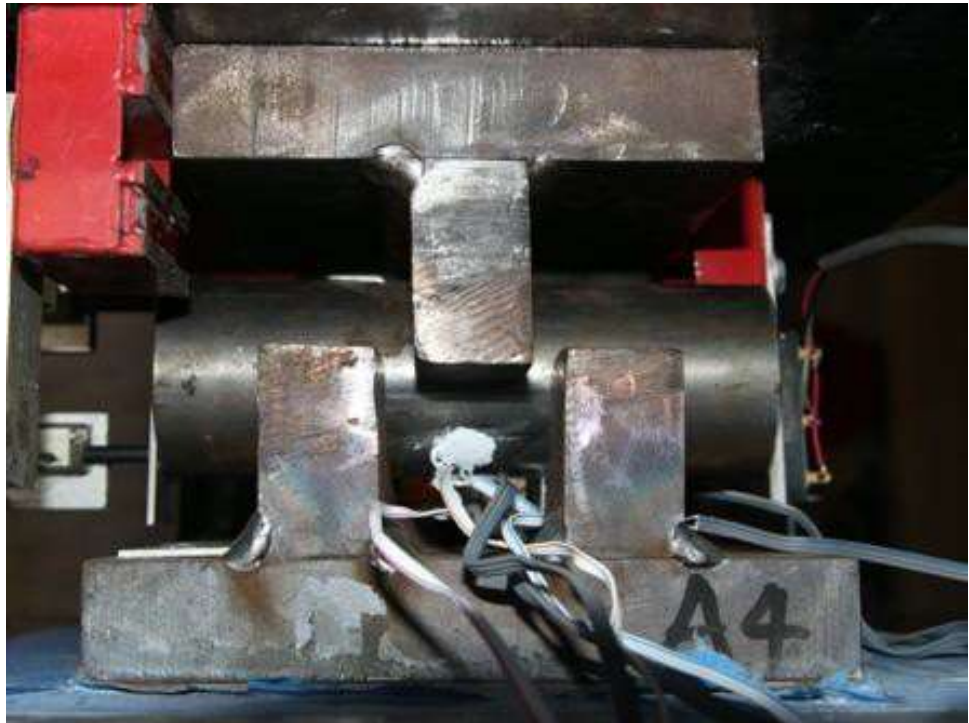
Table 2.3 Chemical Compositions from Mill Certificates

Specimen No.	C	Mn	P	S	Si	Cu	Ni	Cr	Mo	V	CE (%)
Pins A1, A2, A3, A4, A5, A6, A7	0.18	0.77	0.012	0.023	0.30	0.20	0.08	0.08	0.02	0.003	0.35
Pins B1, B2, B3, B4, B5	0.45	0.63	0.015	0.022	0.28	0.30	0.11	0.13	0.04	0.002	0.62
Cradles	0.19	0.87	0.010	0.003	0.32	0.03	0.02	0.58	0.21	0.044	0.51

$$CE = C + \frac{Mn}{6} + \frac{Cr+Mo+V}{5} + \frac{Ni+Cu}{15}$$

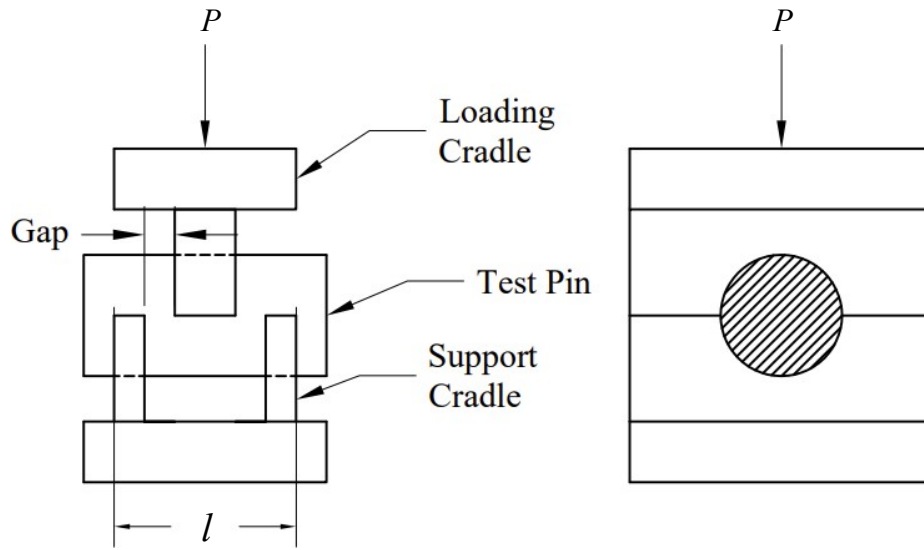


(a) Global View

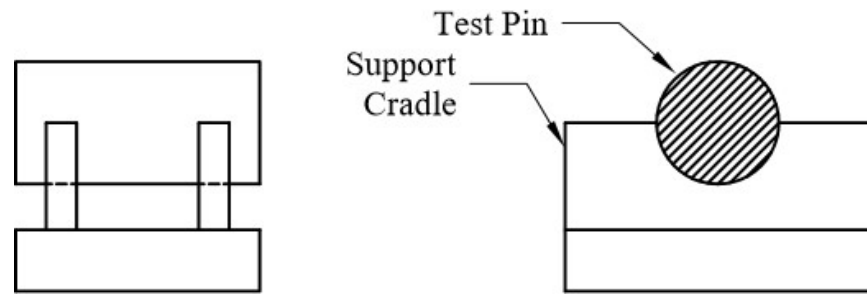


(b) Front View

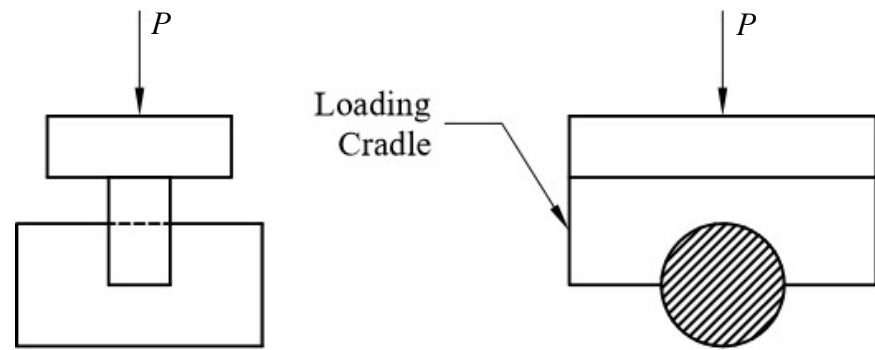
Figure 2.4 Pin Test Setup



(a) Pin Test Configuration

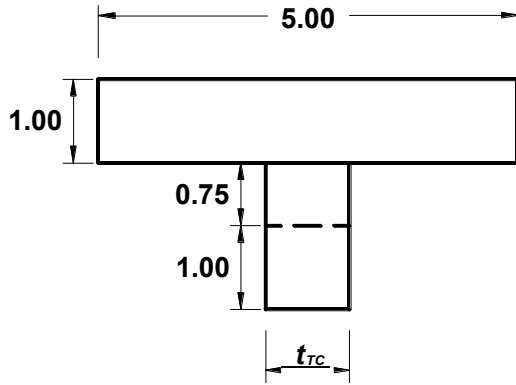


(b) Test Configuration with Loading Cradle Removed



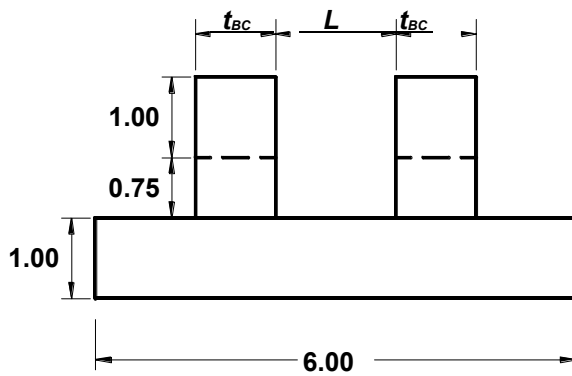
(c) Test Configuration with Support Cradle Removed

Figure 2.5 Pin with Loading and Support Cradles



Cradle No.	Specimen No.	t_{rc} (in.)
TC1	A3, B2	0.87, 0.91
TC2	A2, B1	0.83, 0.91
TC3	A1, A7, B3	0.80
TC4	A4, A5, A6, B4, B5	1.0

(a) Loading Cradles



Specimen No.	t_{bc} (in.)	L (in.)
A1	0.5	1.0
A2	0.75	1.0
A3	1.0	1.0
A4	1.0	1.25
A5	1.0	1.5
A6	1.0	1.75
A7	1.0	3.5
B1	0.75	1.0
B2	1.0	1.0
B3	1.0	1.125
B4	1.0	2.0
B5	1.0	3.0

(b) Support Cradles

Figure 2.6 Dimensions of Loading and Support Cradles for Pin Tests

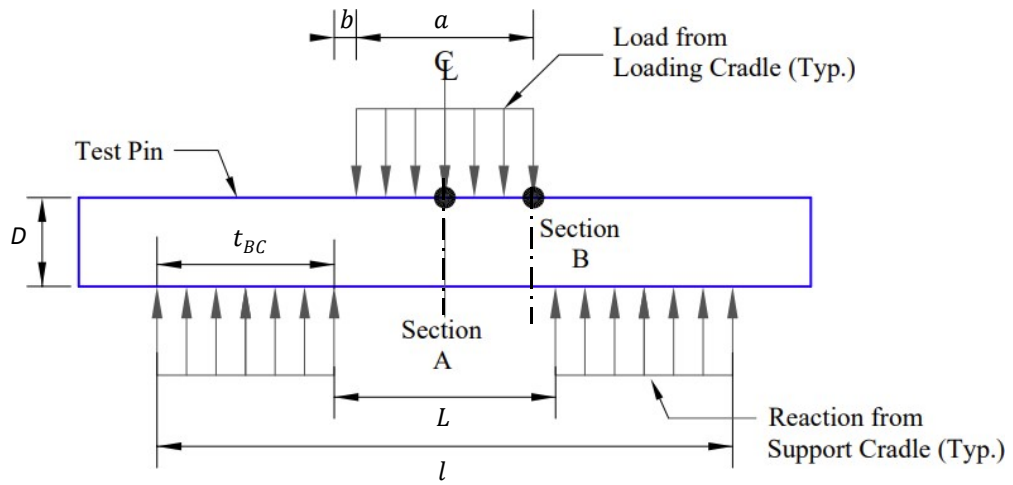


Figure 2.7 Assuming Loading Pattern for Pin Design

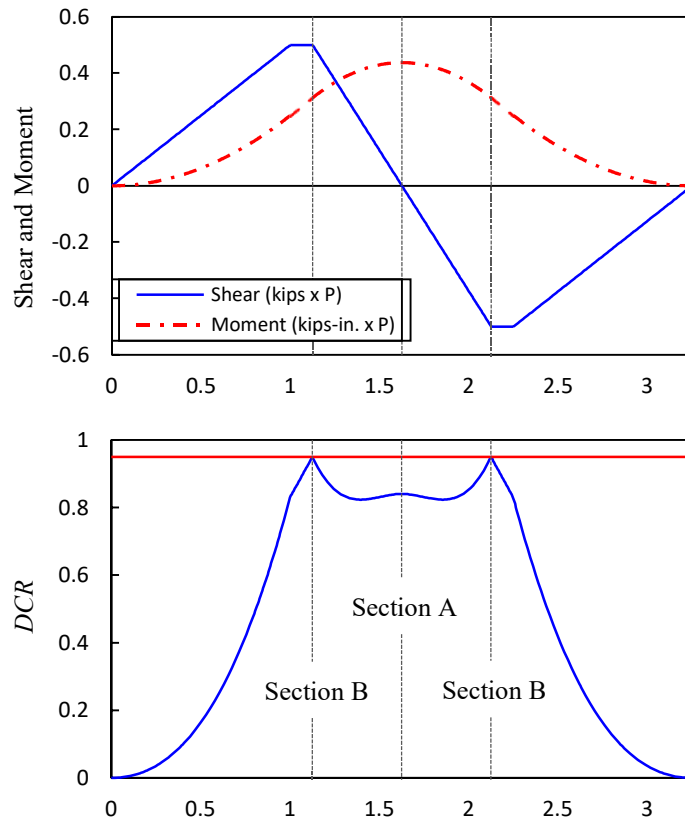


Figure 2.8 Sample Pin Moment-Shear Interaction Check

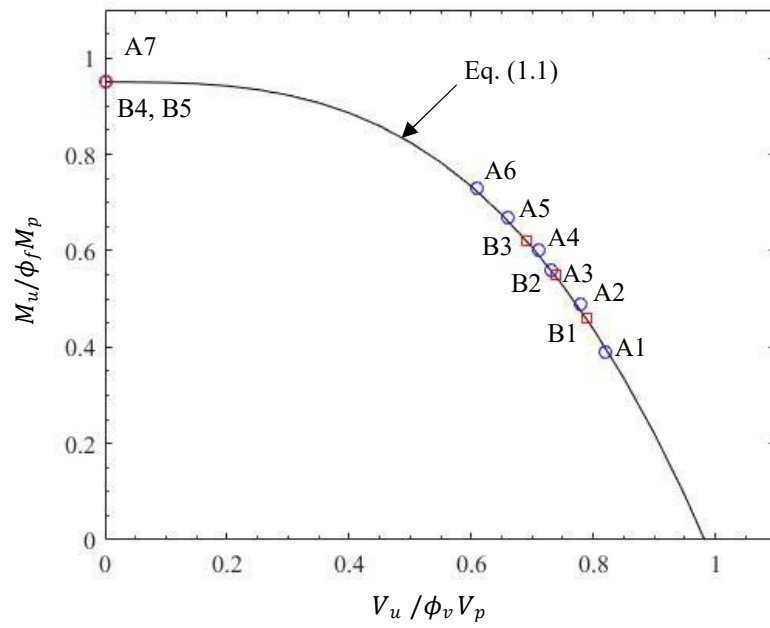
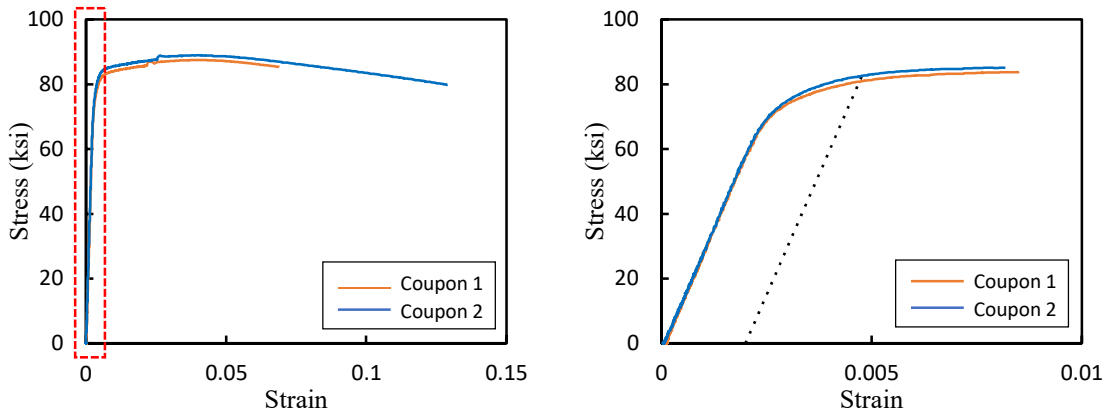
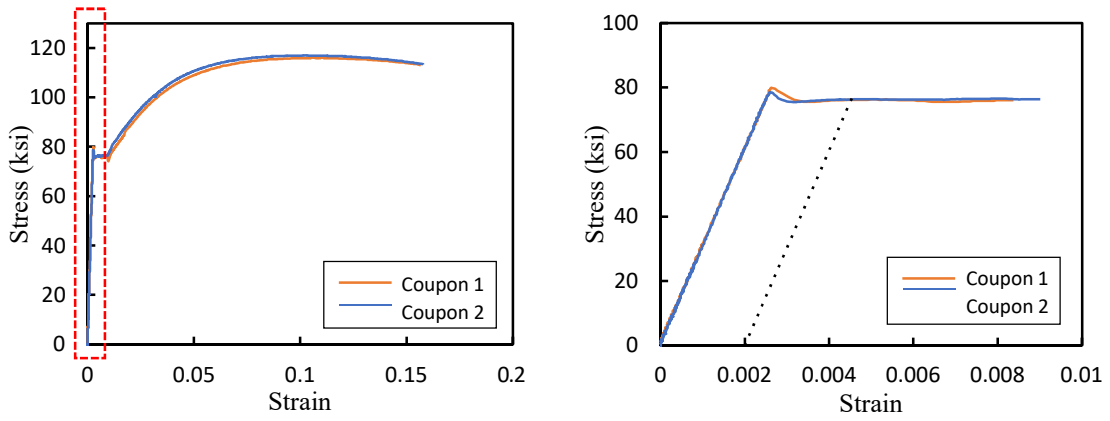


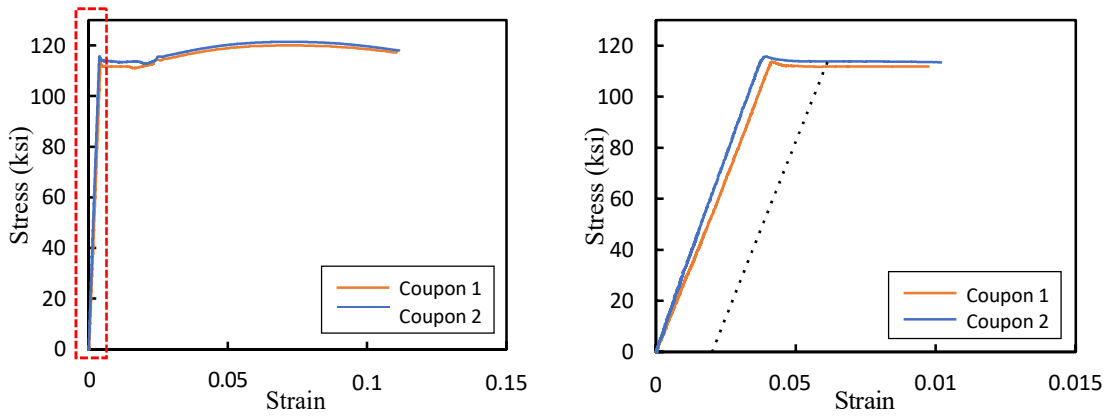
Figure 2.9 Distribution of Pin Specimens in Moment-Shear Domain



(a) A108 Gr.1018 Steel



(b) A668 Class F Steel



(c) A514 Steel

Figure 2.10 Stress-strain Responses from Tensile Coupon Testing (Pin Tests)

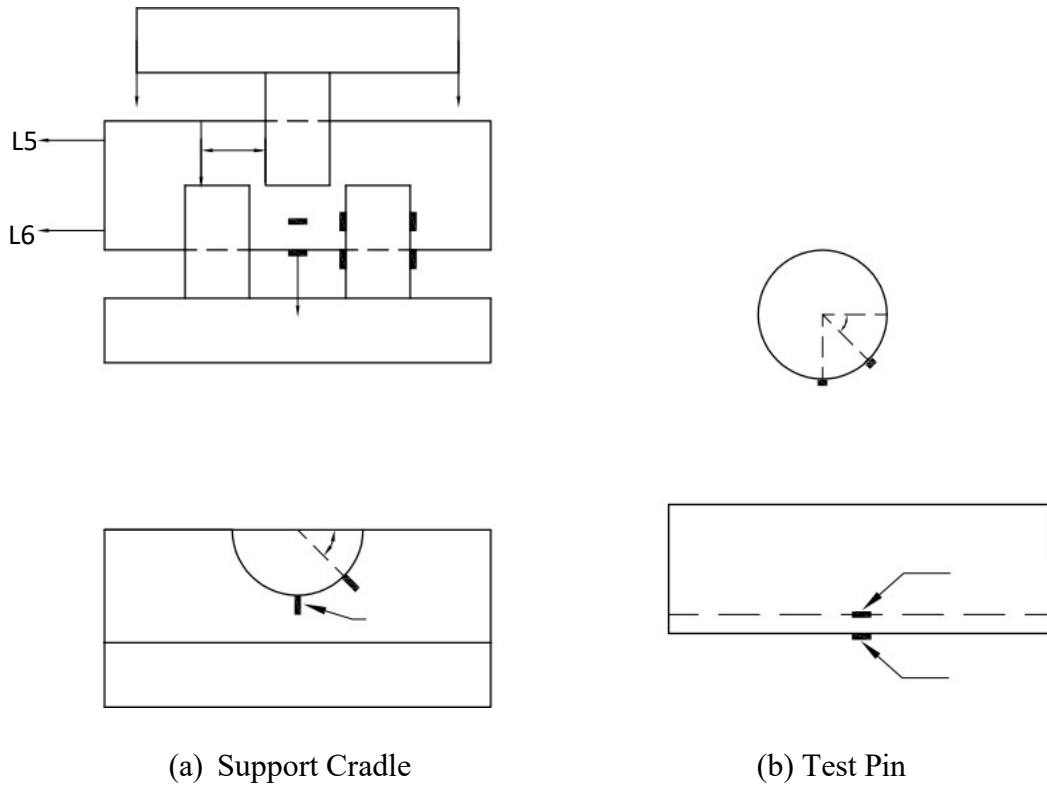


Figure 2.11 Instrumentation for Pin Tests

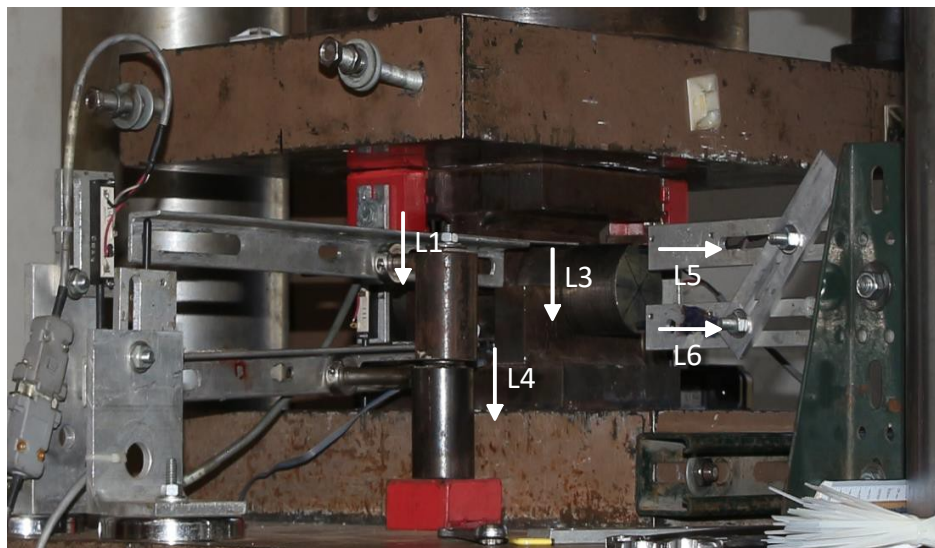


Figure 2.12 Displacement Transducer Layout for Pin Tests

2.3 Test Results

2.3.1 Series A Specimens (A108 Gr. 1018 Steel)

2.3.1.1 Specimen A1

Figure 2.13(b) shows the failure mode of the specimen. The global response is shown in Figure 2.14. The deflection used for the solid-line response in Figure 2.14(a) is the average vertical displacement of the loading cradle as measured by displacement transducers L1 and L2 (see Figure 2.11). This measurement includes both the pin deformation and deformations from the loading and supporting cradles. Note that the pin deformation includes not only the conventional pin deformation in the context of a simply supported beam but also penetrations that the much stronger cradles made into the pin from the top and bottom surfaces. The deflection for the dashed-line response is the vertical displacement of the pin bottom surface at the midspan as measured by displacement transducer L4. This measurement includes both the pin deformation mentioned above and the deformation of the support cradle. Because each of the two vertical plates of the support cradle was subjected to half that of the vertical plate of the loading cradle, it was observed that the plastic deformation of the latter was significant, but the vertical plates of the support cradle remained essentially elastic. Therefore, measurements from L1 and L2 included the deformation of the loading cradle, and measurement by L4 is predominately due to the pin deformation. Figure 2.14(b) shows the relationship between applied load and end rotation, where the end rotation of the pin was measured by displacement transducers L5 and L6 (see Figure 2.11). For this particular test, the unexpected negative rotation was caused by the malfunction of the displacement transducers.

Guided by a pre-test finite element analysis, the specimen was first loaded to 200 kips [point “a” in Figure 2.14(a)] before the testing was switched to a displacement-control mode up to point “b” when significant deformation was observed. The pin failed into three pieces in a brittle manner when the specimen was loaded to 0.58 in. (point “c”). The maximum strength reached was 318.1 kips.

2.3.1.2 Specimen A2

Figure 2.15 and Figure 2.16 show the failure mode and measured responses, respectively. The maximum strength (= 318.6 kips) was reached at point “b” and the

strength started to degrade. Like Specimen A1, significant penetration to the pin occurred. But the pin specimen was still intact as shown in Figure 2.15(b), not broken into three pieces like Specimen A1.

2.3.1.3 Specimen A3

Figure 2.17 and Figure 2.18 show the failure mode and measured responses, respectively. The specimen was first loaded to point “a” in Figure 2.18. Then the specimen started to break into three pieces at about 0.39 in. (point “b”), beyond which the strength degraded rapidly. The maximum strength reached as 323.9 kips.

2.3.1.4 Specimen A4

Figure 2.19 and Figure 2.20 show the failure mode and measured responses, respectively. The specimen reached its maximum strength (= 338.0 kips) at 0.42 in. (point “b”) before the strength started to degrade.

2.3.1.5 Specimen A5

Figure 2.21 and Figure 2.22 show the failure mode and measured responses, respectively. The specimen reached its maximum strength (= 319.6 kips) at 0.31 in. (point “b”).

2.3.1.6 Specimen A6

Figure 2.23 and Figure 2.24 show the failure mode and measured responses, respectively. The maximum strength (= 313.8 kips) was reached at 0.39 in. (point “b”).

2.3.1.7 Specimen A7

Figure 2.25 and Figure 2.26 show the failure mode and measured responses, respectively. The specimen was first loaded to point “a” in Figure 2.26 (a). Of all the Series A specimens, this one has the longest span. The large flexural deformation caused the pin at both ends to touch the loading cradle when the displacement was increased to 0.44 in. After this stage 1 loading, the specimen was unloaded. A 0.6-in. thick shim plate (A36 steel) was inserted between the pin and top cradle before stage 2 loading was applied to the specimen. Pin ends touched the top cradle again. The same process was repeated for stage 3 loading. The maximum load reached was 246.7 kips; L1 and L2 measurements were not made during stage 3 loading.

2.3.2 Series B Specimens (A668 Class F Steel)

2.3.2.1 Specimen B1

Figure 2.27 and Figure 2.28 show the failure mode and measured responses, respectively. The specimen was first loaded to point “a”. The specimen reached its maximum strength (= 449.6 kips) at 0.52 in. (point “b”), which was followed by a rapid degradation in strength.

2.3.2.2 Specimen B2

Figure 2.29 and Figure 2.30 show the failure mode and measured responses, respectively. Once the specimen reached its maximum strength (= 469.3 kips) at 0.58 in. (point “b”), the pin was sheared into three pieces as shown in Figure 2.29(b).

2.3.2.3 Specimen B3

Figure 2.31 and Figure 2.32 show the failure mode and measured responses, respectively. Testing was stopped at 0.59 in. after the maximum strength (= 460.8 kips) of the pin was reached (point “b”).

2.3.2.4 Specimen B4

Figure 2.33 and Figure 2.34 show the failure mode and measured responses, respectively. The specimen was loaded until both ends of the pin touched the loading cradle, which corresponded to a displacement of 0.54 in. (point “b”). Since the load-deflection curve showed a relatively flat plateau at point “b” and the pin had deformed considerably, it was judged that any increase in strength would be small and, thus, the test was stopped. The maximum load reached was 420.3 kips.

2.3.2.5 Specimen B5

Of all the Series B specimens, this one had the largest span. Figure 2.35 and Figure 2.36 show the failure mode and measured responses, respectively. Both ends of the pin touched the top cradle at 0.57 in. (point “b”). A slight increase of the deflection from 0.57 in. to 0.59 in. (point “c”) caused a significant increase of the applied load. This artificial increase of the load was due to the bearing action between pin ends and the loading cradle. For the same reason as for Specimen B4, the test was stopped for safety considerations.

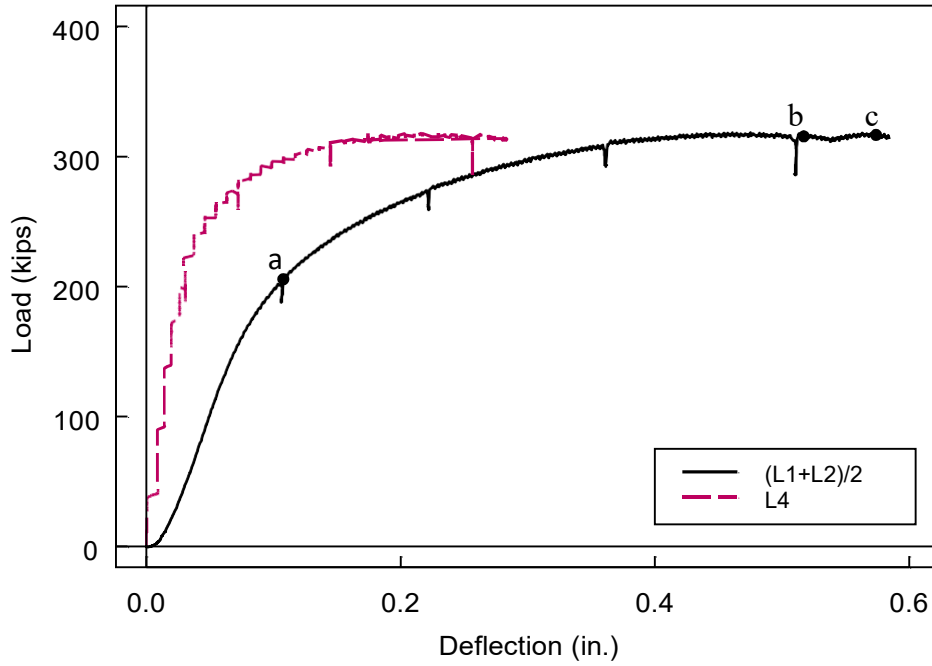


(a) End of Test

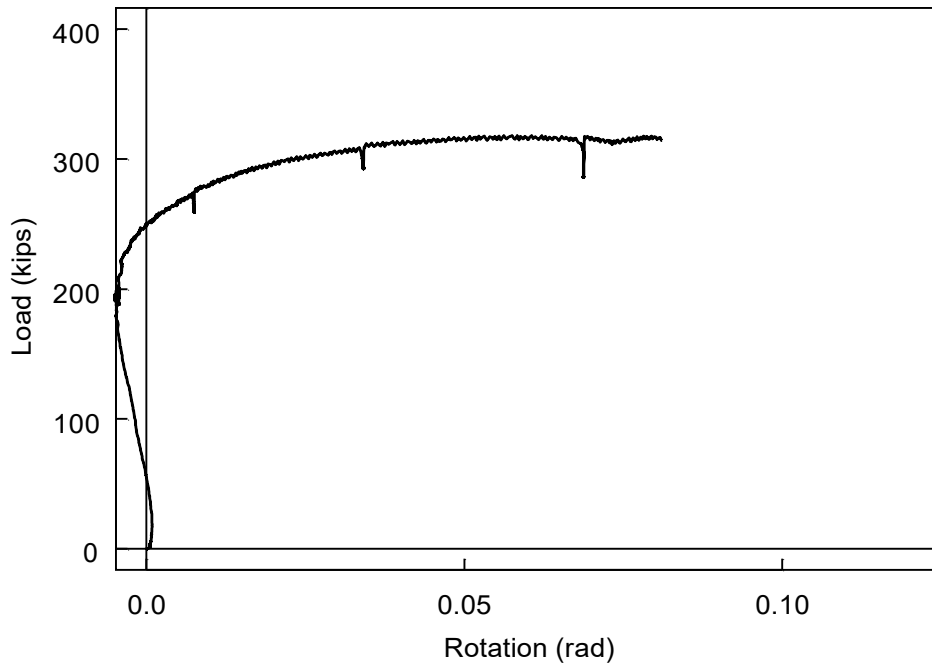


(b) Failure Mode

Figure 2.13 Specimen A1: Deformed Shape

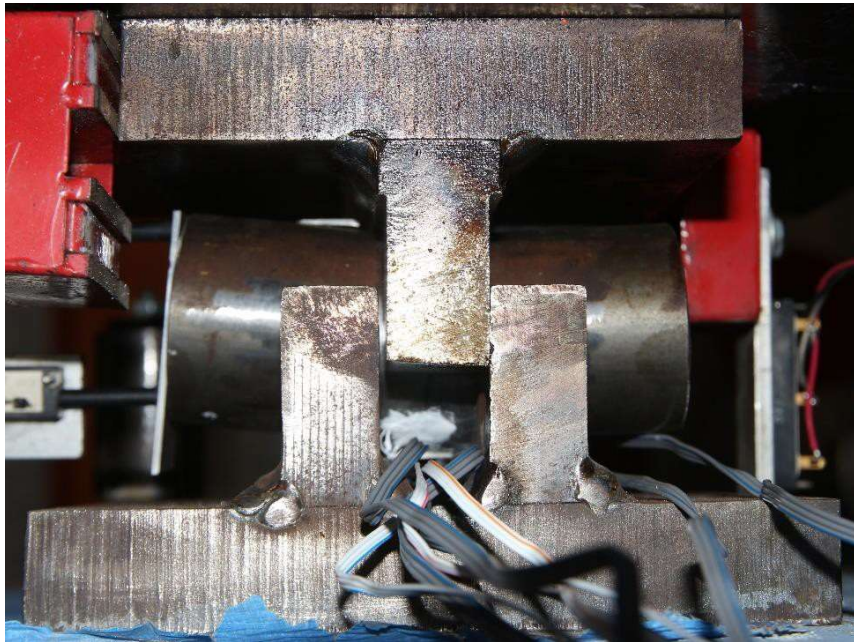


(a) Applied Load versus Deflection



(b) Applied Load versus End Rotation

Figure 2.14 Specimen A1: Global Response

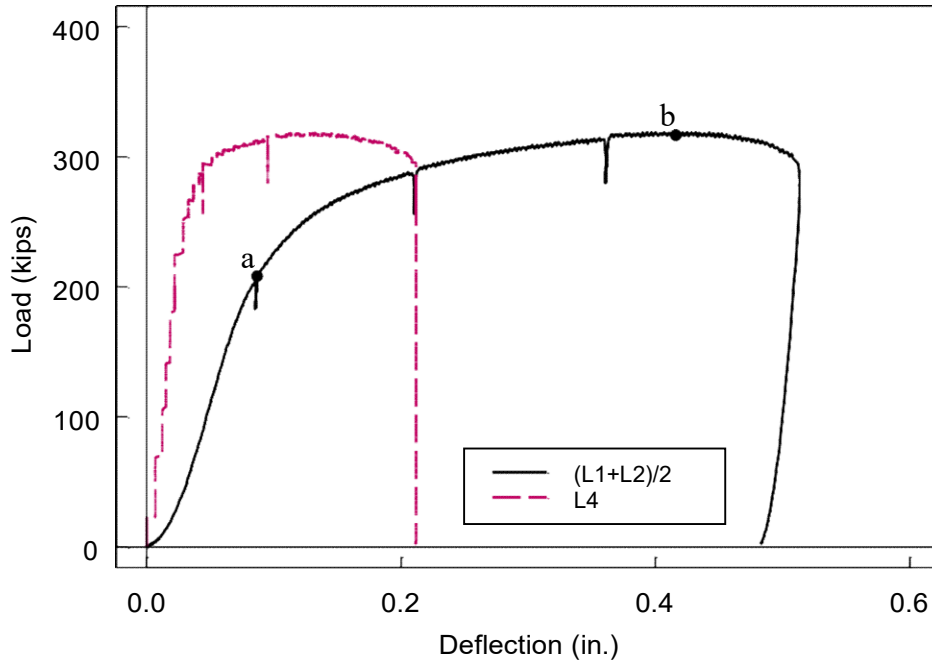


(a) End of Test

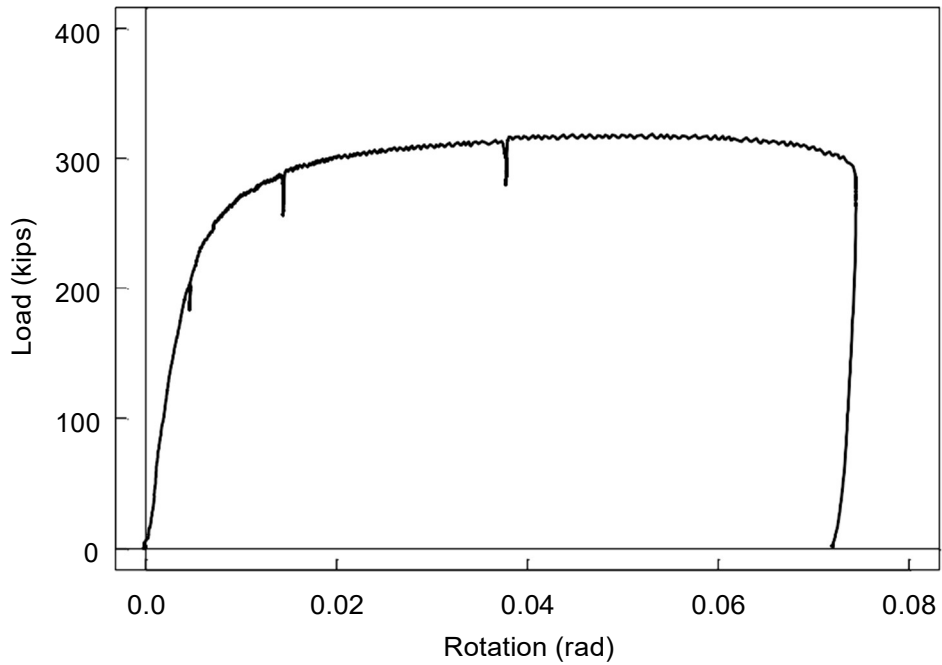


(b) Failure Mode

Figure 2.15 Specimen A2: Deformed Shape

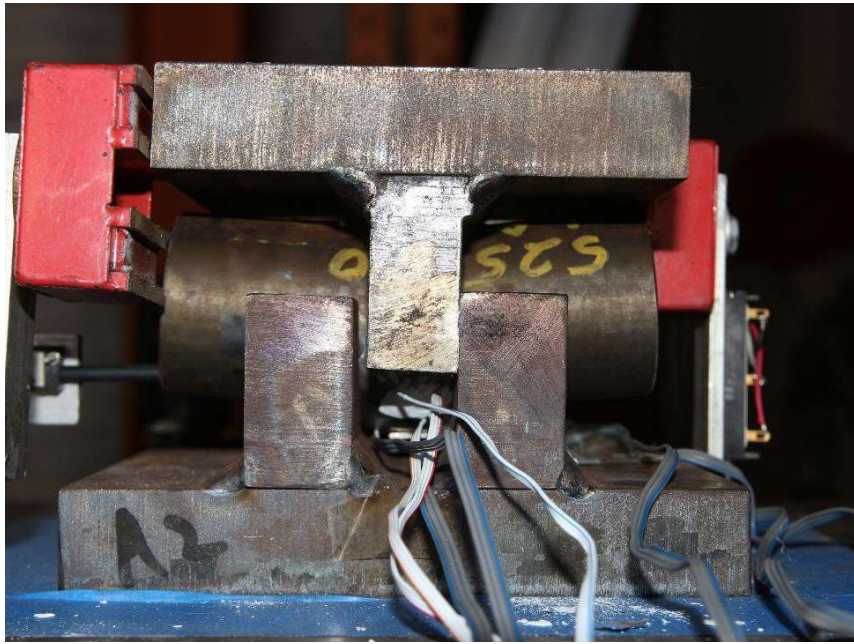


(a) Applied Load versus Deflection



(b) Applied Load versus End Rotation

Figure 2.16 Specimen A2: Global Response

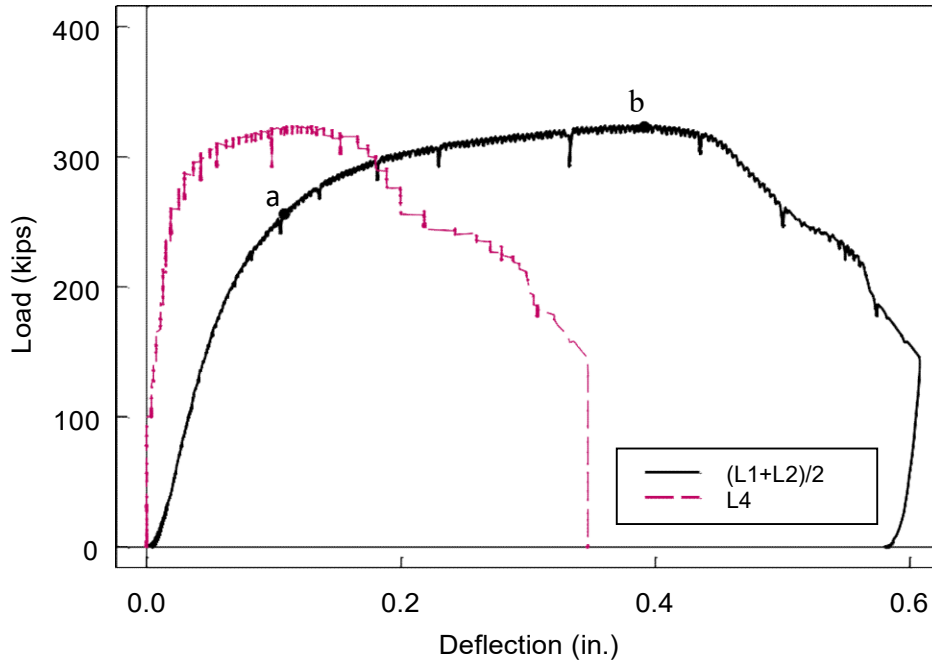


(a) End of Test

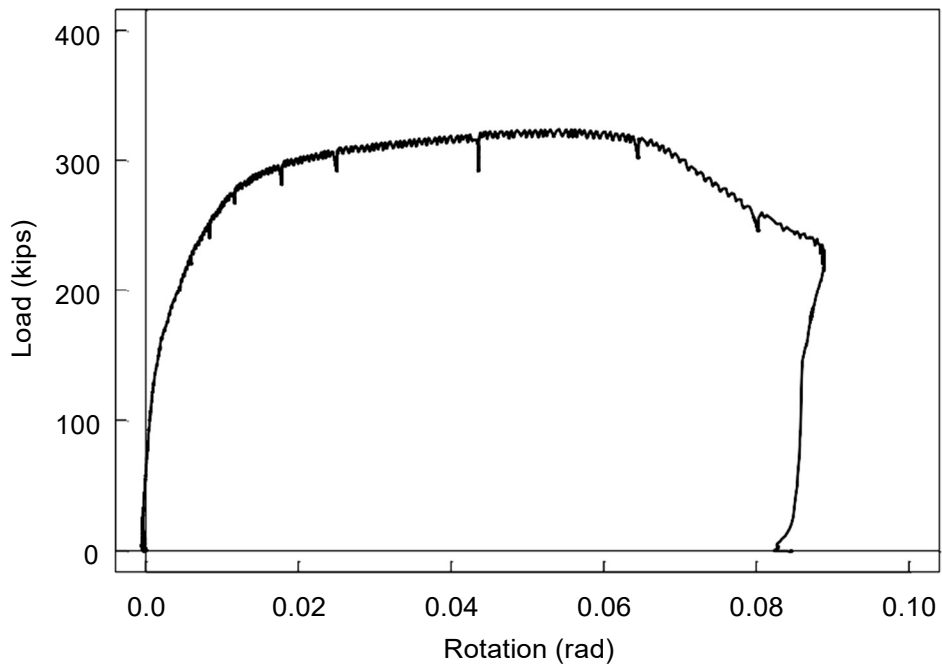


(b) Failure Mode

Figure 2.17 Specimen A3: Deformed Shape

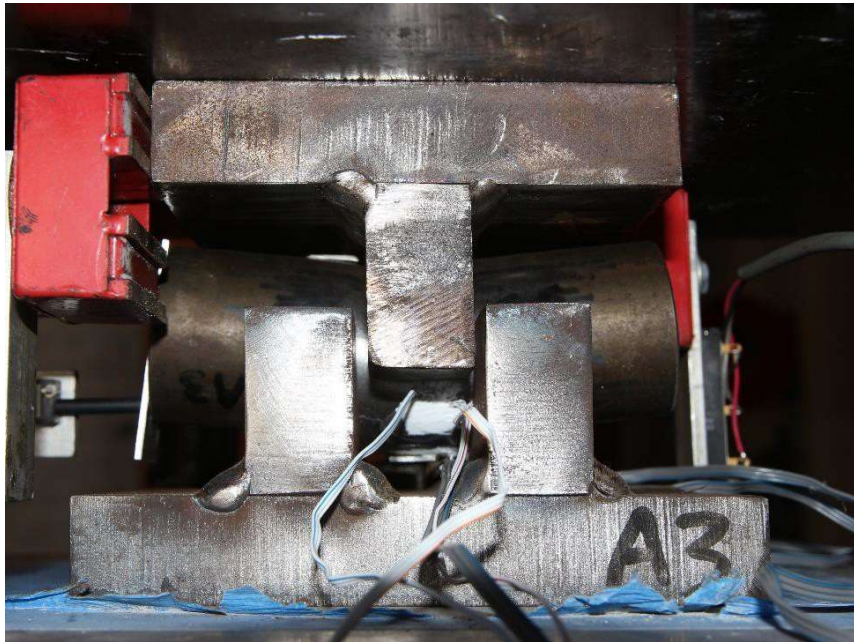


(a) Applied Load versus Deflection



(b) Applied Load versus End Rotation

Figure 2.18 Specimen A3: Global Response

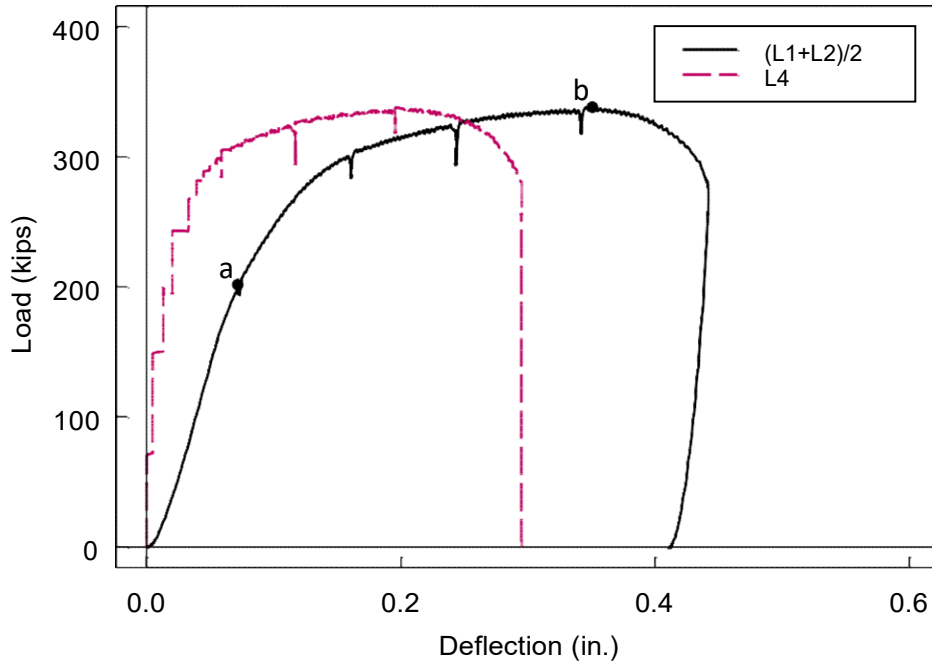


(a) End of Test

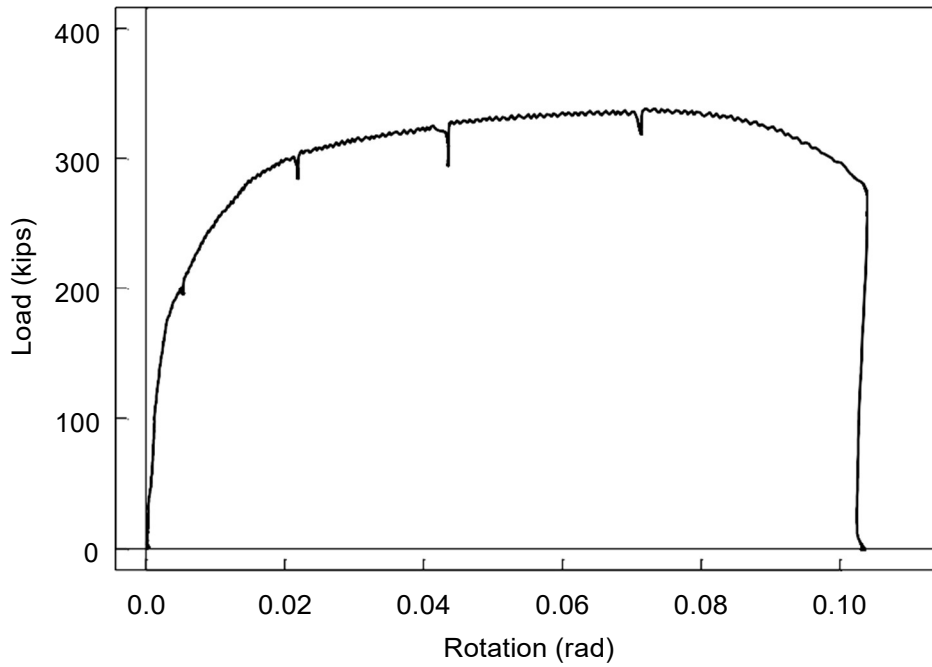


(b) Failure Mode

Figure 2.19 Specimen A4: Deformed Shape

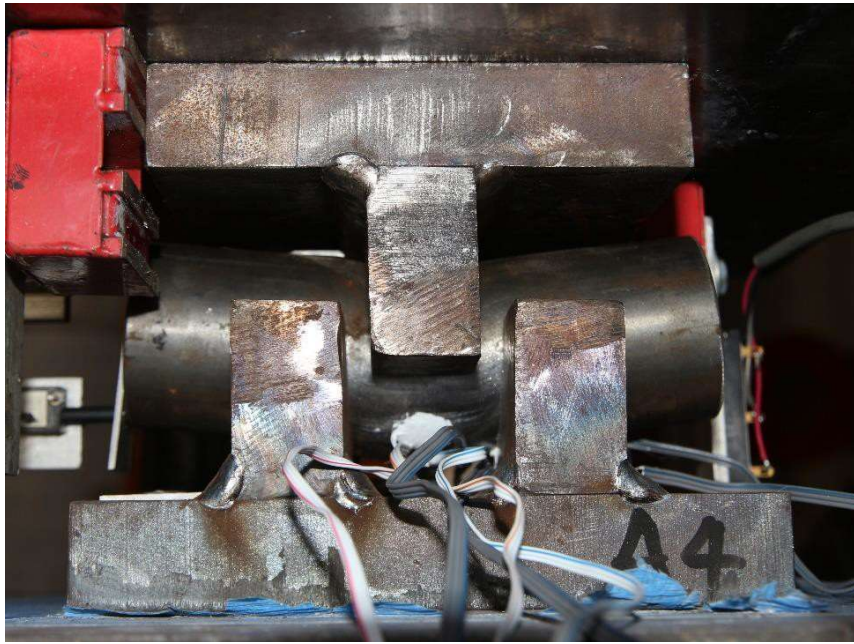


(a) Applied Load versus Deflection



(b) Applied Load versus End Rotation

Figure 2.20 Specimen A4: Global Response

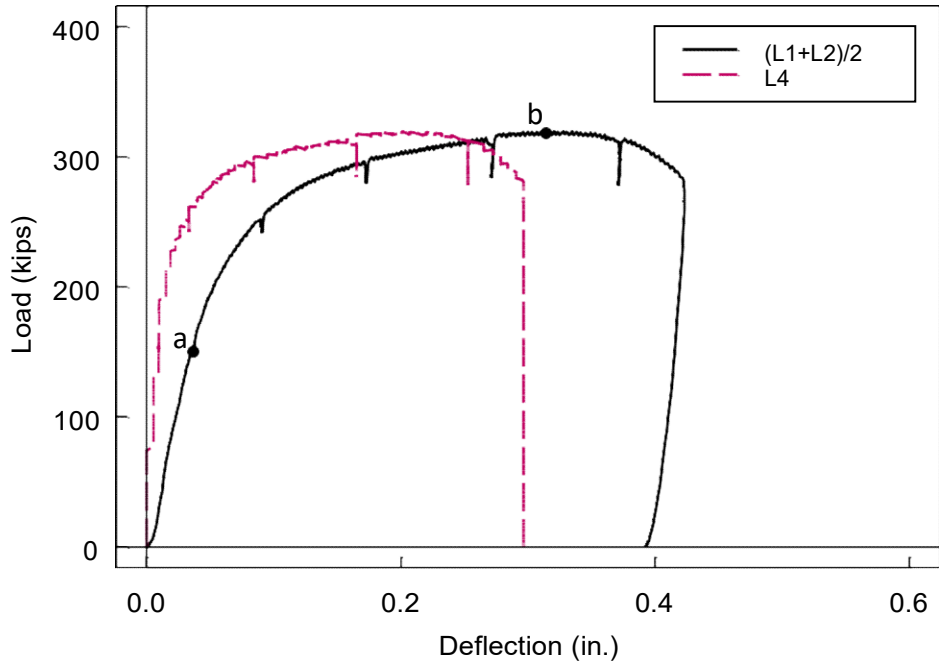


(a) End of Test

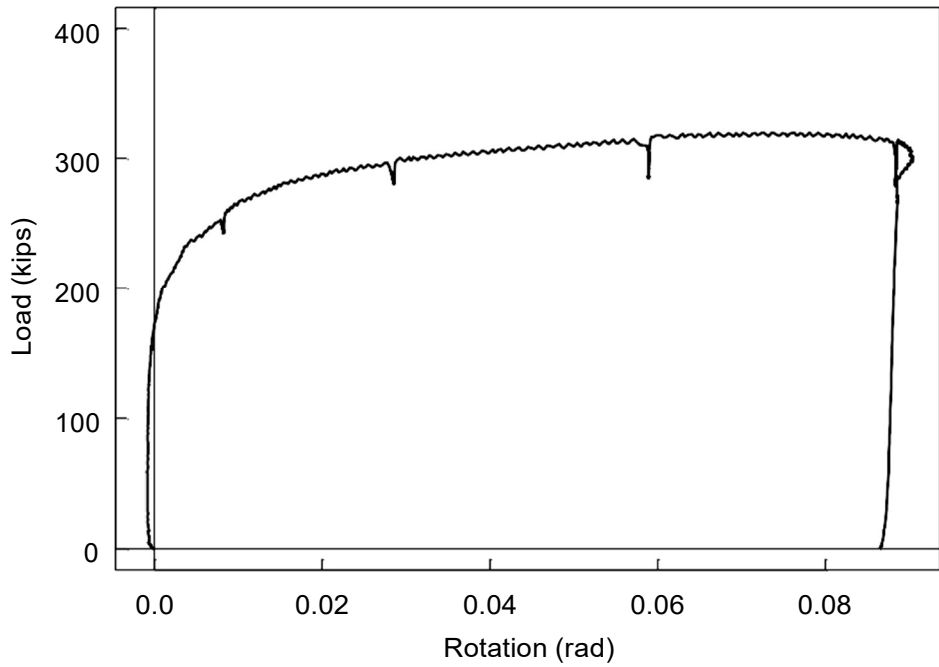


(b) Failure Mode

Figure 2.21 Specimen A5: Deformed Shape

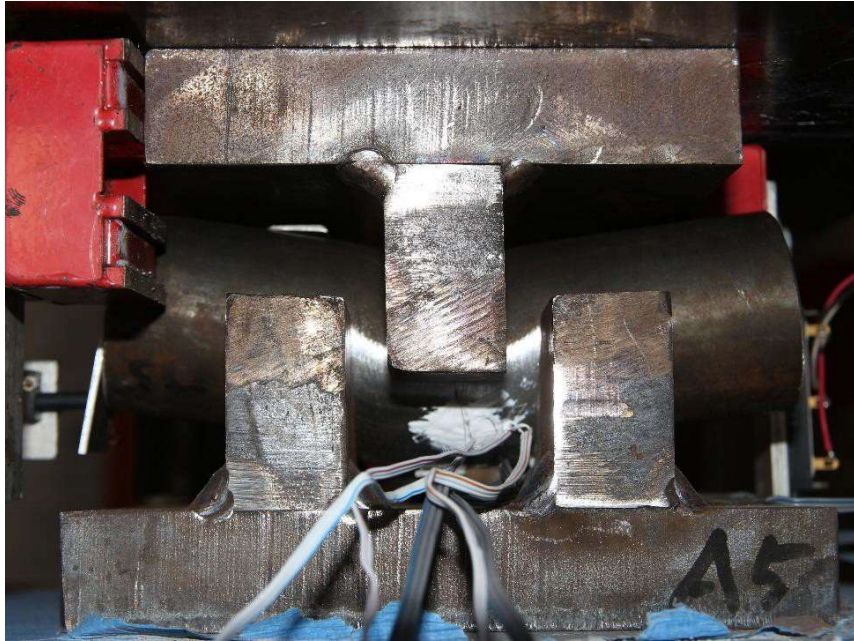


(a) Applied Load versus Deflection



(b) Applied Load versus End Rotation

Figure 2.22 Specimen A5: Global Response

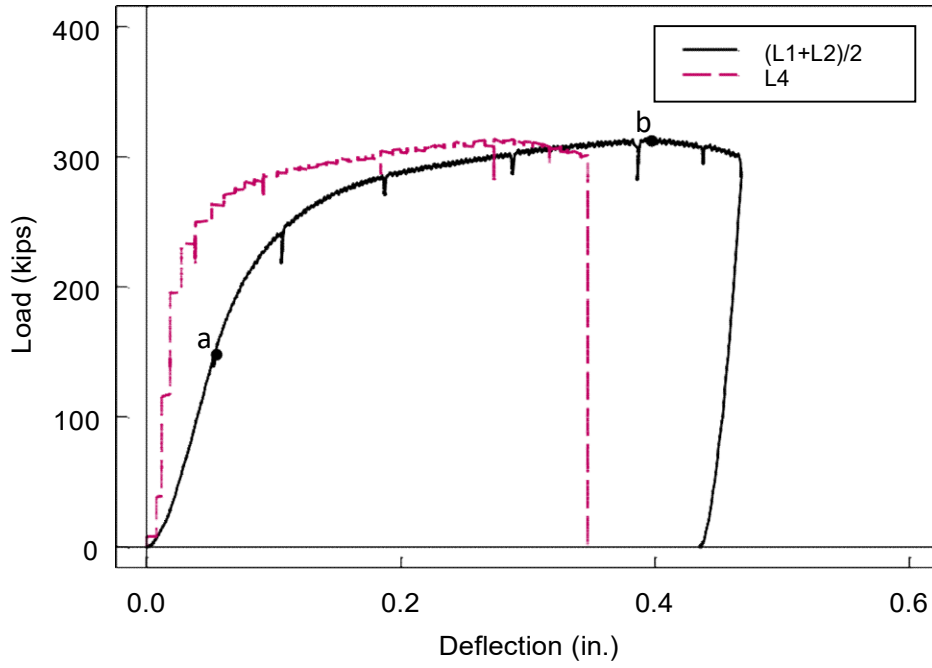


(a) End of Test

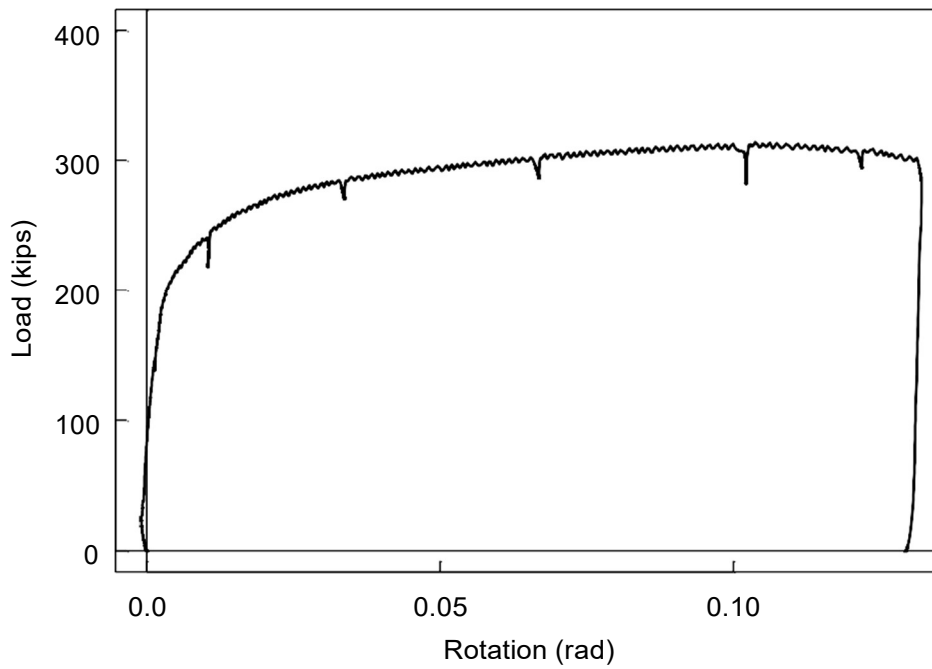


(b) Failure Mode

Figure 2.23 Specimen A6: Deformed Shape

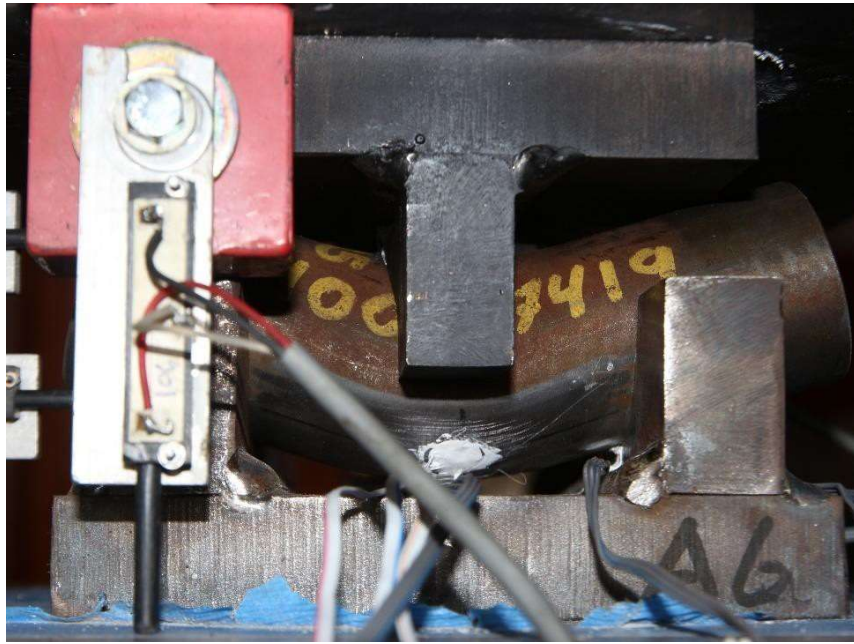


(a) Applied Load versus Deflection



(b) Applied Load versus End Rotation

Figure 2.24 Specimen A6: Global Response

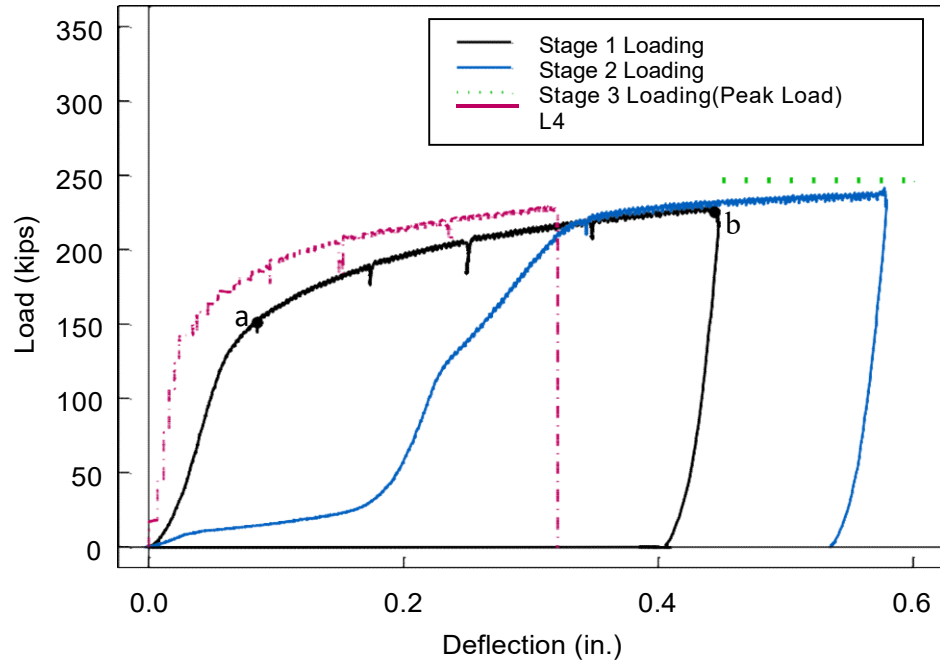


(a) End of Test

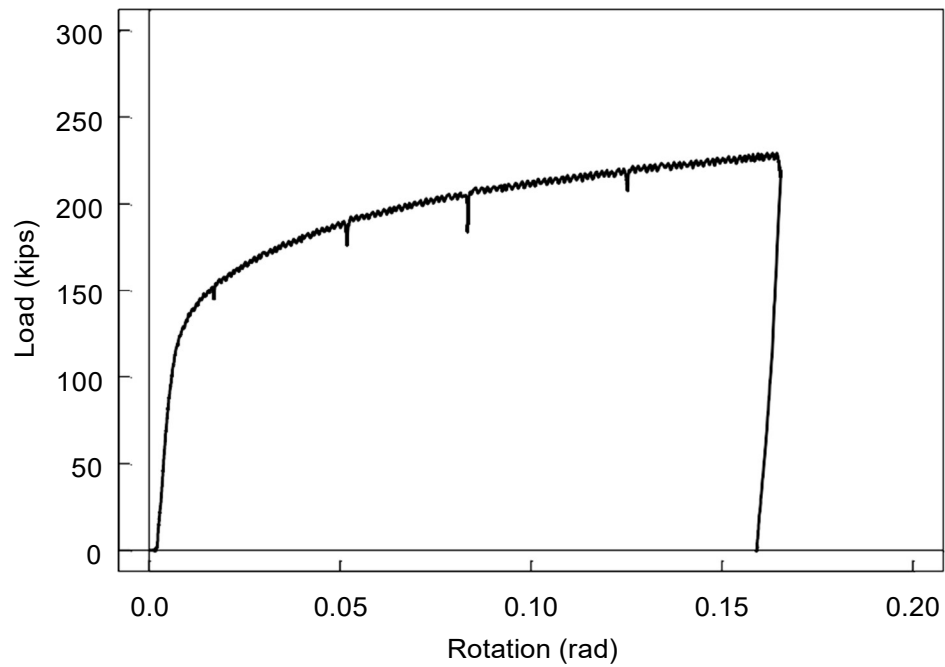


(b) Failure Mode

Figure 2.25 Specimen A7: Deformed Shape

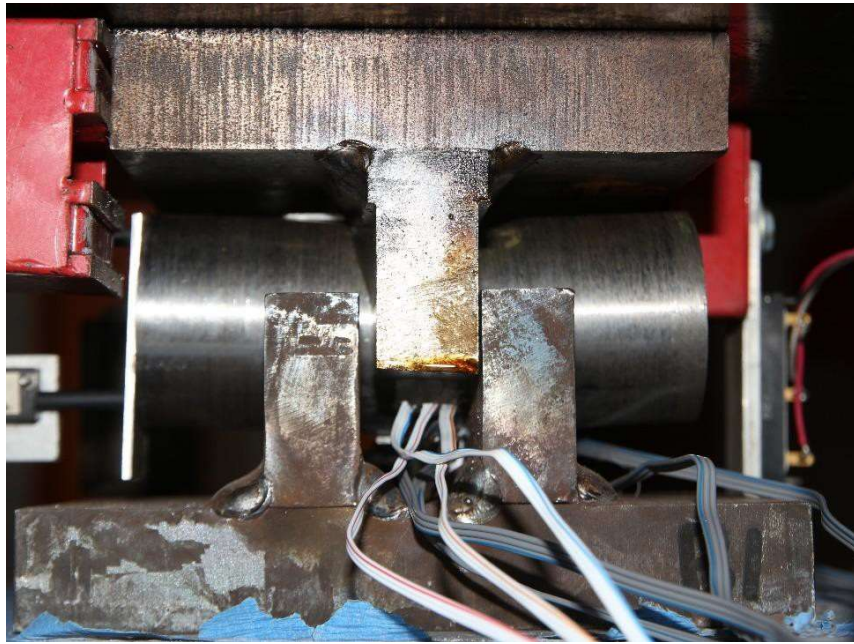


(a) Applied Load versus Deflection



(b) Applied Load versus End Rotation

Figure 2.26 Specimen A7: Global Response

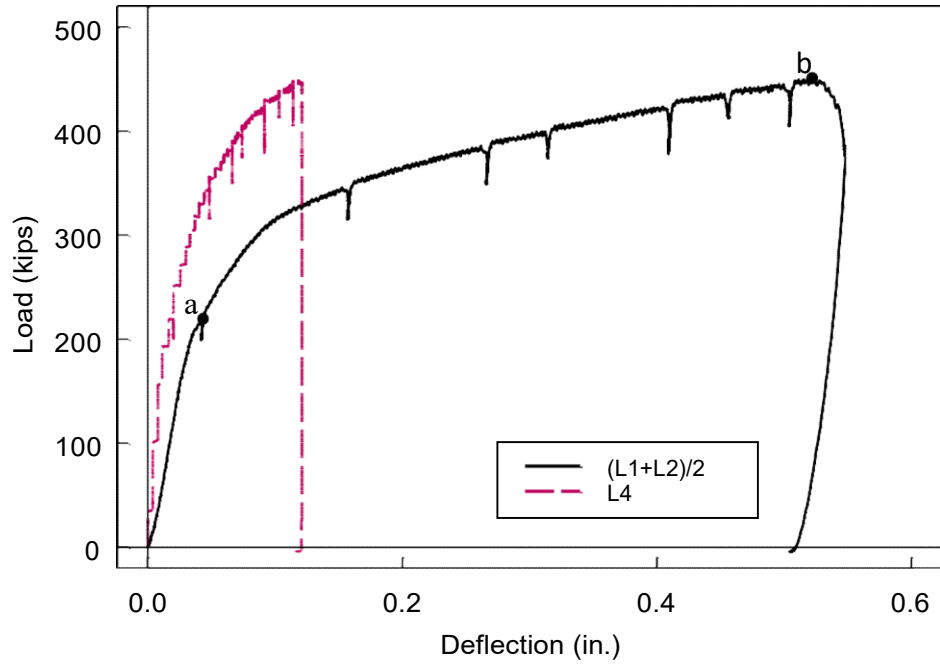


(a) End of Test

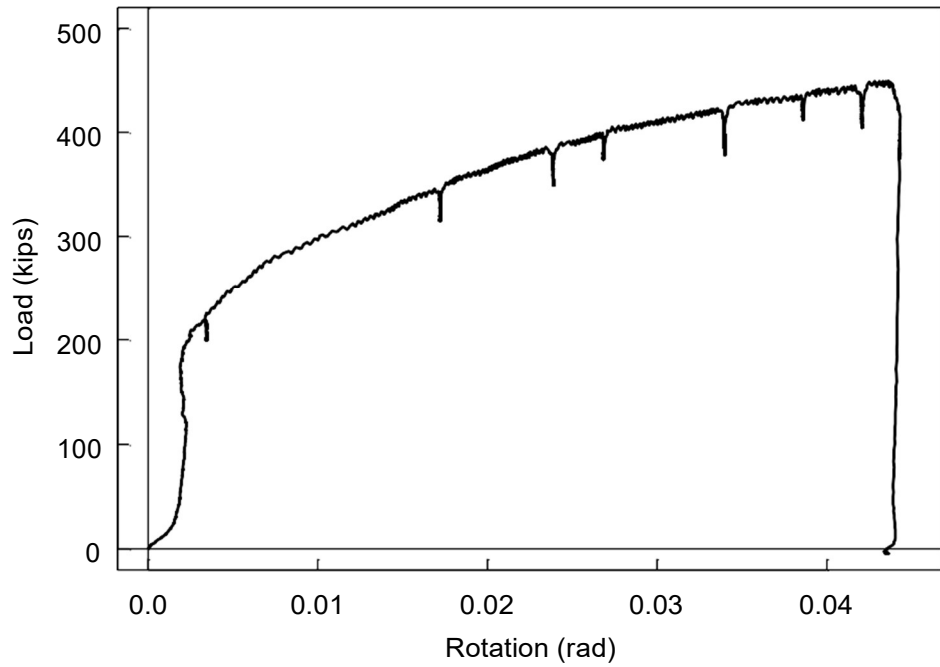


(b) Failure Mode

Figure 2.27 Specimen B1: Deformed Shape

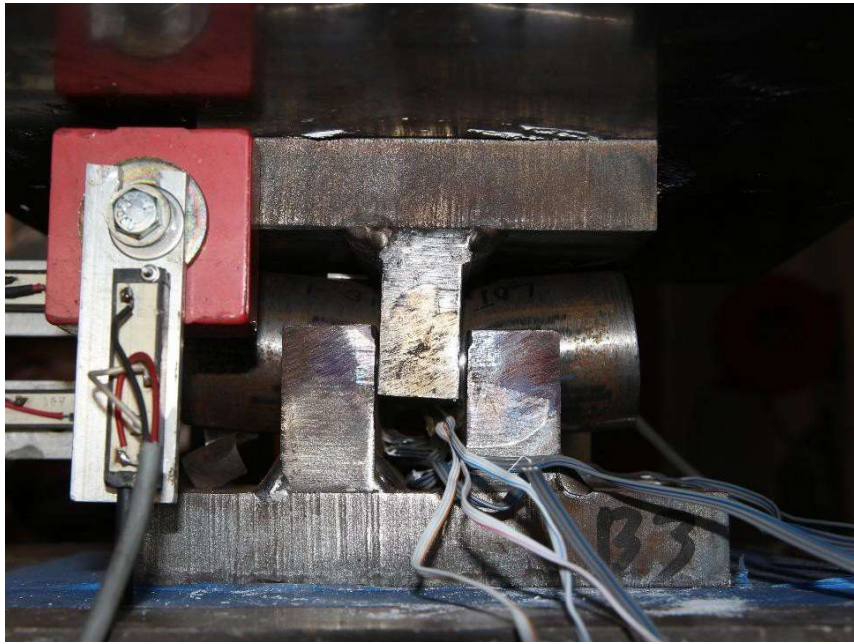


(a) Applied Load versus Deflection



(b) Applied Load versus End Rotation

Figure 2.28 Specimen B1: Global Response

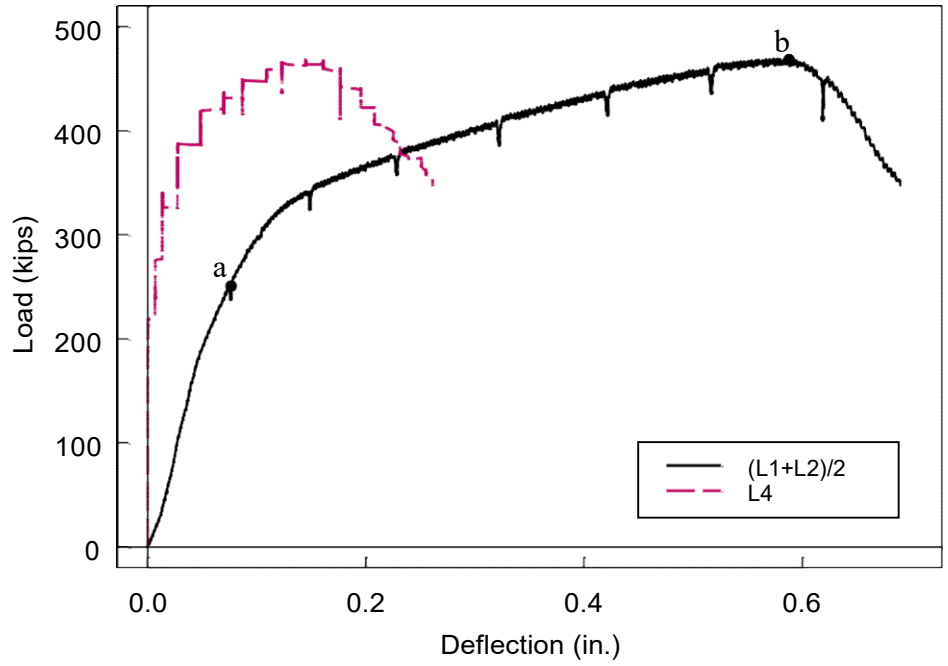


(a) End of Test

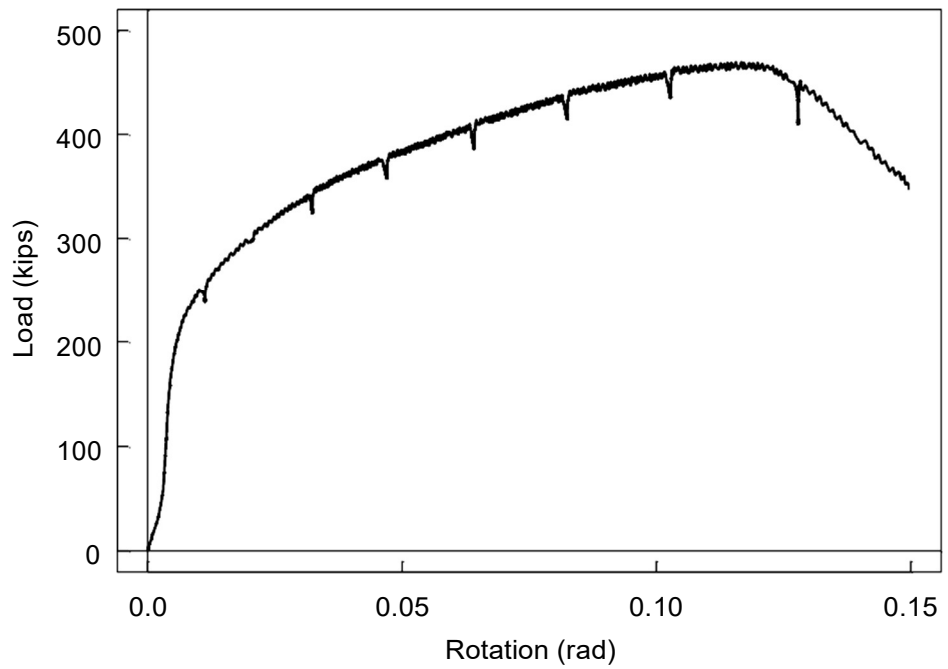


(b) Failure Mode

Figure 2.29 Specimen B2: Deformed Shape

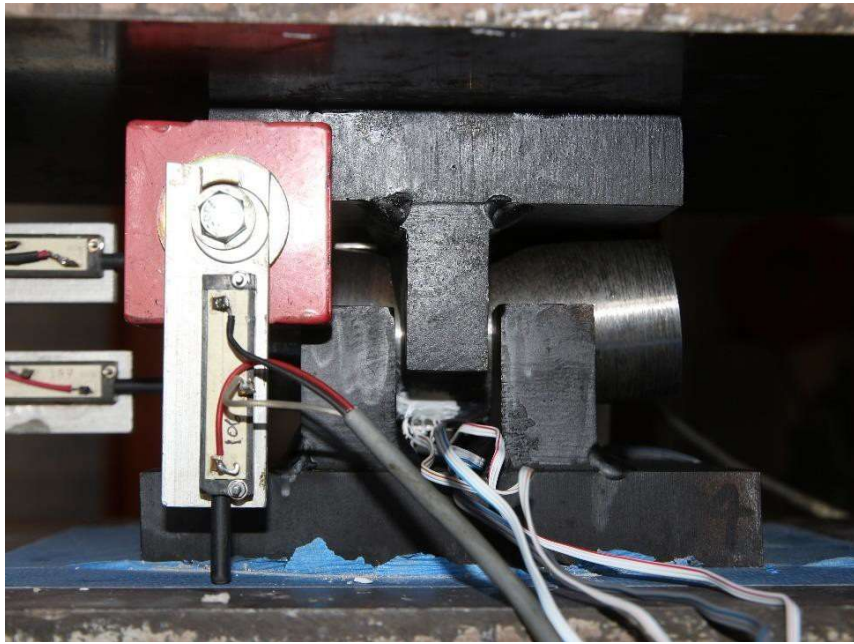


(a) Applied Load versus Deflection



(b) Applied Load versus End Rotation

Figure 2.30 Specimen B2: Global Response

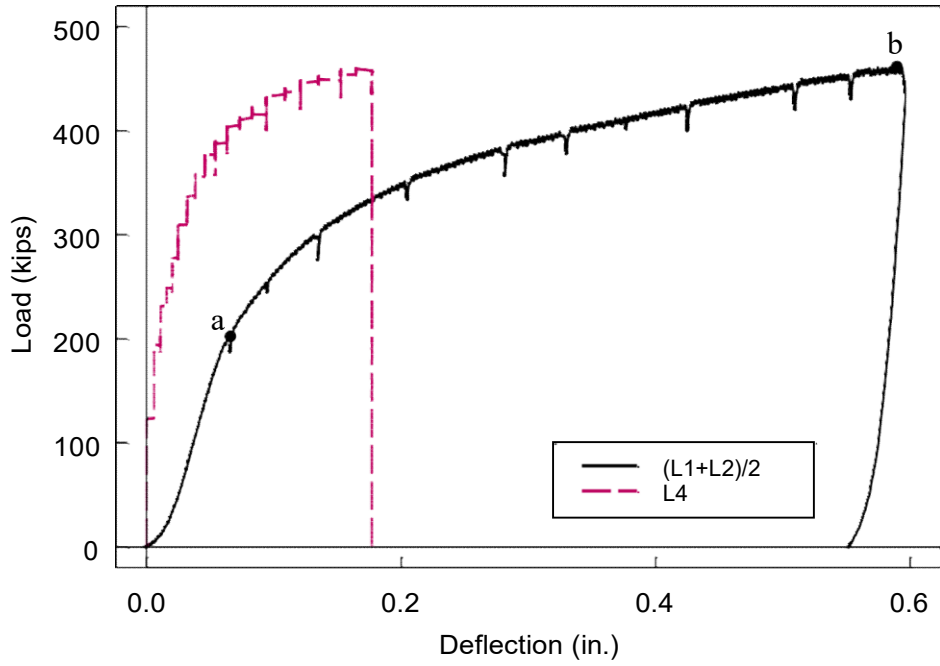


(a) End of Test

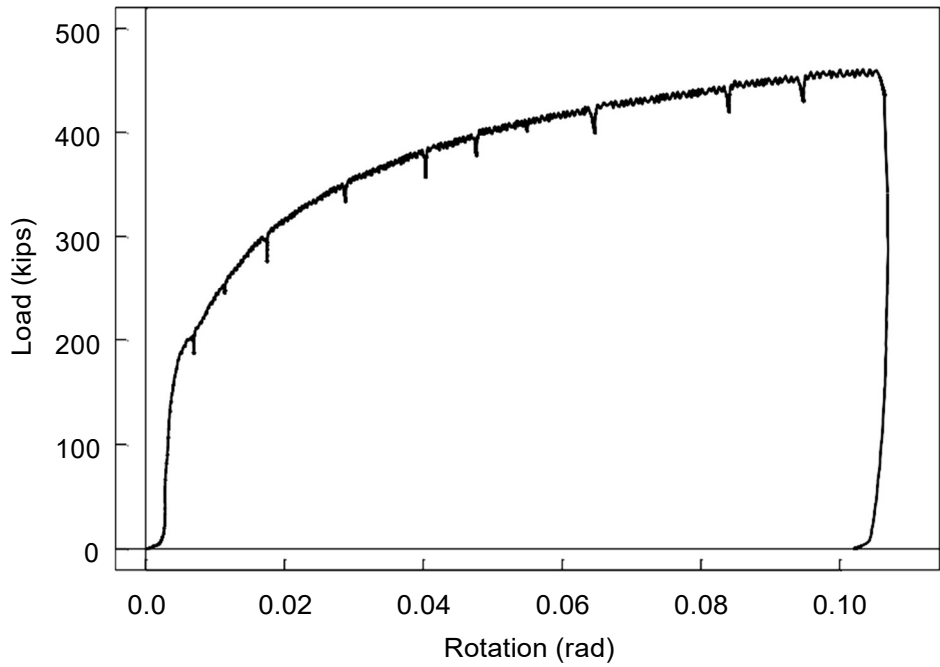


(b) Failure Mode

Figure 2.31 Specimen B3: Deformed Shape

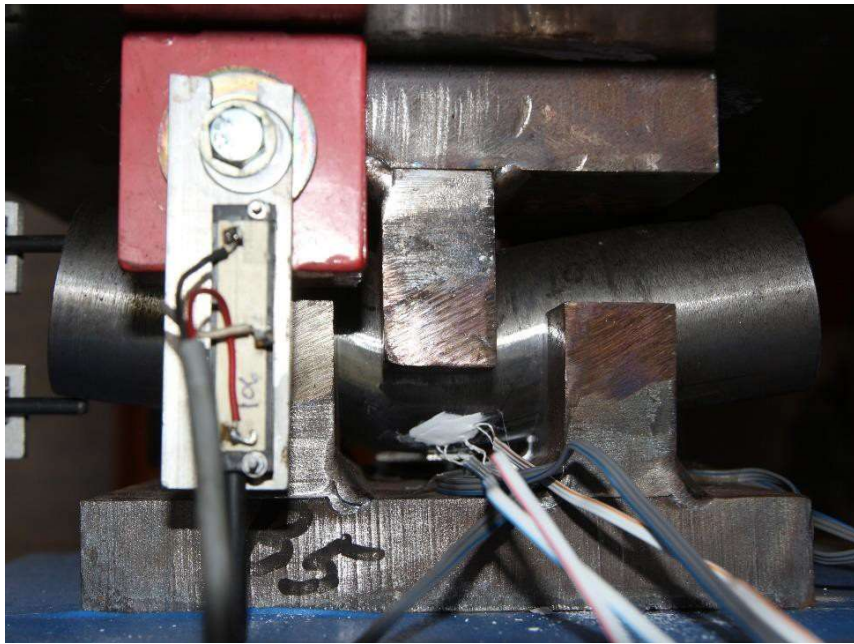


(a) Applied Load versus Deflection



(b) Applied Load versus End Rotation

Figure 2.32 Specimen B3: Global Response

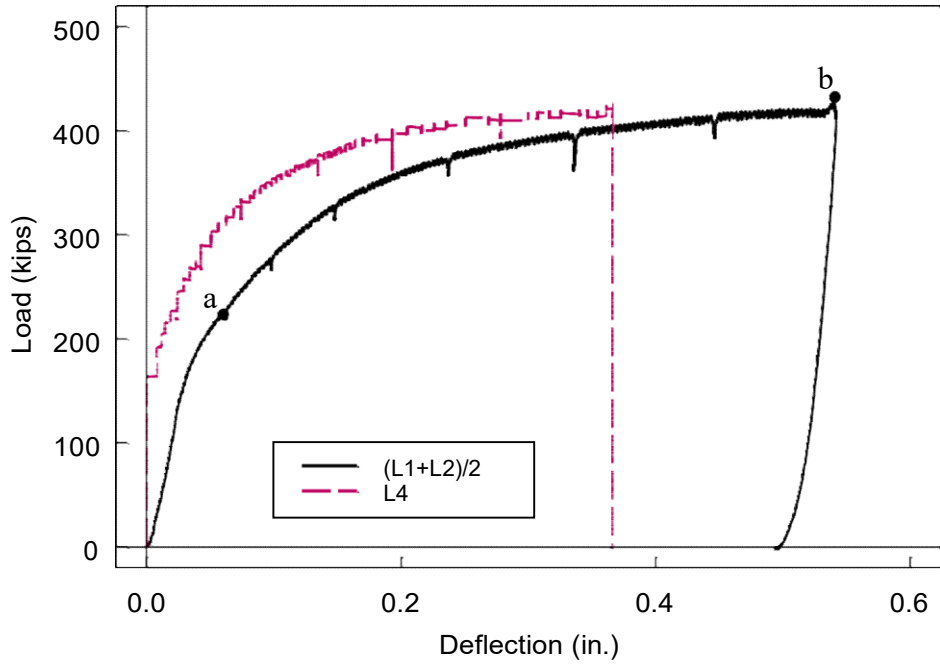


(a) End of Test

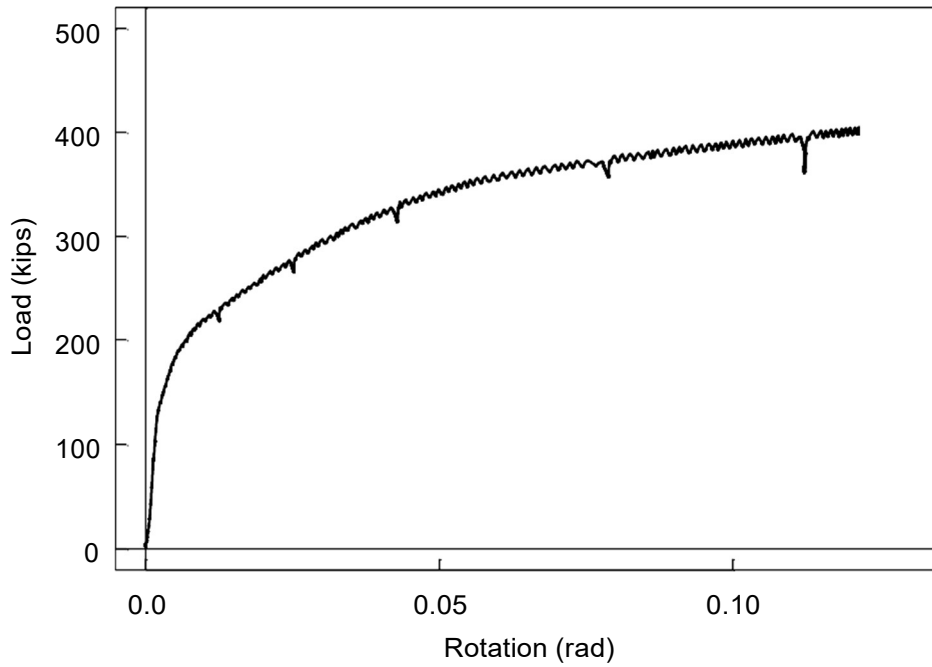


(b) Failure Mode

Figure 2.33 Specimen B4: Deformed Shape

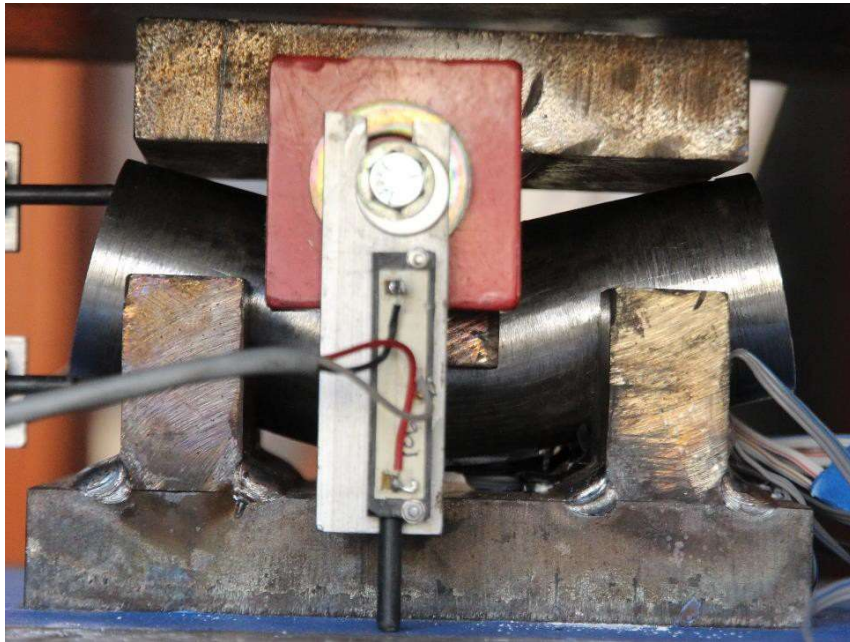


(a) Applied Load versus Deflection



(b) Applied Load versus End Rotation

Figure 2.34 Specimen B4: Global Response

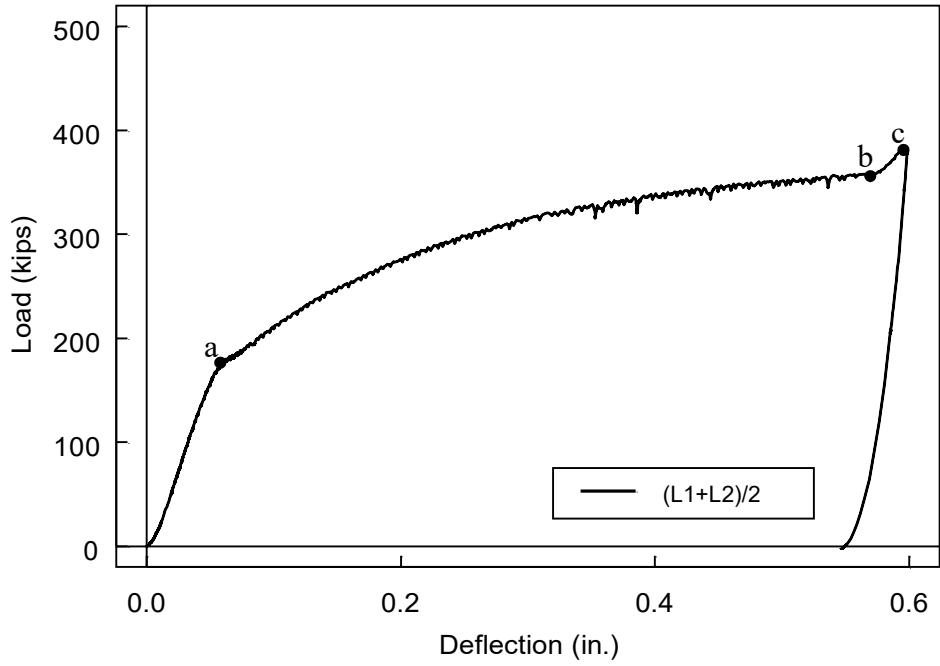


(a) End of Test

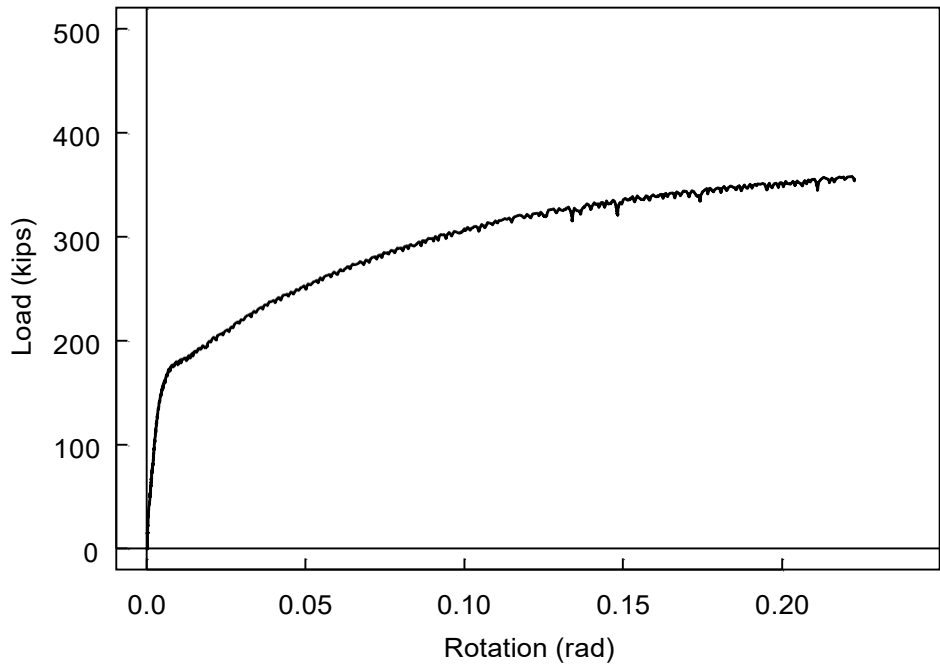


(b) Failure Mode

Figure 2.35 Specimen B5: Deformed Shape



(a) Applied Load versus Deflection



(b) Applied Load versus End Rotation

Figure 2.36 Specimen B5: Global Response

2.4 Analysis of Test Results

2.4.1 Comparison of Test Results

Figure 2.37 summarizes the failure mode of all 12 specimens. The load versus midspan deflection relationships are summarized in Figure 2.38, where the deflection is based on the average of measurements of L1 and L2. The ultimate loads achieved in the test specimens are summarized in Table 2.4. Assuming that the current design practice of treating the pin as a beam is valid, moment and shear at Section B (see Figure 2.7) for each specimen are computed and summarized in Table 2.4. Figure 2.39 and Figure 2.40 show the normalized shear versus deflection relationships, where the plastic shear strengths based on the measured yield stress and tensile strength, respectively, were used for normalization:

$$V_{py} = \frac{\pi D^2}{4} (0.58 F_y) \quad (2.6a)$$

$$V_{pu} = \frac{\pi D^2}{4} (0.58 F_u) \quad (2.6b)$$

Figure 2.40 shows that the maximum shear achieved in all but Specimen A7 and B5 can be approximated by V_{pu} . Specimen A7 and B5, which were pins with the largest span in Series A and B, respectively, did not reach V_{pu} due to the dominating flexural effect. Similarly, Figure 2.41 and Figure 2.42 show the normalized moment versus deflection relationships, where the plastic moment based on the measured yield stress and tensile strength, respectively, were used for normalization:

$$M_{py} = \frac{D^3}{6} (F_y) \quad (2.7a)$$

$$M_{pu} = \frac{D^3}{6} (F_u) \quad (2.7b)$$

Figure 2.42 shows that the maximum moment in all expect Specimens A7 and B5 was significantly below M_{pu} . Specimens A7 and B5 exceeded M_{pu} by at least 20%. Since M_{pu} is the upper-bound flexural strength that cannot be exceeded, it implies that the current design practice to treat the pin as a beam appears flawed. It is hypothesized that it occurs because of an arching-like behavior that develops in the pin.

2.4.2 Comparison of Test Results for Serviceability

The peak strength achieved in each pin represents the ultimate strength, which is associated with large deformations associated with the flexural and shearing deformations and pin plate penetration. Since these deformations would result in the pin losing its ability to function as a pin, it is desirable to establish a pin strength for serviceability considerations which preserves its function. Criteria for serviceability can be in the form of deformation or strain level. For the former, it appears that there is no consensus-based criteria like those for beam or girder design. Before such a criterion can be established, the latter is used herein. Based on the recorded midspan strain at the bottom surface (strain gage S5 in Figure 2.11), strengths at one, two and three times the yield strain are identified as shown in Figure 2.43 and summarized in Figure 2.44 and Table 2.5. This information will be used in Chapter 5 to establish a predictive strength equation for serviceability design.

2.4.3 Comparison of Test Results with AASHTO Specifications

Based on the values in Table 2.4, Figure 2.45 shows the distribution of ultimate strengths of all specimens in the moment-shear domain. For each data point, moment and shear are computed at Section B as defined Figure 2.7 by assuming that simple beam theory applies to the pin. In Figure 2.45(a), the moment and shear have been normalized by M_{py} and V_{py} , respectively, based on the measured yield stresses. The figure shows that the AASHTO moment-shear interaction surface is very conservative and cannot capture the distribution pattern indicated by the test data. The normalization has also been made by M_{pu} and V_{pu} with the measured tensile strengths of the pins, Figure 2.45(b) shows that the test data are more clustered when normalized by the ultimate strength of the steel. But the correlation to the AASHTO equation, where M_p and V_p in Eq. (2.3) are based on the measured tensile strength, is not satisfactory. In particular, Specimens A7 and B5 that were pins with the longest span in each series and were thought to be more like beams, deviate further away from the AASHTO interaction surface.

Table 2.4 Summary of Test Results at Ultimate Strength

Specimen No.	F_y^a (ksi)	F_u^b (ksi)	P_{max} (kips)	a (in.)	b (in.)	L (in.)	M_B (kip-in.)	V_B (kips)	$\frac{M_B}{M_{py}}$	$\frac{V_B}{V_{py}}$	$\frac{M_B}{M_{pu}}$	$\frac{V_B}{V_{pu}}$
A1	81.9	88.0	318.1	0.80	0.100	1.00	15.90	159.04	0.15	1.07	0.14	1.00
A2	81.9	88.0	318.6	0.83	0.085	1.00	13.54	159.30	0.12	1.07	0.12	1.00
A3	81.9	88.0	323.9	0.87	0.065	1.00	10.53	161.95	0.10	1.09	0.09	1.01
A4	81.9	88.0	338.0	1.00	0.125	1.25	21.13	169.00	0.19	1.14	0.18	1.06
A5	81.9	88.0	319.6	1.00	0.250	1.50	39.95	159.80	0.37	1.08	0.34	1.00
A6	81.9	88.0	313.8	1.00	0.375	1.75	58.84	156.90	0.54	1.06	0.50	0.98
A7	81.9	88.0	246.7	0.80	1.350	3.50	166.52	123.35	1.52	0.83	1.42	0.77
B1	76.2	116.6	449.6	0.91	0.045	1.00	10.12	224.80	0.10	1.63	0.07	1.06
B2	76.2	116.6	469.3	0.91	0.045	1.00	10.56	234.65	0.10	1.70	0.07	1.11
B3	76.2	116.6	460.8	0.80	0.163	1.13	37.44	230.40	0.37	1.67	0.24	1.09
B4	76.2	116.6	420.3	1.00	0.500	2.00	105.08	210.15	1.03	1.52	0.68	0.99
B5	76.2	116.6	357.7	1.00	1.000	3.00	178.85	178.85	1.76	1.29	1.15	0.85

^a Yield strength from coupon test.

^b Tensile strength from coupon test.

^c For Series A specimens, $V_{py} = 148.6$ kips and $M_{py} = 109.2$ kips.

For Series B specimens, $V_{py} = 138.2$ kips and $M_{py} = 101.6$ kips.

Table 2.5 Strengths at ϵ_y , $2\epsilon_y$, and $3\epsilon_y$

Specimen No.	P_{ϵ_y} (kips)	$P_{2\epsilon_y}$ (kips)	$P_{3\epsilon_y}$ (kips)
A1	237.8	280.9	301.8
A2	226.1	281.3	303.1
A3	192.1	247.0	282.2
A4	173.7	215.6	246.2
A5	210.8	239.0	261.1
A6	176.5	217.3	238.2
A7	85.1	118.4	132.6
B1	235.4	293.9	327.6
B2	223.8	260.5	283.8
B3	209.3	248.2	281.3
B4	147.2	195.3	209.2
B5	107.3	157.0	176.4

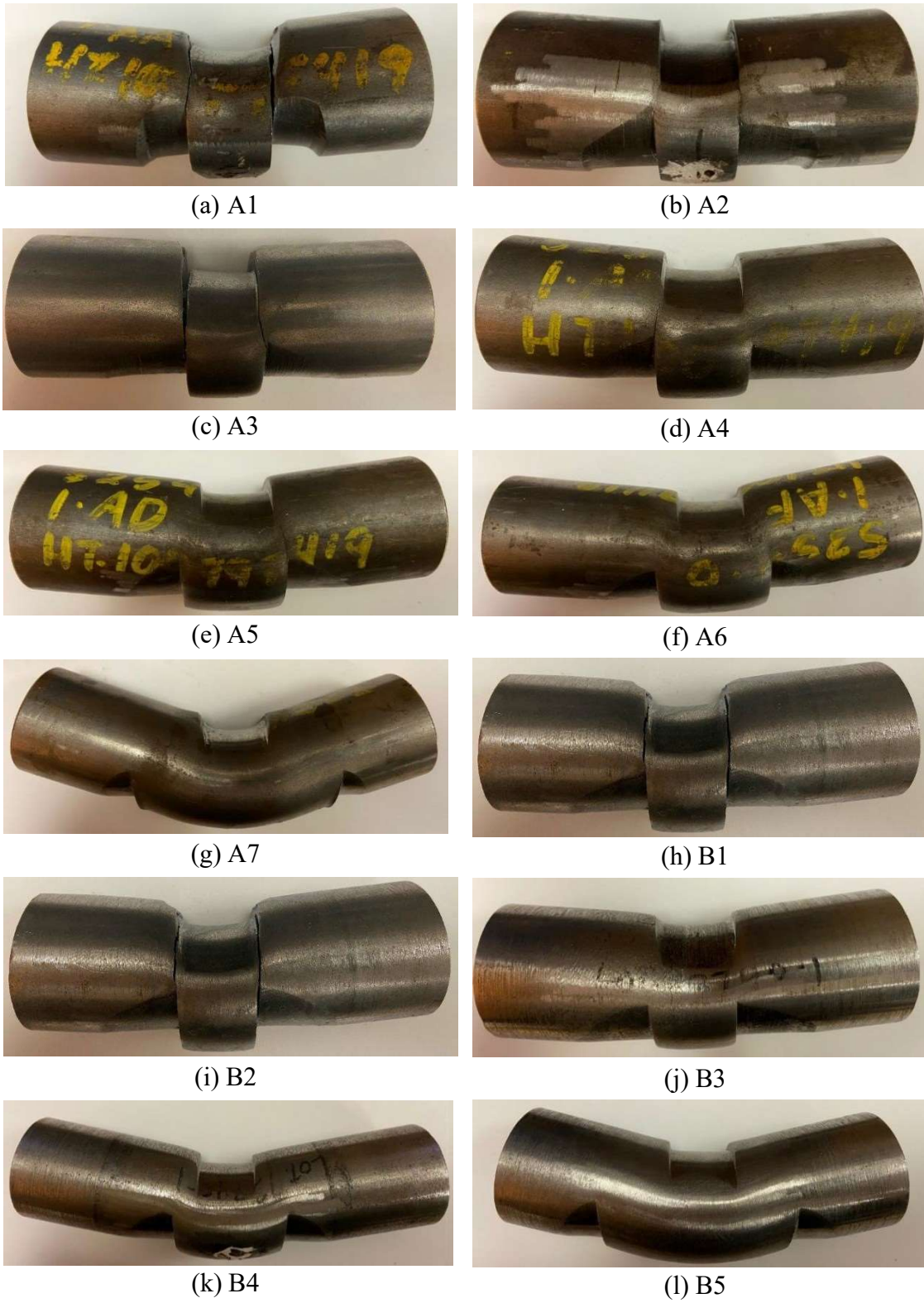


Figure 2.37 Failure Mode

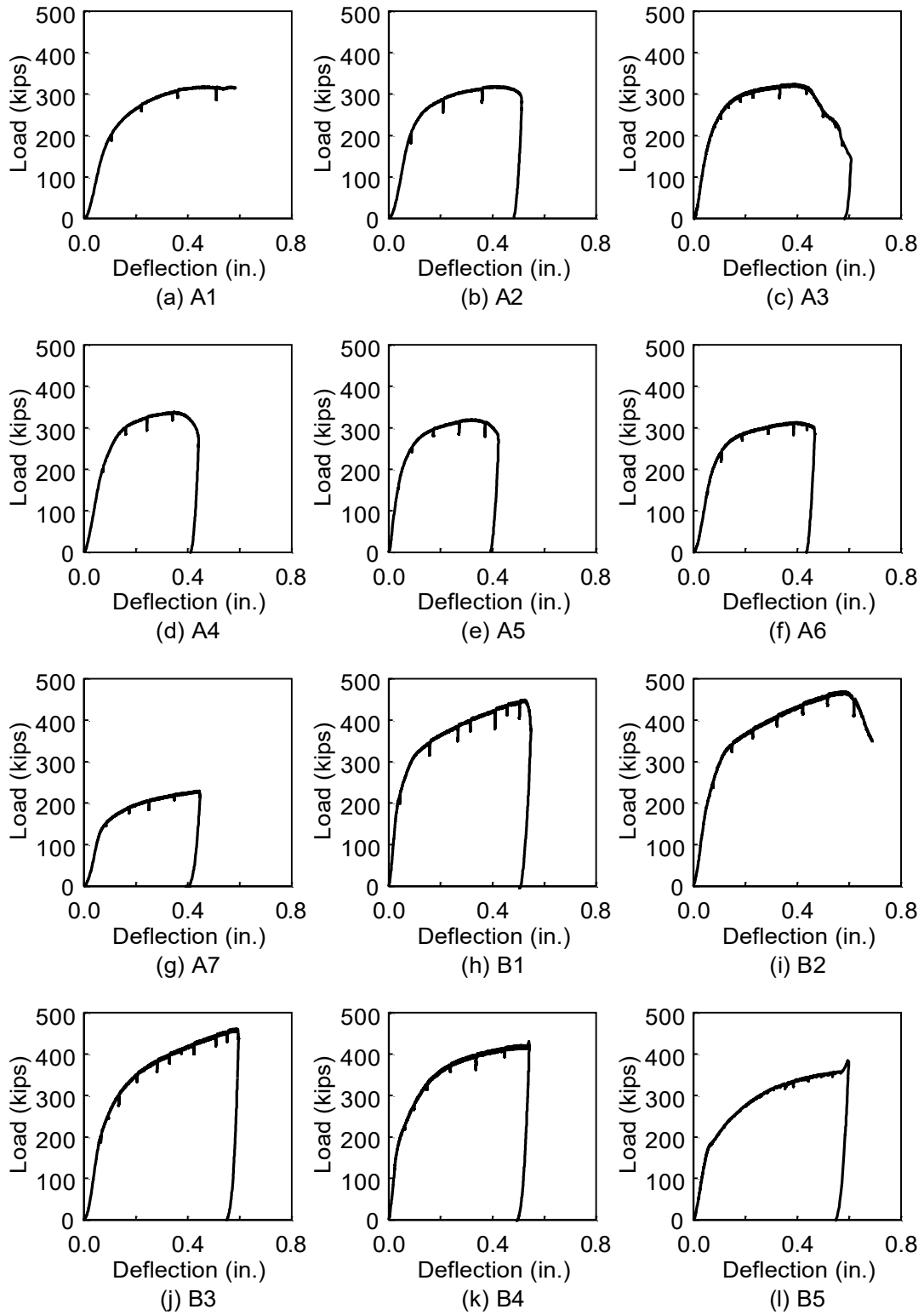


Figure 2.38 Summary of Global Response

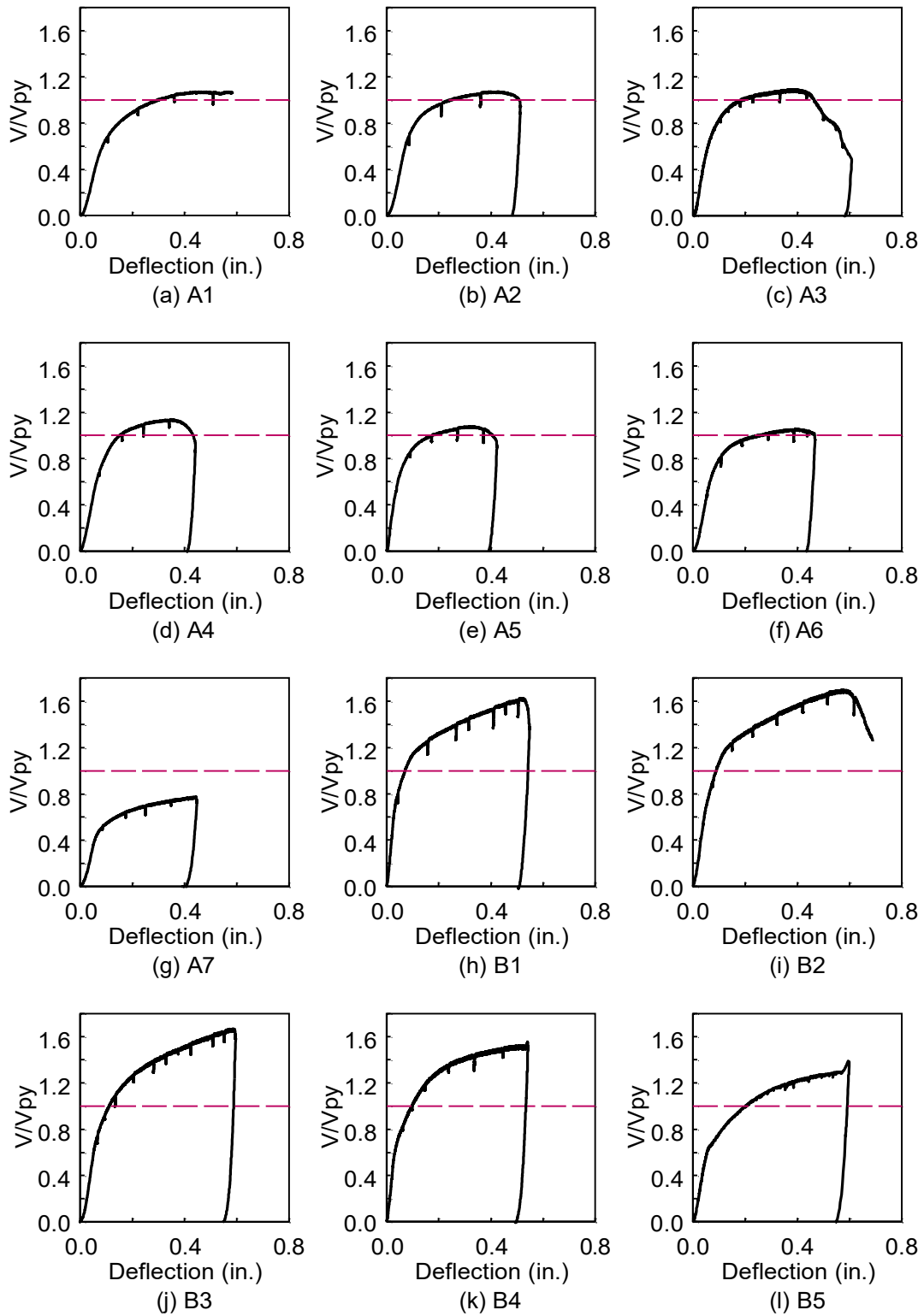


Figure 2.39 Summary of Normalized Shear versus Midspan Deflection Relationship
(Normalization Based on Measured Yield Stress)

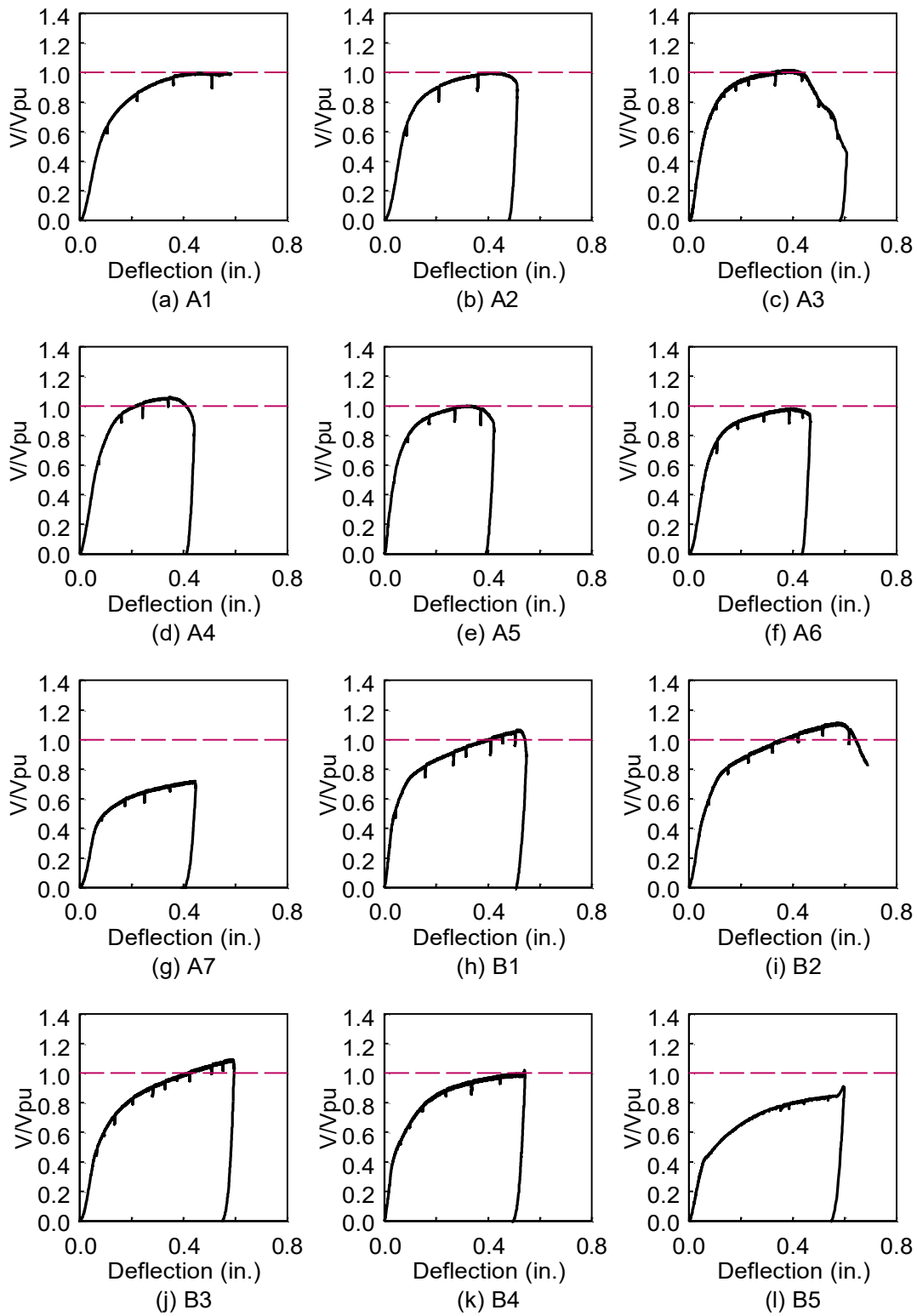


Figure 2.40 Summary of Normalized Shear versus Midspan Deflection Relationship
(Normalization Based on Measured Tensile Strength)

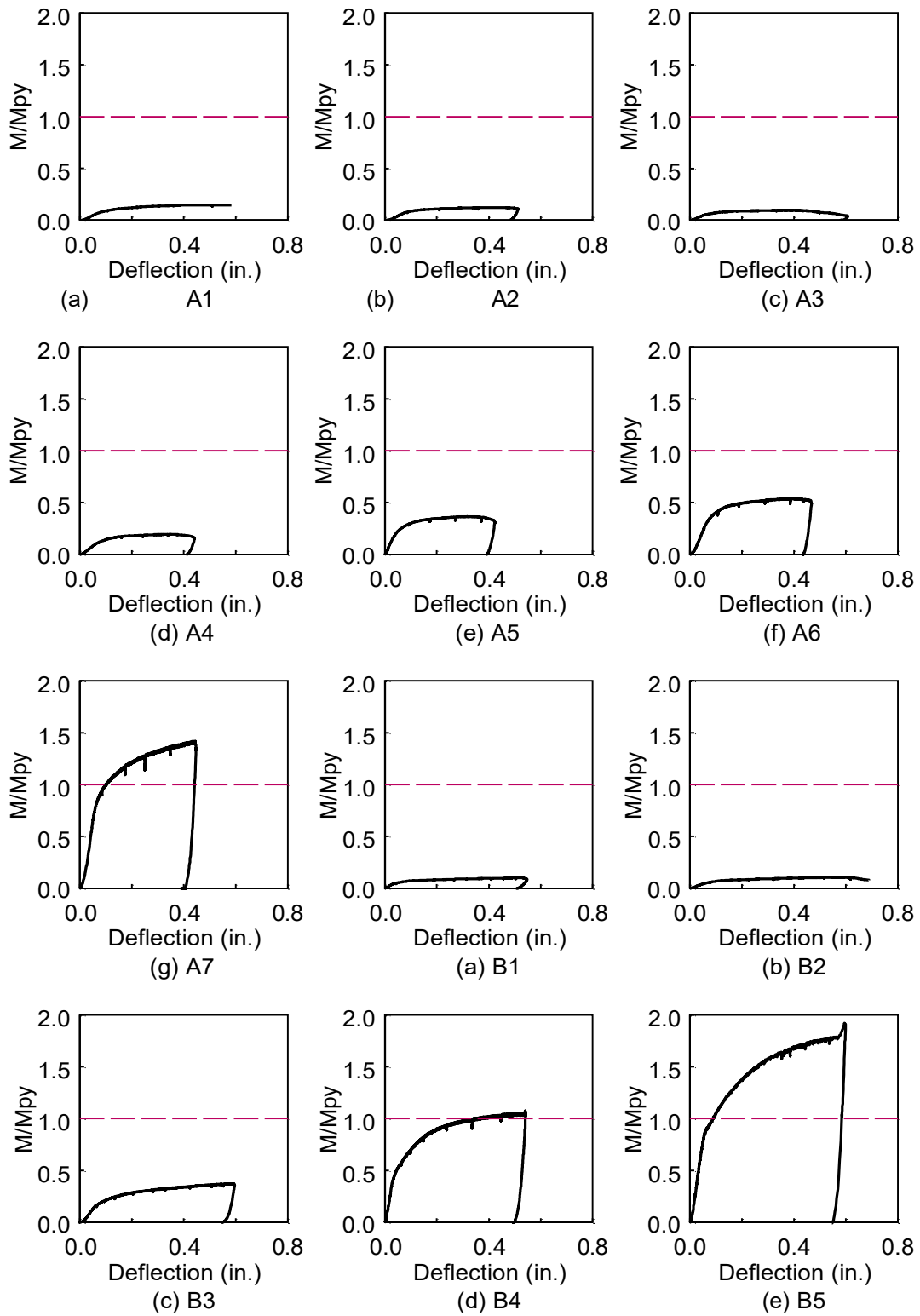


Figure 2.41 Summary of Normalized Moment versus Midspan Deflection Relationship (Normalization Based on Measured Yield Stress)

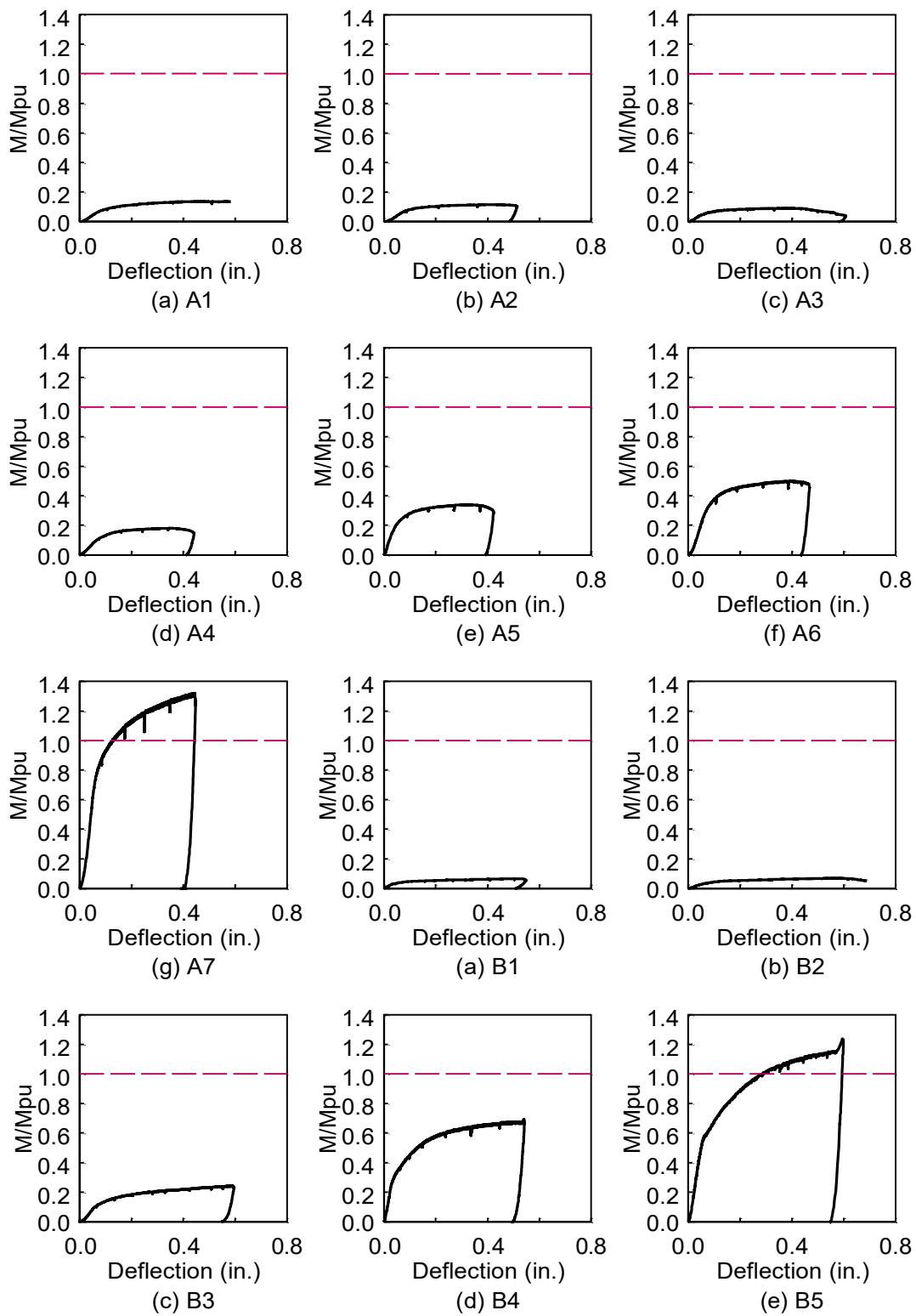


Figure 2.42 Summary of Normalized Moment versus Midspan Deflection Relationship
(Normalization Based on Measured Tensile Strength)

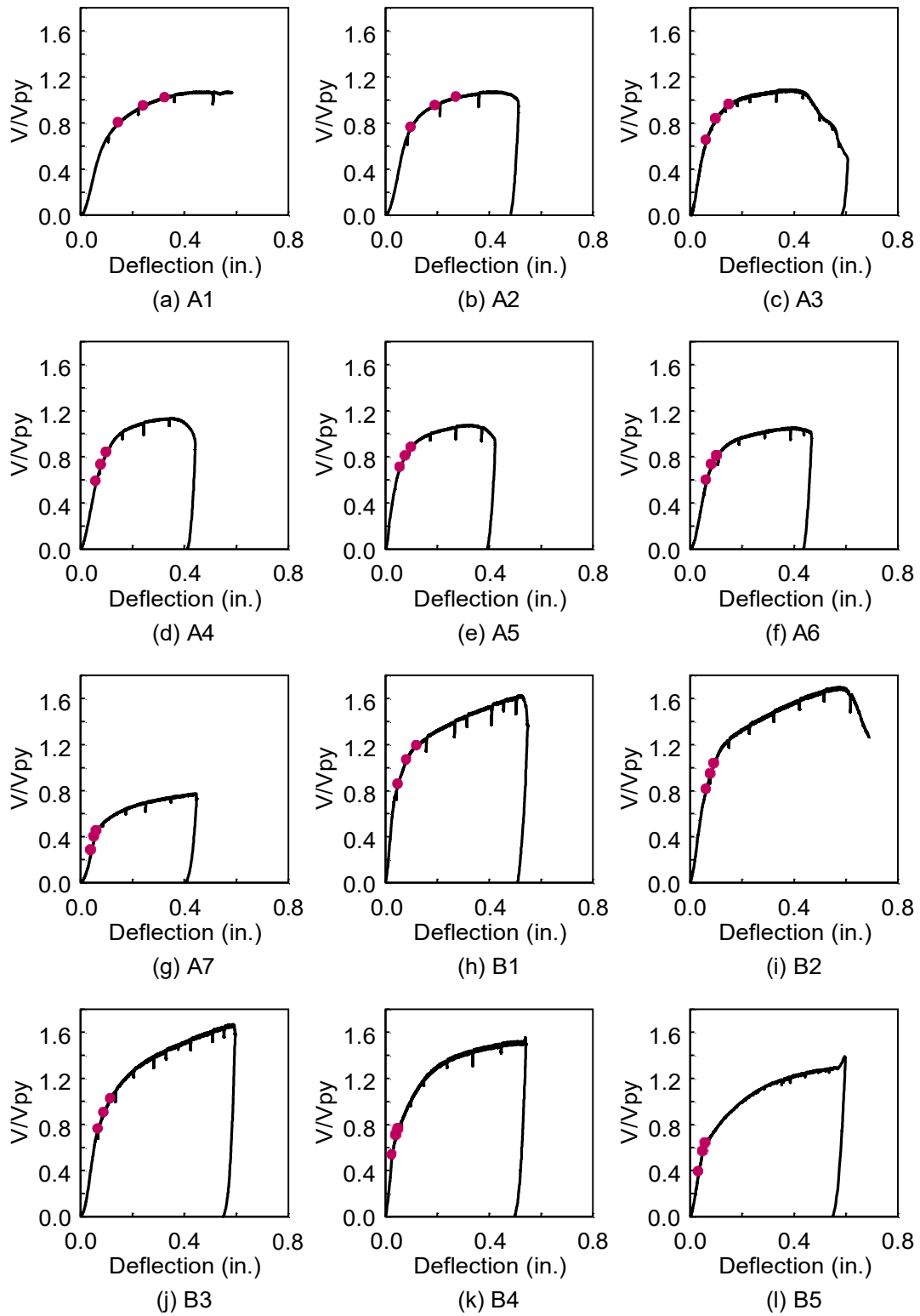


Figure 2.43 Normalized Shear versus Midspan Deflection with Events at ϵ_y , $2\epsilon_y$ and $3\epsilon_y$

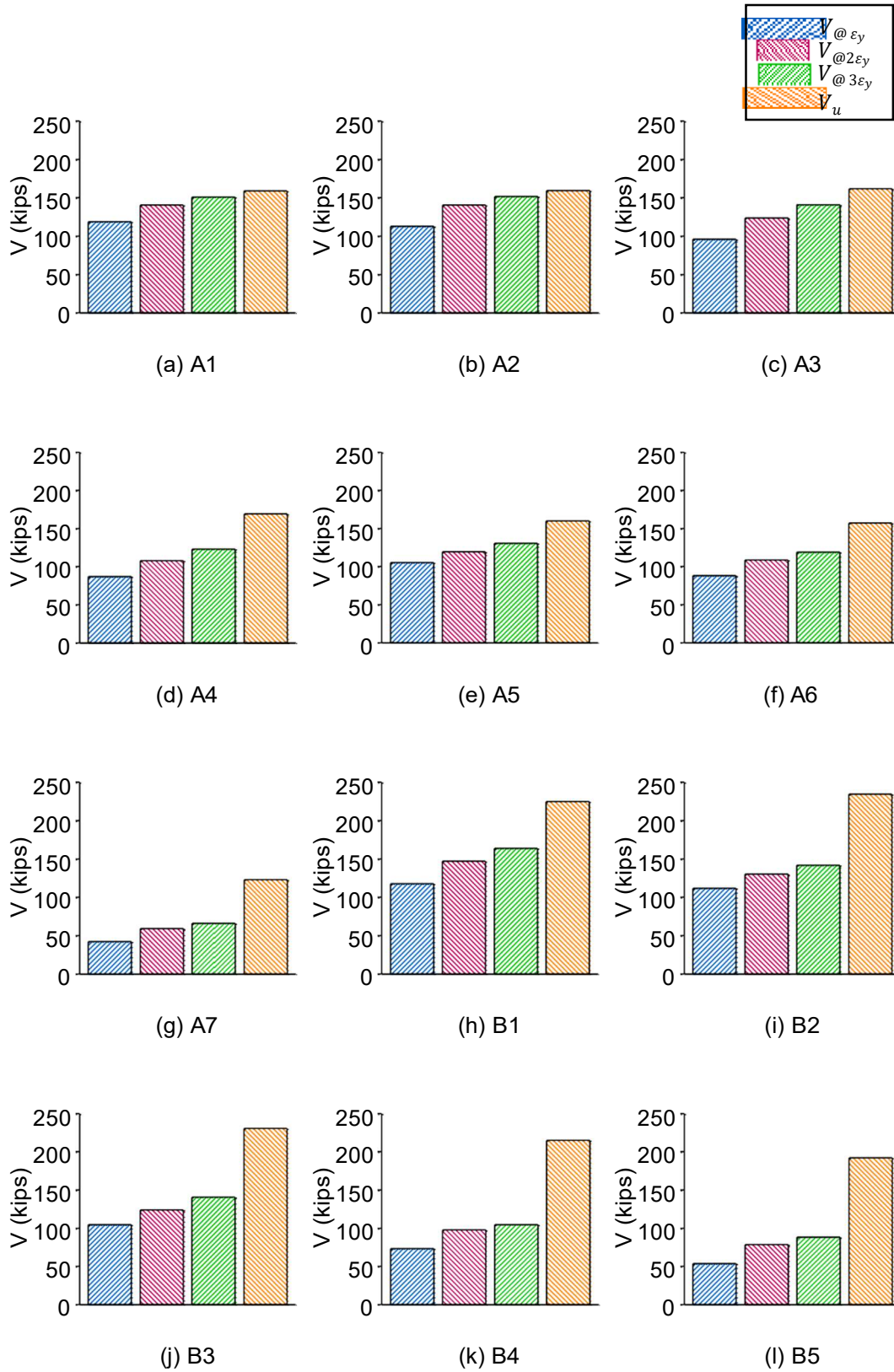
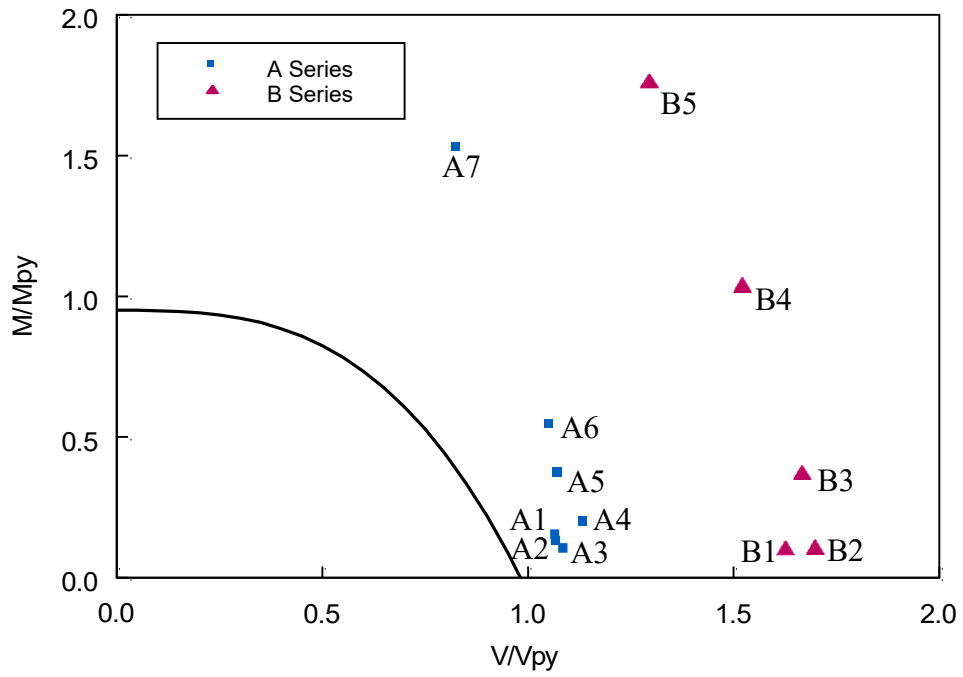
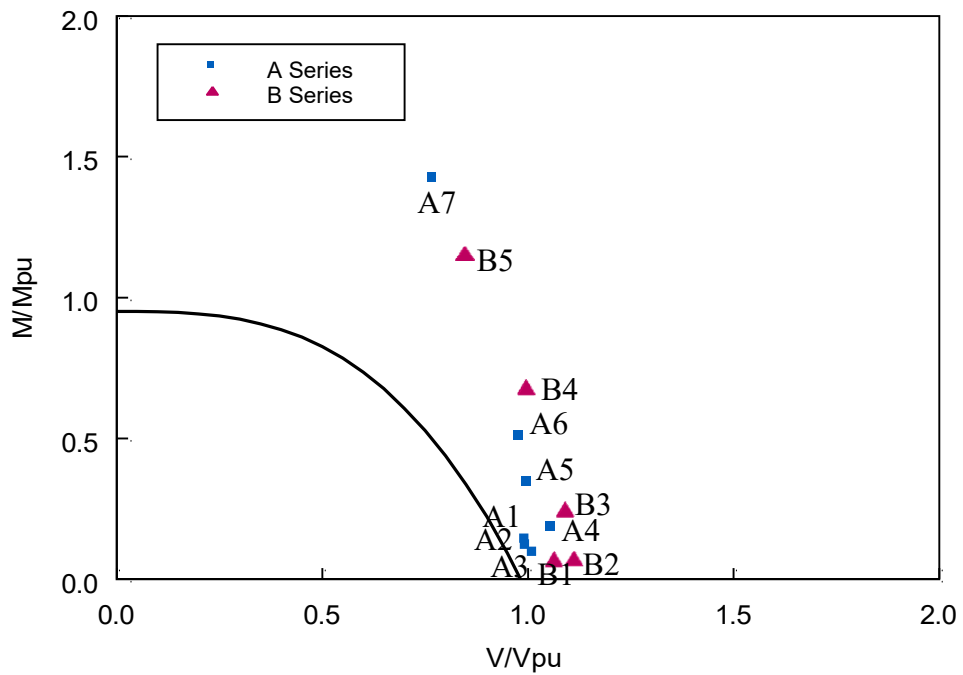


Figure 2.44 Summary of Pin Shear Strength at Different Limit States



(a) Based on Yield Stress



(b) Based on Tensile Strength

Figure 2.45 Comparison of Pin Test Data with AASHTO Moment-Shear Interaction Curve

2.5 FINITE ELEMENT ANALYSIS

2.5.1 General

This chapter presents results from finite element analysis (FEA) of steel pins. FEA was performed using the commercial finite element analysis software package, ABAQUS (2014). Results from FEA were used to correlate the measured responses of the 2-in. pin specimens. Using the same modeling technique, additional models were constructed and analyzed to fill gaps in the moment-shear domain that was not investigated in the test program. To generalize the findings from 2-in. pins, additional analyses were also conducted on 1-in. and 4-in. diameter pins.

2.5.2 Finite Element Models

Figure 2.46(a) shows the typical finite element model. Standard 3-D solid eight-node linear brick elements with reduced integration (C3D8R) were used to model all 12 steel pin specimens including the loading and supporting cradles. For example, Figure 2.46(a) is the model for Specimen B1. The numbers of brick elements are 21,879, 4,195, and 5,587 for the pin, loading cradle, and support cradle, respectively. Surface-to-surface interaction techniques were used to connect the surfaces between the pin and cradles [Figure 2.46(b)]. To implement a proper contact modeling, a penalty method was used; this method approximates hard pressure-overclosure behavior. This study assumed a linear penalty method, i.e., the amount of penetration is linearly proportional to the contact pressure for an assumed stiffness:

$$f_p = k \cdot \delta \quad (2.8)$$

where f_p is the contact pressure, k is the penalty stiffness, and δ is the penetration when the contact occurs between the contacting bodies.

When two surfaces are in contact, they usually transmit shear (or friction) as well as normal forces across the interface. The Coulomb model of friction with an assumed coefficient of friction, μ , is used. The tangential motion is zero until the surface traction reaches a critical shear stress value:

$$\tau_{crit} = \mu \cdot f_p \quad (2.9)$$

Boundary conditions for the models simulated the experimental test setup. The load was applied monotonically to the top surface of the loading cradle in a displacement-control mode.

2.5.3 Material Stress-Strain Characteristics

The steel properties (modulus of elasticity of 29,000 ksi and Poisson's ratio of 0.3) were used to describe the elastic material characteristics, while the yield stress and plastic strain extracted from the tensile coupon test results were used to define the plastic behavior. Since ABAQUS requires the user to input true plastic stress and strain (σ_T and ε_T), the engineering stress and strain (σ and ε) measured from the tensile coupon tests were converted to the true stress and strain as follows:

$$\sigma_T = \sigma(1 + \varepsilon) \quad (2.10)$$

$$\varepsilon_T = \ln(1 + \varepsilon) \quad (2.11)$$

Figure 2.47 shows the true stress-strain relationships of steels.

2.5.4 Calibration of Finite Element Models

As was mentioned in Section 4.2 that two parameters (k and μ) need to be assumed to model the penetration phenomenon. A series of analyses were first conducted so that consistent values could be used in the correlation study. Consider Specimen B1 for example. Figure 2.48 shows the sensitivity study. It is observed from Figure 2.48(a) that the value of penalty stiffness, k , has a significant effect on the initial stiffness, but not the ultimate strength of the global response. Conversely, the ultimate strength is affected by the coefficient of friction, μ . Based on this observation, it was possible to select a pair of k and μ values to optimize the correlation to the test data. But it was then decided to select a pair of k and μ for each test series. These values are provided in Table 2.6.

2.5.5 Correlation between Test Results and FEA

Based on the assumed k and μ values in Table 2.6, a correlation of the predicted and measured responses of each pin specimen is provided in Figure 2.49; a correlation of the deformed shapes is summarized in Figure 2.50. Overall, the correlation is satisfactory. Table 2.7 summarizes the ultimate strengths for both tests and FEA analyses. The prediction-to-test ratio has a mean value of 1.0 and a standard deviation of 0.03.

2.5.6 Simulated Results to Supplement Test Database ($D = 2$ in.)

Assuming that the beam theory is valid, the distribution of the test data in the moment-shear domain was presented in Figure 2.45. Note that that the experimental database did not include specimens with V/V_{py} less than, say, 0.5. Pins in this range usually are long and the gap (i.e., dimension b in Figure 2.7) is large. To fill this gap, Series C models with 22 simulated pins that covered a much wider range in the moment-shear domain were constructed and analyzed; see Table 2.8 for the dimensions of these 2-in. pin models. The same steel material properties as those of Series B specimens were assumed.

Figure 2.51 shows the deformed shapes of selected pin models. Note that models like C22 do behave like beams due to the large span/depth ratios. Figure 2.52 shows the simulated results in the moment-shear domain. Presenting the results in the moment-shear domains requires that moment and shear be computed, which in turn implies beam theory is valid. Following the current design practice, moment and shear were thus computed at Section B (see Figure 2.11) based on the predicted ultimate load. [Note in current design practice that all sections along the pin span need to be checked; see Figure 2.8 for the design of pin specimens.] Referring to Figure 2.52(b), where the moment and shear have been normalized by M_{pu} and V_{pu} , the simulated results show a clear trend. Each data point in the figure is associated with a gap-to-diameter ratio (b/D , where b is defined in Figure 2.7). Several observations can be made. First, the observed “yield surface” from the simulated data can be divided into two branches: the ascending branch ($b/D > 1.0$) and descending branch ($b/D \leq 1.0$). These two branches can be separated by $b/D = 1.0$. Test data from Series A and B specimens are also shown in the figure, these test data fall in the descending branch. Comparing to the simulated results, the second observation is that test data, in the normalized form with respect to the ultimate strength of the steel, not the yield stress as shown in Figure 2.52(a), do show a trend consistent to finite element simulation. The third observation is related to the ascending branch. For a long beam to behave like a beam, the maximum moment that can theoretically develop is M_{pu} . Extrapolating the simulated data in this branch to zero shear does show that the trend line will converge to $M/M_{pu} = 1.0$. These observations justify the observed yield surface in the complete moment-shear interaction domain.

2.5.7 Simulated Results of Pins with $D = 1$ in. and $D = 4$ in.

All the test and FEA results presented so far are for 2-in. diameter pins. To confirm that the observed yield surface also applies to other diameters, additional pin models (see Table 2.9 and Table 2.10) with both 1-in. and 4-in. diameters were constructed and analyzed. The results of these Series D and E models are presented in Figure 2.53 to Figure 2.56. These results support the same trend as observed in the 2-in. pin results.

Table 2.6 Contact Parameters for Finite Element Analysis

Series	Contact Stiffness (kips/in. ³)	Friction Coefficient
A (A108 Gr. 1018)	3,500	0.3
B (A668 Class F)	3,500	0.5

Table 2.7 Ultimate Strength Comparison between FEM and Tests

Specimen No.	Ultimate Strength (kips)		$\frac{P_{FEM}}{P_{TEST}}$
	FEM (P_{FEM})	Test (P_{TEST})	
A1	300.9	318.1	0.95
A2	324.5	318.6	1.02
A3	336.3	323.9	1.04
A4	331.4	338.0	0.98
A5	322.8	319.6	1.01
A6	311.3	313.8	0.99
A7	229.1	246.7	0.93
B1	453.7	449.6	1.01
B2	478.2	469.3	1.02
B3	466.1	460.8	1.01
B4	421.3	420.3	1.00
B5	353.5	357.7	0.99

Table 2.8 Matrix of Additional Data of Finite Element Modeling

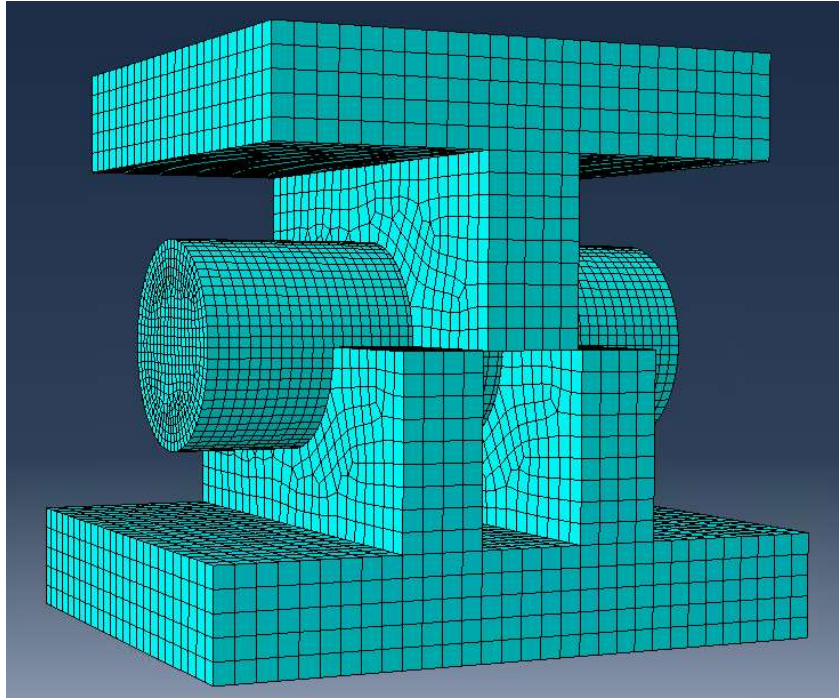
Model No.	a (in.)	b (in.)	$\frac{b}{D}$	L (in.)	Ultimate Strength, P_u (kips)
C1	0.8	0.1	0.05	1.6	457.3
C2	0.8	0.2	0.1	1.6	449.8
C3	0.7	0.3	0.15	1.4	432.3
C4	1	0.4	0.2	2	417
C5	1.2	0.5	0.25	2.4	407
C6	1	0.6	0.3	2	393.6
C7	1.2	0.7	0.35	2.4	382.7
C8	1.4	0.8	0.4	2.8	370.3
C9	1.3	0.9	0.45	2.6	355.4
C10	1.7	1	0.5	3.4	343.6
C11	1.7	1.1	0.55	3.4	324.2
C12	1.6	1.2	0.6	3.2	313
C13	1.8	1.3	0.65	3.6	299.7
C14	2	1.4	0.7	4	283.5
C15	2	1.5	0.75	4	272
C16	2	1.6	0.8	4	258.7
C17	2.5	2	1.0	5	214.6
C18	3	2.5	1.25	6	168.9
C19	3.5	3	1.5	7	135.4
C20	4	3.5	1.75	8	111.9
C21	5	4.5	2.25	10	81.4
C22	6	5.5	2.75	12	62.5

Table 2.9 Matrix of Additional Data of FEM Series D Models ($D = 1.0$ in.)

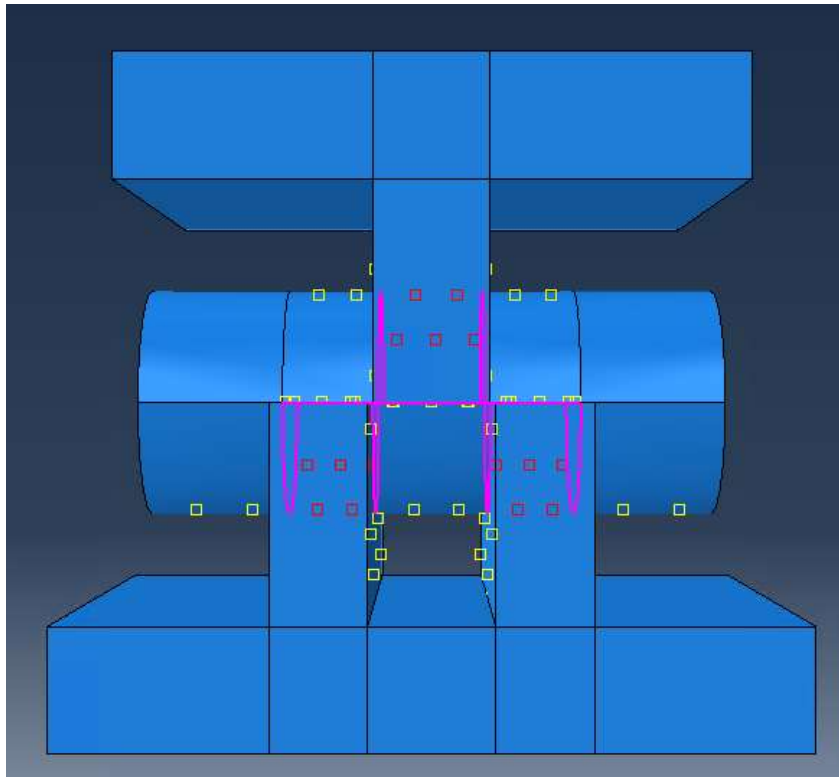
Model No.	a (in.)	b (in.)	$\frac{b}{D}$	L (in.)	Ultimate Strength, P_u (kips)
D1	0.7	0.1	0.1	0.7	124.5
D2	1	0.3	0.3	1	106.7
D3	1.6	0.5	0.5	1.6	87.0
D4	2	0.8	0.8	2	62.0
D5	2.5	1	1	2.5	50.3
D6	2.9	1.2	1.2	2.9	41.5
D7	3.6	1.5	1.5	3.6	31.9
D8	4.1	1.8	1.8	4.1	25.9
D9	4.5	2	2	4.5	23.7
D10	5.5	2.5	2.5	5.5	18.8
D11	6.5	3	3	6.5	15.4

Table 2.10 Matrix of Additional Data of FEM Series E Models ($D = 4.0$ in.)

Model No.	a (in.)	b (in.)	$\frac{b}{D}$	L (in.)	Ultimate Strength, P_u (kips)
E1	0.7	0.5	0.125	1.5	1850.0
E2	1	1	0.25	2.5	1715.0
E3	1.6	2	0.5	4.5	1486.5
E4	2	3	0.75	6.5	1213.2
E5	2.5	4	1	8.5	918.2
E6	2.9	5	1.25	10.5	696.6
E7	3.6	7.5	1.875	15.5	416.5
E8	4.1	10	2.5	20.5	296.6

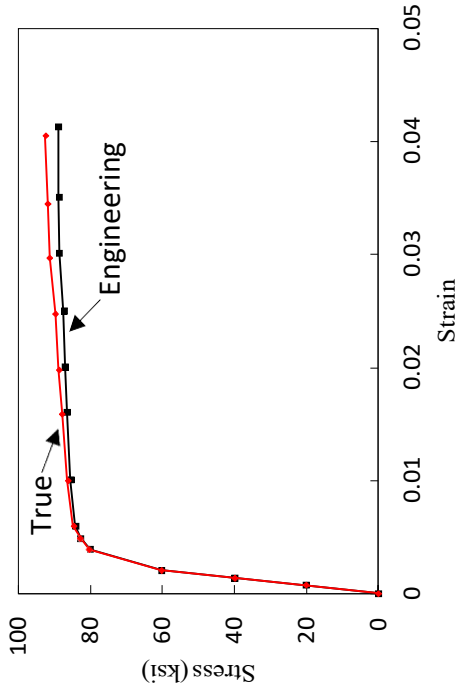


(a) FEA Model

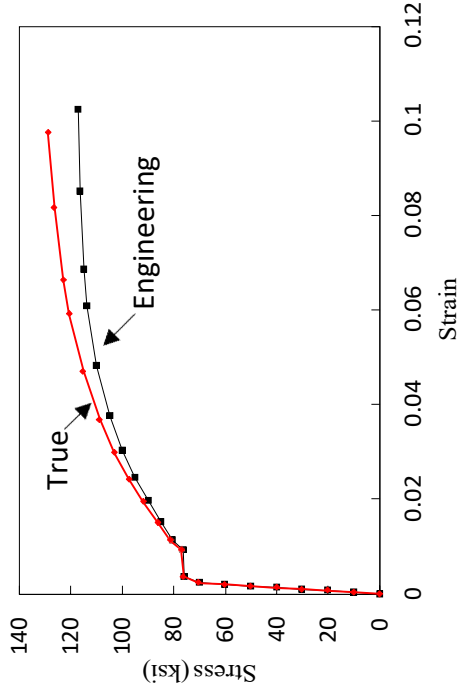


(b) Global View with Surface-to-Surface Contact

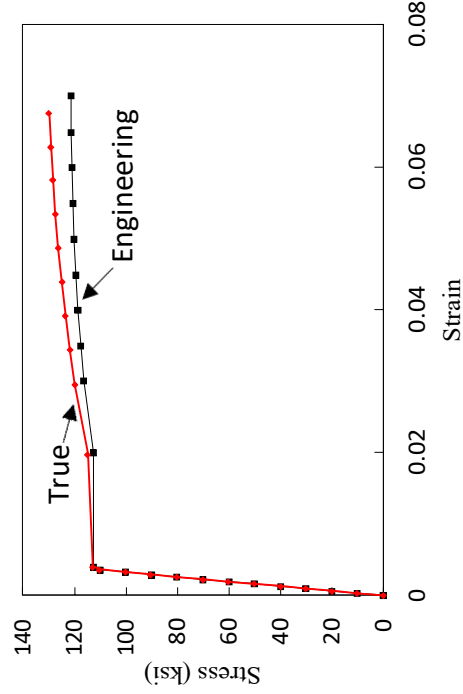
Figure 2.46 Typical Finite Element Model of Pin Test



(a) A108 Gr.1018 Steel

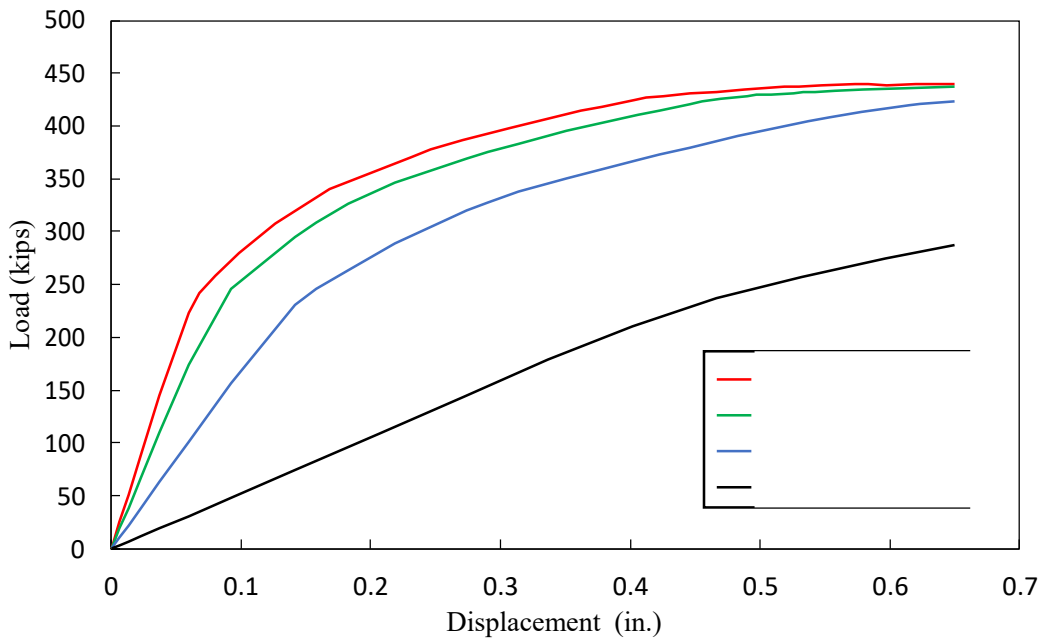


(b) A668 Class F steel

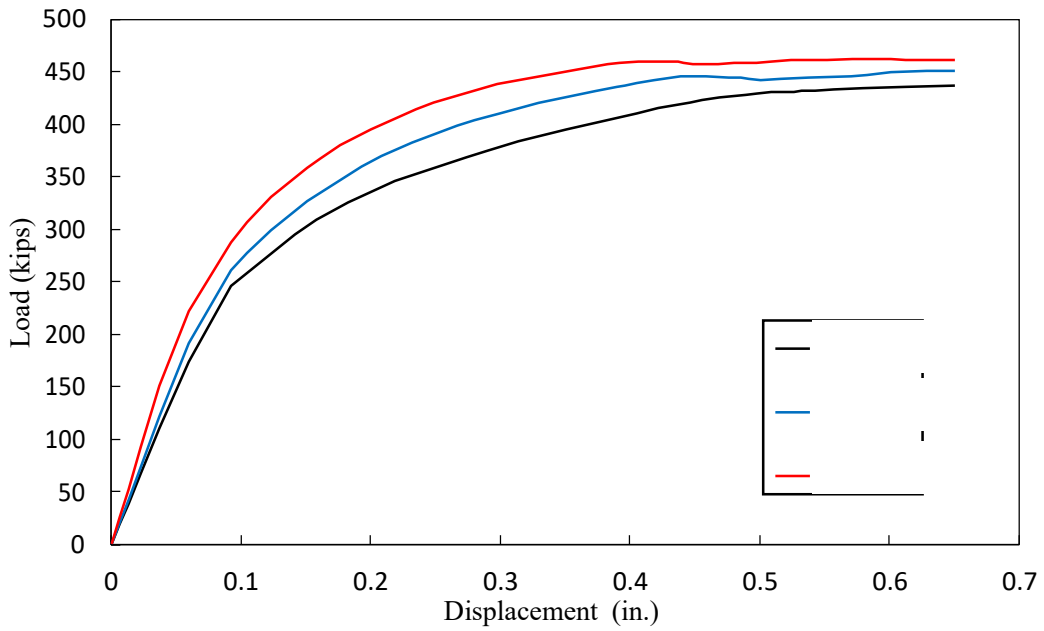


(a) A514 Steel

Figure 2.47 True and Engineering Stress-Strain Relationships

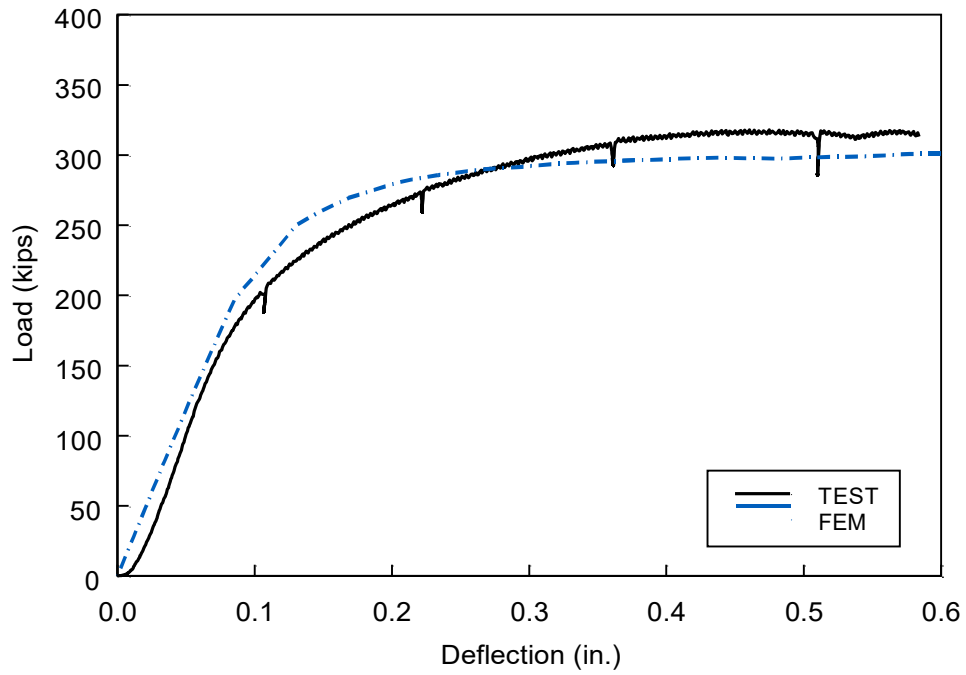


(a) Effect of Contact Stiffness ($\mu = 0.3$)

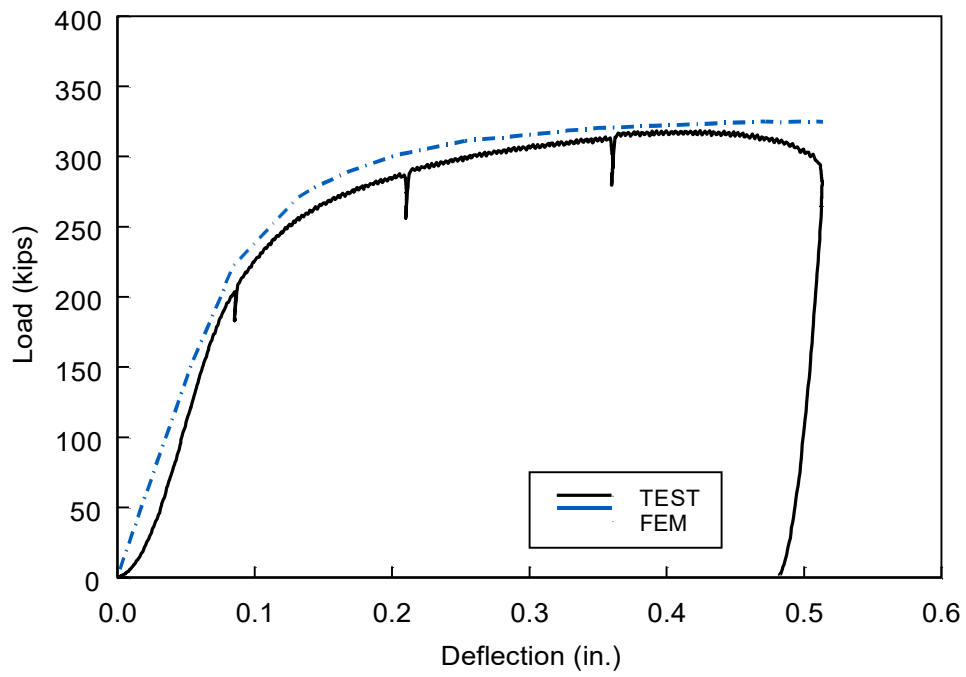


(b) Effect of Friction Coefficient ($k = 3500$ kips/in.³)

Figure 2.48 Sensitive Study

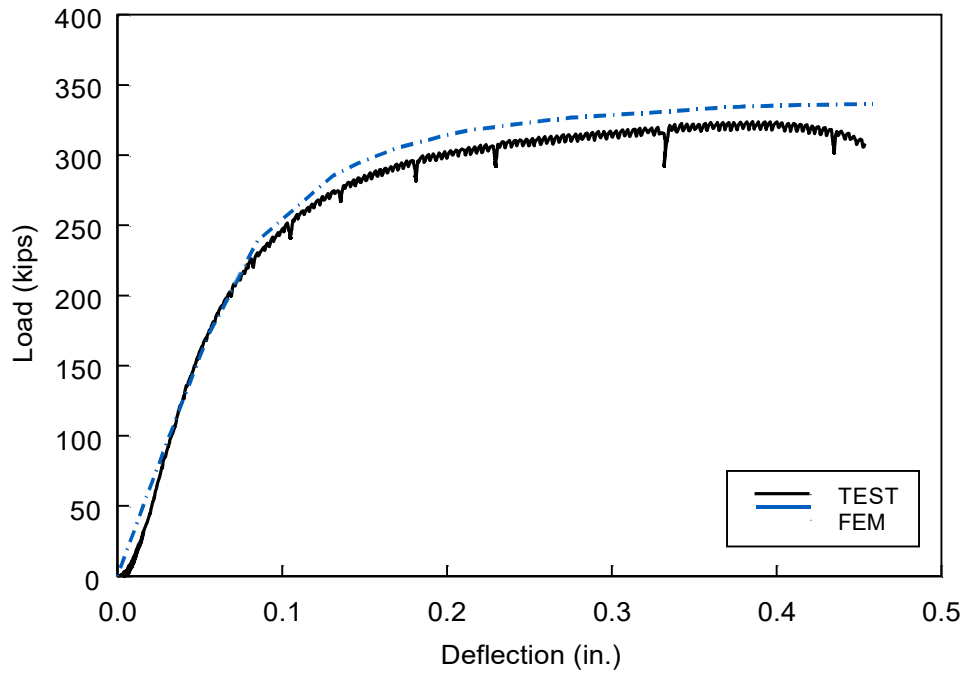


(a) Specimen A1

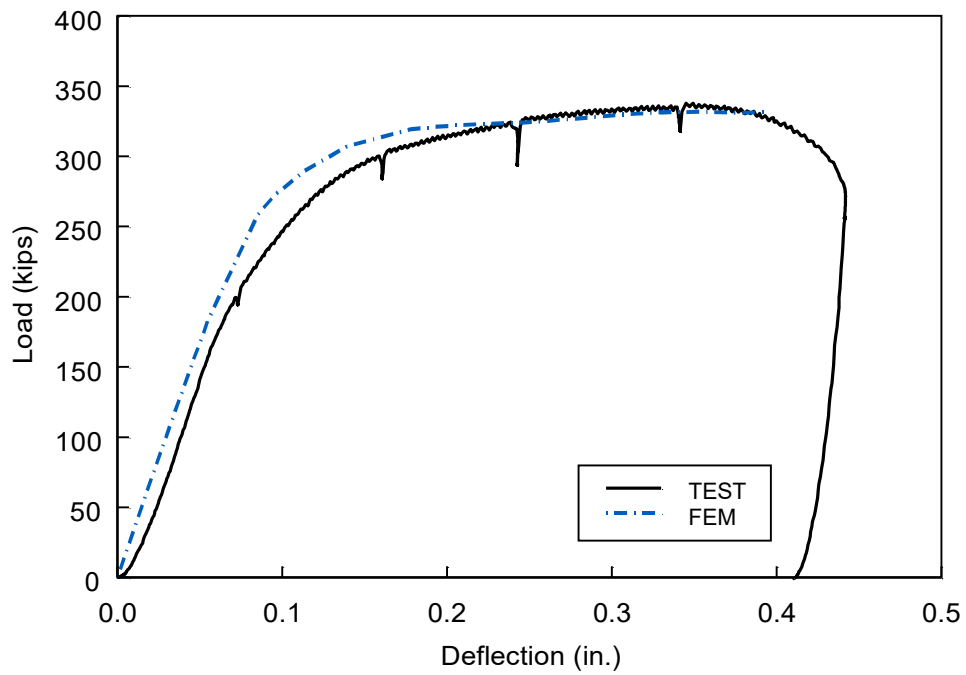


(b) Specimen A2

Figure 2.49 Correlation between Test Results and FEM Analyses

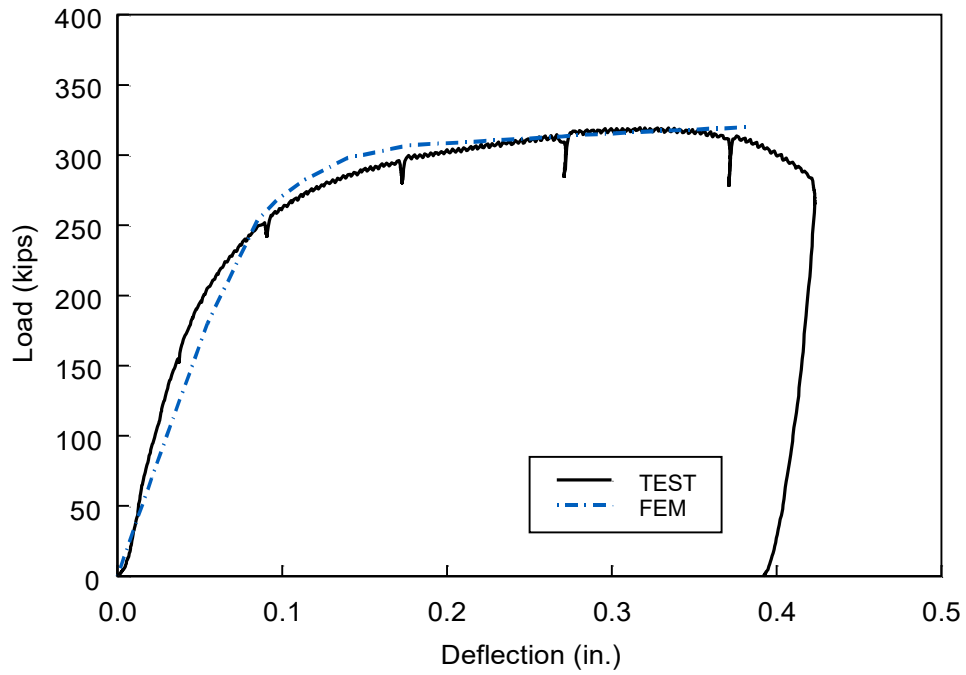


(c) Specimen A3

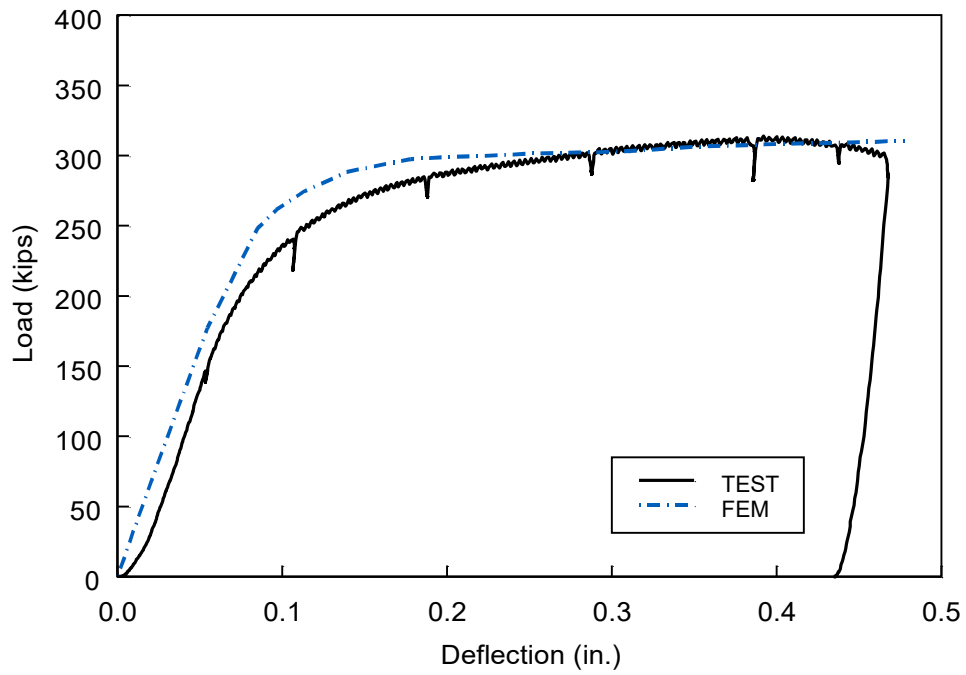


(d) Specimen A4

Figure 2.49 Correlation between Test Results and FEM Analyses (continued)

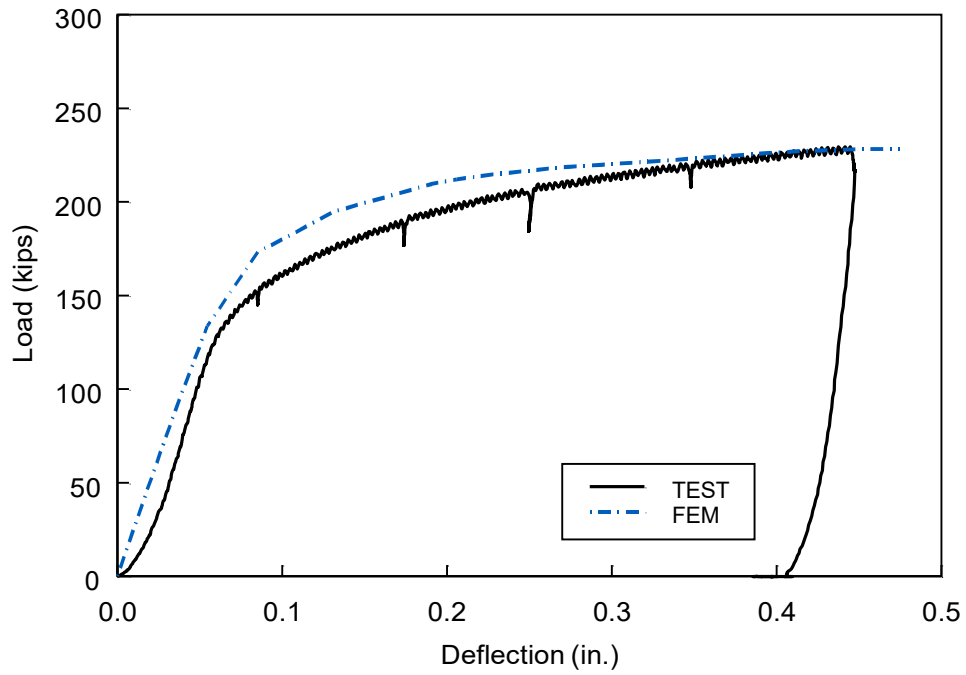


(e) Specimen A5

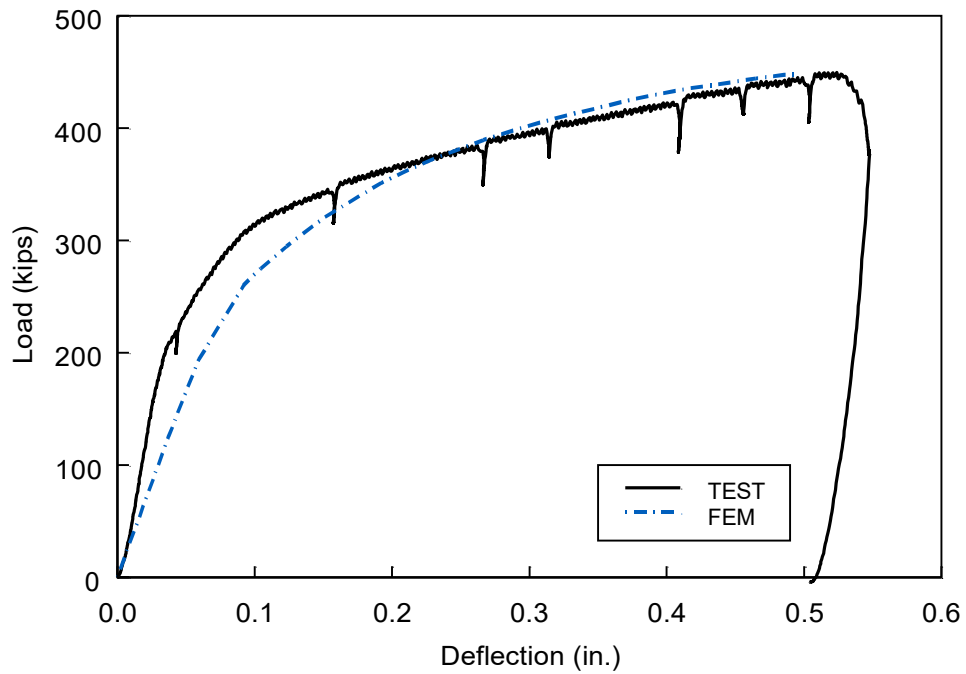


(f) Specimen A6

Figure 2.49 Correlation between Test Results and FEM Analyses (continued)

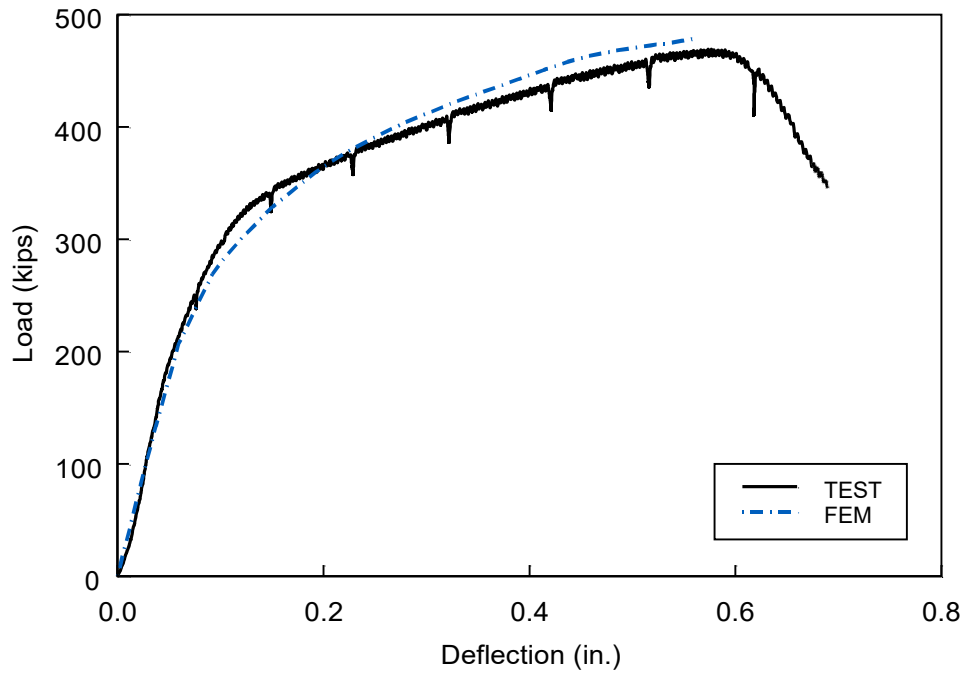


(g) Specimen A7

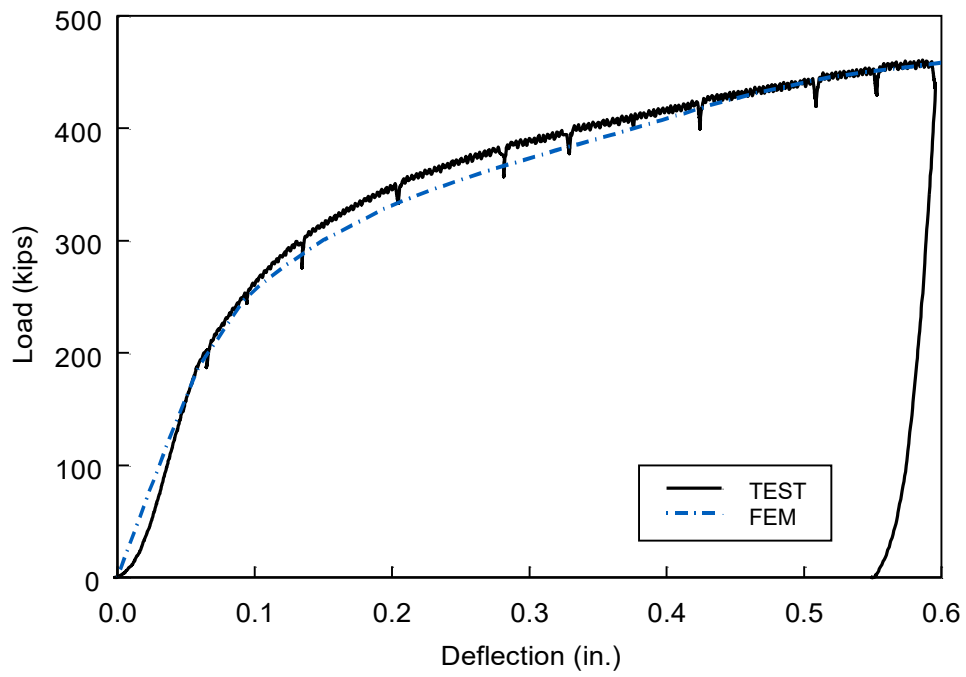


(h) Specimen B1

Figure 2.49 Correlation between Test Results and FEM Analyses (continued)

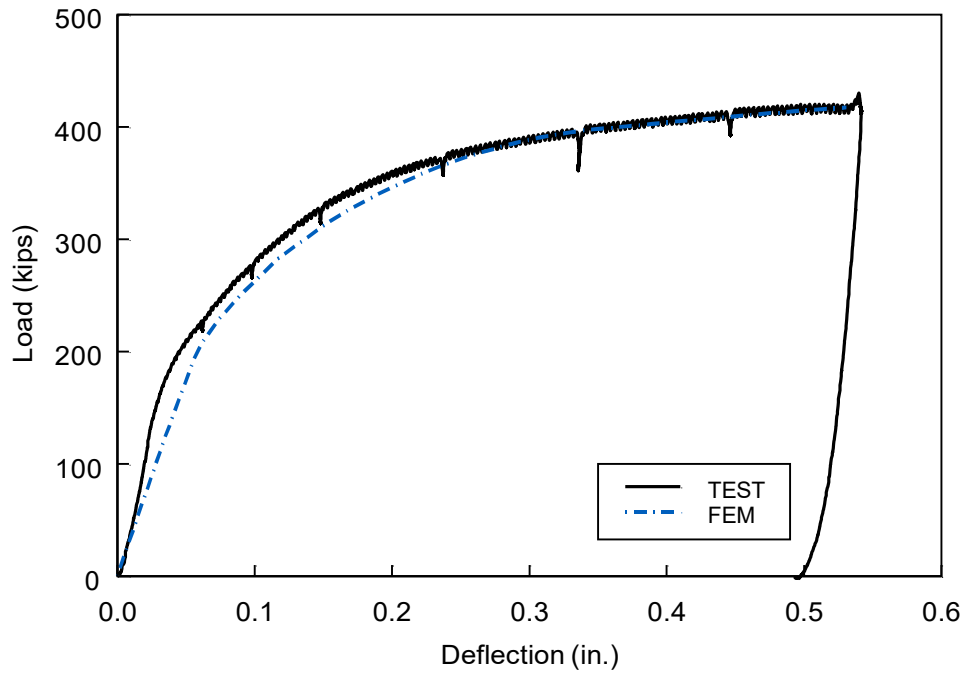


(i) Specimen B2

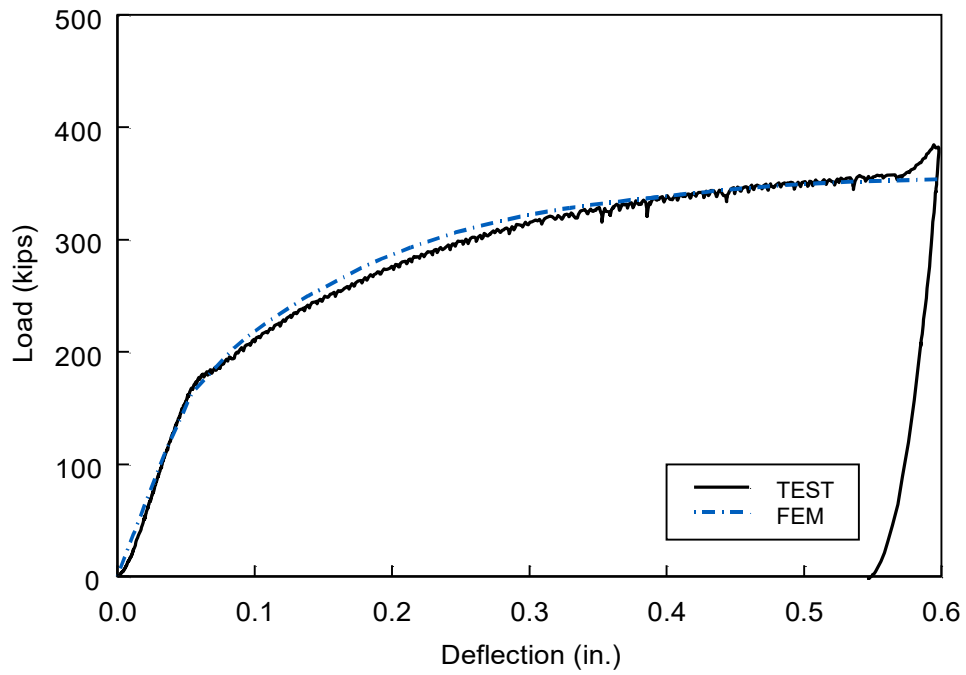


(j) Specimen B3

Figure 2.49 Correlation between Test Results and FEM Analyses (continued)

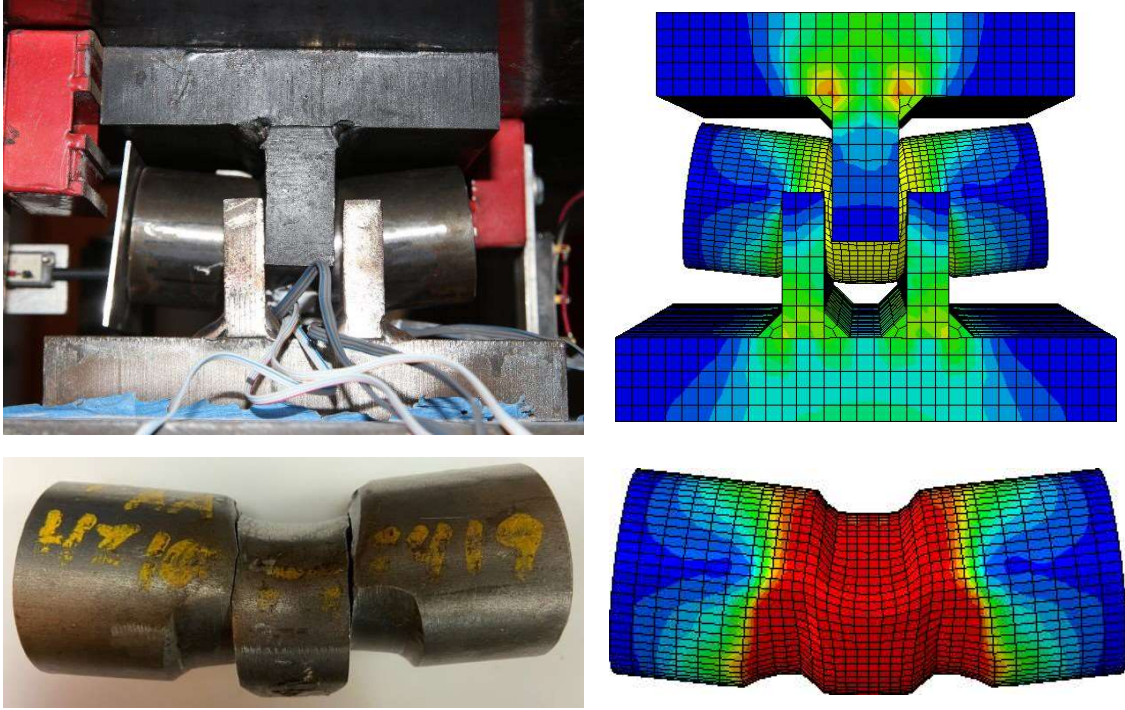


(k) Specimen B4

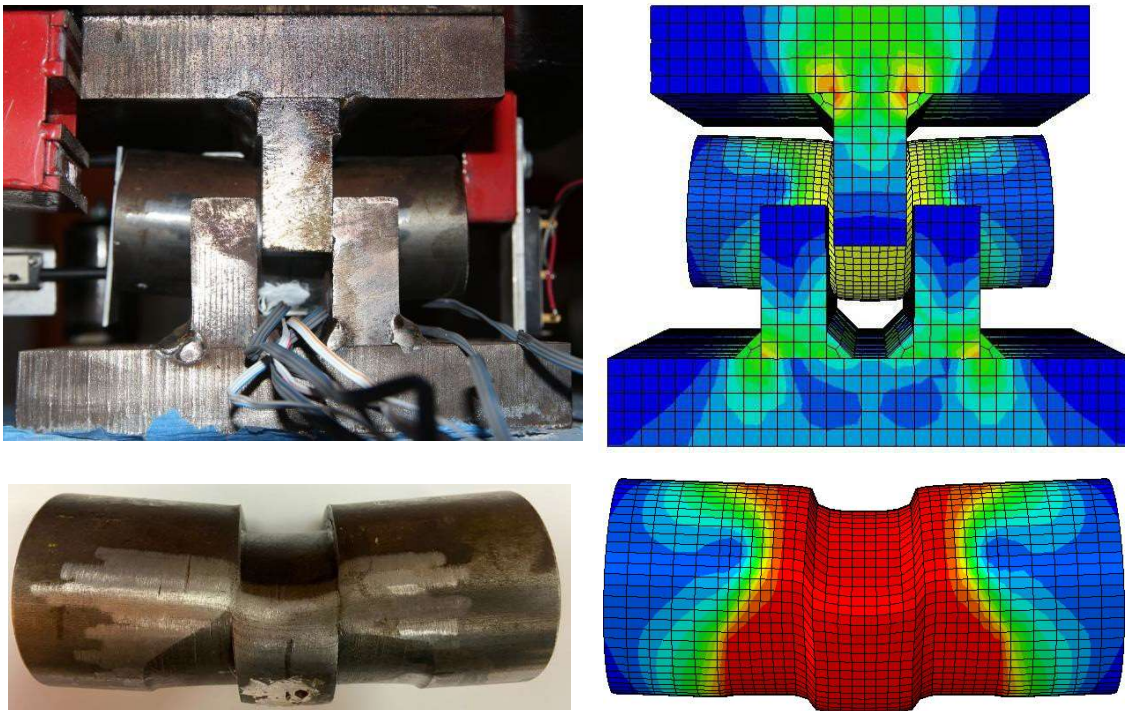


(l) Specimen B5

Figure 2.49 Correlation between Test Results and FEM Analyses (continued)

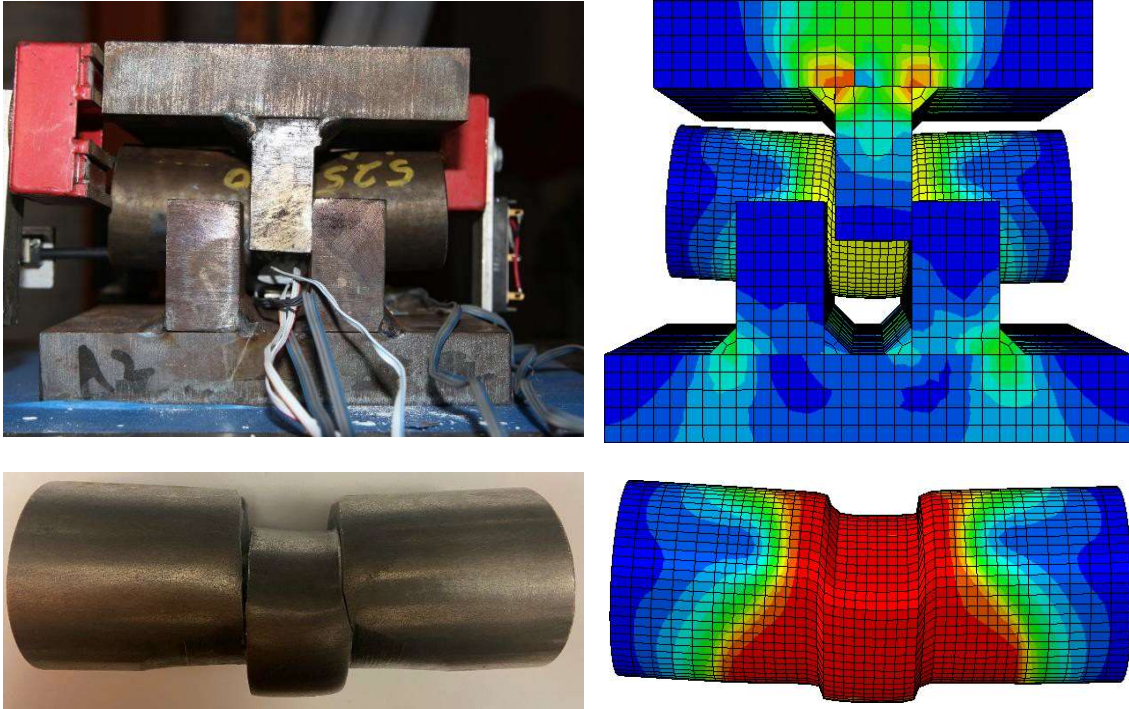


(a) Specimen A1

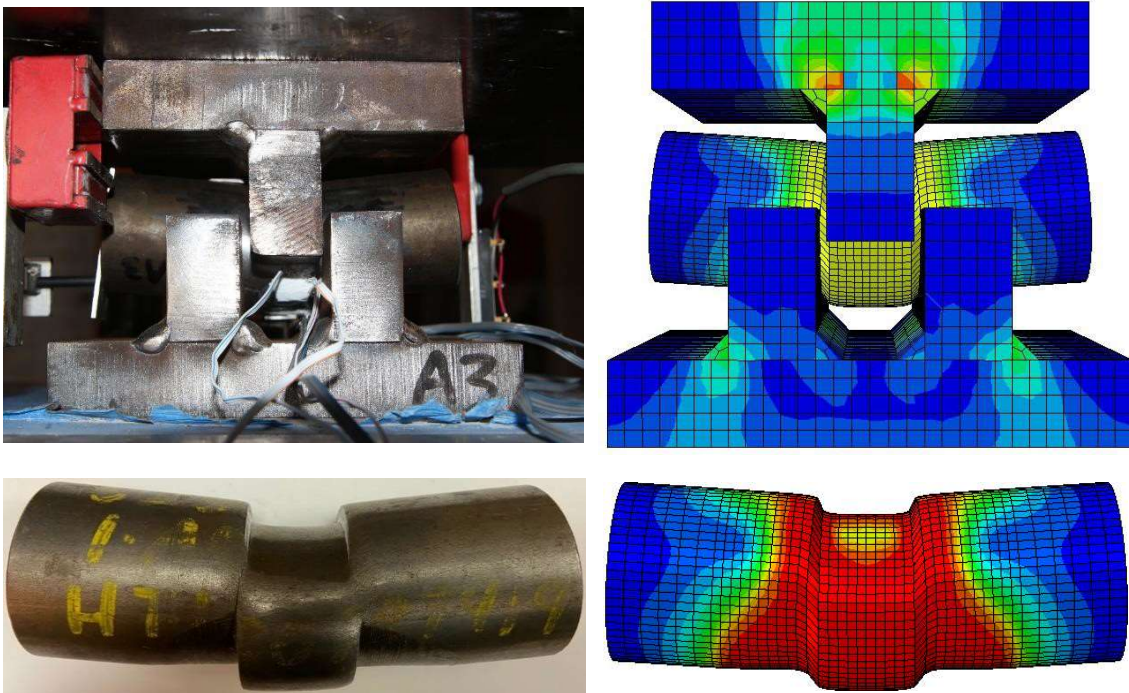


(b) Specimen A2

Figure 2.50 Comparison of Deformed Shape

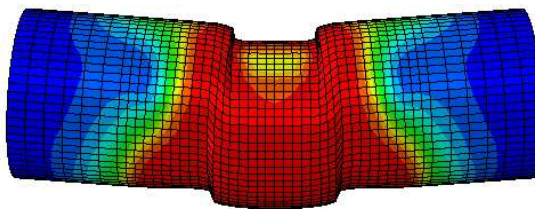
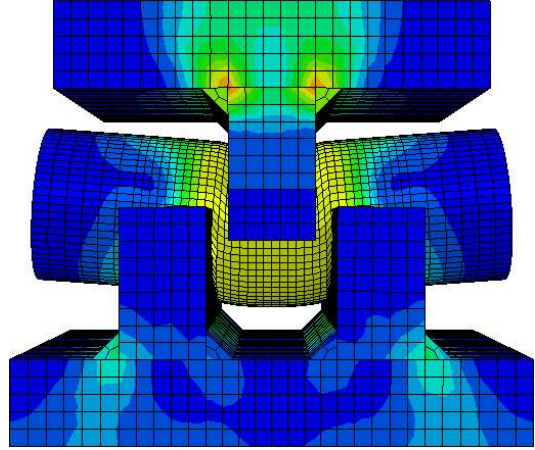
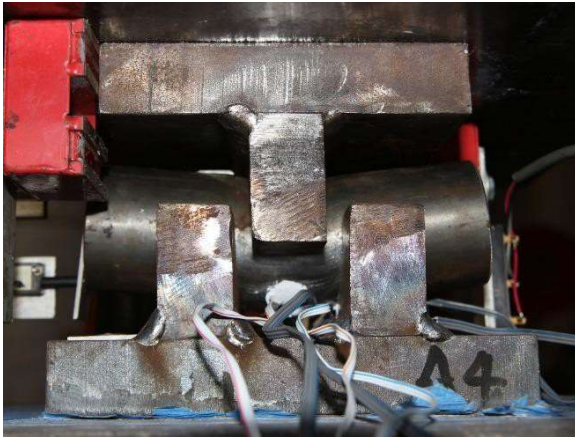


(c) Specimen A3

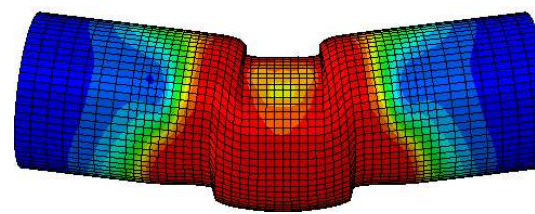
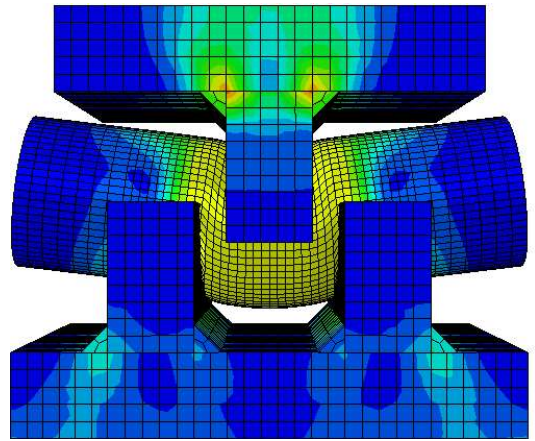
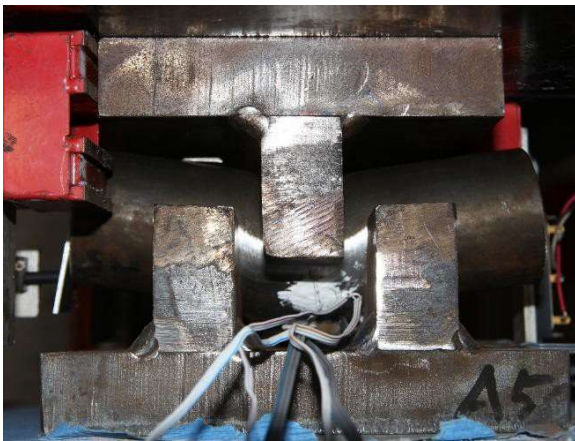


(d) Specimen A4

Figure 2.50 Comparison of Deformed Shape (continued)

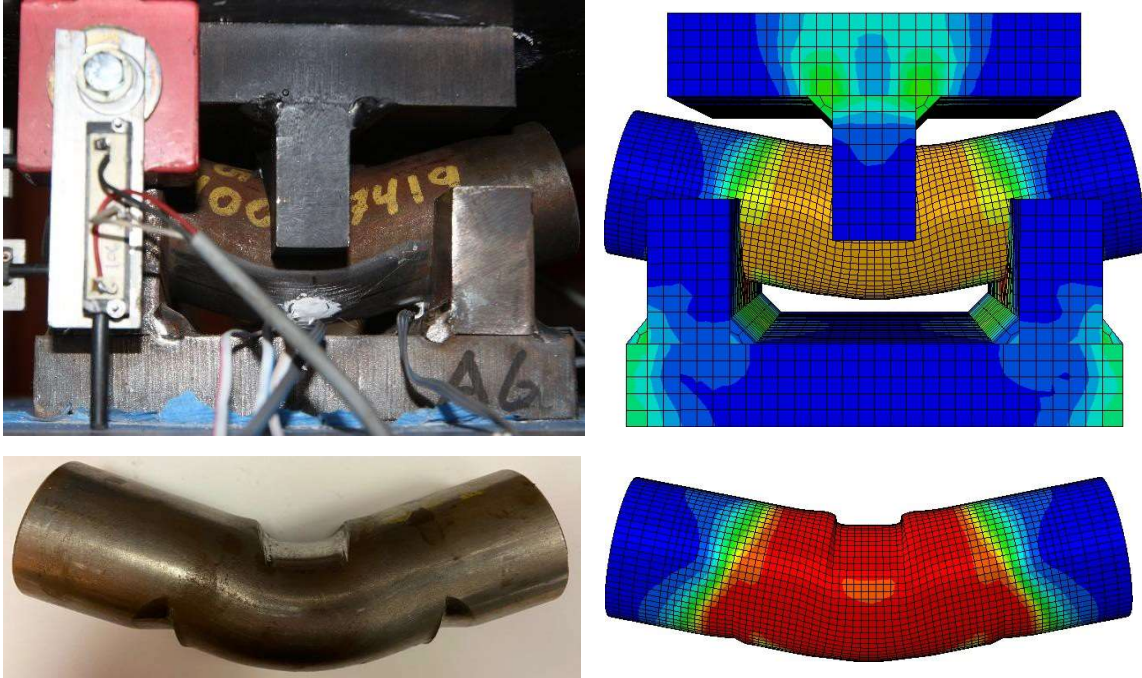


(e) Specimen A5

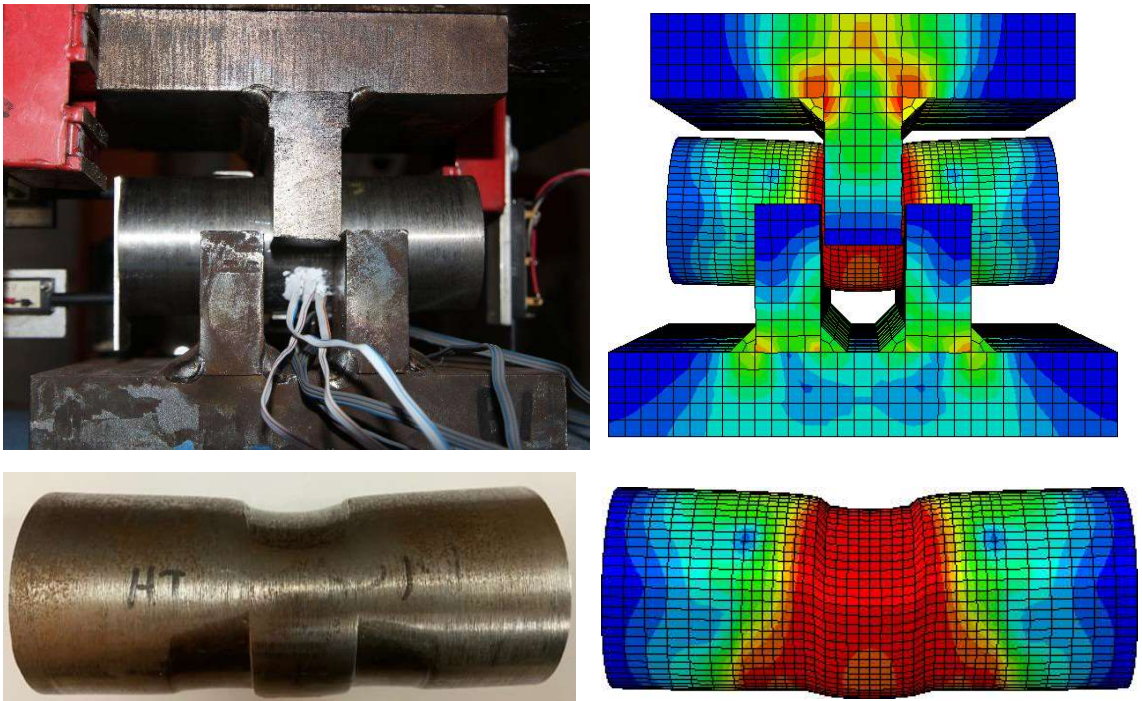


(f) Specimen A6

Figure 2.50 Comparison of Deformed Shape (continued)

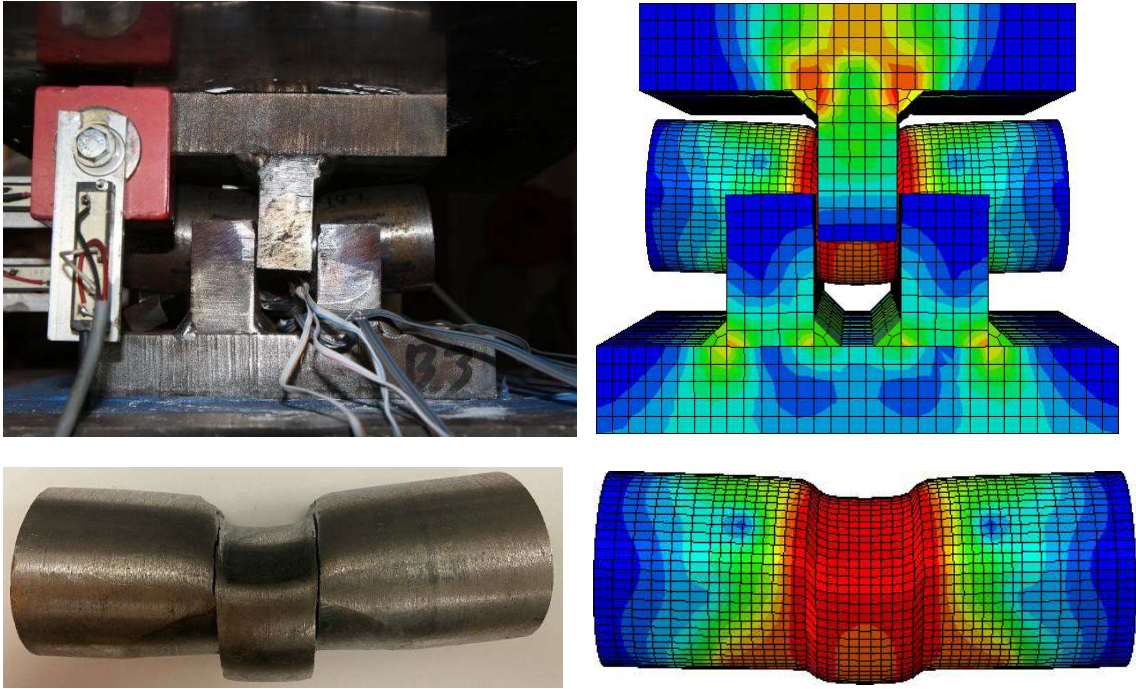


(g) Specimen A7

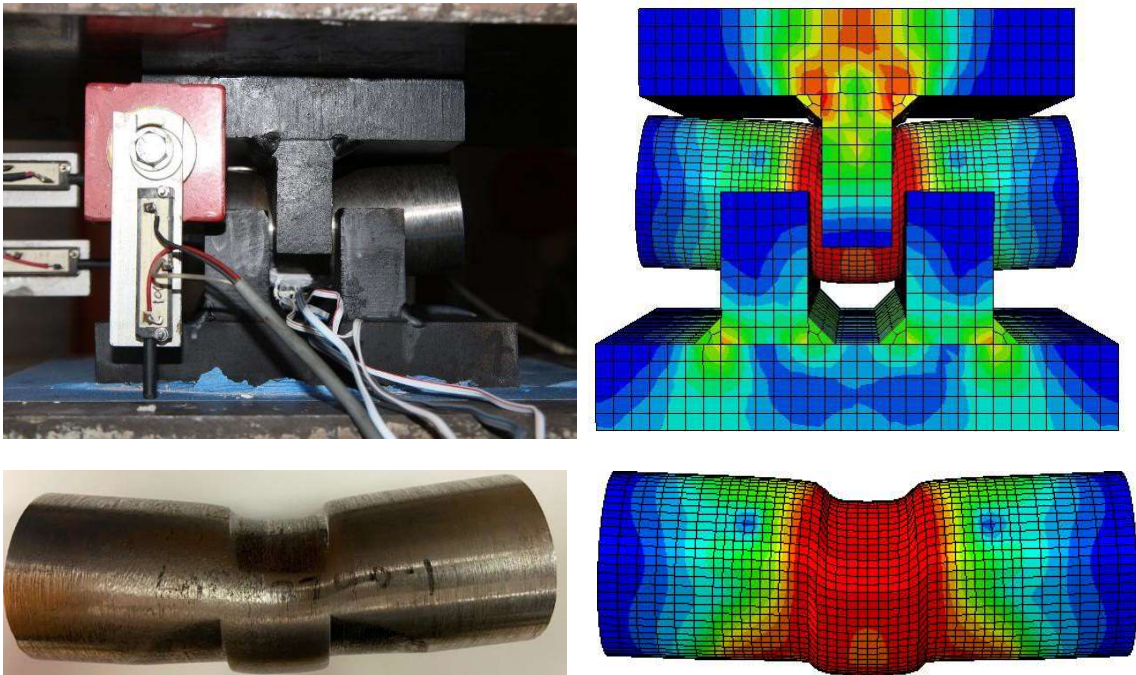


(h) Specimen B1

Figure 2.50 Comparison of Deformed Shape (continued)

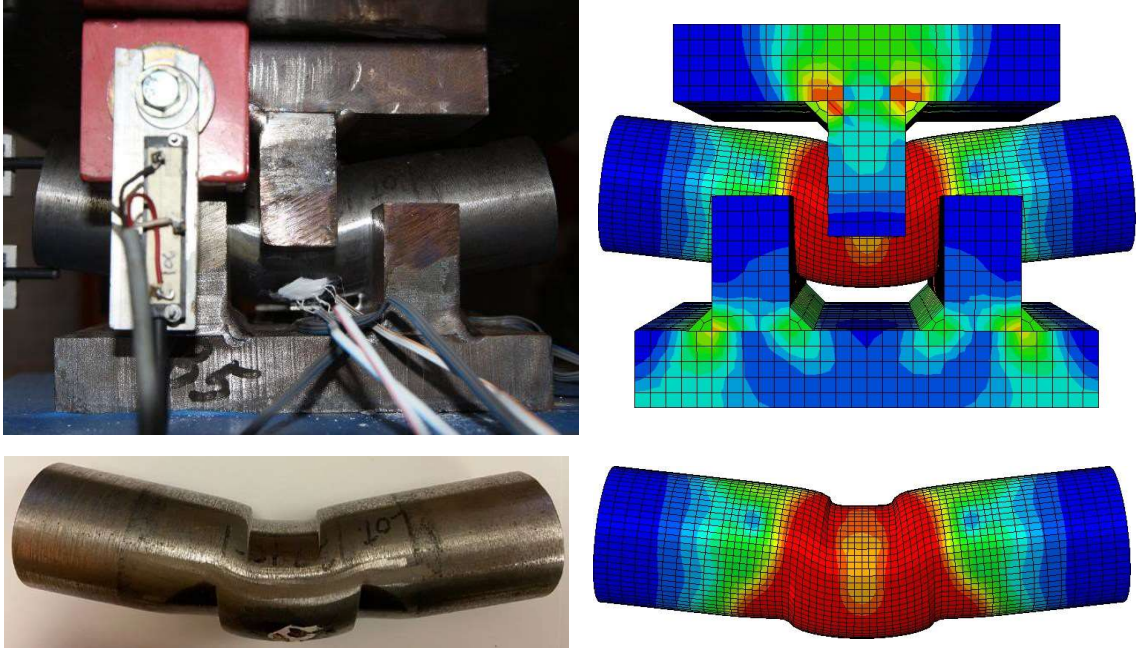


(i) Specimen B2

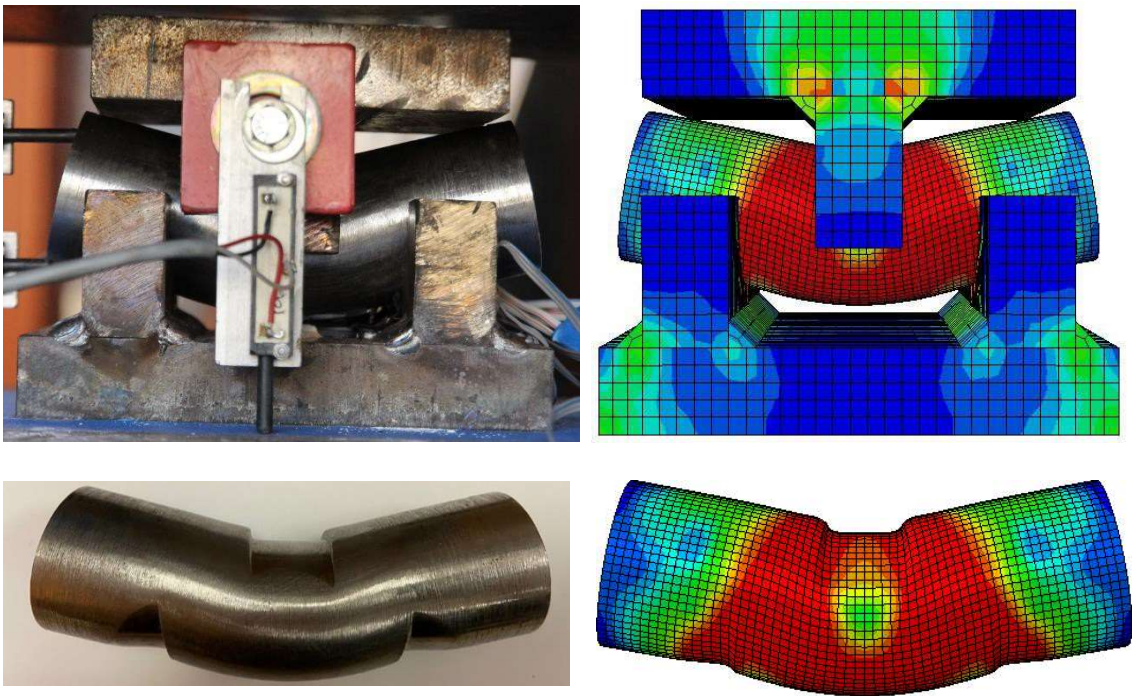


(j) Specimen B3

Figure 2.50 Comparison of Deformed Shape (continued)

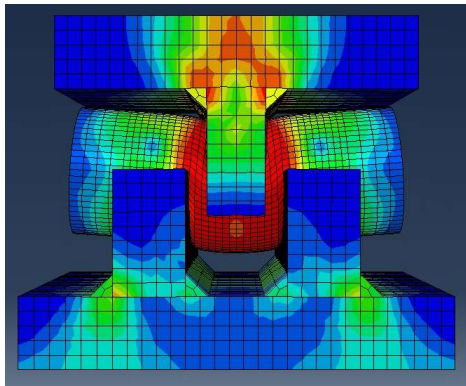


(k) Specimen B4

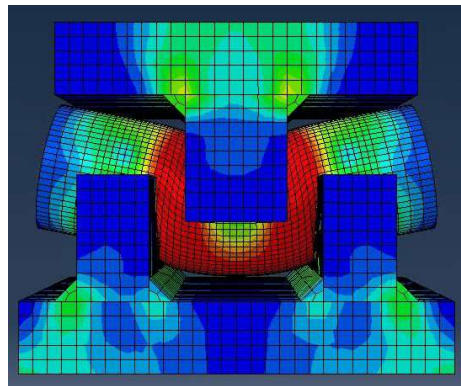


(l) Specimen B5

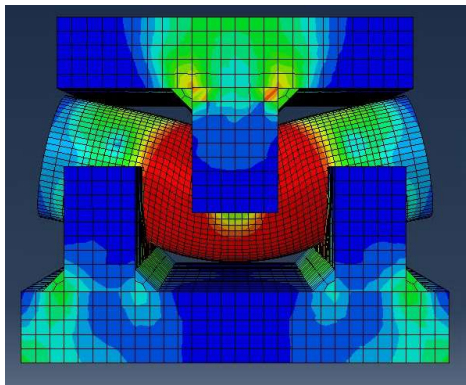
Figure 2.50 Comparison of Deformed Shape (continued)



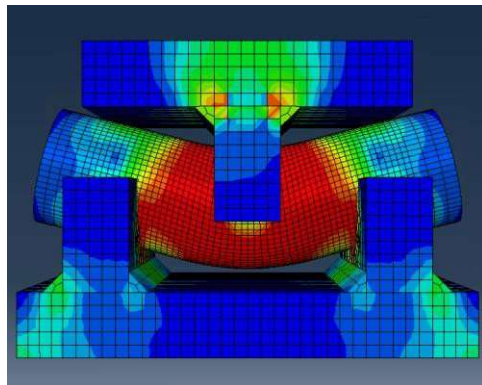
(a) C3 ($b/D = 0.15$)



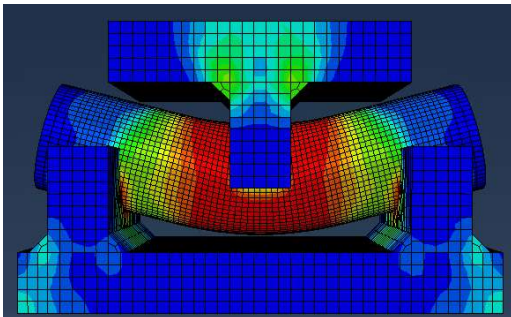
(b) C5 ($b/D = 0.25$)



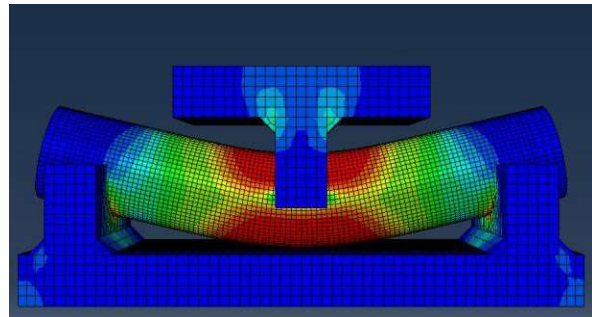
(c) C8 ($b/D = 0.40$)



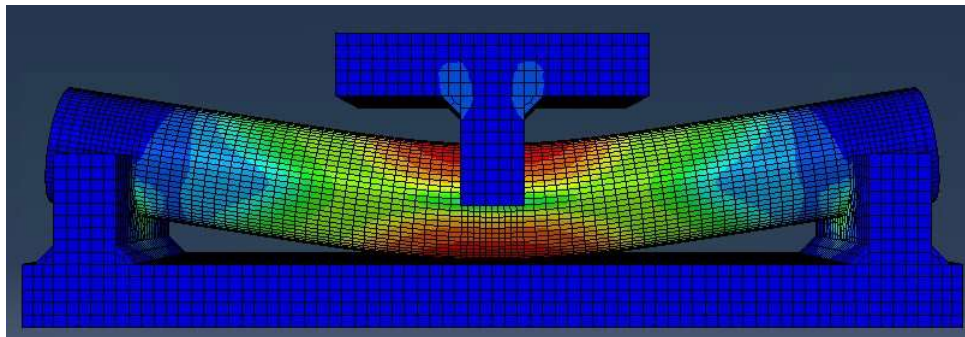
(d) C13 ($b/D = 0.65$)



(e) C17 ($b/D = 1.0$)



(f) C20 ($b/D = 1.75$)



(g) C22 ($b/D = 2.75$)

Figure 2.51 Deformed Shape of Selected Series C Models ($D = 2.0$ in.)

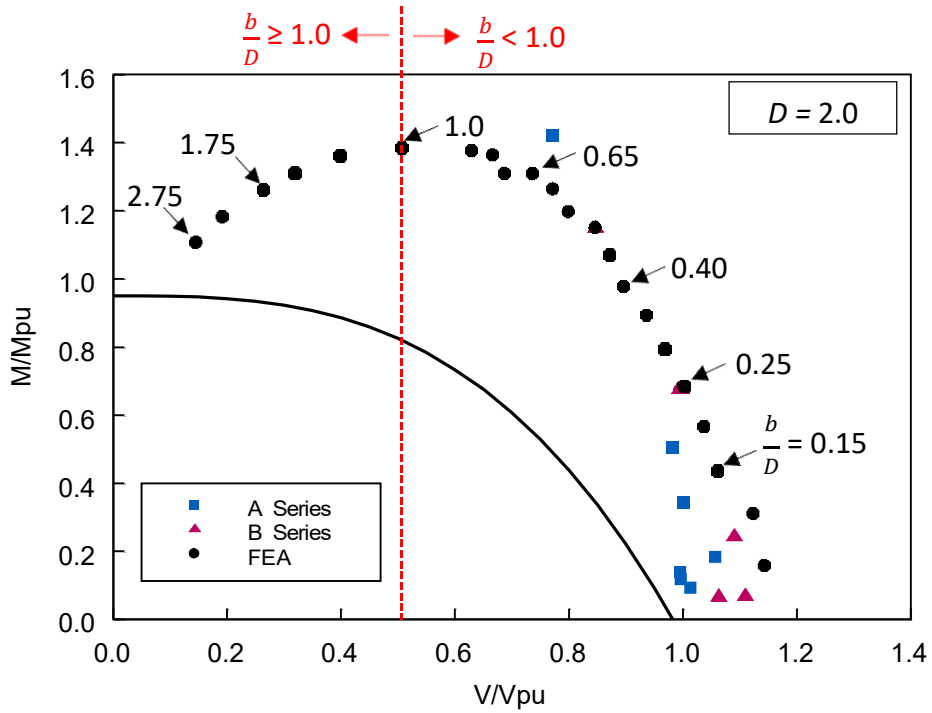
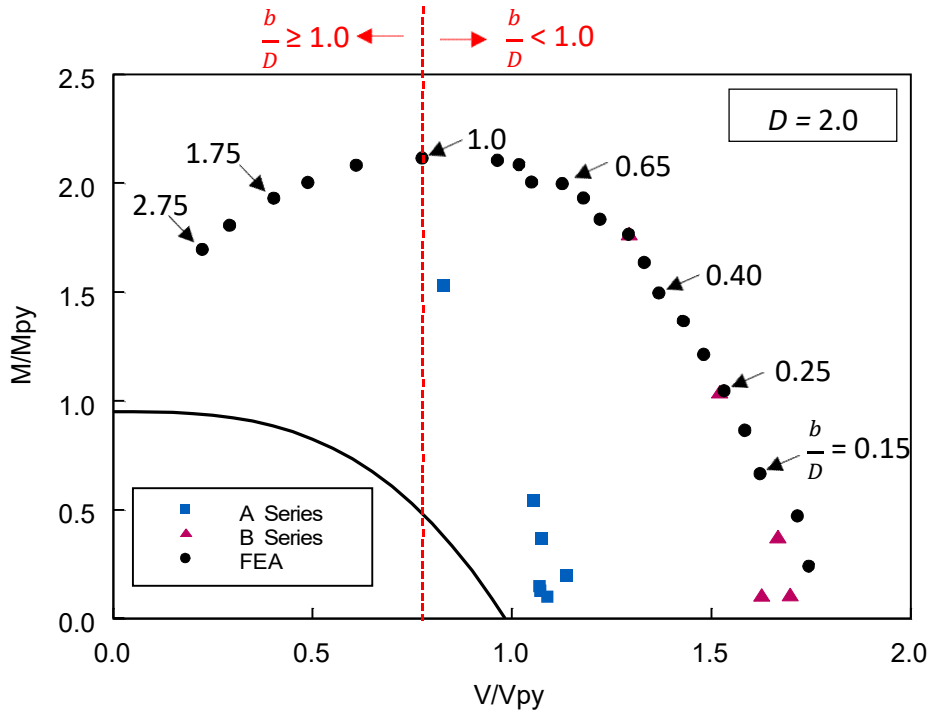
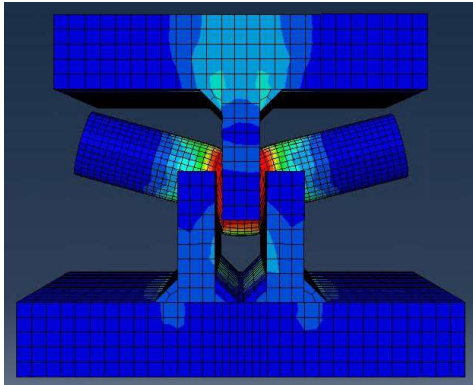
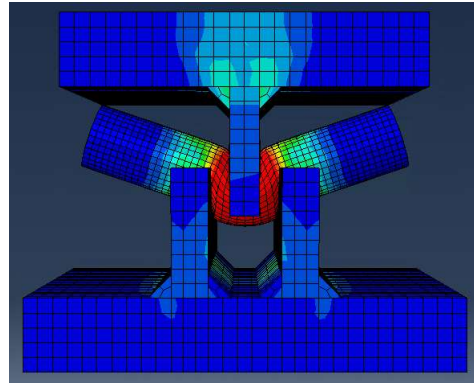


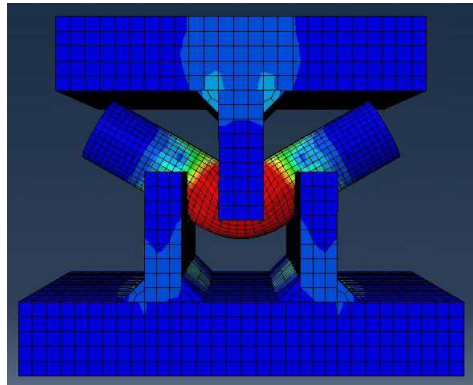
Figure 2.52 Results of Test and Simulated Series C Pin Models in Moment-Shear Domain ($D = 2.0$ in.)



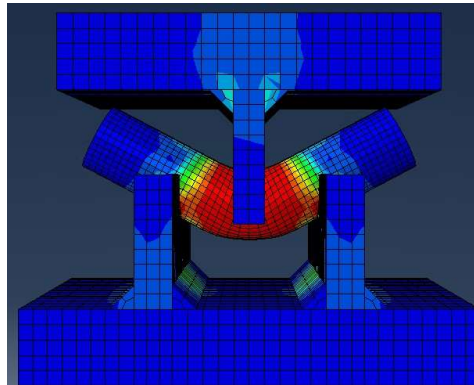
(a) D1 ($b/D = 0.1$)



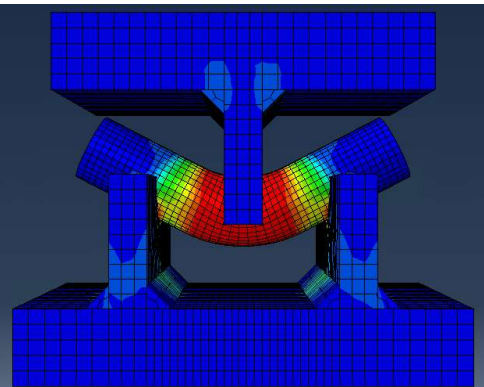
(b) D2 ($b/D = 0.3$)



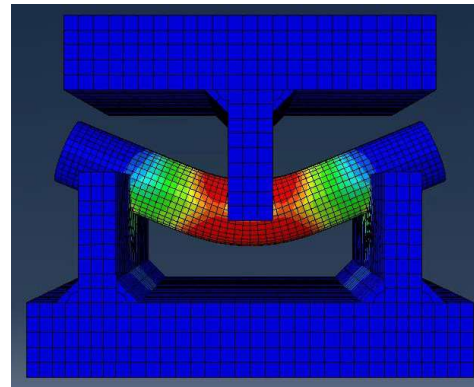
(c) D3 ($b/D = 0.5$)



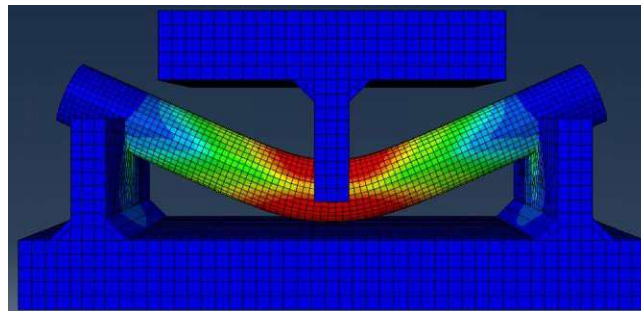
(d) D4 ($b/D = 0.8$)



(e) D5 ($b/D = 1.0$)

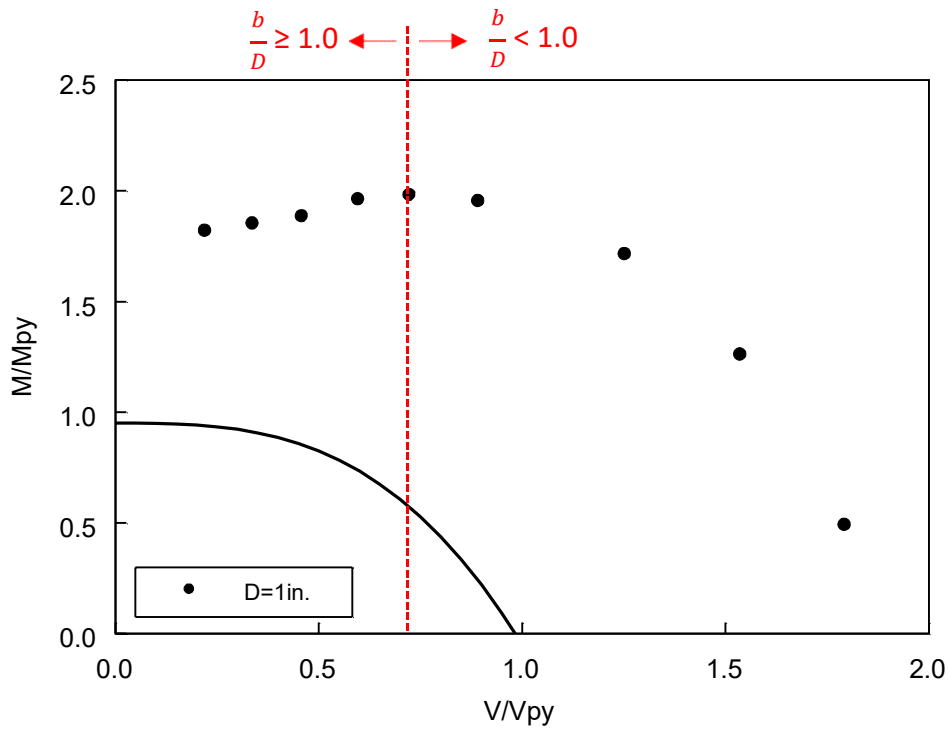


(f) D6 ($b/D = 1.5$)

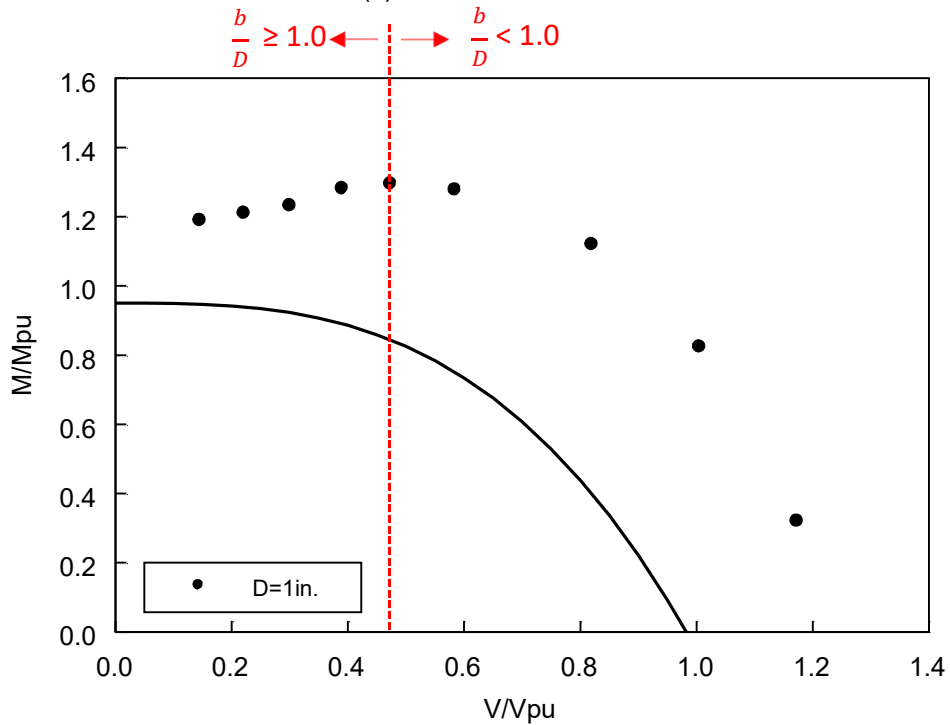


(g) D7 ($b/D = 3.0$)

Figure 2.53 Deformed Shape of Selected Series D Models ($D = 1.0$ in.)

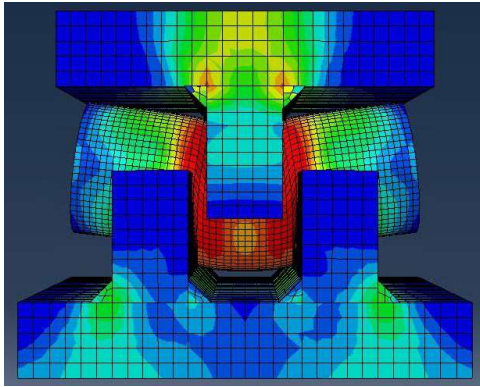


(a) Based on Yield Stress

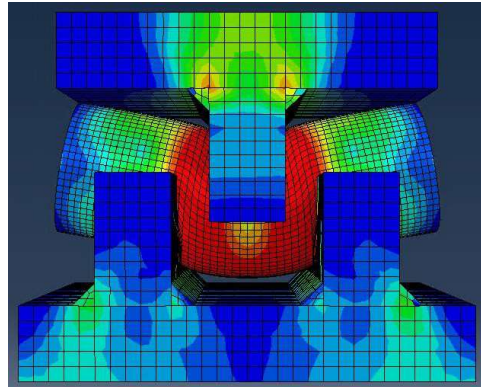


(b) Based on Tensile Stress

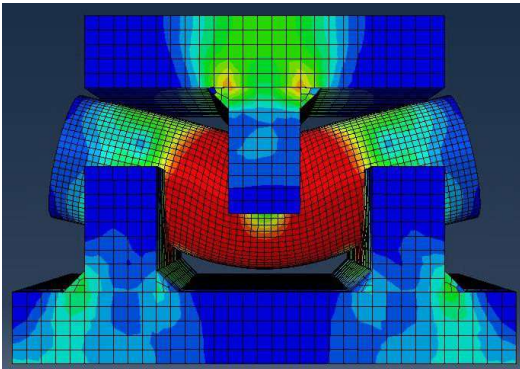
Figure 2.54 Results of Simulated Series D Models in the Moment-Shear Domain ($D = 1.0\text{ in.}$)



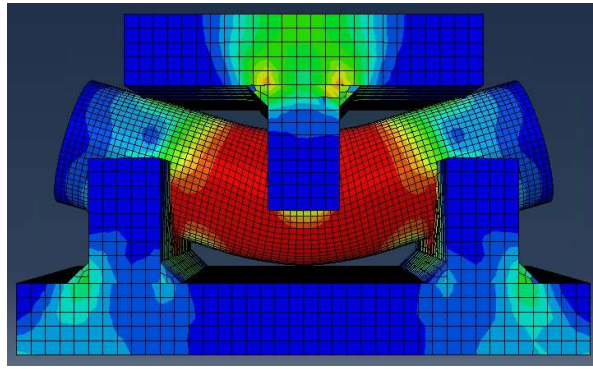
(a) E1 ($b/D = 0.125$)



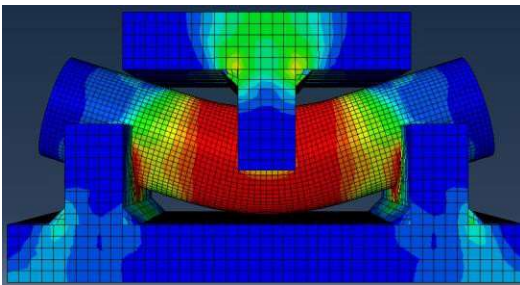
(b) E2 ($b/D = 0.25$)



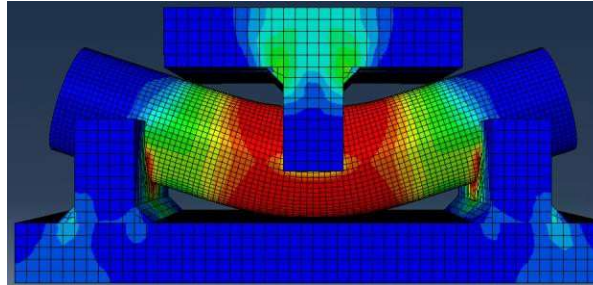
(c) E3 ($b/D = 0.50$)



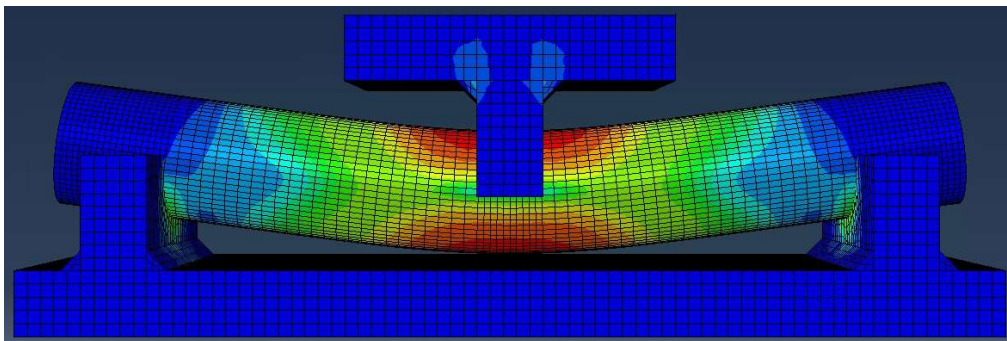
(d) E4 ($b/D = 0.75$)



(e) E5 ($b/D = 1.0$)

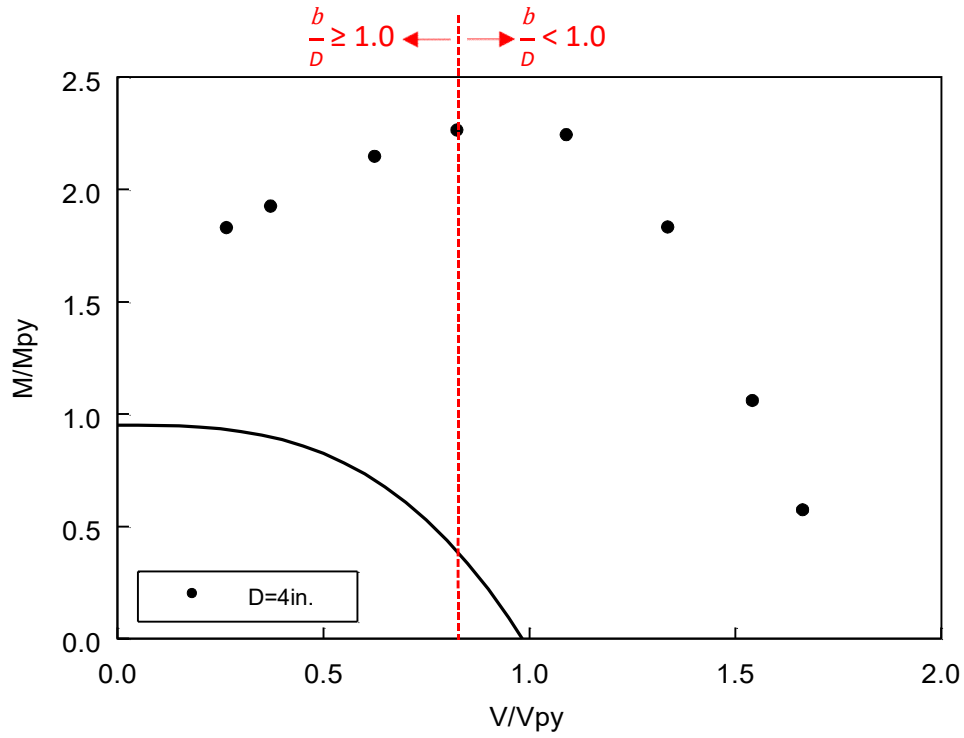


(f) E6 ($b/D = 1.875$)

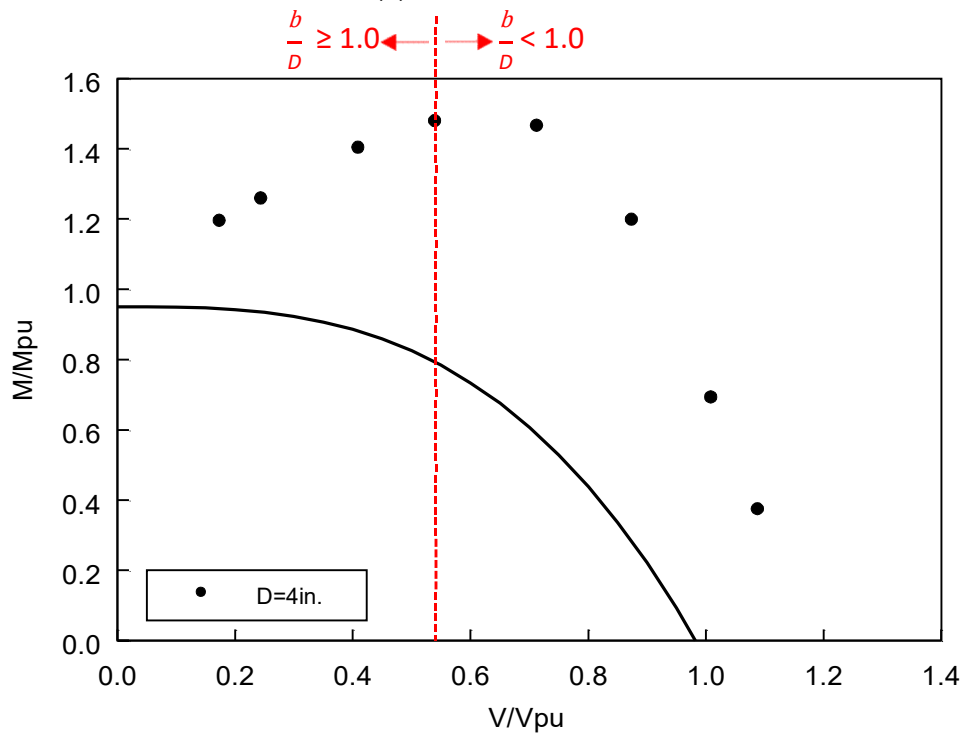


(g) E7 ($b/D = 2.5$)

Figure 2.55 Deformed Shape of Selected Series E Models ($D = 4.0$ in.)



(a) Based on Yield Stress



(b) Based on Tensile Strength

Figure 2.56 Results of Simulated Series D Models in the Moment-Shear Domain ($D = 4.0$ in.)

2.6 DEVELOPMENT OF PIN STRENGTH PREDICTIVE EQUATIONS

2.6.1 General

Based on the results from both testing and finite element simulation, it is concluded that treating the pin as a beam and using the AASHTO moment-shear interaction equation in Eq. (2.1) would significantly underestimate the ultimate strength of the pin. Even if the beam-analogy is valid, the actual shape of the moment-shear interaction curve does not resemble that assumed in the AASHTO Specifications. In this chapter, alternative pin strength equations that do not rely on the beam analogy and moment-shear interaction design procedure are developed. The development considers both the strength and service limit states.

2.6.2 Proposed Model

A designer following the current design practice is required to define not only the span of the pin but also the applied load pattern. For the latter, it is common to assume a distributed load (uniform or non-uniform). For strength prediction purposes, the proposed pin model is shown in Figure 2.57. The applied load is P and the pin shear, V , equals $P/2$. The clear span, L , of the pin is α times the pin diameter, D . The transverse load from the loading plate is assumed to be distributed in a width that is β times the pin diameter. Unlike the current design practice, it not necessary to assume if the distributed load is uniform or not because the proposed model does not treat the pin as a beam and, therefore, computing moment and shear is unnecessary. Also, a check on moment-shear interaction equation is not used.

The shear strength of the pin, V_u , is expressed in the following form:

$$\frac{V_u}{V_{pu}} = C_1 \cdot \alpha^{C_2} \cdot \beta^{C_3} \quad (2.12)$$

where V_{pu} is the plastic shear strength based on the tensile strength [see Eq. (2.6b)]. V_{py} is not used in Eq. (2.12) because normalization by V_{py} provided a more scattered data distribution than that by V_{pu} (see Figure 2.45). For each pin specimen tested, α and β are uniquely defined (see Table 2.11). Coefficients C_1 , C_2 and C_3 are to be determined from regression.

2.6.3 Strength Limit State

The ultimate strength, V_u , α , and β values for each specimen are listed in Table 2.11. A regression analysis resulted in the following expression:

$$\frac{V_u}{V_{pu}} = 1.21 \cdot \alpha^{-0.22} \cdot \beta^{0.34} = 1.21 \frac{\beta^{0.34}}{\alpha^{0.22}} \quad (2.13)$$

To improve the significance of regression, it is desirable to increase the size of experimental database. Unfortunately, available pin test is very limited. A literature review shows that Bridge et al. (2001) tested 13 pins. The diameter of the pins, steel material strengths, α and β values, as well as pin shear strengths are provided in Table 2.12. A regression analysis that considered test data from both this research and Bridge et al. resulted in the following equation:

$$\frac{V_u}{V_{pu}} = 1.17 \frac{\beta^{0.3}}{\alpha^{0.26}} \quad (2.14)$$

Since the exponents for α and β are close, Eq. (2.12) is further simplified as

$$\frac{V_u}{V_{pu}} = C_1 \cdot \alpha^{-C_2} \cdot \beta^{C_2} = C_1 \left(\frac{\beta}{\alpha} \right)^{C_2} \quad (2.15)$$

Another regression based on the above expression gives the following:

$$\frac{V_u}{V_{pu}} = 1.14 \left(\frac{\beta}{\alpha} \right)^{0.28} \quad (2.16)$$

Figure 2.58(a) shows a comparison of the shear strengths from testing and prediction based on Eq. (2.16). The prediction is very satisfactory; the coefficient of determination (R^2) is 0.995.

Of the 12 pin specimens tested in this research, Specimens A7 and B5 had the largest span in the A and B series specimens, respectively. The deformed shape (see Figure 2.37) shows that their response was dominated by flexure. Since it is not common in practice to have pins with a large gap between the loading plate and supporting plates, the regression presented above was repeated by excluding these two data points from the database, and Eqs. (2.13), (2.14), (2.16) become

$$\frac{V_u}{V_{pu}} = 1.11 \cdot \alpha^{-0.13} \cdot \beta^{0.17} = 1.11 \frac{\beta^{0.17}}{\alpha^{0.13}} \quad (2.17)$$

$$\frac{V_u}{V_{pu}} = 1.17 \frac{\beta^{0.3}}{\alpha^{0.27}} \quad (2.18)$$

$$\frac{V_u}{V_{pu}} = 1.14 \left(\frac{\beta}{\alpha} \right)^{0.29} \quad (2.19)$$

Figure 2.58(b) shows a comparison of the test results with the prediction based on Eq. (2.19). This equation is very similar to Eq. (2.16), and the coefficient of determination (R^2) remains at 0.995. It is recommended that Eq. (2.19) be used. Substituting (2.6b) for V_{pu} into the above equation gives the following expression for the ultimate pin shear strength:

$$V_u = 1.14 \left(\frac{\beta}{\alpha} \right)^{0.29} \left[\frac{\pi D^2}{4} (0.58 F_u) \right] = 0.52 F_u D^2 \left(\frac{\beta}{\alpha} \right)^{0.29} \quad (2.20)$$

Based on their test data, Bridge et al. (2001) proposed the following equation to calculate the shear resistance of the pin:

$$V_u = 0.62 F_u \left(\frac{\pi D^2}{4} \right) \quad (2.21)$$

Figure 2.59 shows a comparison of the predicted and test results.

2.6.4 Service Limit State

Figure 2.60 summarize the global response plots for all 12 specimens. The vertical axis is the pin shear normalized by V_{py} , and the horizontal axis is the midspan deflection measured by L4. (The average of L1 and L2 is not used here because this midspan deflection also includes the deformation of the loading cradle.) In this study, the serviceability criterion is based on the midspan flexural strain at the bottom surface; see strain gage S5 in Figure 2.11. For each test, three events corresponding to ϵ_y , $2\epsilon_y$, and $3\epsilon_y$ are labelled on the response curve, where ϵ_y is the actual yield strain. Figure 2.44 shows a comparison of the pin shear strength at these strain levels with respect to the ultimate shear strength. Using $1\epsilon_y$ to define pin service strength is a natural choice. Selecting $3\epsilon_y$ is questionable because Figure 2.60 shows that the global response at this strain level has deviated from the elastic response for most of the specimens. But using ϵ_y as the serviceability criterion may be too conservative. The figure shows that using $2\epsilon_y$ still appears acceptable; except for Specimen A1, it is reasonable to assume that the response

up to $2\varepsilon_y$ remained more or less elastic. Based on the test data presented in Table 2.11, the shear strength at ε_y is presented below.

The following expression is used for regression:

$$\frac{V_s}{V_y} = C_4 \cdot \alpha^{C_5} \cdot \beta^{C_6} \quad (2.22)$$

In the above equation V_y , is the shear yield force of the pin:

$$V_y = \frac{\pi D^2}{4} (0.44F_y) \quad (2.23)$$

With 10 data points (Specimens A7 and B5 excluded) from this test program, the following equation results:

$$\frac{V_s}{V_y} = 0.64 \frac{1}{\alpha^{0.42}\beta^{0.21}} \quad (2.24)$$

or

$$V_s = 0.64 \frac{1}{\alpha^{0.42}\beta^{0.21}} \left[\frac{\pi D^2}{4} (0.44F_y) \right] = 0.22 \left(\frac{F_y D^2}{\alpha^{0.42}\beta^{0.21}} \right) \quad (2.25)$$

A comparison of the predicted and actual service shear strengths is presented in Figure 2.61. The coefficient of determination is 0.61.

Note that AASHTO LRFD Specifications in Section 6.10.4.2.2 uses 95% of the yield stress to define the service strength of I-section flexural members. Applying the same safety factor to Eq. (2.25) gives the following for service design:

$$V_s = 0.95 \times 0.22 \left(\frac{F_y D^2}{\alpha^{0.42}\beta^{0.21}} \right) = 0.2 \left(\frac{F_y D^2}{\alpha^{0.42}\beta^{0.21}} \right) \quad (2.26)$$

Table 2.11 Summary of UCSD Test Data

Specimen	α	β	Pin Shear (kips)		
			Ultimate	@ ϵ_y	@ $2\epsilon_y$
A1	0.5	0.4	159.1	118.9	140.4
A2	0.5	0.415	159.3	113.0	140.7
A3	0.5	0.435	162.0	96.0	123.5
A4	0.625	0.5	169.0	86.9	107.8
A5	0.75	0.5	159.8	105.4	119.5
A6	0.875	0.5	156.9	88.3	108.7
A7	1.75	0.4	123.4	42.6	59.2
B1	0.5	0.455	224.8	117.7	146.9
B2	0.5	0.455	234.7	111.9	130.2
B3	0.563	0.4	230.4	104.6	124.1
B4	1.0	0.5	210.2	73.6	97.7
B5	1.5	0.5	178.9	53.6	78.5

Table 2.12 Summary of Test Data by Bridge et al. (2001)

Specimen No.	D (in.)	F_y (ksi)	F_u (ksi)	V_u (kips)	α	β	V_{py} (kips)	V_{pu} (kips)
1	0.40	36.3	66.0	6.0	0.310	0.310	2.6	4.7
2	0.40	36.3	66.0	6.1	0.595	0.595	2.6	4.7
3	0.40	36.3	66.0	6.1	0.979	0.979	2.6	4.7
5	0.64	43.5	72.4	16.9	0.623	0.623	8.0	13.3
6	0.64	43.5	72.4	16.5	0.983	0.983	8.0	13.3
8	1.06	39.2	70.3	38.9	0.367	0.367	20.1	36.1
9	1.06	39.2	70.3	38.7	0.740	0.740	20.1	36.1
10	0.39	69.6	80.9	6.0	0.315	0.315	4.9	5.7
11	0.40	69.6	80.9	6.4	0.607	0.607	5.0	5.8
12	0.39	69.6	80.9	6.3	1.011	1.011	4.9	5.7
14	0.63	66.7	75.9	15.4	0.617	0.617	12.0	13.7
15	0.63	66.7	75.9	14.7	0.996	0.996	12.0	13.7
18	1.06	65.3	75.9	39.3	0.739	0.739	33.3	38.8

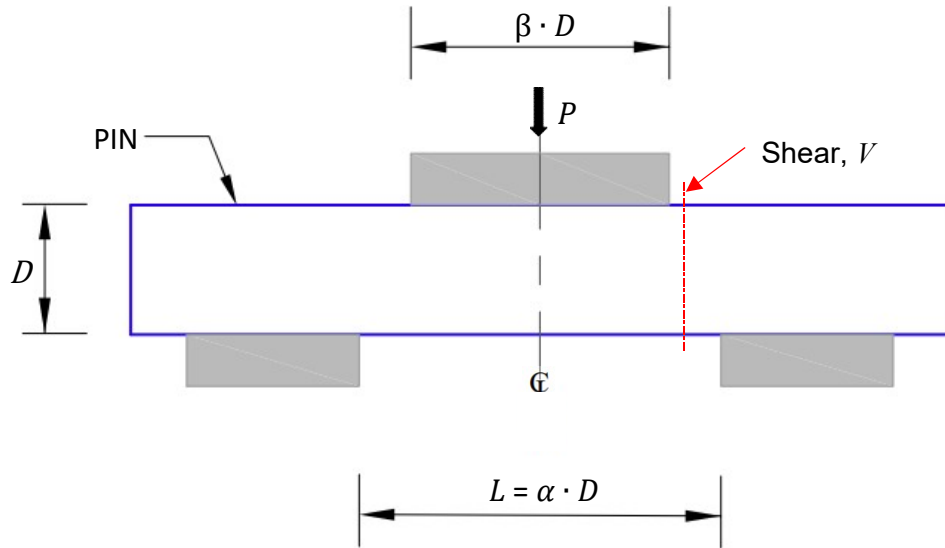
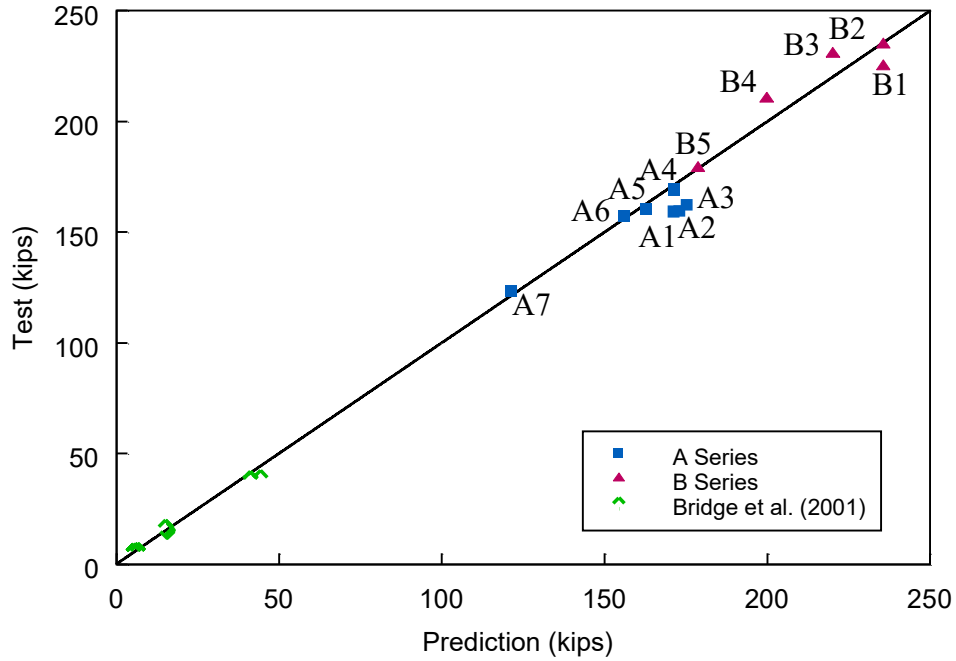
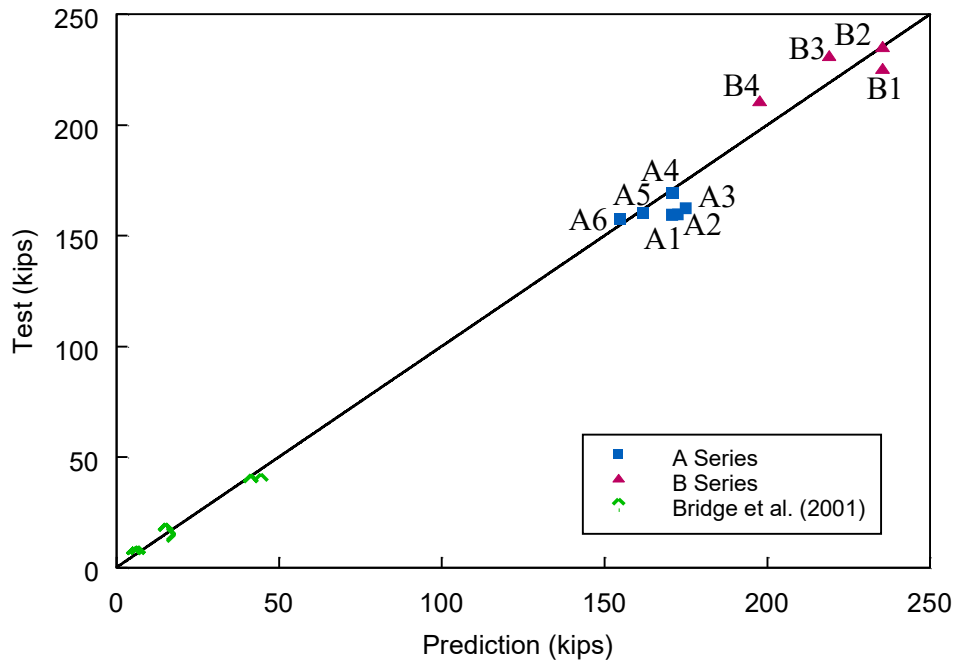


Figure 2.57 Definition of α and β for Pin Strength Prediction



(a) Prediction Based on Eq. (2.16)



(b) Prediction Based on Eq. (2.19)

Figure 2.58 Comparison of Measured and Predicted Pin Ultimate Shear Strengths

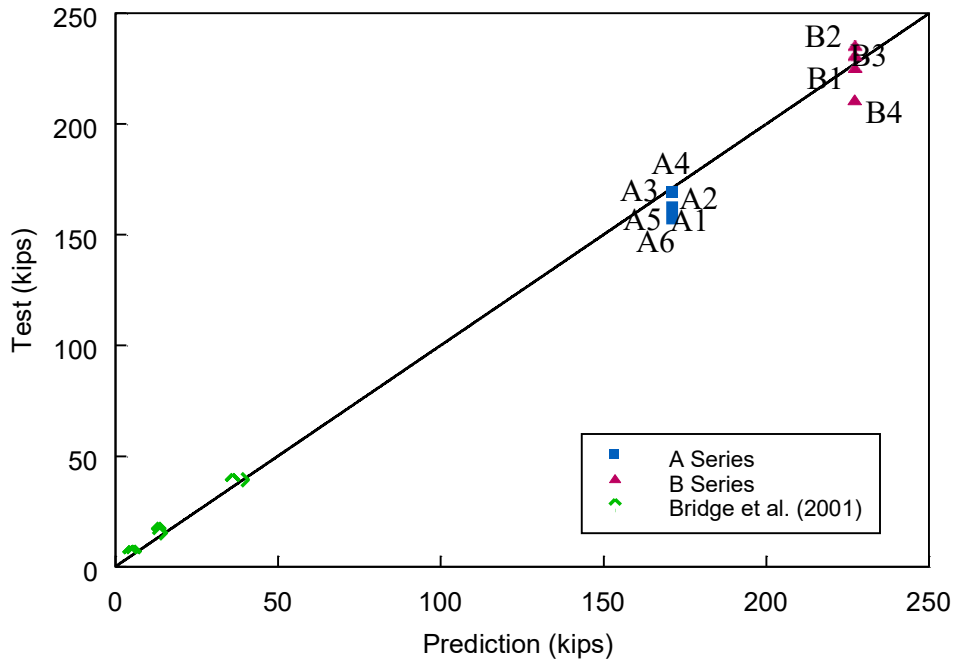


Figure 2.59 Comparison of Measured and Bridge et al. (2001) Predicted Pin Ultimate Shear Strength

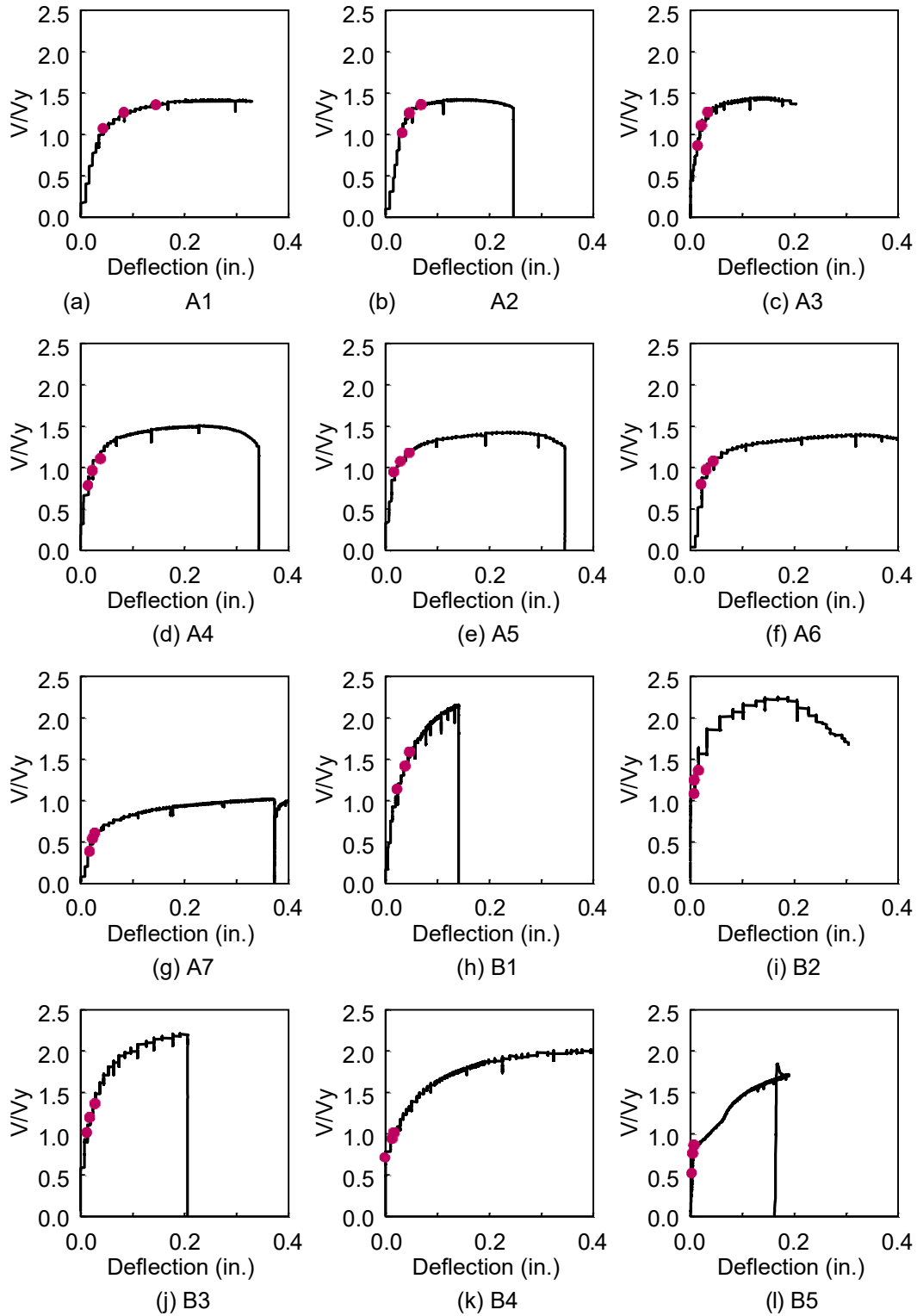


Figure 2.60 Global Response with Service Shear Strength

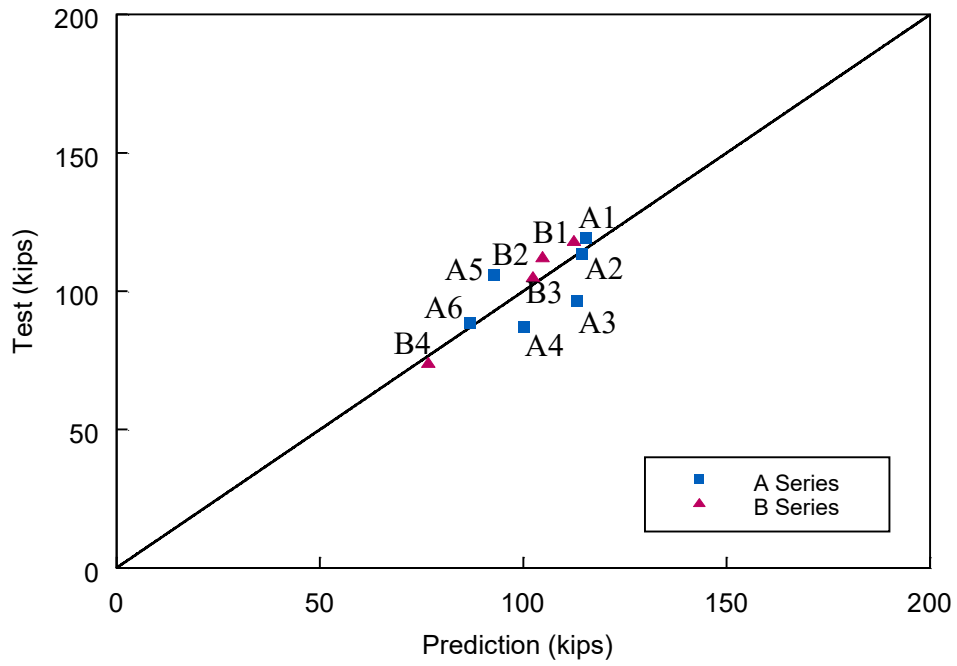


Figure 2.61 Comparison of Measured and Predicted Pin Service Shear Strengths

2.7 Summary and Concluding Remarks

2.7.1 Summary

A full-scale test program with twelve 2-in. diameter pins was conducted. Two steel grades were considered: A108 Grade 1018 and A668 Class F. The design of these specimens followed the current practice that treats the pin as a beam. With the assumed beam span and uniform loading pattern, the computed moment and shear are then checked against the AASHTO moment-shear interaction equation to identify the critical section.

A series of finite element analyses with ABAQUS were conducted. First, A correlation study with all the test specimens was conducted. After achieving a satisfactory correlation, additional models were analyzed to (i) fill the gap in the 2-in. pin experimental database, and (ii) expand the database to other pin diameters (1 in. and 4 in.).

Based on results from both tests and finite element simulation, an alternate pin strength equation for factored load design was proposed; the proposed model does not treat the pin as a beam. In addition, predicted strength equations for serviceability considerations are proposed.

2.7.2 Concluding Remarks

The following conclusions can be made from this research.

- (1) Assuming that the current design practice that treats the pin as a beam is valid, test results of twelve pins showed that the pin strength based on the AASHTO moment-shear interaction was exceeded by a very large margin (see Figure 2.45).
- (2) Based on results from both testing and finite element simulation, it was concluded that the shape of the moment-shear yield surface—assuming that the pin can be treated as a beam—does not resemble that assumed in the AASHTO Specifications (see Figure 2.52). The yield surface is composed of ascending and descending branches, separately by $b/D = 1.0$, where b is the gap (see Figure 2.7) and D is the pin diameter. This observation is also confirmed from finite element simulation of 1-in. (Figure 2.54) and 4-in. (Figure 2.56) diameter pins.
- (3) Based on (2), the strength of pins should not be treated as a beam in design. By using the beam analogy and the experimentally determined ultimate load, the computed maximum moment exceeded the plastic moment based on the measured ultimate strength (F_u) of the pin material for some specimens (Specimens A7 and B5 in Figure

2.42) by at least 20%, which is theoretically not permissible. This is hypothesized to be a result of arching that occurs in the pin.

- (4) Nonlinear finite element analysis with solid elements were found to simulate the observed failure mode and measured response. Most of the specimens with a shorter span experienced localized damage (or penetration) due to the concentrated load (see Figure 2.37). To simulate the pin behavior, it is essential that the penetration phenomenon be considered. With a proper calibration, using a penalty stiffness and friction between contact surfaces provided a satisfactory correlation to the test results.
- (5) The pin strength predictive model proposed in this research, which deviates from the current design practice, considers two nondimensional length parameters (α and β in Figure 2.57). For the strength limit state, a regression analysis with the test data from both this research and Bridge et al. (2001) resulted in Eq. (2.20) for the ultimate shear strength of the pin. This equation is valid for α ranging from 0.31 and 1.75 and β ranging from 0.31 to 1.01.
- (6) No consensus-based criterion to establish a pin service strength is available. In this research, the condition that the flexural tensile strain at midspan reaching the yield strain was first chosen as the limit state. From test data generated in this research, Eq. (2.25) was established, which after multiplying a safety factor of 0.95 resulted in Eq. (2.26) for service design.

3 BEARING STRENGTH OF STEEL PIN PLATES

3.1 Introduction

3.1.1 Statement of Problem

This research aims to evaluate the bearing resistance of pin plates. Both the AASHTO LRFD Specifications (AASHTO 2020) and the AISC Specification (AISC 2016) provide design requirements for pin plates and pin-connected tension members. The design requirements are summarized below.

Section 6.7.6.2.2 of the AASHTO Specifications specify the factored bearing resistance of steel pins as

$$\phi P_b = \phi_b 1.5tDF_y \quad (3.1)$$

where t is the thickness of plate, D is the diameter of pin F_y is the yield strength of the pin, and resistance factor for bearing, ϕ_b , equals 1.00. Section 6.8.7 provides design requirements for *pin-connected plates*. Section 6.8.7.1 states that “Pin-connected plates should be avoided whenever possible.” When used, the factored resistance of the pinplate needs to be checked for the gross section yielding

$$\phi P_r = \phi_y F_y A_g \quad (3.2)$$

and net section rupture

$$\phi P_r = \phi_u F_u A_n R_p U \quad (3.3)$$

where the resistance factors for yielding, ϕ_y , and rupture, ϕ_u , are 0.95 and = 0.85, respectively. The gross area, A_g , and net area, A_n are used in conjunction with the tensile strength of the plate, F_u , to compute the resistances of two limit states. The final two factors, R_p and U both equal 1.0. Figure 3.1 shows the section to be checked in each of these two limit states.

Section 6.8.7.2 further provides design requirements for *pin plates* and specifies the factored bearing resistance on pin plates as

$$\phi P_b = \phi_b A_b F_y = \phi_b tDF_y \quad (3.4)$$

where $A_b (= tD)$ equals the projected bearing area on the plate, and F_y is the yield strength of the plate. A comparison of this equation with Eq. (3.1) shows that the AASHTO Specifications take a conservative approach by removing the 1.5 factor for pin plates. Section 6.8.7.2 also states that “The main plate may be strengthened in the region of the hole by attaching pin plates to increase the thickness of the main plate.” Therefore, a pin-connected plate is composed of a main plate, and pin plates are added to strengthen the main plate if needed. However, the AASHTO Specifications do not mention the factored bearing resistance of main plate. A common practice is to apply Eq. (3.4) to both the main plate and pin plates. In this research the bearing resistance of main plate without pin plates was investigated, Although a pin-plate refers to that used to strengthen the main plate at the pin hole according to the Specifications, the terms “pin plate” and pin-connected “main plate” were used interchangeably in this report.

Section D5 of the AISC Specification (AISC 2016) considers four limit states in determining the design tensile strength of pin-connected members. For bearing on the projected area of pin,

$$\phi P_n = \phi 1.8 F_y A_{pb} \quad (3.5)$$

where $\phi = 0.75$, and the projected bearing area $A_{pb} = Dt$. For yielding on the gross section,

$$\phi P_n = \phi_t F_y A_g \quad (3.6)$$

where $\phi_t = 0.90$. For tensile rupture on the net effective area,

$$\phi P_n = \phi_t F_u (2t b_e) \quad (3.7)$$

where $\phi_t = 0.75$, and the effective edge distance $b_e = 2t + 0.63$ in., but not more than the actual distance from the edge of the hole to the edge of the part measured in the direction normal to the applied force. For shear rupture on the effective area,

$$\phi P_n = \phi_{sf} 0.6 F_u A_{sf} \quad (3.8)$$

where $\phi_{sf} = 0.75$, area on the shear failure path $A_{sf} = 2t(a + D/2)$, and a is the shortest distance from edge of the pin hole to the edge of the member measured parallel to the direction of the force (see Figure 3.1).

The Canadian code (CSA, 2014) defines the factored bearing resistance of both the pin and pin plate as

$$\phi V_n = \phi_s 1.50 F_y t D \quad (3.9)$$

where $\phi_s = 0.90$. The Eurocode (CEN 2005) defines the factored bearing resistance for both the pin and plate as

$$\phi P_b = \frac{1.5 t D F_y}{\gamma_{M0}} \quad (3.10)$$

where γ_{M0} is equal to 1.00.

A comparison of these code provisions shows that AASHTO Specifications provides the lowest nominal bearing resistance for the pin plates. The nominal value provided by AISC Specification is 80% higher, and the value provided by the Canadian code and Eurocode is 50% higher.

3.1.2 Research Objective

The goal of this research is to evaluate the adequacy of the AASHTO design requirement of pin bearing strength and determine if the level of apparent conservatism is warranted.

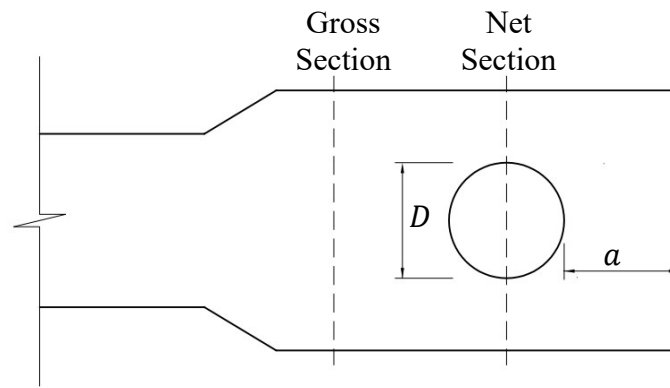


Figure 3.1 Notation and Location of Limit State Sections

3.2 Test Program

3.2.1 General

A total of 8 test specimens (4 pairs, with two nominally identical specimens in each pair) were fabricated. See Table 3.1 for the test matrix. Figure 3.2 shows the pull-plate test assembly. The test plate, which was either A36 steel or A572 Gr. 50 steel, was loaded to bear against a 4-in. diameter pin (6-in. long). The load was then transferred by two splice plates that were bolted to a loading plate. The test plate and the loading plate were 9 in. wide at the connection region. The width of these two plates was reduced to 6 in. so they can fit into the test machine for clamping at the ends. The assemblies were tested with a 600-kip hydraulic test system in the UCSD's Powell Structures Laboratory. The test setup is shown in Figure 3.3.

To ensure that damage would occur in the pin plates, higher strength steels were specified for the reusable 4-in. diameter pin, splice plates, and loading plate. The grade of the pin was A668 Class N, which had a specified minimum yield stress of 140 ksi. A514 steel Grade 100 was specified for both the splice plates and loading plate.

3.2.2 Material Properties

Figure 3.4 shows the stress-strain relationships obtained from tensile coupon tests conducted at UCSD (two coupons were tested for each steel grade.) Table 3.2 summarizes the mechanical properties of the steel pin plate materials. Table 3.3 shows the chemical composition of the materials obtained from Certified Mill Test Reports.

3.2.3 Specimen Design

The specimens were designed based on the AASHTO Specifications. Table 3.4 shows the capacities of the test assemblies based on three limit states, i.e., Eqs. (3.2) to (3.4); the design goal was to ensure that bearing on the test plate would govern the design. The table shows the capacities of three limit states based on both the nominal and actual material strengths. The design goal was achieved by providing a sufficient margin of safety to ensure that bearing of the test plate is the governing failure mode (see bold-faced values). Taking Table 3.4(a) for example, the nominal strengths (P_n) for gross section yielding and net section rupture are at least 2.25 and 1.61, respectively, higher than that for plate bearing.

The test specimens were also checked against the design provisions of the AISC Specification. Table 3.5 shows the results based on four limit states, i.e., Eqs. (3.5) to (3.8). Although the allowable bearing stress provided the AISC Specification is 1.8 times that of AASHTO Specifications, bearing on the plate still governs for Specimens C1 and C2. However, AISC Specification predicts that net section rupture, not plate bearing, would govern for Specimens D1 and D2.

3.2.4 Instrumentation

The instrumentation is shown in Figure 3.5. Displacement transducers L1 and L2 measured the vertical displacement at the center of the 4-in. pin relative to the base. L3 and L4 measured the vertical displacement of the test plate at a location 1.0 in. from the end (free edge) of test plate. Then the bearing deformation of the tension plate is estimated as follows.

$$\Delta_b = \frac{L1 + L2}{2} - \frac{L3 + L4}{2} \quad (3.11)$$

Figure 3.5 also shows the location of uniaxial strain gauges. Uniaxial strain gauges measured the strain at the test plate (S1 to S3).

Table 3.1 Plate Bearing Test Matrix

Test Plate	Specimen Pair			
	C1	C2	D1	D2
Thickness (in.)	1.0	1.5	1.0	1.5
Steel Grade	A36		A572 Gr. 50	

Table 3.2 Plate Mechanical Characteristics

Specimen No.	Steel Grade (Heat No.)	Yield Stress (ksi)	Tensile Strength (ksi)	Elong. (%)
Pin	A668 Class N (237P237)	[165.0]	[181.0]	[15.0]
Test Plate	C1	A36 (PL16104091) 41.9, 40.0 (41.0) [53.5]	65.9, 65.9 (65.9) [77.6]	45.8, 45.6 (45.7) [24.5]
	C2	A36 (N161770) 42.5, 43.2 (42.9)	69.7, 71.3 (70.5)	47.4, 47.4 (47.4)
	D1	A572 Gr.50 (A113014) 51.2, 51.2 (51.2) [57.6]	78.4, 78.1 (78.3) [80.9]	40.3, 34.5 (37.4) [25.0]
	D2	A572 Gr.50 (A8N0697) 51.6, 54.9 (53.3) [54.9]	78.9, 77.9 (78.4) [79.3]	47.8, 42.4 (45.1) [34.9]
Loading & Splice Plates	A514 (LE0250)	111.8, 113.8 (112.8) [114.5]	120.1, 121.5 (120.8) [122.0]	27.1, 26.4 (26.7) [40.0]

Note: Values in () are mean values from two coupon tests; values in [] are from Certified Mill Test Reports.

Table 3.3 Chemical Compositions from Mill Certificates

Specimen No.	C	Mn	P	S	Si	Cu	Ni	Cr	Mo	V	CE (%)
Pin	0.42	0.72	0.009	0.009	0.26	0.12	1.89	0.81	0.23	0.043	0.85
Plates C1	0.17	0.84	0.01	0.05	0.25	0.24	0.08	0.11	0.02	0.018	0.36
Plates C2	-	-	-	-	-	-	-	-	-	-	-
Plates D1	0.17	1.10	0.021	0.003	0.21	0.02	0.01	0.02	0.01	0.002	0.36
Plates D2	0.19	1.16	0.013	0.004	0.18	0.17	0.05	0.06	$\frac{0.02}{3}$	0.073	0.44
Loading & Splice Plates	0.19	0.87	0.010	0.003	0.32	0.03	0.02	0.58	0.21	0.044	0.51

$$CE = C + \frac{Mn}{6} + \frac{Cr+Mo+V}{5} + \frac{Ni+Cu}{15}$$

Table 3.4 Tensile Strength of Pin-Connected Plates Based on AASHTO Specifications

(a) Based on Nominal Yield and Tensile Strengths

Test Specimens		C1		C2		D1		D2	
t (in.)		1.0		1.5		1.0		1.5	
F_y (ksi)		36.0		36.0		50.0		50.0	
F_u (ksi)		58.0		58.0		65.0		65.0	
A_g (in. ²)		6.0		9.0		6.0		9.0	
A_n (in. ²)		4.97		7.45		4.97		7.45	
Capacity		P_n	$\phi_t P_n$						
Limit State	Plate bearing	144	144	216	216	200	200	300	300
	Gross section yielding	324	308	486	462	450	428	675	641
	Net section rupture	288	245	432	367	323	275	484	412

(b) Based on Actual Yield and Tensile Strengths

Test Specimens		C1		C2		D1		D2	
t (in.)		1.0		1.5		1.0		1.5	
F_y (ksi)		41		42.9		51.2		53.3	
F_u (ksi)		65.9		70.5		78.3		78.4	
A_g (in. ²)		6.0		9.0		6.0		9.0	
A_n (in. ²)		4.97		7.45		4.97		7.45	
Capacity		P_n	$\phi_t P_n$						
Limit State	Plate bearing	164	164	257	257	205	205	320	320
	Gross section yielding	369	351	579	550	461	438	720	684
	Net section rupture	328	278	525	446	389	331	584	496

Table 3.5 Tensile Strengths of Pin-Connected Plates Based on AISC Specification
(a) Based on Nominal Yield and Tensile Strengths

Test Specimens		C1		C2		D1		D2	
t (in.)		1.0		1.5		1.0		1.5	
F_y (ksi)		36.0		36.0		50.0		50.0	
F_u (ksi)		58.0		58.0		65.0		65.0	
b_e (in.)		2.63		3.63		2.63		3.63	
A_{sf} (in. ²)		11.94		17.91		11.94		17.91	
A_g (in. ²)		6.0		9.0		6.0		9.0	
A_n (in. ²)		4.97		7.45		4.97		7.45	
Capacity		P_n	$\phi_t P_n$						
Limit State	Plate bearing	259	194	389	292	360	270	540	405
	Gross section yield	324	292	486	437	450	405	675	608
	Net section rupture	288	216	432	324	323	242	484	363
	Shear rupture	415	312	623	467	466	349	698	524

(b) Based on Actual Yield and Tensile Strengths

Test Specimens		C1		C2		D1		D2	
t (in.)		1.0		1.5		1.0		1.5	
F_y (ksi)		41.0		42.9		51.2		53.3	
F_u (ksi)		65.9		70.5		78.3		78.4	
b_e (in.)		2.63		3.63		2.63		3.63	
A_{sf} (in. ²)		11.94		17.91		11.94		17.91	
A_g (in. ²)		6.0		9.0		6.0		9.0	
A_n (in. ²) ^a		4.97		7.45		4.97		7.45	
Capacity		P_n	$\phi_t P_n$						
Limit State	Plate bearing	295	221	463	347	369	276	576	432
	Gross section yield	369	332	579	521	461	415	720	648
	Net section rupture	328	246	525	394	389	292	584	438
	Shear rupture	472	354	757	568	561	421	842	632

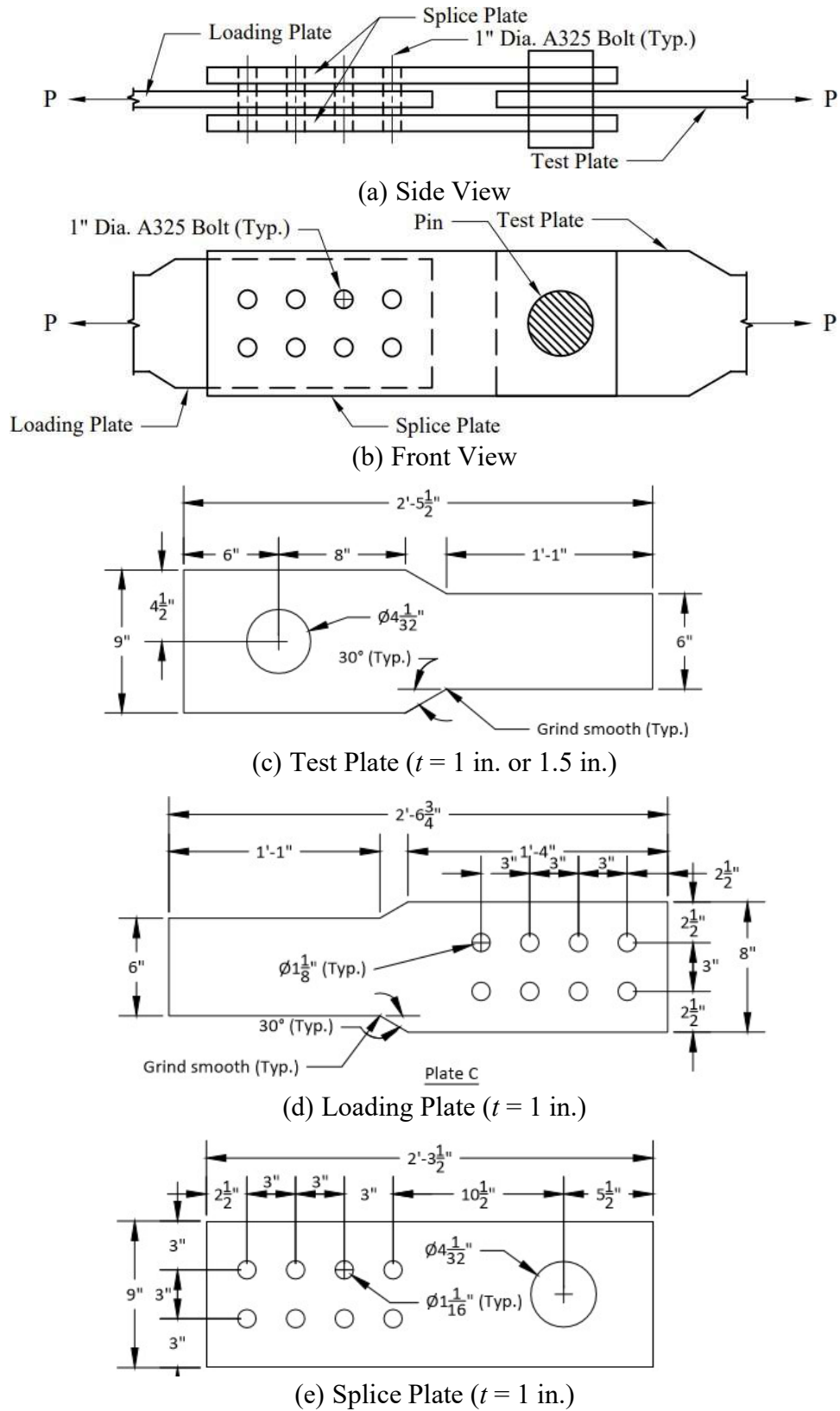
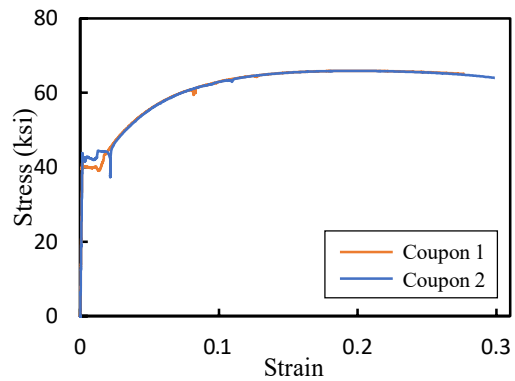


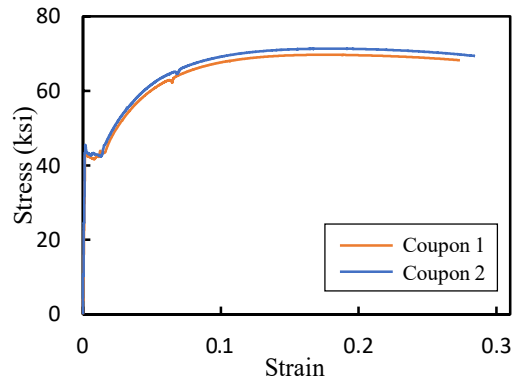
Figure 3.2 Pin Plate Test Assembly



Figure 3.3 Pin Plate Test Setup

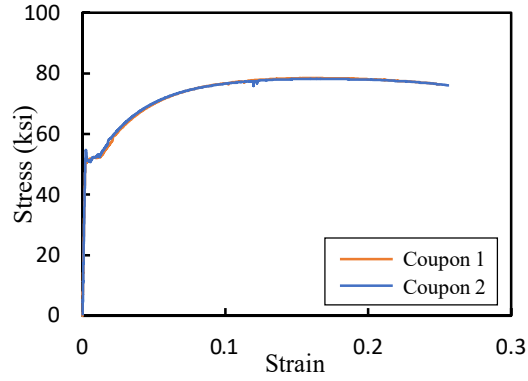


(a) A36 Steel (Plates C1)

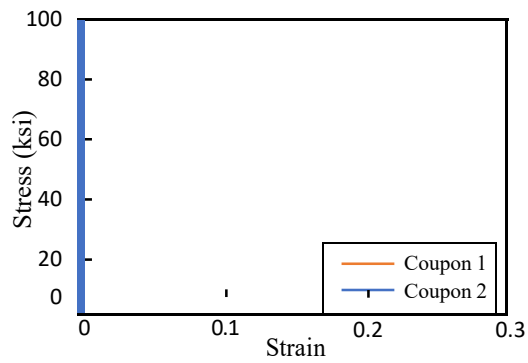


(b) A36 Steel (Plates C2)

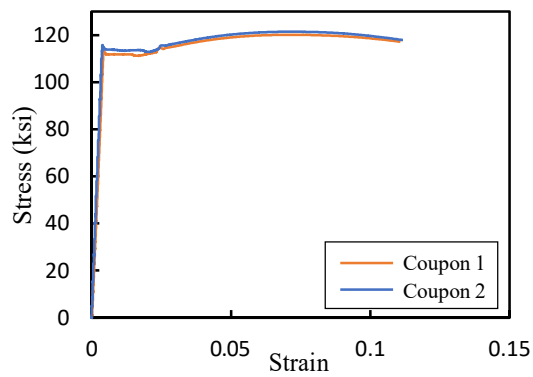
Figure 3.4 Stress-strain Responses from Tensile Coupon Testing (Pin Plate Tests)



(c) A572 Gr. 50 Steel (Plates D1)

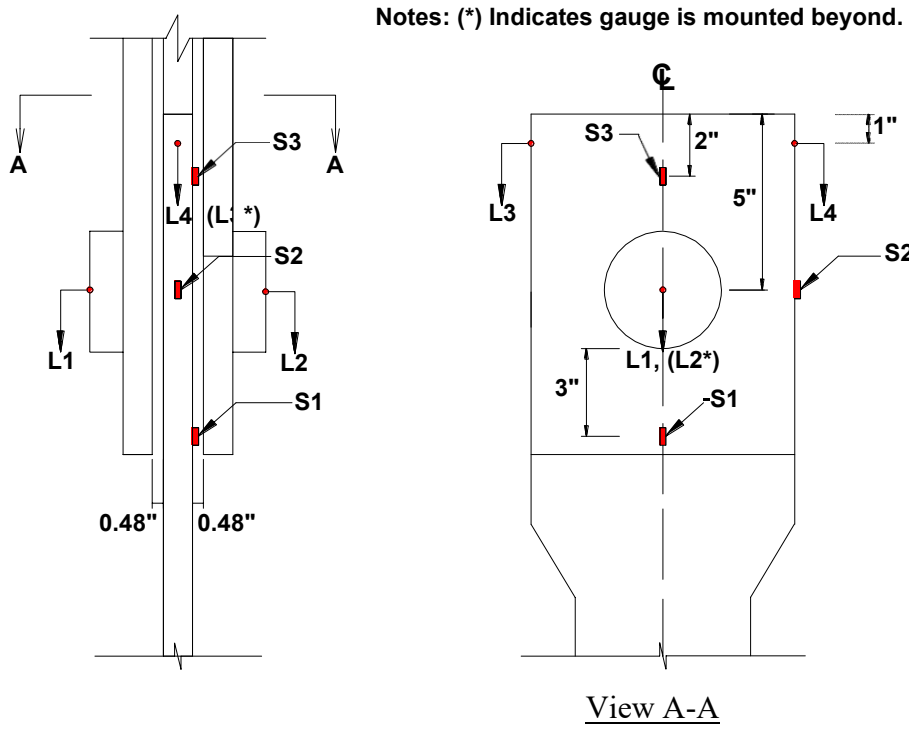


(d) A572 Gr. 50 Steel (Plates D2)



(e) A514 Steel

Figure 3.4 Stress-strain Responses from Tensile Coupon Testing (Pin Plate Tests)
(continued)



(a) Displacement Transducer and Strain Gauge Locations



(b) Mounting of Displacement Transducers

Figure 3.5 Instrumentation for Pin Plate Tests

3.3 Test Results

3.3.1 Series C Specimens (A36 Steel)

3.3.1.1 Specimens C1 ($t = 1.0$ in.)

Figure 3.6 and Figure 3.7 show the failure mode of Specimens C1-1 and C1-2, respectively. Both specimens failed in net section fracture, not the plate bearing mode predicted by both the AASHTO Specifications and the AISC Specification. Necking in the net sections was obvious in these figures.

The global responses are shown in Figure 3.8. In Figure 3.8(a), the moving head displacement of the test machine was used as the abscissa, while the bearing deformation of the test plate estimated by Eq. (3.11) was used in Figure 3.8(b). The measured strains in the test plate are shown in Figure 3.9. Measurement of strain gage S1 indicates that the enlarged section of the test plate in front of the pin remained elastic. S2 measurement showed significant yielding before rupture at the net section. Strain gage S3 showed compressive strains behind the pin due to the bearing action of the pin.

3.3.1.2 Specimens C2 ($t = 1.5$ in.)

The same net section rupture failure mode was observed in Specimens C2-1 and C2-2. See Figure 3.10 to Figure 3.13 for the failure mode and measured responses. Again, the failure mode was not consistent to that predicted by either the AASHTO Specifications or AISC Specification.

3.3.2 Series D Specimens (A572 Gr. 50 Steel)

3.3.2.1 Specimens D1 ($t = 1.0$ in.)

With a higher strength steel grade for the test plates, the failure mode of these two specimens remained the same as that observed in the Series C specimens. See Figure 3.14 to Figure 3.17 for the failure mode and measured responses. Note that the observed failure mode was consistent to that predicted by the AISC Specification, but not the AASHTO Specifications, when the nominal yield and tensile stresses were used; see Table 3.5(a).

3.3.2.2 Specimens D2 ($t = 1.5$ in.)

This pair of specimens had the highest capacity. The yielding pattern was very similar to the other specimens (see Figure 3.18 and Figure 3.19). But testing had to be stopped

before net section rupture occurred due to the capacity limitation of the test machine (about 600 kips). Figure 3.20 shows the measured responses. Both the yielding pattern and measured strain responses in Figure 3.21 indicate that these two specimens would also fail in net section rupture had more load been applied to the specimens. Therefore, the measured peak loads represent the lower-bound strengths of these two specimens.



(a) End of Test



(b) Failure Mode

Figure 3.6 Specimen C1-1: Deformed Shape

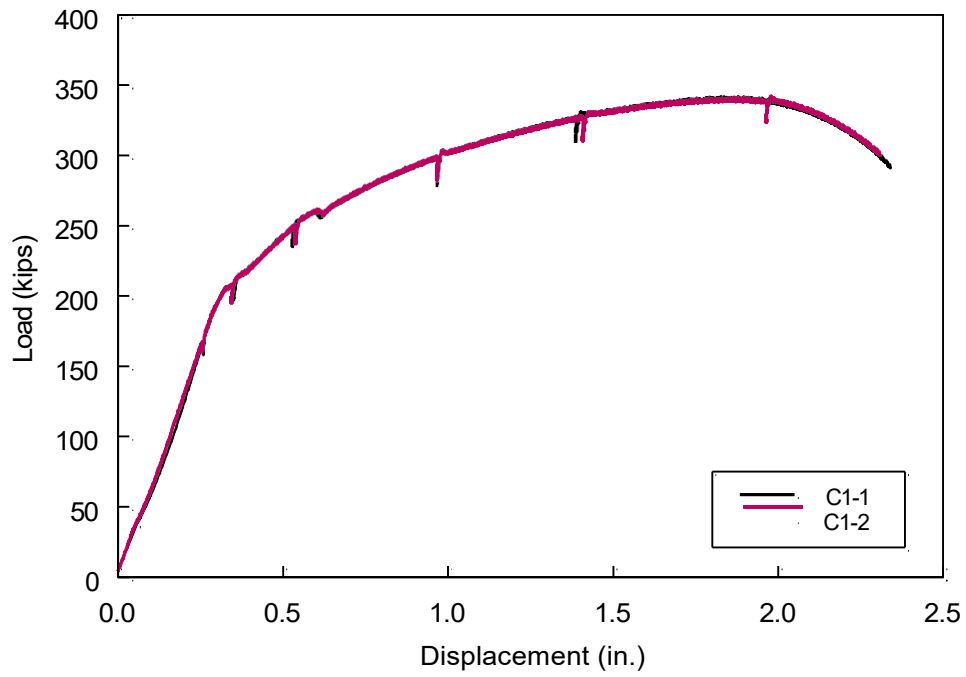


(a) End of Test

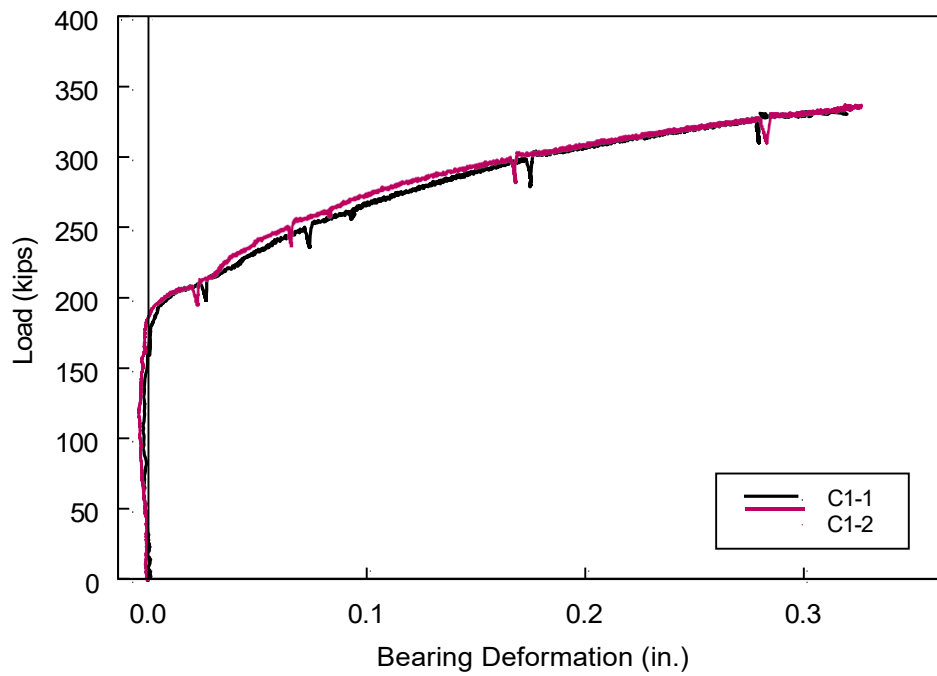


(b) Failure Mode

Figure 3.7 Specimen C1-2: Deformed Shape

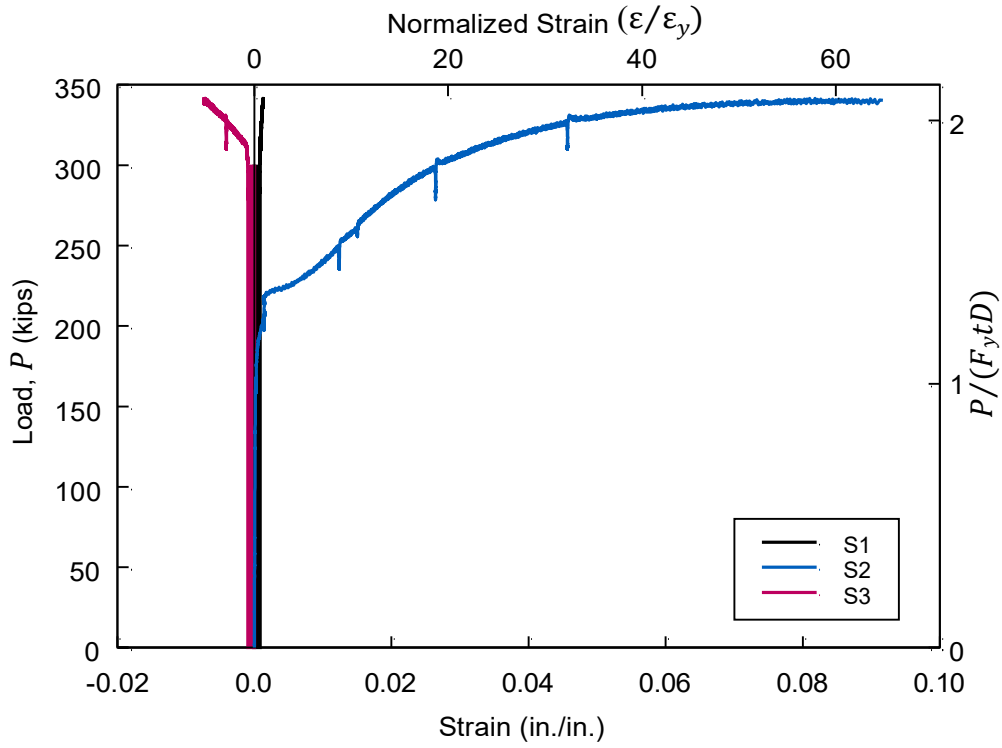


(a) Applied Load vs. Moving Head Displacement

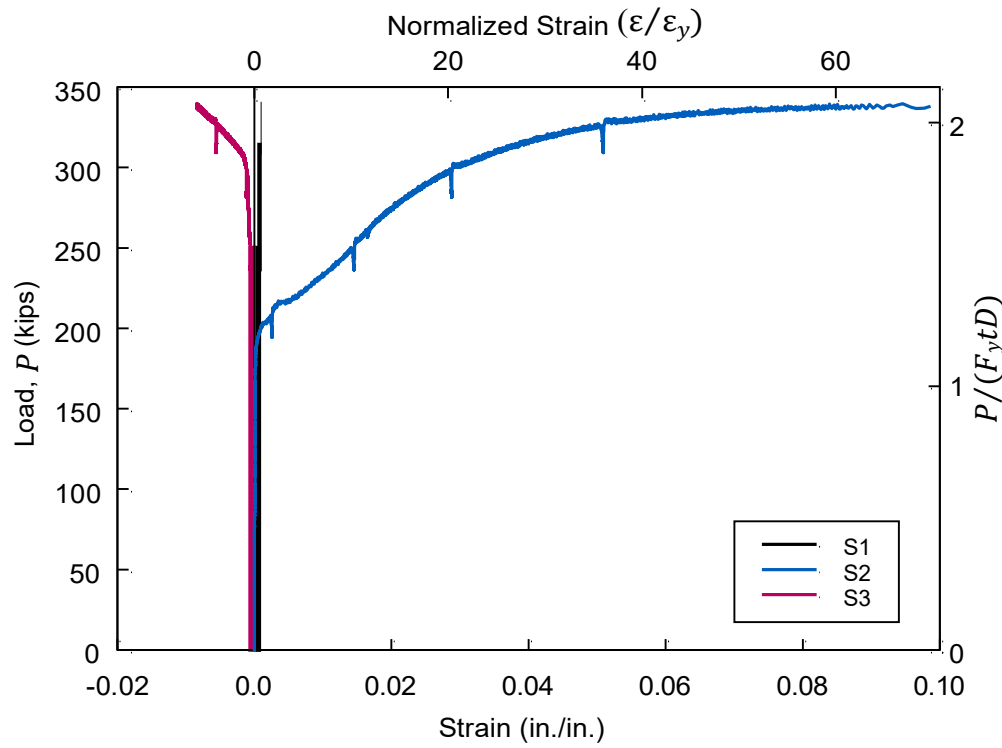


(b) Applied Load vs. Bearing Deformation

Figure 3.8 Specimen C1: Global Response



(a) Specimen C1-1

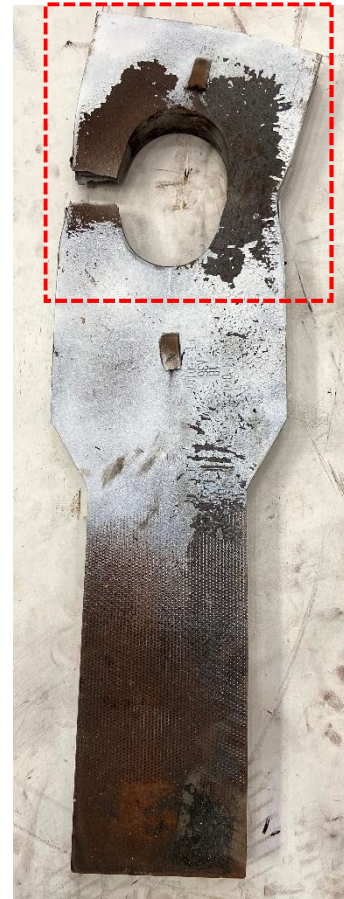


(b) Specimen C1-2

Figure 3.9 Specimen C1: Strain Response



(a) End of Test

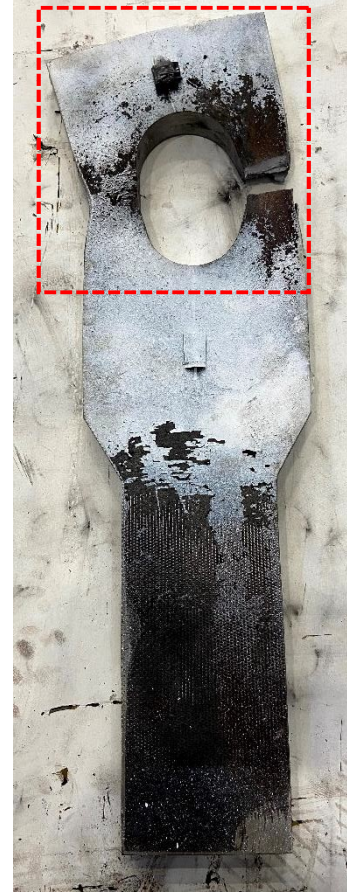


(b) Failure Mode

Figure 3.10 Specimen C2-1: Deformed Shape

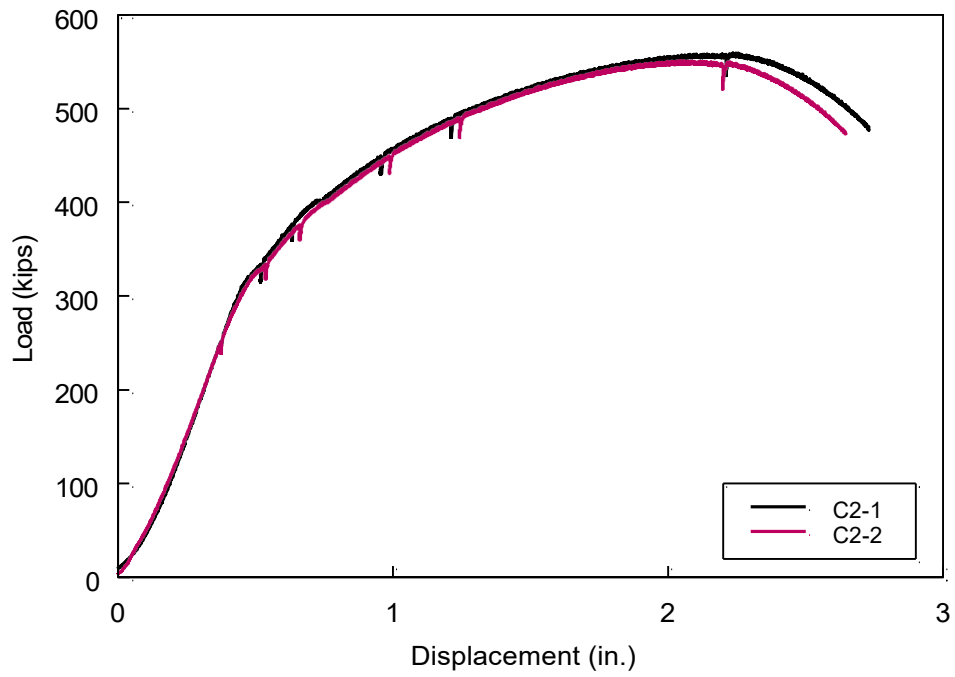


(a) End of Test

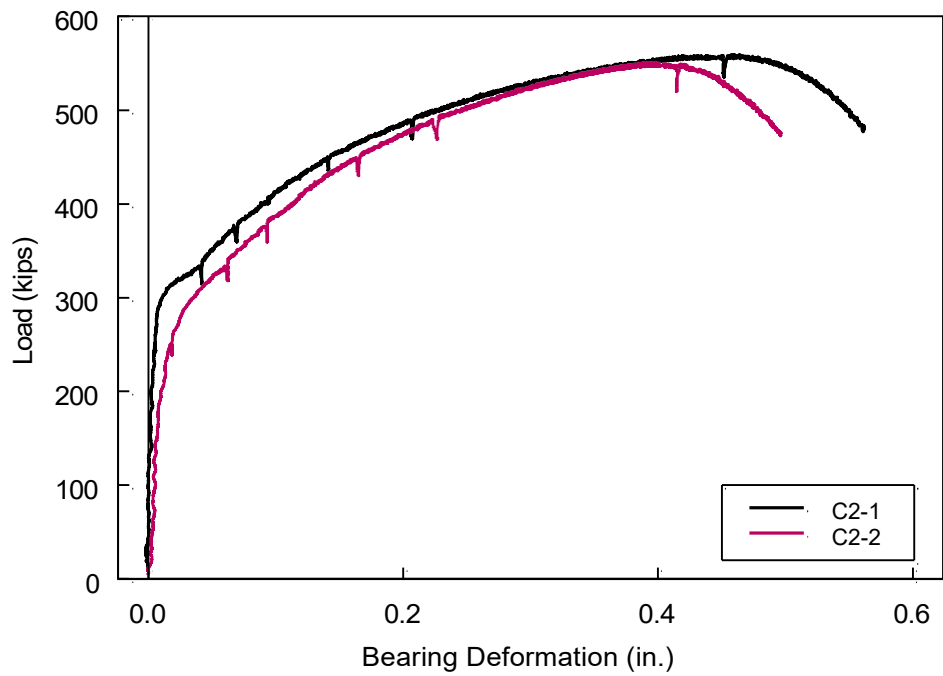


(b) Failure Mode

Figure 3.11 Specimen C2-2: Deformed Shape



(a) Applied Load vs. Moving Head Displacement



(b) Applied Load vs. Bearing Deformation

Figure 3.12 Specimen C2: Global Response

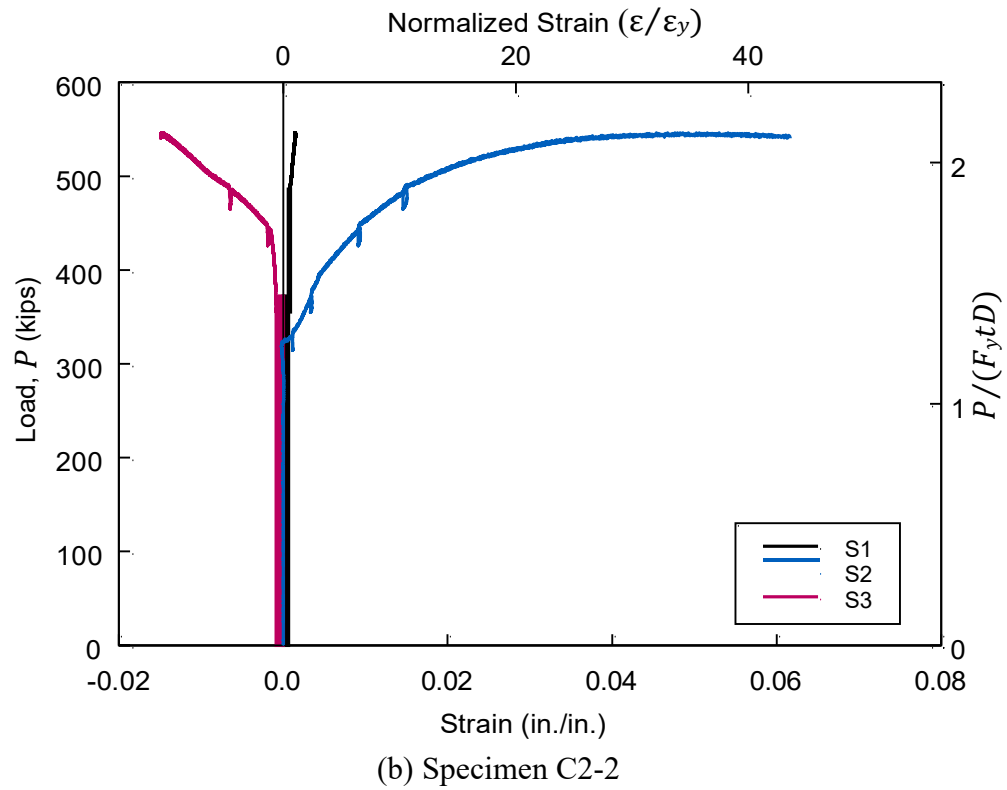
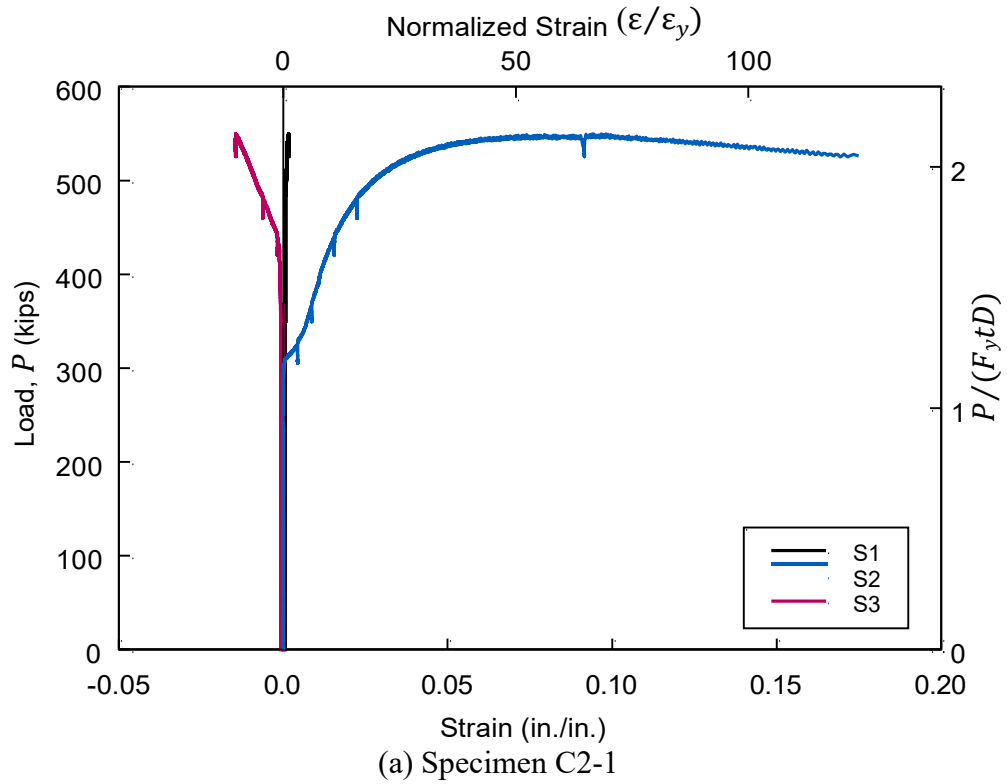
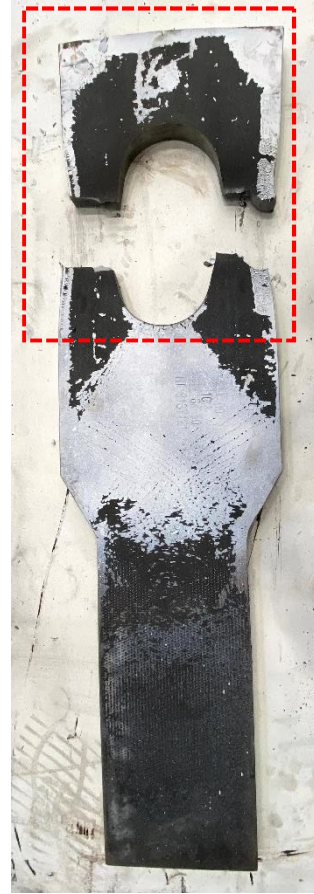


Figure 3.13 Specimen C2: Strain Response



(a) End of Test



(b) Failure Mode

Figure 3.14 Specimen D1-1: Deformed Shape

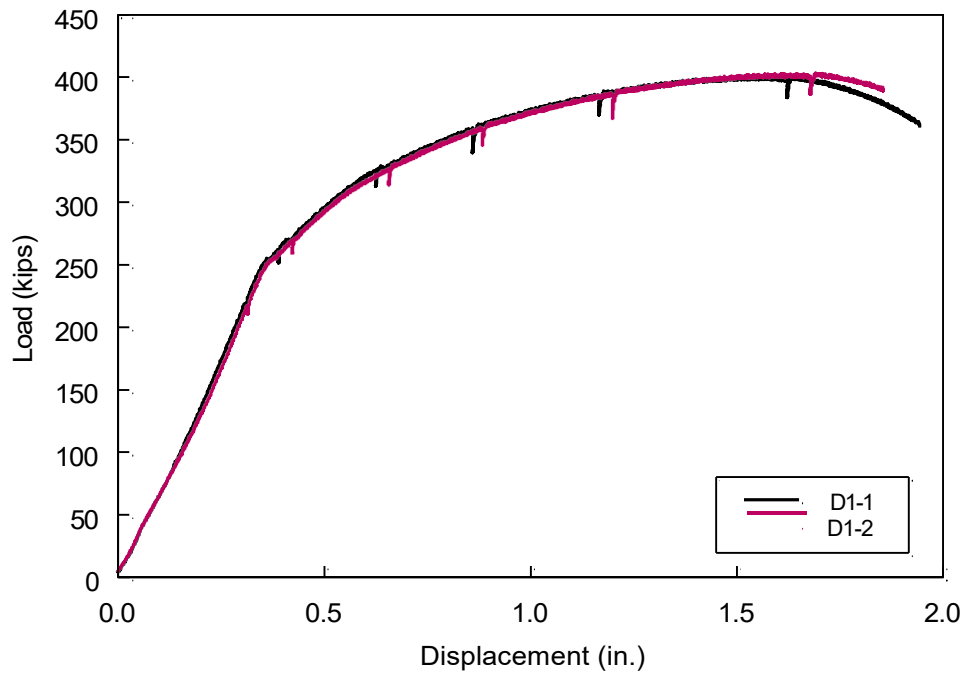


(a) End of Test

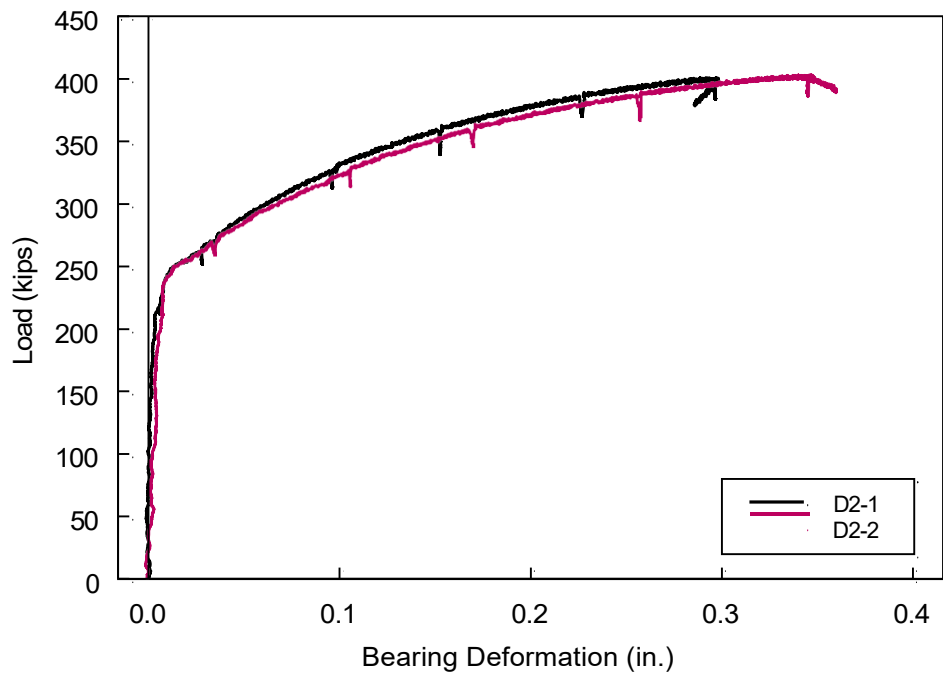


(b) Failure Mode

Figure 3.15 Specimen D1-2: Deformed Shape

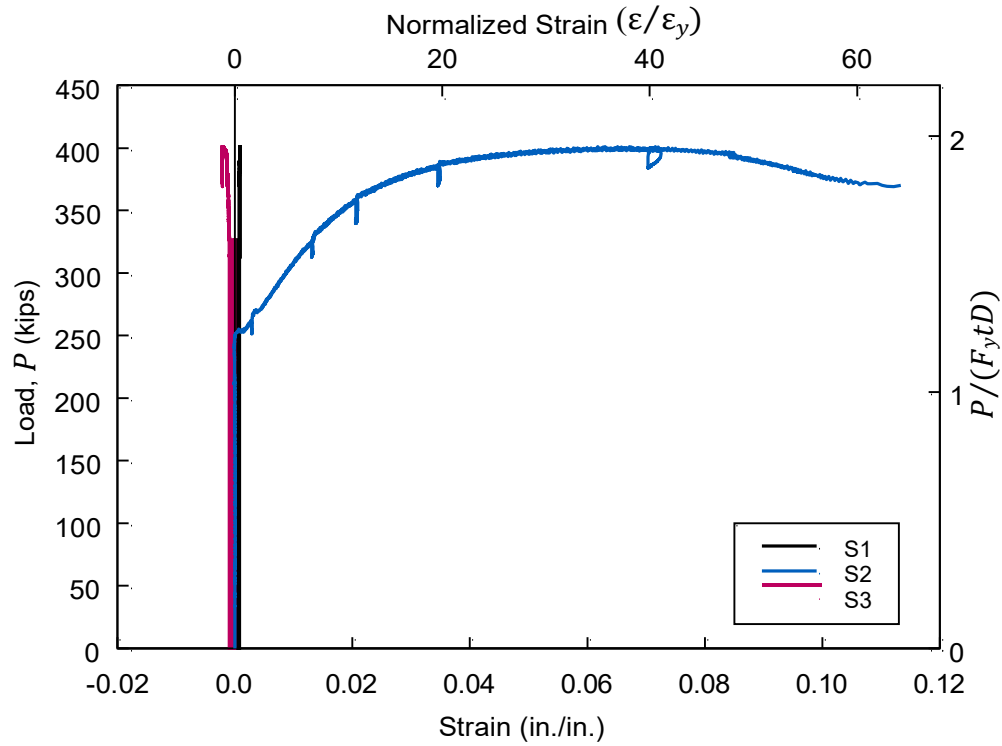


(a) Applied Load vs. Moving Head Displacement

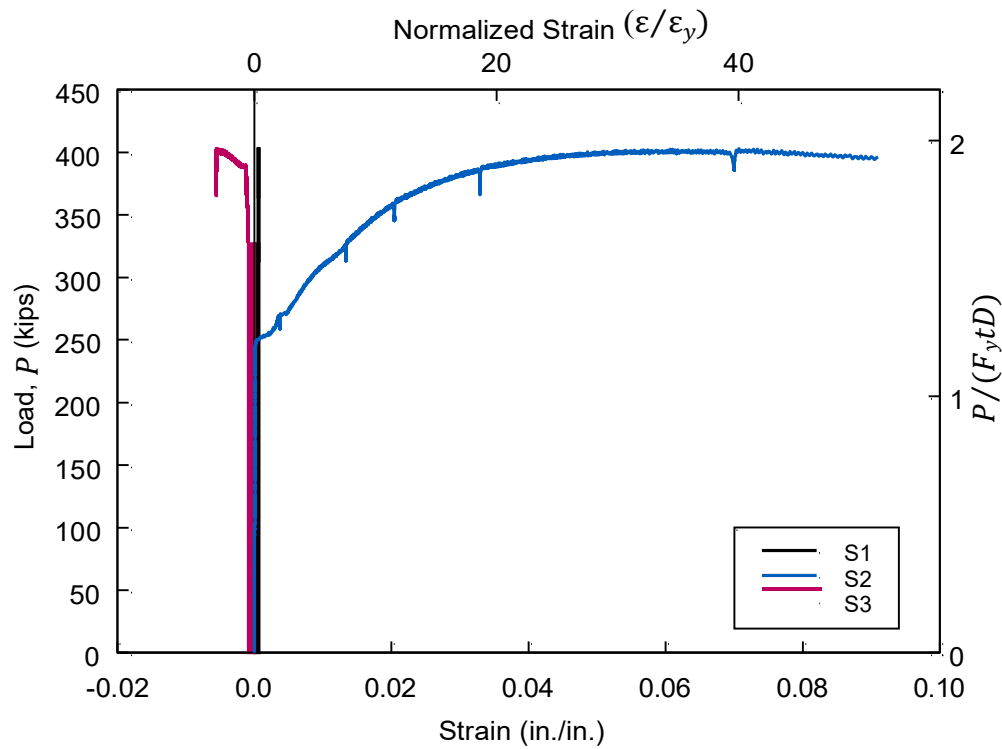


(b) Applied Load vs. Bearing Deformation

Figure 3.16 Specimen D1: Global Response



(a) Specimen D1-1



(b) Specimen D1-2

Figure 3.17 Specimen D1: Strain Response



(a) End of Test



(b) Failure Mode

Figure 3.18 Specimen D2-1: Deformed Shape

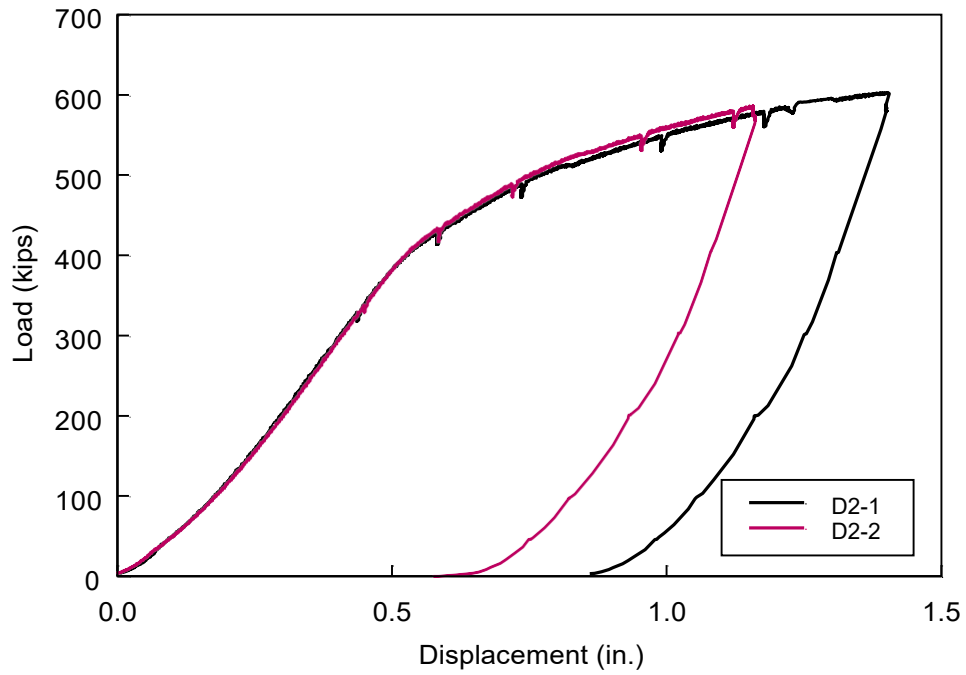


(a) End of Test

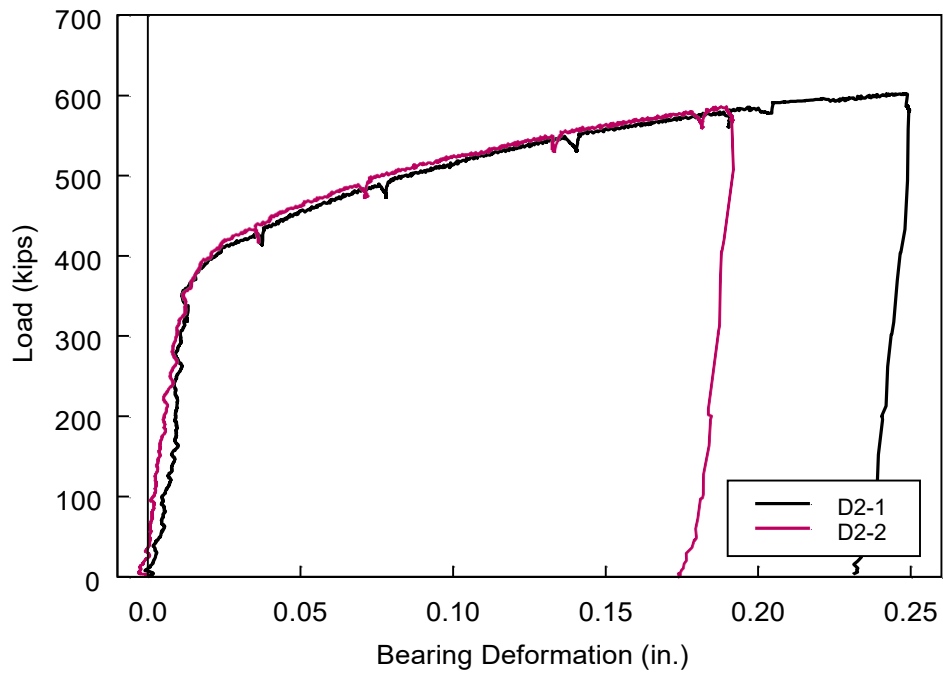


(b) Failure Mode

Figure 3.19 Specimen D2-2: Deformed Shape

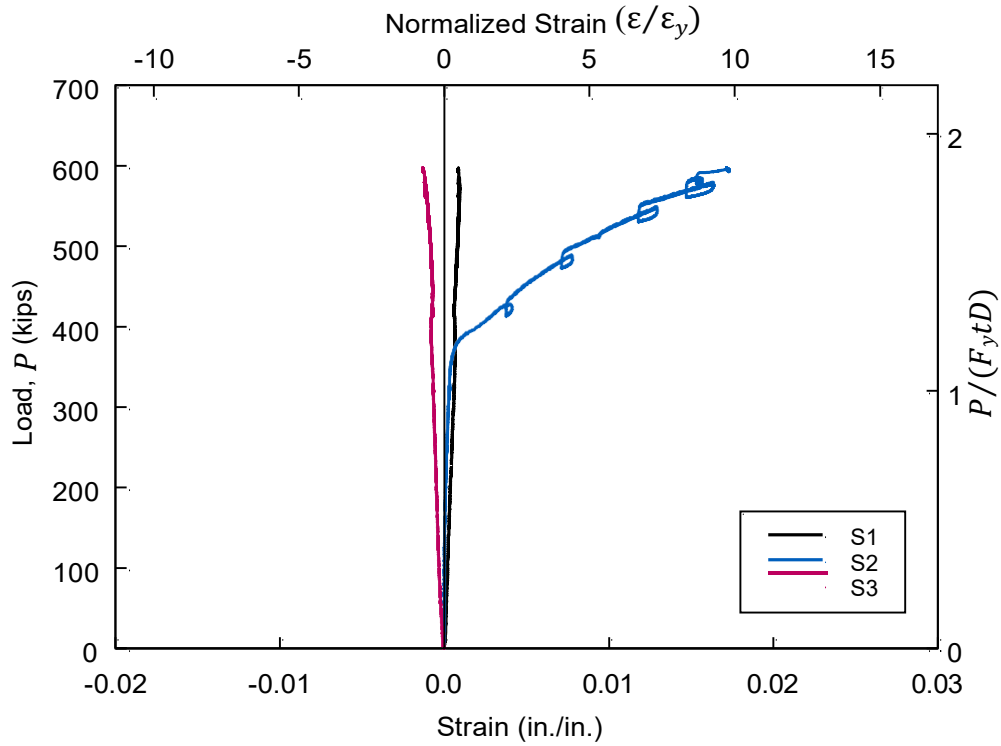


(a) Applied Load vs. Moving Head Displacement

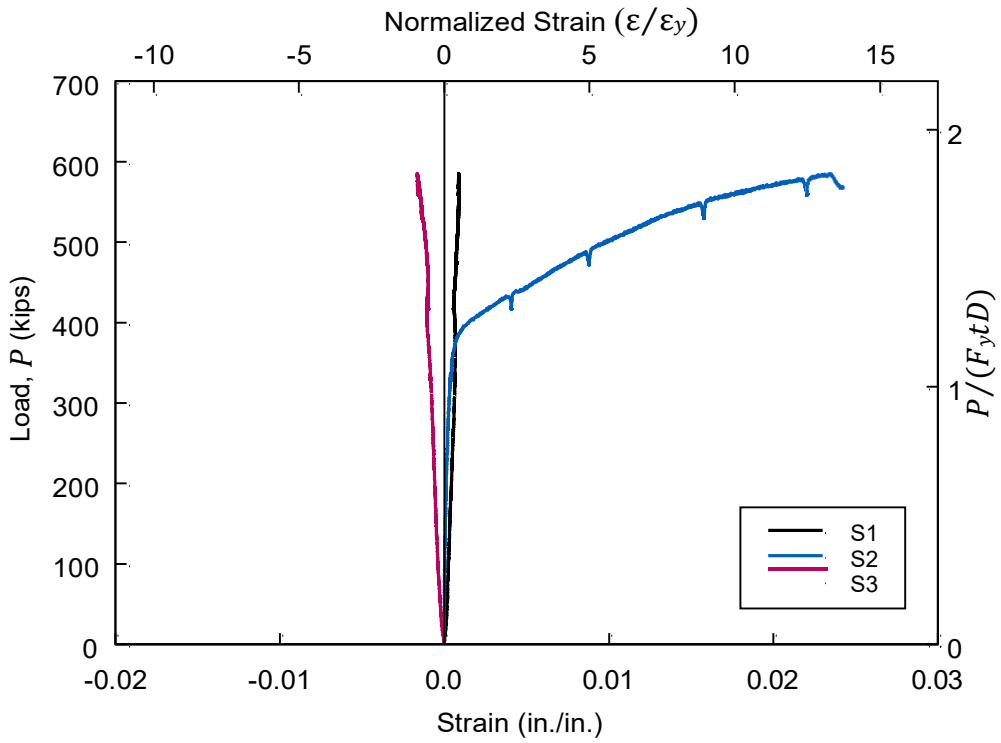


(b) Applied Load vs. Bearing Deformation

Figure 3.20 Specimen D2: Global Response



(a) Specimen D2-1



(b) Specimen D2-2

Figure 3.21 Specimen D2: Strain Response

3.4 Analysis of Test Results and FEM Correlation

3.4.1 Summary of Test Results

Figure 3.22 summarizes the failure mode. Although the AASHTO Specifications predict a plate bearing failure mode for all specimens (Table 3.4), the actual failure is governed by net section rupture at the 4-in. pin hole. The AISC Specification predicts that all specimens would fail in plate bearing, except that net section rupture would govern when the nominal yield and tensile stresses are used to compute the nominal strength [see Table 3.5(a)].

Figure 3.23 summarizes the global responses of the test specimens. Two nominally identical test specimen were tested for each pair. This figure shows that the response in each pair is very reproducible. A summary of the peak strength achieved in each test is provided in Table 3.6.

3.4.2 Comparison of Test and Code-Predicted Strengths

Eq. (3.4) is the factored bearing resistance on pin plates per the AASHTO Specifications. The applied load in the global response plots in Figure 3.23 is normalized by (tDF_y) , where the measured yield stress of the tension plate is used as F_y ; the normalized results are summarized in Figure 3.24(a). Since the response of two nominally identical specimen in each pair behaved similarly, only one specimen from each pair is presented in the figure for clarity. It shows that the capacity specified in the AASHTO Specifications is very conservative. The nominal bearing strength of the plate based on the AISC Specification is 1.8 times that of the AASHTO Specifications [see Eq. (3.5)]. The figure shows that the AISC Specification provides a much reasonable, yet still somewhat conservative, prediction of the ultimate bearing strength.

The AASHTO Specifications do not provide a bearing resistance for serviceability considerations. If, however, such a requirement is needed, Figure 3.24(a) shows that the following can be used:

$$\phi P_b = \phi_b(1.2tD)F_y \quad (3.12)$$

For comparison purposes, Bridge et al. (2001) also proposed an equation for serviceability load condition which limits the bearing deformation to 2% of the pin diameter:

$$\phi P_b = \phi_b(1.6tD)F_y \quad (3.13)$$

But Figure 3.24(a) shows that using a coefficient of 1.6 instead of 1.2 is not conservative as plastic deformation would result. With the proposed service strength in (3.12), the bearing deformation is no more than 0.5 % of the 4-in. pins tested.

By using the measured F_u of the pin plate to normalize the measured load, Figure 3.24(b) shows that the ultimate bearing resistance of the plate can also be predicted, still conservatively but to a less extent, by the following expression:

$$\phi P_b = \phi_b(1.2tD)F_u \quad (3.14)$$

Bridge et al. (2001) also proposed an ultimate bearing resistance:

$$\phi P_b = \phi_b(3.2tD)F_u \quad (3.15)$$

Note that this equation uses F_u , not F_y , to compute the bearing strength. The strength is 267% that from Eq. (3.14), probably because the specimens tested in this research program all failed prematurely in net section rupture. Eqs. (3.12) and (3.14) proposed for both the service and strength limit states effectively means that the effective bearing width is $1.2D$ (see Figure 3.25).

Eq.(3.14) provides a lower-bound prediction for the strength limit state of plate bearing because the governing failure mode is net section fracture instead. Therefore, it is meaningful to use test data to evaluate the limit state of net section fracture. To compute the nominal resistance per the AASHTO Specifications, A_n in Eq. (3.3) is the net area across the pin hole. The AISC Specifications uses an effective net area $2tb_e$ [see Eq. (3.8)], where b_e is the effective edge distance and shall not be taken larger than the actual distance from the edge of the hole to the edge of the part measured in the direction normal to the applied force. For the specimens tested in this research, the latter governs the value of b_e , resulting in an effective net area which is identical to that used in the AASHTO Specifications. That is, the nominal strength is identical in both specifications. Figure 3.26 shows a summary of the global response of four specimens, where the load has been normalized by $F_u A_n$, with F_u being the measured ultimate strength of the pin plate. It shows that the code equations reliably predict the resistance associated with the net section fracture.

3.4.3 Response Correlation with Finite Element Analysis

Finite element analysis (FEA) using the commercial finite element analysis software package, ABAQUS (2014), was performed to provide additional insight into the observed performance. The modeling technique is similar to that use for pin research (see Section 2.5). Figure 3.27 to Figure 3.30 show the correlation. FEA shows significant necking at the net section, which is consistent with the rupture that eventually occurred in testing. In addition, measured strains from S2 (Figure 3.5) that was installed at the edge of the test plate to monitor net section response also correlate reasonably well with the responses predicted by FEA.

Table 3.6 Summary of Peak Strengths (Pin Plate Tests)

Specimen No.		P_u (kips)	$\frac{P_u}{tDF_y}$ (AASHTO)	$\frac{P_u}{1.8F_yA_{pb}}$ (AISC)	$\frac{P_u}{1.2tDF_u}$ (Proposed)
C1	C1-1	341.9	2.08	1.16	1.08
	C1-2	341.7	2.08	1.16	1.08
C2	C2-1	559.3	2.17	1.21	1.10
	C2-2	550.7	2.14	1.19	1.08
D1	D1-1	401.1	1.96	1.09	1.07
	D1-2	402.9	1.97	1.09	1.07
D2	D2-1	602.0	1.88	1.05	1.07
	D2-2	585.2	1.83	1.02	1.04



(a) C1-1



(b) C1-2



(c) C2-1



(d) C2-2



(e) D1-1



(f) D1-2

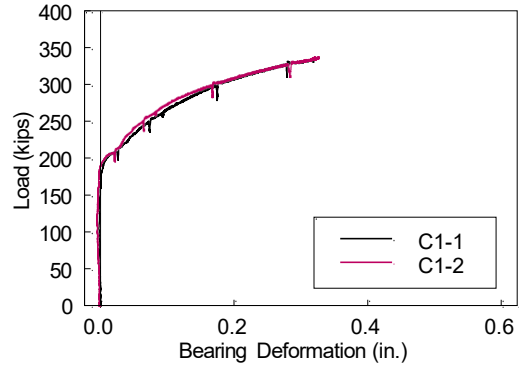


(g) D2-1

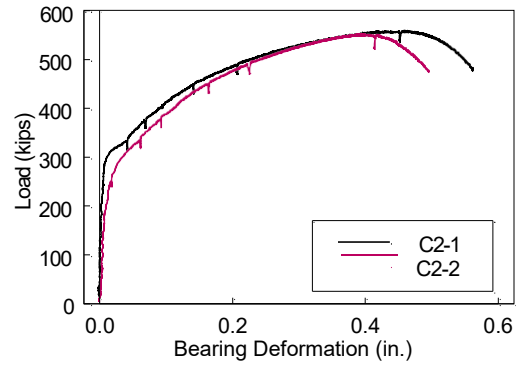


(h) D2-2

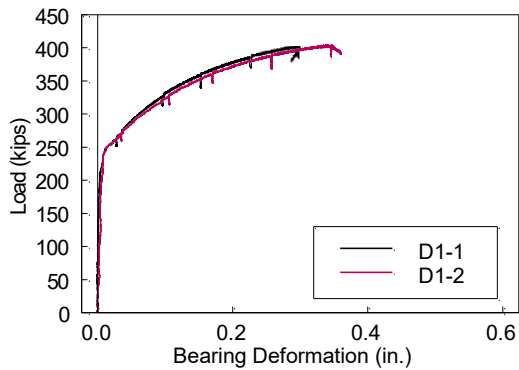
Figure 3.22 Summary of Failure Pattern (Pin Plate Tests)



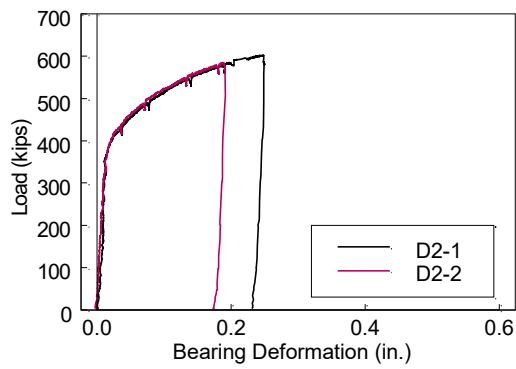
(a) Specimens C1



(b) Specimens C2

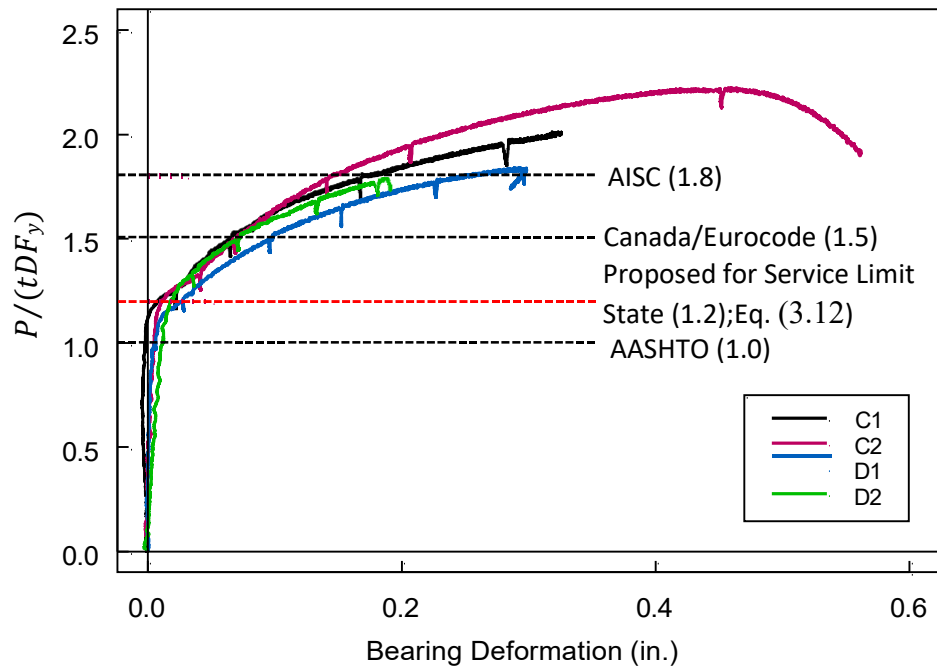


(c) Specimens D1

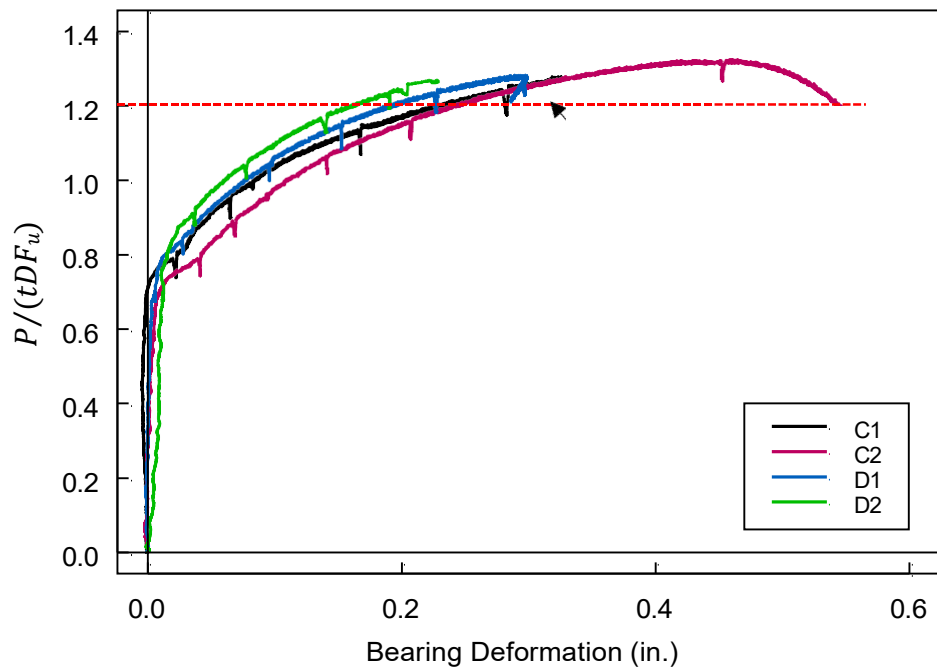


(d) Specimens D2

Figure 3.23 Summary of Global Responses (Pin Plate Tests)



(a) Load Normalized Based on Measured F_y



(b) Load Normalized Based on Measured F_u

Figure 3.24 Normalized Response for Comparison with Bearing Limit State (Pin Plate Tests)

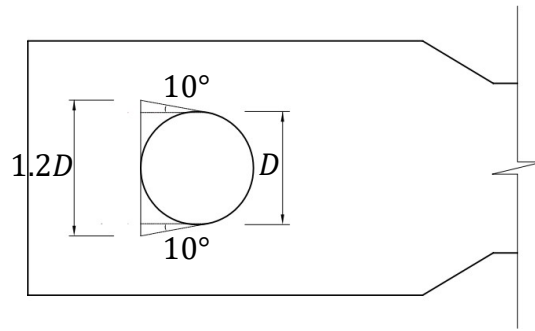


Figure 3.25 Proposed Projected Width for Plate Bearing Strength Prediction

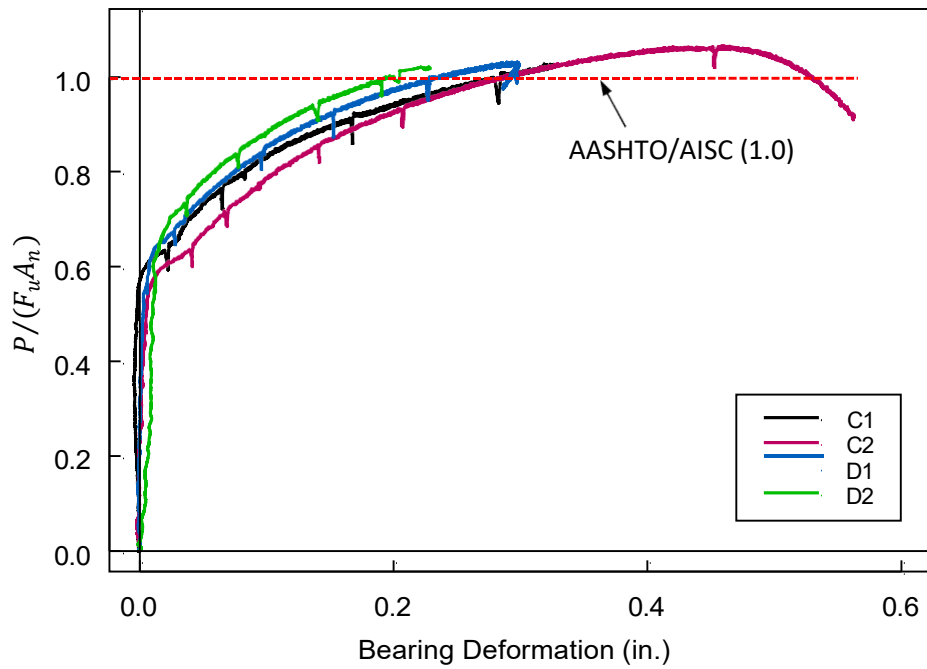
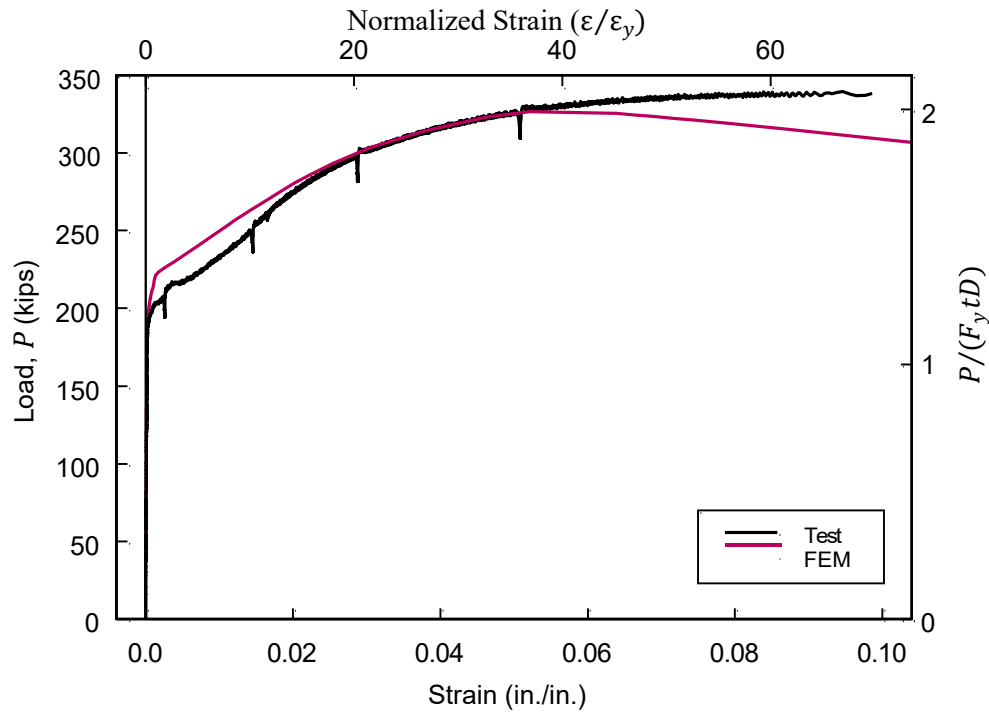
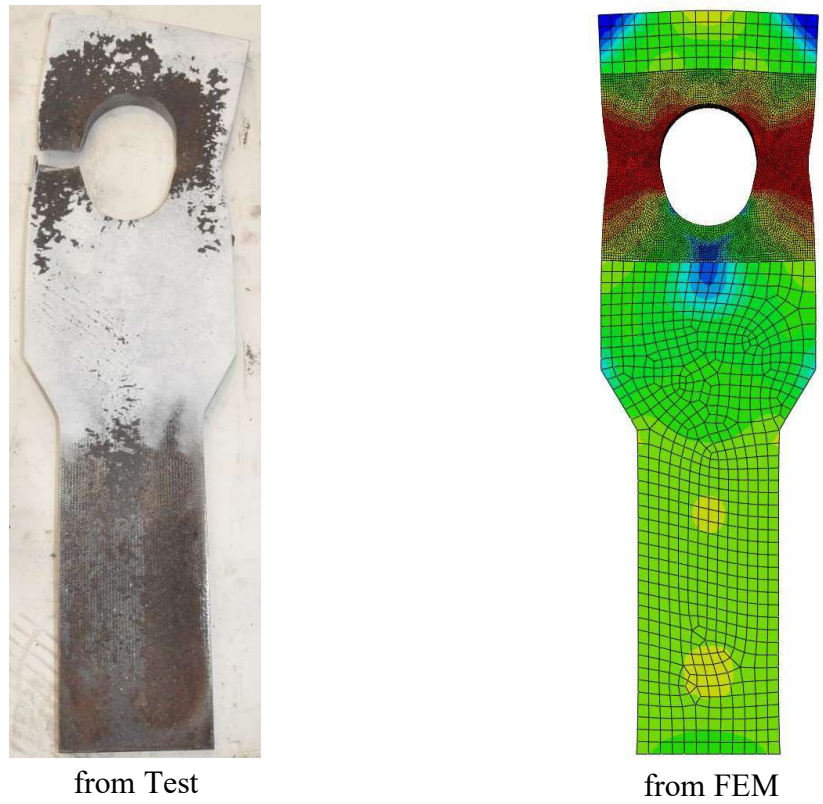


Figure 3.26 Normalized Response for Comparison with Net Section Rupture Limit State (Pin Plate Tests)

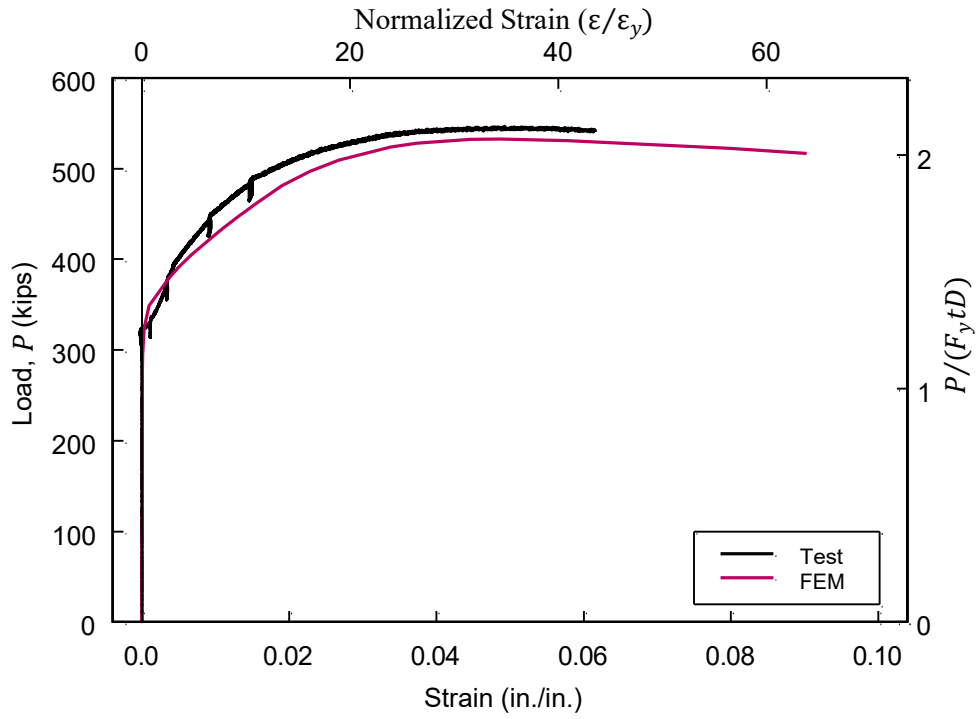


(a) Strain Response at Net Section



(b) Failure Pattern

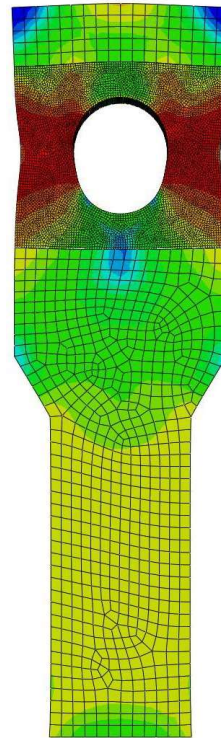
Figure 3.27 FEM Correlation of Specimen C1



(a) Strain Response at Net Section



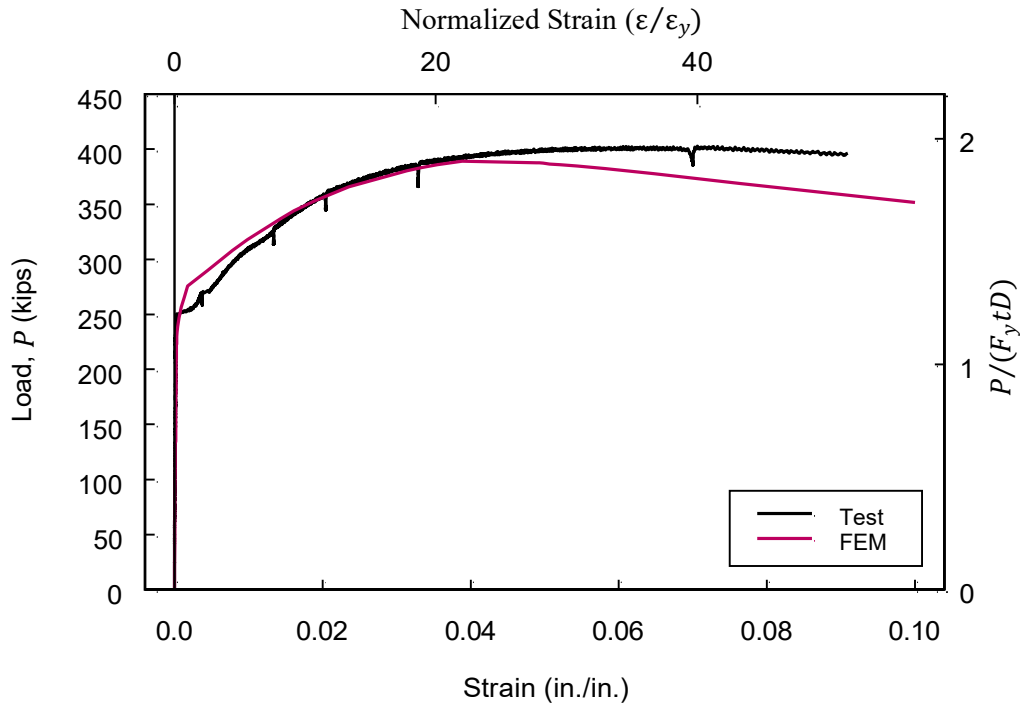
from Test



from FEM

(b) Failure Pattern

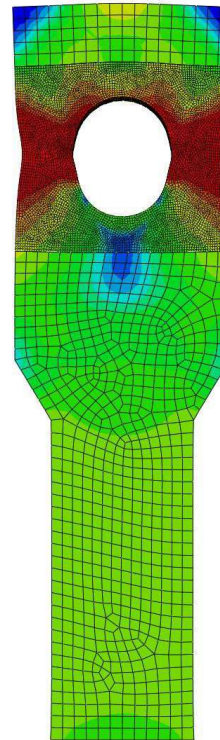
Figure 3.28 FEM Correlation of Specimen C2



(a) Strain Response at Net Section



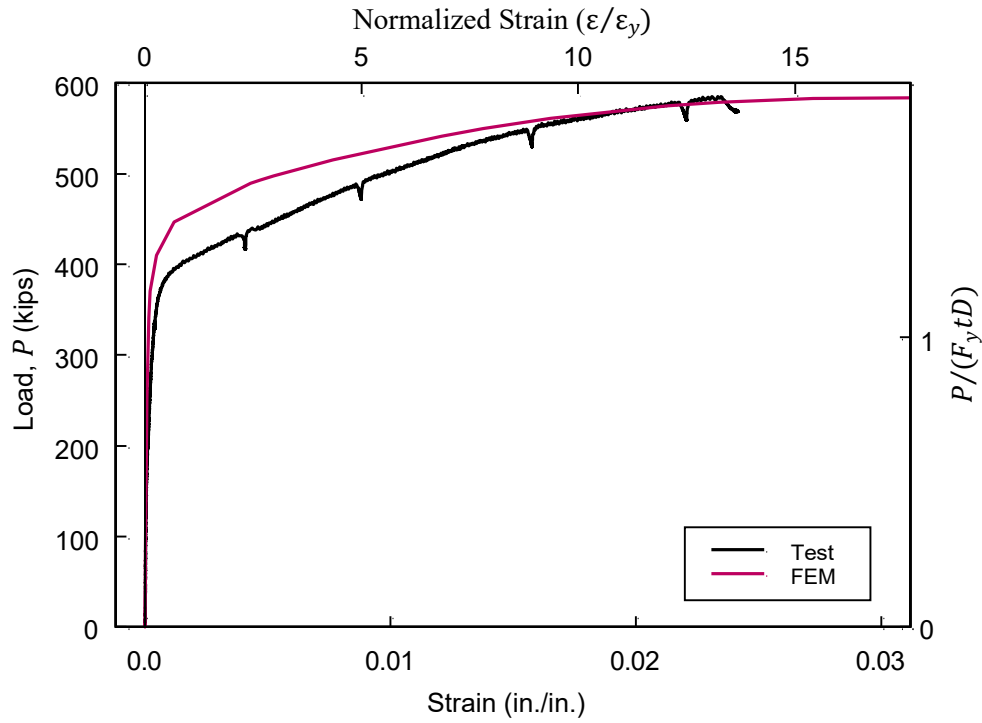
from Test



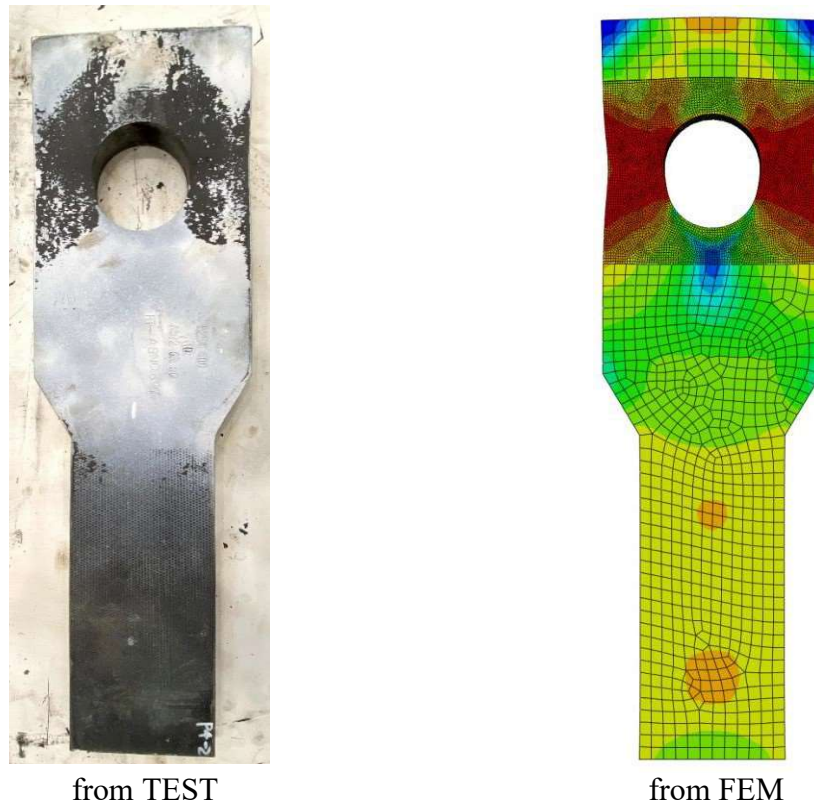
from FEM

(b) Failure Pattern

Figure 3.29 FEM Correlation of Specimen D1



(a) Strain Response at Net Section



(b) Failure Pattern

Figure 3.30 FEM Correlation of Specimen D2

3.5 Summary and Concluding Remarks

3.5.1 Summary

The AASHTO Specifications predict a plate bearing resistance which is significantly lower than those predicted by the AISC Specification, Canadian code, and Eurocode. Four pairs of tension plate assemblies, with two nominally identical specimens in each pair, were tested to failure (see Table 3.1 for the test matrix and Figure 3.2 for the test assembly). Both A36 steel and A572 Gr. 50 steels were included in the test program. High-strength steels were specified for the 4-in. pin, splice plates, and loading plate such that damage would occur in the test plate only. The specimens were designed based on the AASHTO Specifications such that other limit states of the test specimen have a factor of safety of at least 1.6 against plate bearing. A universal test machine was used for testing (Figure 3.3).

3.5.2 Concluding Remarks

The following conclusions can be made from this research.

- (1) While the AASHTO Specifications predict a plate bearing failure mode (Table 3.4), all eight specimens failed in net section rupture at the pin hole (Figure 3.22). The AISC Specification also predicts plate bearing failure mode for Specimens C1 and C2, but net section rupture is predicted for Specimens D1 and D2 when the nominal yield stress and strength are used for the calculations [Table 3.5(a)].
- (2) Since all specimens failed in net section rupture, the measured peak strengths represent the lower-bound resistance of plate bearing. Using these test results to evaluate, conservatively, the plate bearing resistance as a strength limit state, the AISC equation [Eq. (3.5)] predicts reasonably well the ultimate strength but with some conservatism. An improved equation [Eq. (3.14)] is proposed as it reduces the level of conservatism [Figure 3.24(b)]. This equation uses an effective bearing width of $1.2D$ when using the tensile strength of the material (Figure 3.25).
- (3) For serviceability considerations, test results indicated that increasing the current AASHTO bearing resistance by 20% [Figure 3.24(a)] can be used; see Eq. (3.12) for the proposed equation. This equation also uses an effective bearing width of $1.2D$ when using the yield strength of the material.
- (4) Design equations for the limit state of net section rupture in both the AASHTO and AISC Specifications predict well the failure load.

4 BEARING STRENGTH OF STEEL PINS

4.1 Introduction

4.1.1 Statement of Problem

This chapter evaluates the bearing resistance of steel pins. Both the AASHTO LRFD Specifications (AASHTO 2020) and the AISC Specification (AISC 2016) provide design requirements for pin plates and pin-connected tension members. The design requirements are summarized below.

As was mentioned in Section 3.1.1, Section 6.7.6.2.2 of the AASHTO Specifications specify the factored bearing resistance on steel pins as

$$\phi P_b = \phi_b 1.5tDF_y \quad (3.1)$$

where t is thickness of plate, D is the diameter of pin, F_y is the yield strength of the pin, and $\phi_b = 1.00$. But Section 6.8.7 specifies the factored bearing resistance on pin plates by removing the factor 1.5 from the above equation as follows:

$$\phi P_b = \phi_b A_b F_y = \phi_b t D F_y \quad (3.4)$$

where $A_b (= tD)$ is the projected bearing area on the plate, F_y is the yield strength of the plate. Section J7 of the AISC Specification (AISC 2016) considers the limit state of bearing. For bearing on the projected area of pin,

$$\phi P_n = \phi 1.8 F_y A_{pb} \quad (3.5)$$

where $\phi = 0.75$, and the projected bearing area $A_{pb} = Dt$.

The Canadian code defines the factored bearing resistance of both the pin and pin plate as

$$\phi V_n = \phi_s 1.50 F_y D t \quad (3.9)$$

where $\phi_s = 0.90$. The Eurocode defines the factored bearing resistance for both the pin and plate as

$$\phi P_b = \frac{1.5tDF_y}{\gamma_{M0}} \quad (3.10)$$

where γ_{M0} is equal to 1.00.

4.1.2 Research Objective

The goal of this study is to evaluate the adequacy of the AASHTO design requirement of pin bearing strength.

4.2 Test Program

4.2.1 General

A total of five test specimens were fabricated. See Table 4.1 for the test matrix. 3 grades of steel pin (A108 Gr. 1018, A668 Class F, and A668 Class G) and two diameters (2 in. and 3 in.) were used for the test specimens. The original plan was to use the setup similar to that shown in Figure 2.4. Since this test setup would not only introduce localized bearing but also shearing and bending of the pin, it was decided to modify the test setup as that shown in Figure 4.1 and Figure 4.2. That is, the bottom 0.5-in. portion of the pin was removed to produce a flat surface for support directly on a flat surface to eliminate the shearing and bending effect of the pin. The pin was loaded from the top by a loading cradle comprised of a single loading plate attached to a 1-in. thick base, thus producing localized bearing on the pin only. To ensure that damage would occur in the pin, high strength steel (A514 steel with a specified yield stress of 100 ksi) was specified for the loading cradle. The testing was conducted with a 600-kip hydraulic test system at the UCSD's Powell Structures Laboratory.

4.2.2 Material Properties

Figure 4.3 shows the stress-strain relationships obtained from tensile coupon tests conducted at UCSD (two coupons were tested for each steel grade). Table 4.2 summarizes the mechanical properties of the steel materials. Table 4.3 shows the chemical composition of the materials obtained from Certified Mill Test Reports.

4.2.3 Specimen Design

The specimens were designed based on the AASHTO Specifications. Table 4.4 shows the capacities of the test assemblies based on pin and plate limit states, i.e., Eqs. (3.1) and (3.4); the design goal was to ensure that bearing on the test pin would govern the design. When designing the test specimens based on the nominal yield strength of the materials, Table 4.4(a) shows that the design goal was met and a sufficient margin of safety

was provided to ensure that pin bearing would occur. After the pin test specimens were fabricated by a commercial fabricator, tensile coupon testing was conducted. With the actual yield stresses, a design check was performed again, and the results are summarized in Table 4.4(b). It shows that all except Specimen E3 violated the original design intent to have pin bearing as the governing failure mode. Nevertheless, it was shown in pin plate bearing tests (Section 3.4.2) that Eq. (3.4) used in the AASHTO Specifications is very conservative. Conservatively using the proposed Eq. (3.12) instead of Eq. (3.14) to recompute the bearing strength of the loading plate, Table 4.4(b) shows that the original design goal was met.

4.2.4 Instrumentation

The instrumentation is shown in Figure 4.4. Displacement transducers L1 and L2 measured the vertical displacement of the loading cradle relative to the base; also see Figure 4.2. Then the bearing deformation of the pin is estimated as follows.

$$\Delta_b = \frac{L1 + L2}{2} \quad (4.1)$$

Figure 4.4 also shows the location of a rosette strain gauge (R1) on the pin.

Table 4.1 Pin Bearing Test Matrix

Test Plate	Specimen No.				
	E1	E2	E3	F1	F2
Diameter of Pin, D (in.)	3			2	
Steel Grade	A108 Gr. 1018	A108 Gr. 1018	A668 Class G	A108 Gr. 1018	A668 Class F
Thickness of Loading Plate, t (in.)	1/2	3/4	1/2	1	1

Table 4.2 Plate Mechanical Characteristics (Pin Bearing Tests)

Specimen No.	Steel Grade (Heat No.)	Yield Stress (ksi)	Tensile Strength (ksi)	Elong. (%)
Pins E1, E2	A108 Gr. 1018 (A192101)	76.5	85.6	21.7
Pin E3	A668 Class G (A183610)	62.4 [64.0] ^c	100.8 [98.5] ^c	30.6 [27.0] ^c
Pin F1	A108 Gr. 1018 (100797419)	82.7, 81.1 (81.9) ^b	87.5, 88.9 (88.2) ^b	19.5, 22.4 (21.0) ^b
Pin F2	A668 Class F (A113014)	76.2, 76.2 (76.2) ^b [75.0] ^c	116.0, 117.0 (116.5) ^b [114.0] ^c	26.4, 26.7 (26.5) ^b [26.4] ^c
Loading Cradle	A514 (LE0250)	111.8, 113.8 (112.8) ^b [114.5] ^c	120.1, 121.5 (120.8) ^b [122.0] ^c	27.1, 26.4 (26.7) ^b [40.0] ^c

Note: Values in () are mean values from two coupon tests; values in [] are from Certified Mill Test Reports.

Table 4.3 Chemical Compositions from Mill Certificates (Pin Bearing Tests)

Specimen No.	C	Mn	P	S	Si	Cu	Ni	Cr	Mo	V	CE (%)
Pins E1, E2	0.17	0.65	0.006	0.020	0.27	0.21	0.08	0.09	0.02	0.001	0.32
Pin E3	0.40	0.92	0.008	0.007	0.23	0.15	0.09	1.03	0.23	0.002	0.82
Pin F1	0.18	0.77	0.012	0.023	0.30	0.20	0.08	0.08	0.02	0.003	0.35
Pin F2	0.45	0.63	0.015	0.022	0.28	0.30	0.11	0.13	0.04	0.002	0.62
Loading Cradle	0.19	0.87	0.010	0.003	0.32	0.03	0.02	0.58	0.21	0.044	0.51

$$CE = C + \frac{Mn}{6} + \frac{Cr+Mo+V}{5} + \frac{Ni+Cu}{15}$$

Table 4.4 Bearing Strength of Pin Based on AASHTO Specifications

(a) Based on Nominal Yield Strengths

Test Specimens		E1	E2	E3	F1	F2
t (in.)		0.5	0.75	0.5	1.0	1.0
$F_{yn, Pin}$ (ksi)		40.0	40.0	50.0	40.0	50.0
$F_{yn, Plate}$ (ksi)		100.0	100.0	100.0	100.0	100.0
Capacity (kips)		$P_n(\phi_b=1)$	$P_n(\phi_b=1)$	$P_n(\phi_b=1)$	$P_n(\phi_b=1)$	$P_n(\phi_b=1)$
Limit State	Bearing on Pin ^a	90	135	112.5	120	150
	Bearing on Loading Cradle ^b	150	225	150	200	200
	Bearing on Loading Cradle ^c	180	270	180	240	240

(b) Based on Actual Yield Strengths

Test Specimens		E1	E2	E3	F1	F2
t (in.)		0.5	0.75	0.5	1.0	1.0
$F_{ya, Pin}$ (ksi)		81.9	81.9	64.0	81.9	75.9
$F_{ya, Plate}$ (ksi)		112.5	112.5	112.5	112.5	112.5
Capacity (kips)		$P_n(\phi_b = 1)$				
Limit State	Bearing on Pin ^a	184.3	276.4	144	245.7	227.7
	Bearing on Loading Cradle ^b	168.8	253.2	168.8	225	225
	Bearing on Loading Cradle ^c	202.5	303.8	202.5	270	270

^a Eq. (3.1), where F_y is based on pin.

^b Eq. (3.4), where F_y is based on cradle.

^c Eq. (3.12), from pin plate bearing research, where F_y is based on cradle.

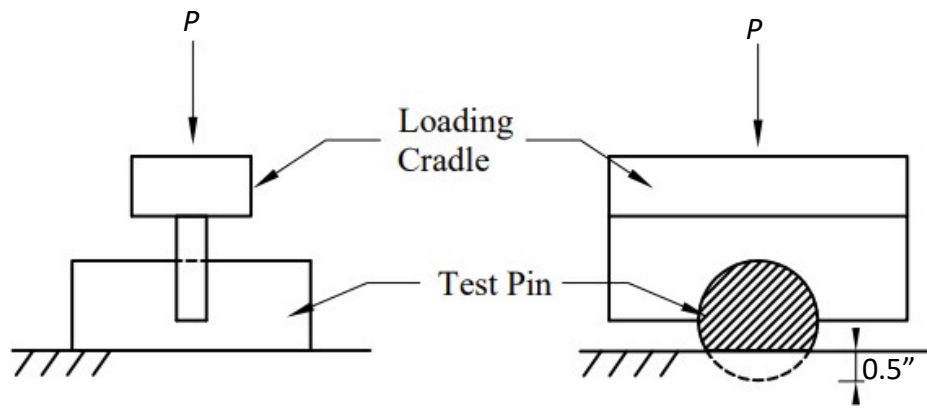


Figure 4.1 Test Assembly (Pin Bearing Tests)

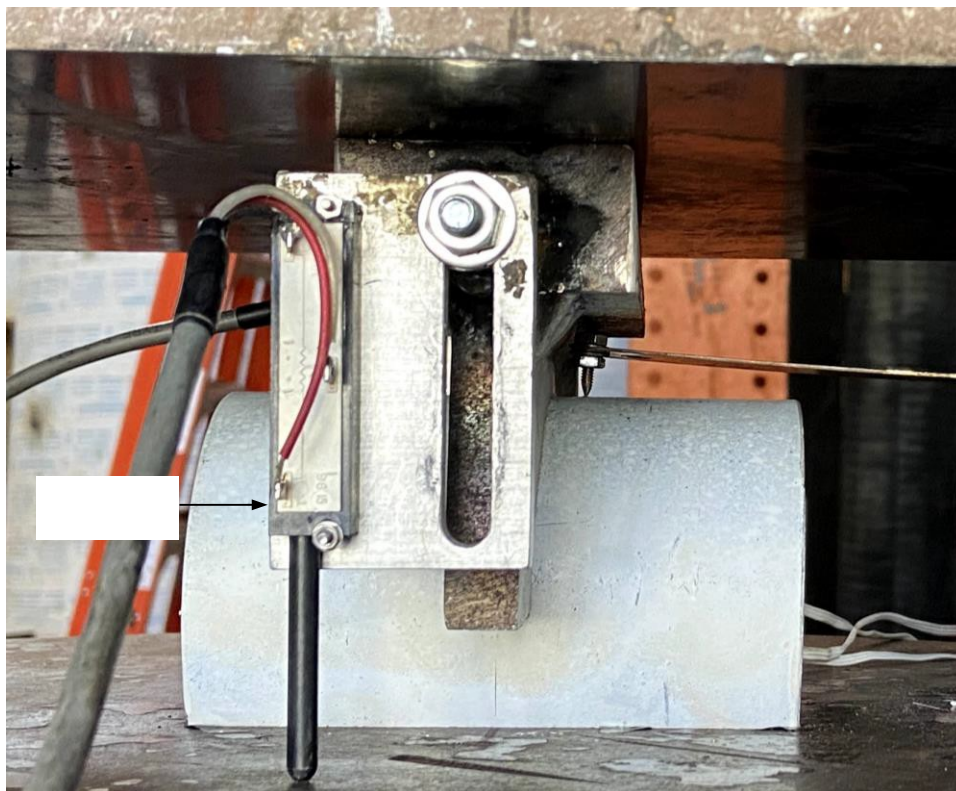
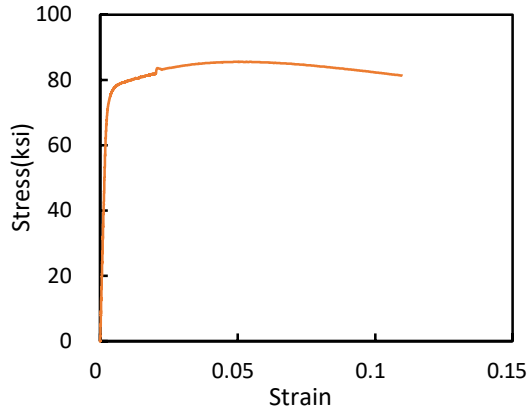
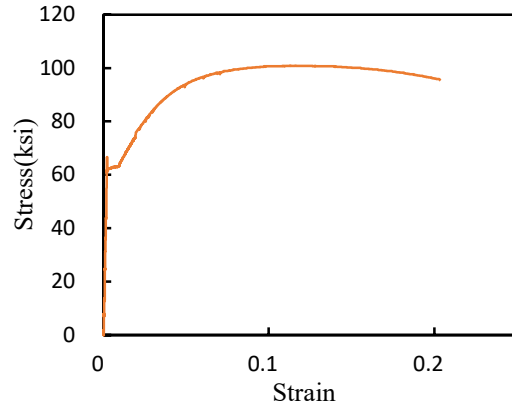


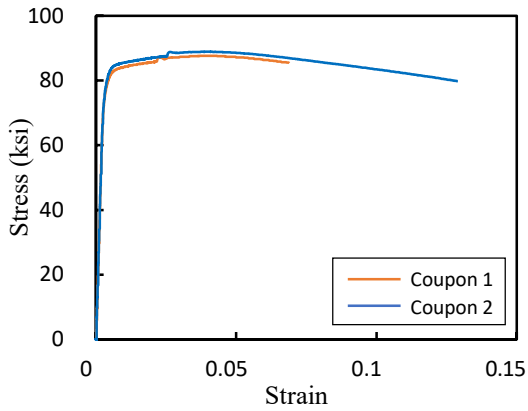
Figure 4.2 Test Setup (Pin Bearing Tests)



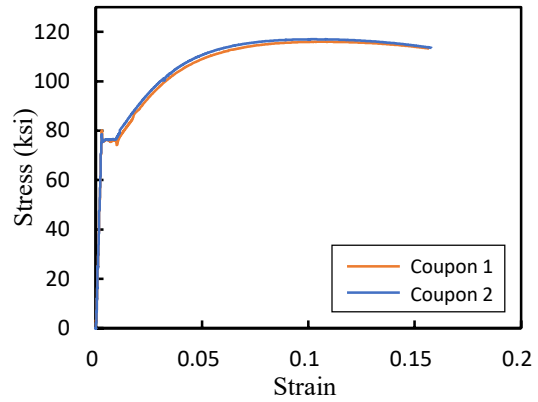
(a) A108 Gr.1018 Steel (Specimens E1, E2)



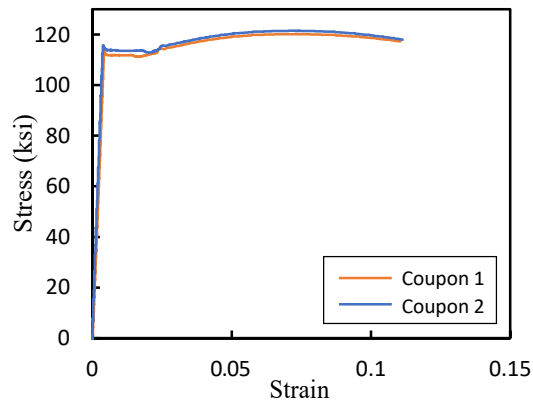
(b) A668 Class G Steel (Specimens E3)



(c) A108 Gr.1018 Steel (Specimen F1)

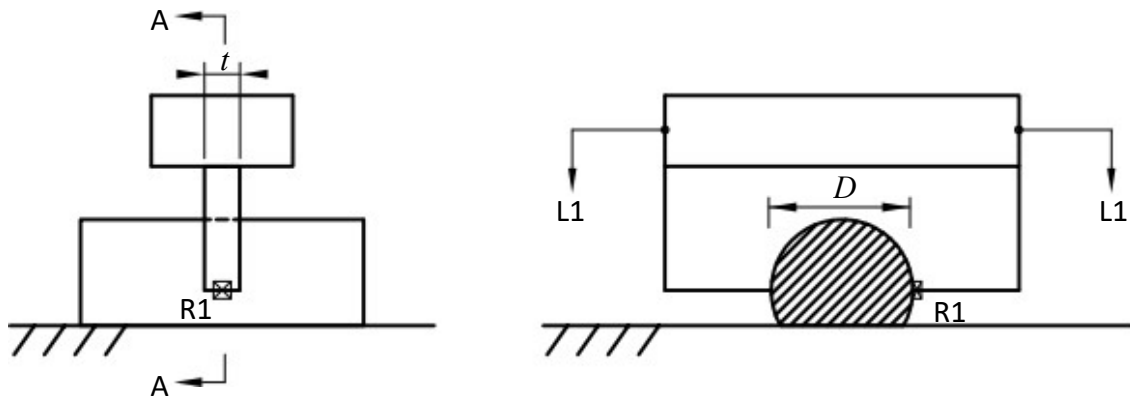


(d) A668 Class F Steel (Specimen F2)



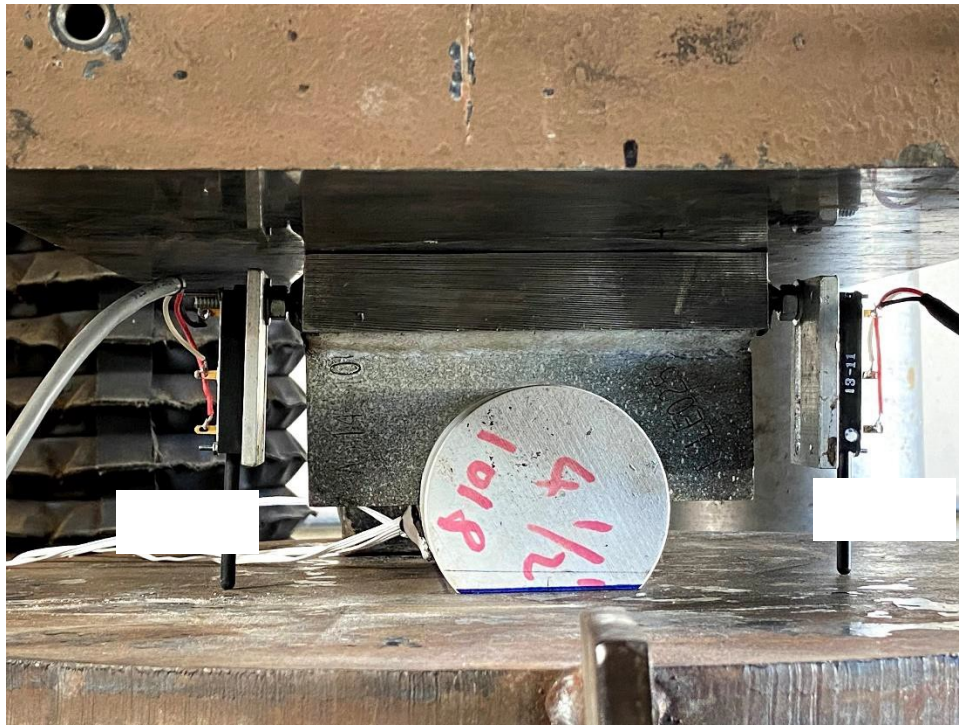
(e) A514 Steel (Loading Cradle)

Figure 4.3 Stress-strain Responses from Tensile Coupon Testing (Pin Bearing Tests)



Section A-A

(a) Displacement Transducer and Strain Gauge Locations



(b) Side View

Figure 4.4 Instrumentation (Pin Bearing Tests)

4.3 Test Results

4.3.1 Series E Specimens ($D = 3.0$ in.)

Figure 4.5 to Figure 4.7 show the deformed shape and measured response of the Series E specimens. Unlike simply supported pin testing reported in Chapter 2, where the pin would eventually fail with a drop of strength, it was expected that the load would continue to increase in this pin bearing testing. Note that the intent of this testing was to introduce bearing in the pin, not the loading plate. To avoid permanent deformation to the re-usable loading plate, recall that a conservative bearing strength of the plate, i.e., Eq. (3.12) that was proposed in Chapter 3, was used for computing the bearing strength [see the last row in Table 4.4(b)], although the actual bearing strength based on the proposed Eq. (3.14) could be much higher. Guided by the values in the last row of Table 4.4(b), therefore, pin bearing testing was stopped before actual failure occurred. Extrapolation of bearing response beyond the test range by finite element analysis will be presented in Section 4.5.

4.3.2 Series F Specimens ($D = 2.0$ in.)

Figure 4.8 and Figure 4.9 show the deformed shape and measured response of the Series F specimens. Again, testing was stopped based on the criterion mentioned above.

4.4 Analysis of Test Results

A summary of the global response of five specimens is presented in Figure 4.10. For a meaningful comparison, the load has been normalized by $F_y t D$. Because the specimens were not tested to failure, the ultimate bearing strength of the pins could not be evaluated. But this figure shows that the current AASHTO requirement on pin bearing strength, i.e., Eq. (3.1), is very conservative.

The effect of the plate thickness on the bearing strength of the pin can be observed from Figure 4.11. Specimens E1 and E2 have the same steel grade (A108) and pin diameter, but the loading plate thicknesses were 0.5 and 0.75 in., respectively. For a given stress level, a thicker plate would produce more bearing deformation.

Two pairs of specimens were used to evaluate the effect of steel grade; A668 steel shows significant strain hardening while A108 steel does not (Figure 4.3). Figure 4.12(a) shows the comparison of Specimens E1 and E3. Both of them had the same pin diameter

(3 in.) and loading plate thickness (0.5 in.). As expected, both specimens showed very similar elastic response and Specimen E3 (A668 steel) showed more hardening. Figure 4.12(b) shows the comparison of another pair (Specimens F1 and F2). Both had the same pin diameter (2 in.) and loading plate thickness (1 in.). Although Specimen F2 (A668 steel) also showed more hardening, it is not clear what caused the elastic stiffness to deviate from each other.

The effect of pin diameter on the bearing response can be observed by comparing two pairs of specimens in Figure 4.13. First consider Specimens E1 and F1, both with a steel grad of A108. For a given stress level in the elastic range, Specimen F1 showed a much larger bearing deformation due to two factors. The first contributing factor is the thickness effect as observed above (Figure 4.11); Specimen F1 had twice the thickness as that of E1. The smaller diameter (2 in.) of Specimen F1, which had a less volumetric constraint for bearing deformation, may have contributed to a further increase of the observed bearing deformation. A similar trend can also be observed from the second pair of specimens, Specimens E3 and F2 (A668 steel); see Figure 4.13(b).

4.5 Correlation between Test Results and FEA

Finite element analysis (FEA) using the commercial finite element analysis software package, ABAQUS (2014), was performed to correlate the test results. The modeling technique is similar to that use of pin research (see Section 2.5). Two parameters (k and μ) were needed to model the penetration phenomenon. Based on the previous FEA presented in Section 2.5, values listed in Table 2.6 were first used. It was observed that a good correlation could be achieved for the two F series specimens, but not for the three E Series specimens. For the latter case, these two parameters were then adjusted by trial-and-error until a satisfactory correlation could be achieved. See Table 4.5 for the values of the parameters used for each specimen. The correlations are presented in Figure 4.14 to Figure 4.18.

FEA was then used to extend the range of bearing deformation beyond that tested for each specimen. Figure 4.19 shows a summary of the global responses. The effect of significant material strain hardening of the A668 steel on the response of the Series F specimens is obvious.

4.6 Summary and Concluding Remarks

Five pin specimens were tested to evaluate the adequacy of the pin bearing strength in the AASHTO Specifications (see Table 4.1 for the test matrix and Figure 4.1 for the test assembly). Three parameters (thickness of loading plate, steel grade of steel, and pin diameter) were considered in this test program. Since it was expected that the specimen would not “fail” in bearing until a very large deformation, testing was stopped when a modest amount of bearing deformation was observed such that the re-usable loading plate would not be damaged. FEA correlation of the test data was also conducted and used to extend the test range to a higher deformation level. Based on these results, the following conclusions can be made.

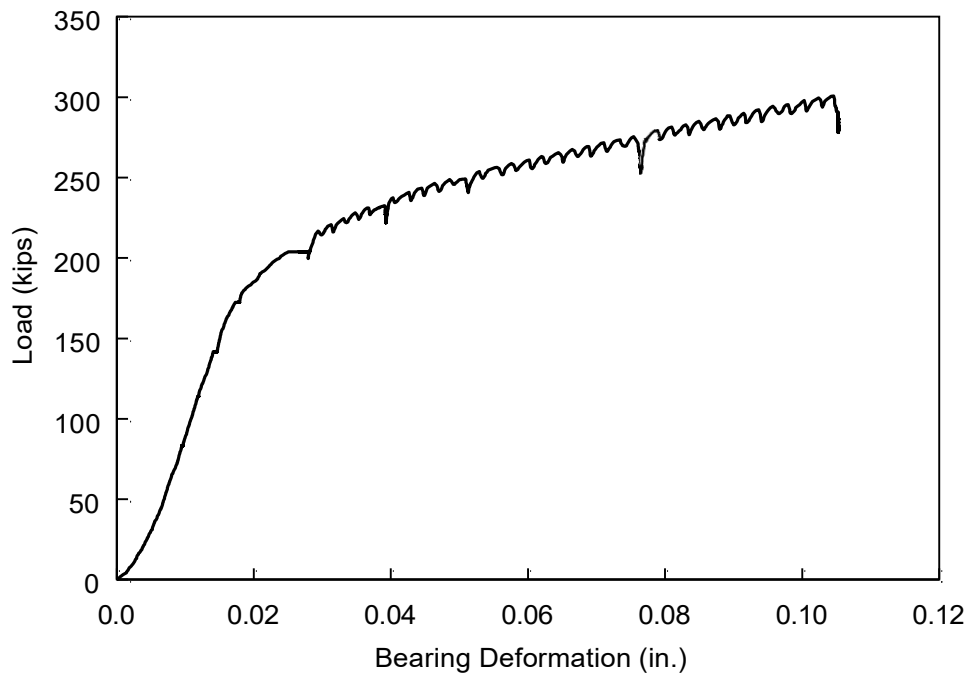
- (1) The pin bearing resistance [Eq. (3.1)] in the AASHTO Specifications underestimates the bearing strength of the pin by a large margin (see Figure 4.10 and Figure 4.19).
- (2) The bearing deformation is affected by the loading plate thickness and pin diameter.

Table 4.5 Contact Parameters for Finite Element Analysis (Pin Bearing Tests)

Specimen No.	Contact Stiffness (kips/in. ³)	Friction Coefficient
E1, E2	14,000	0.3
E3	14,000	0.4
F1	3,500	0.3
F2	3,500	0.5



(a) Deformed Shape

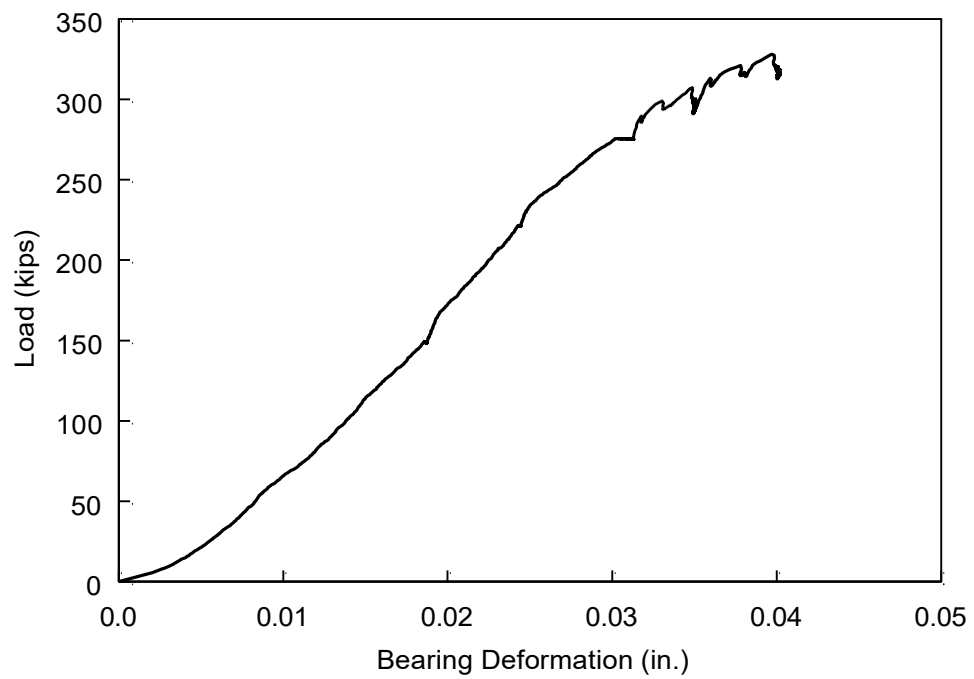


(b) Global Response

Figure 4.5 Specimen E1: Deformed Shape and Global Response

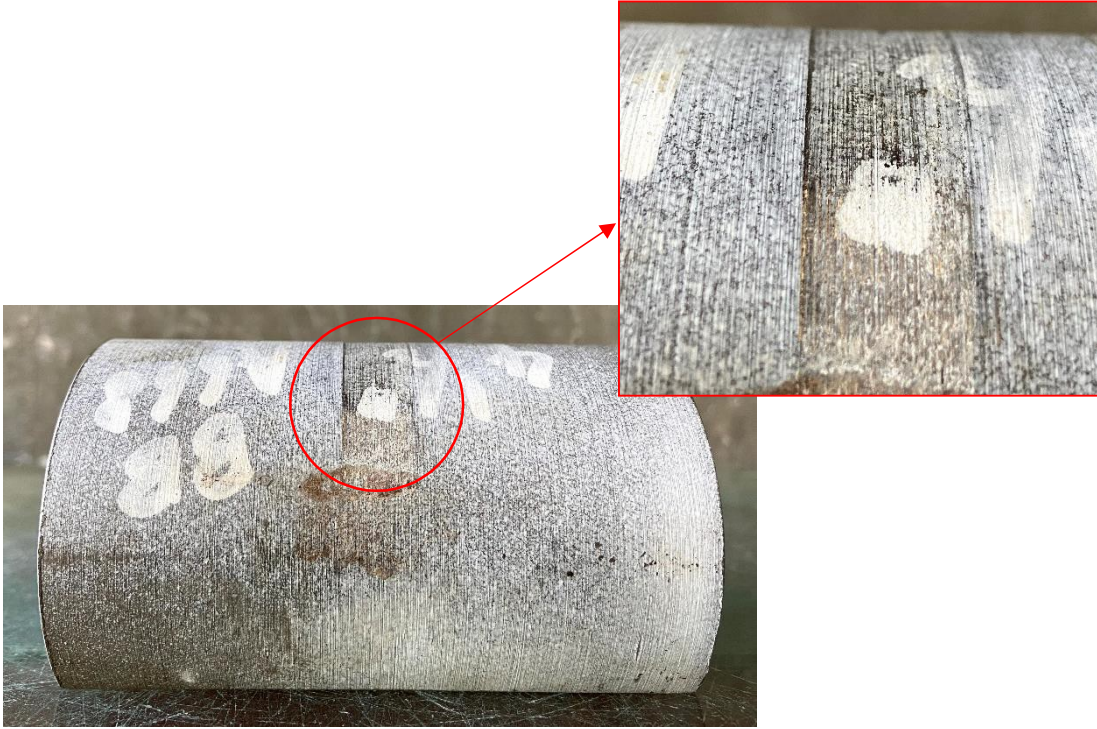


(a) Deformed Shape

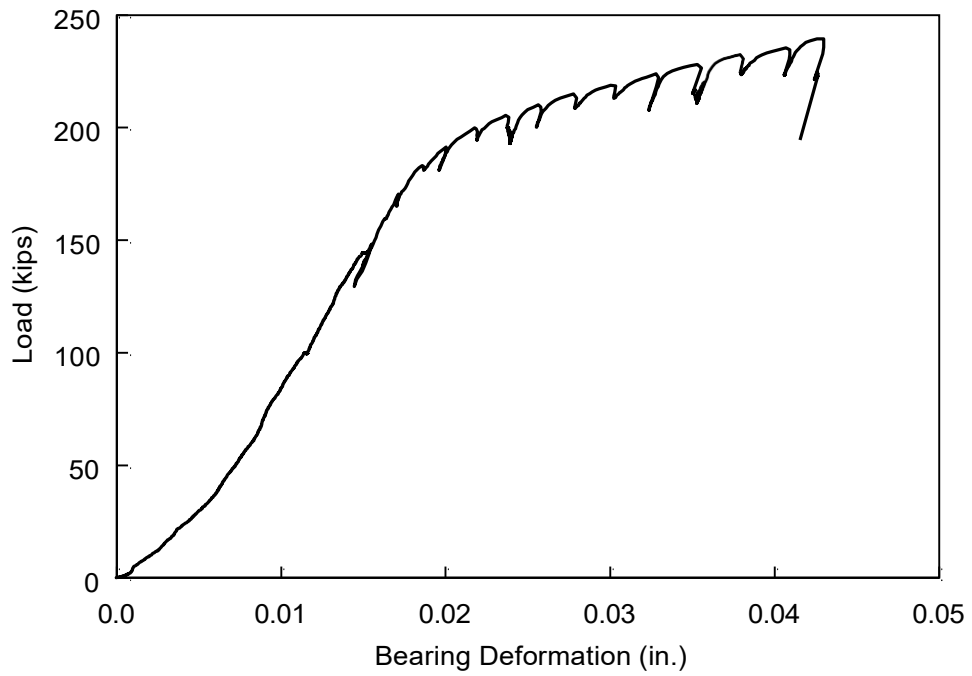


(b) Global Response

Figure 4.6 Specimen E2: Deformed Shape and Global Response

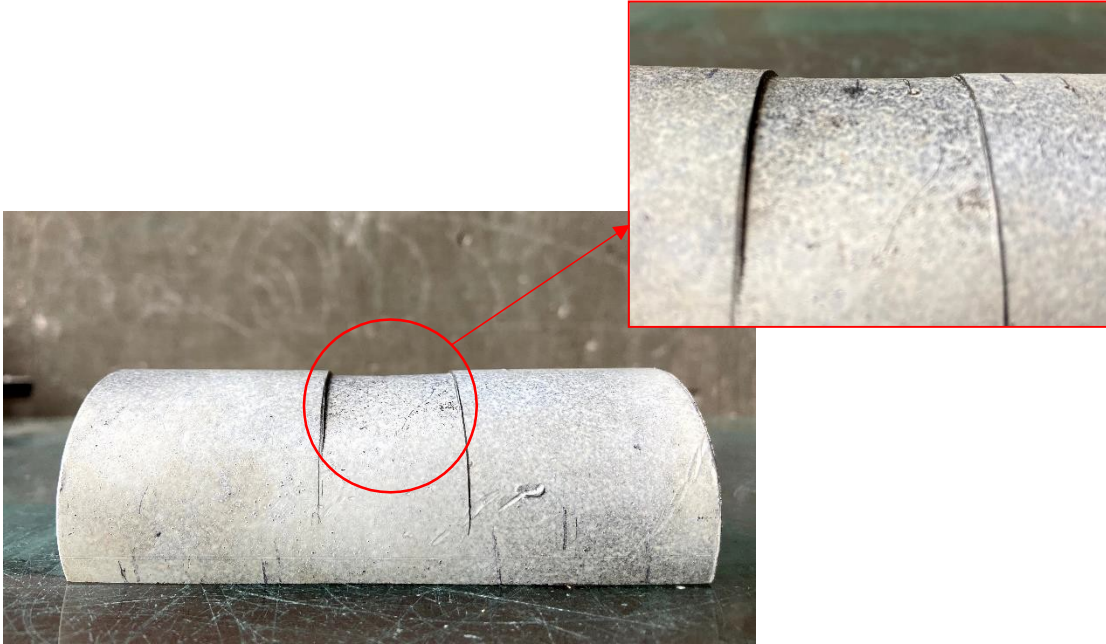


(a) Deformed Shape

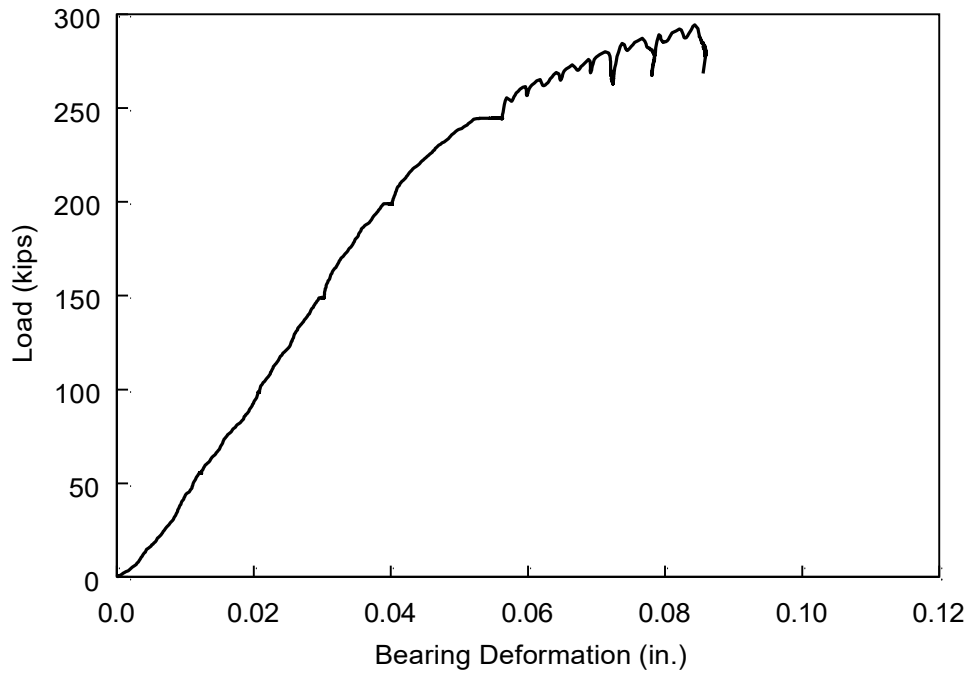


(b) Global Response

Figure 4.7 Specimen E3: Deformed Shape and Global Response

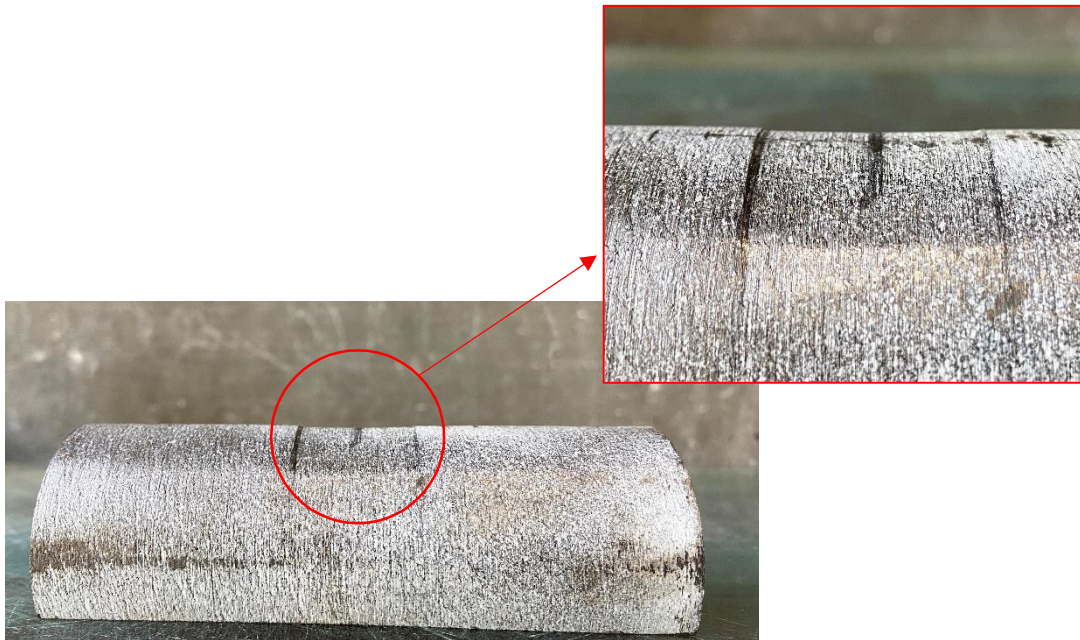


(a) Deformed Shape

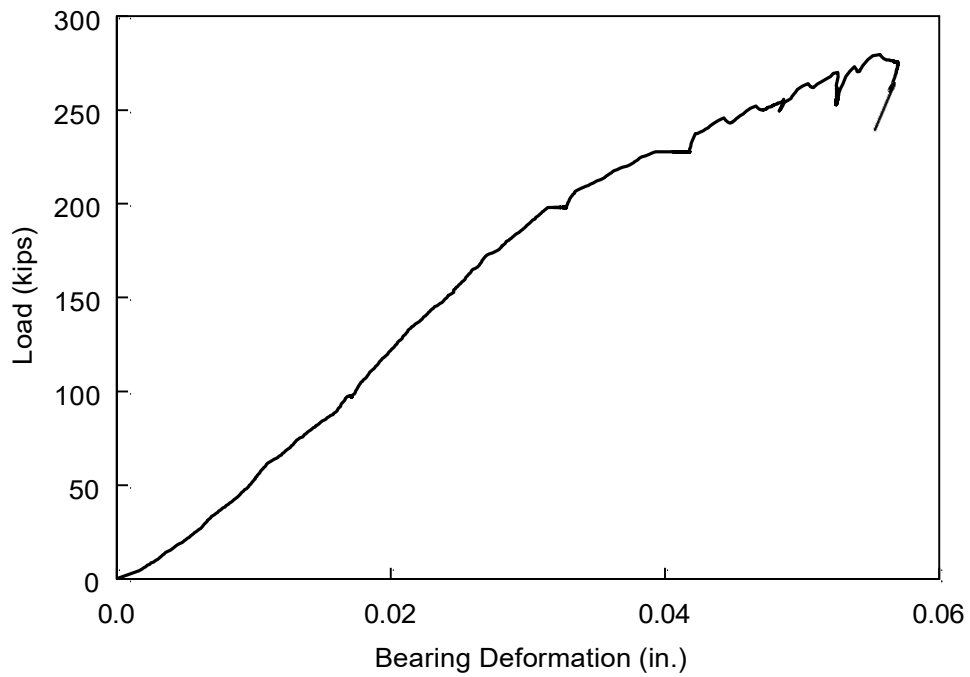


(b) Global Response

Figure 4.8 Specimen F1: Deformed Shape and Global Response



(a) Deformed Shape



(b) Global Response

Figure 4.9 Specimen F2: Deformed Shape and Global Response

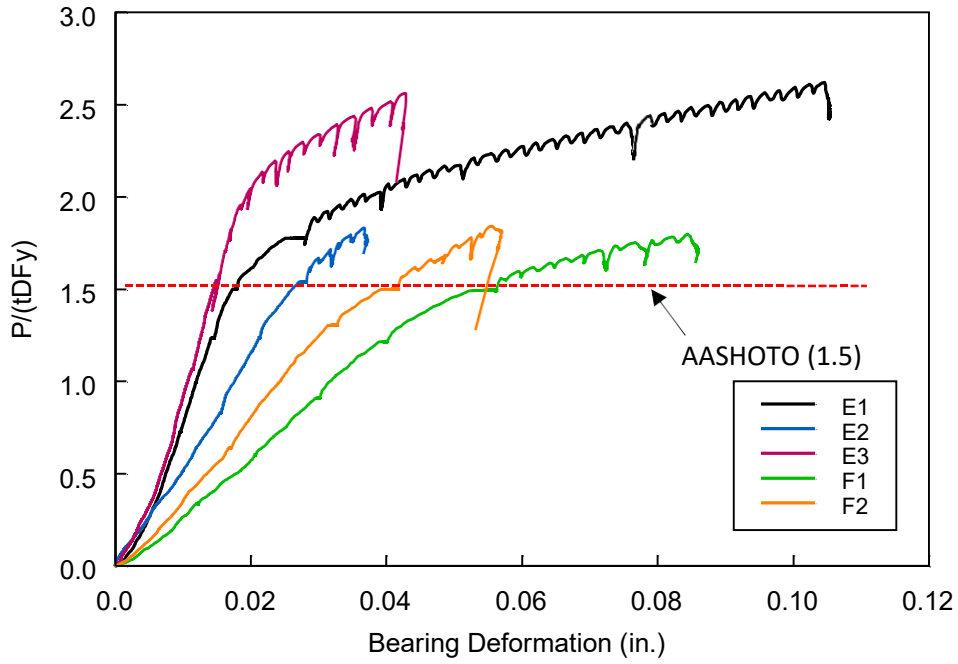


Figure 4.10 Summary of Global Response (Pin Bearing Tests)

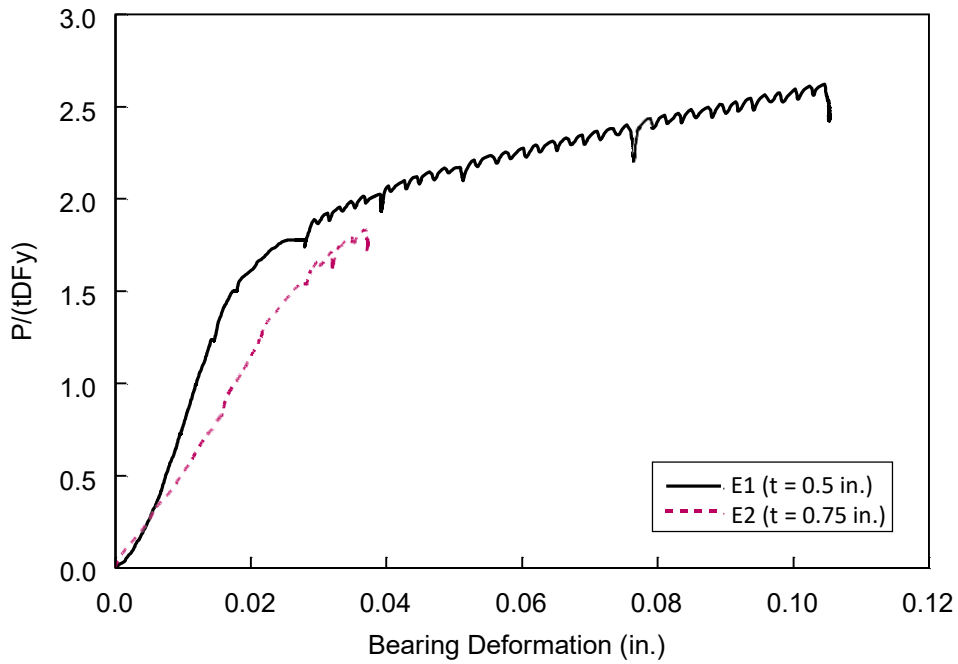
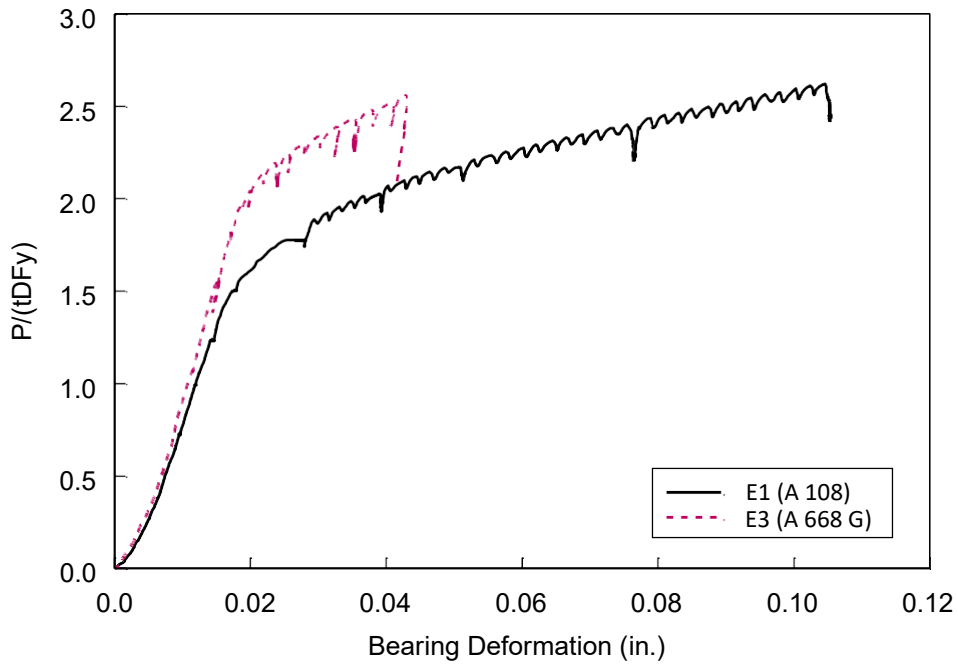
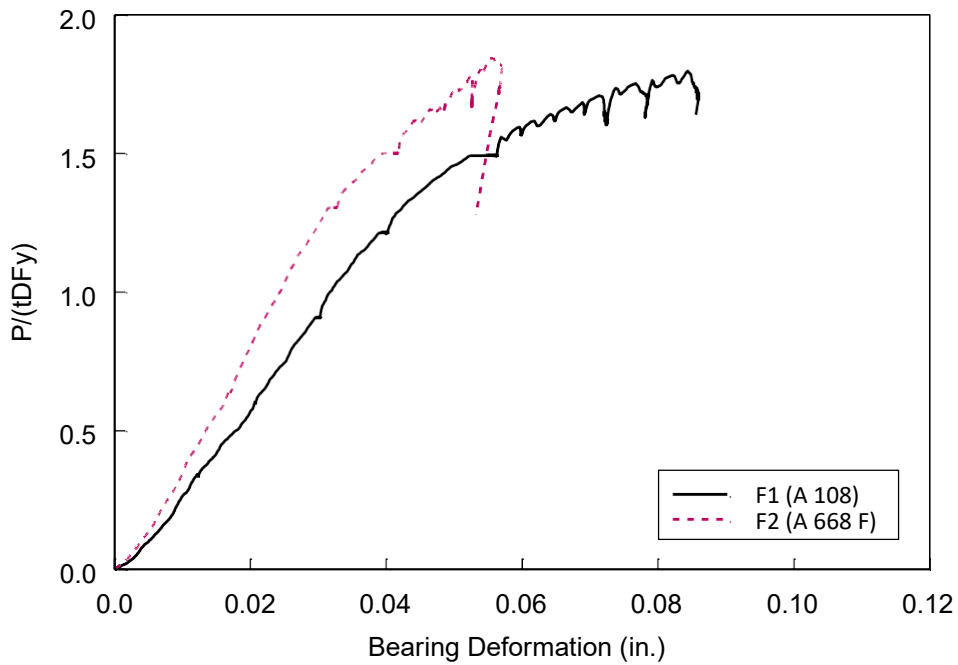


Figure 4.11 Effect of Plate Thickness on Pin Bearing Response

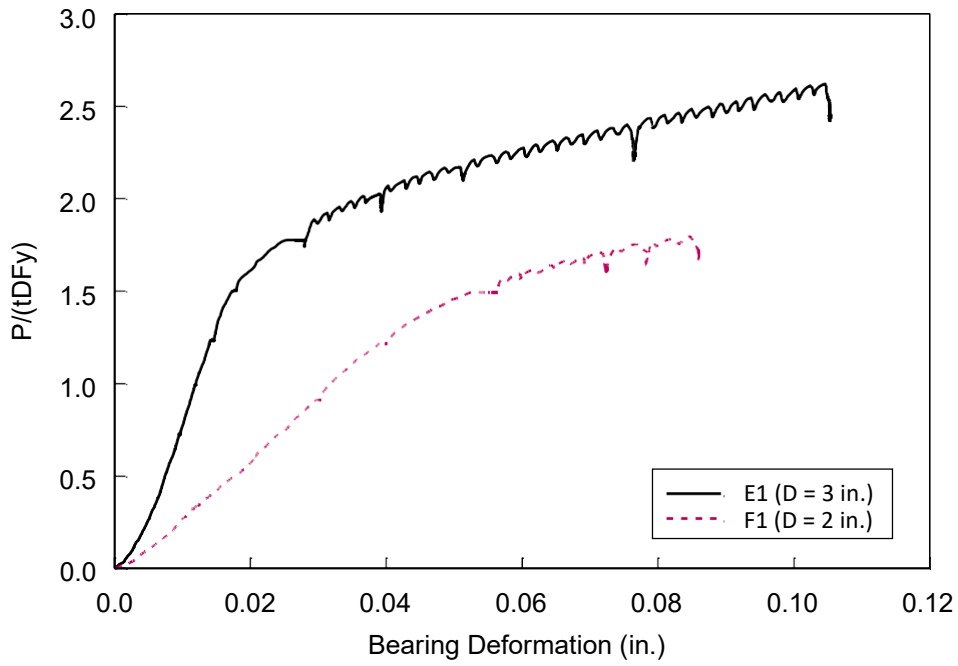


(a) Specimen E1 vs. Specimen E3

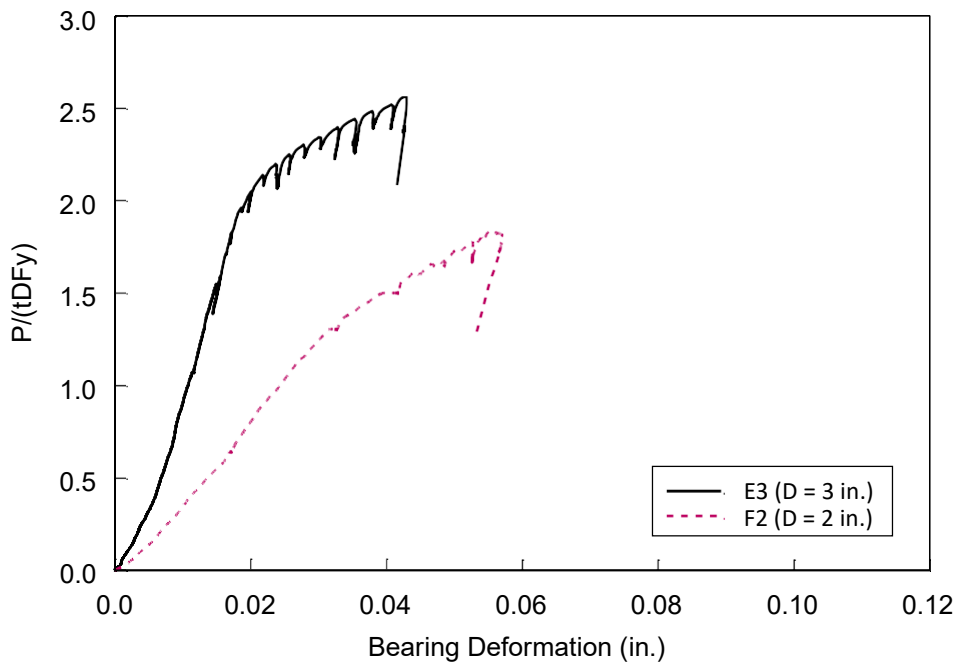


(b) Specimen F1 vs. Specimen F2

Figure 4.12 Effect of Steel Grade on Pin Bearing Response

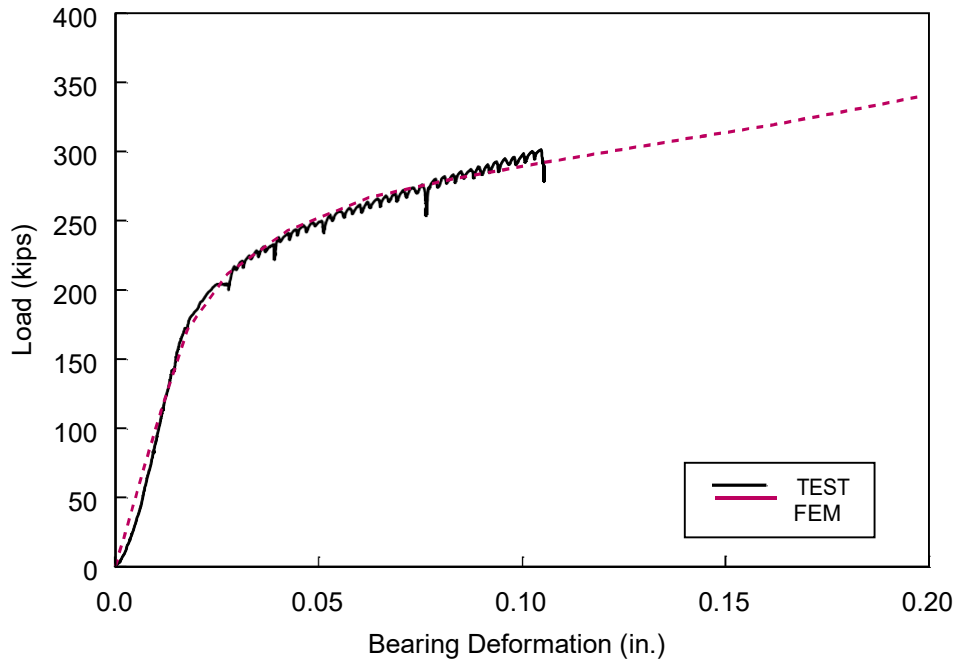


(a) Specimen E1 vs. Specimen F1



(b) Specimen E3 vs. Specimen F2

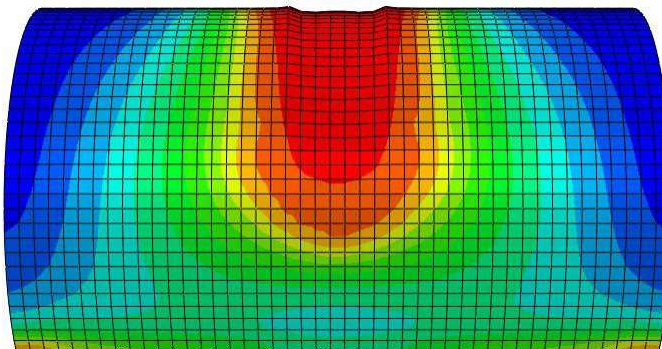
Figure 4.13 Effect of Pin Diameter on Pin Bearing Response



(a) Global Response

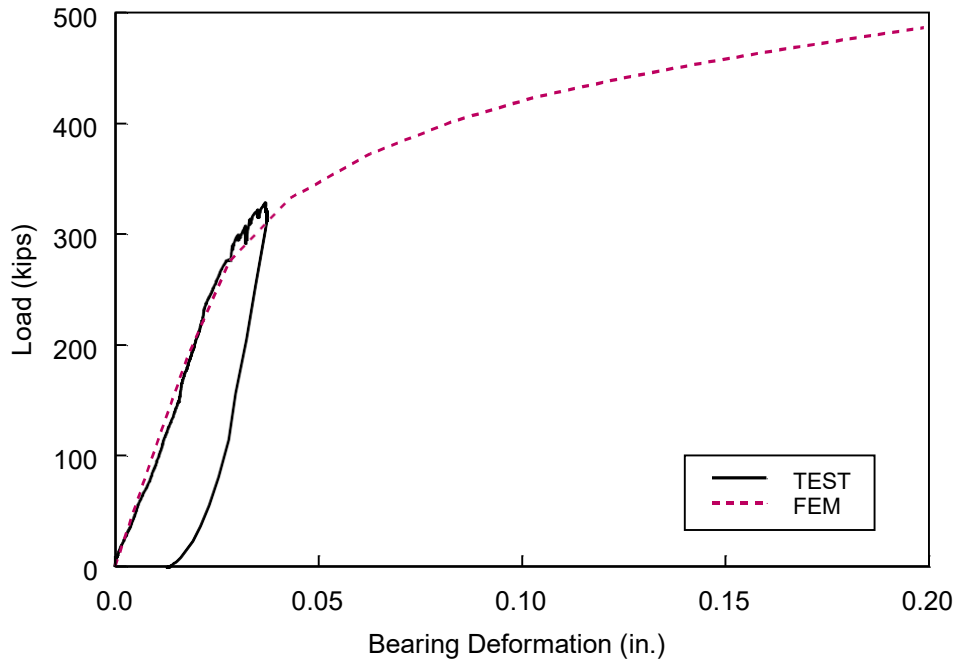


(b) Test



(c) FEM

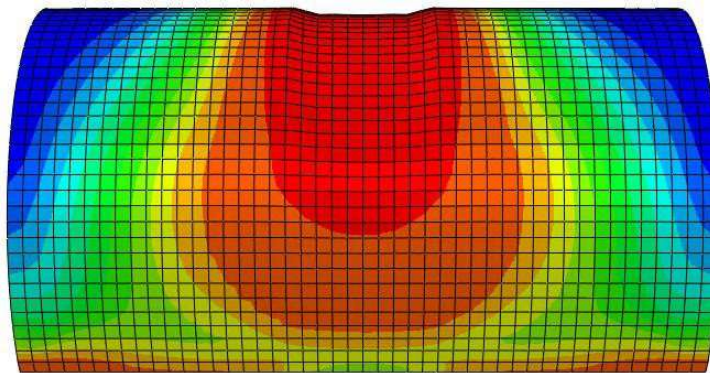
Figure 4.14 FEM Correlation of Specimen E1



(a) Global Response

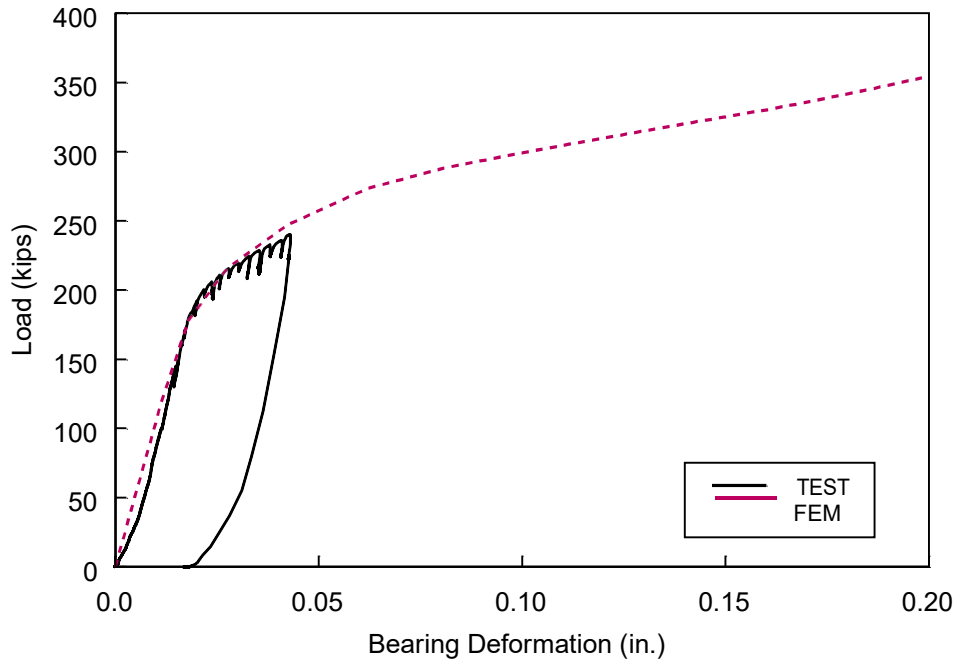


(b) Test



(c) FEM

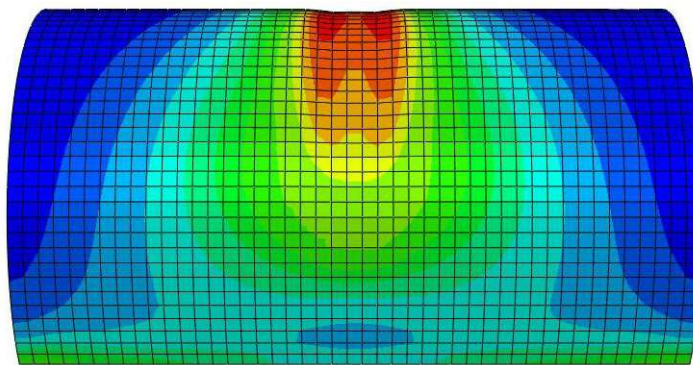
Figure 4.15 FEM Correlation of Specimen E2



(a) Global Response

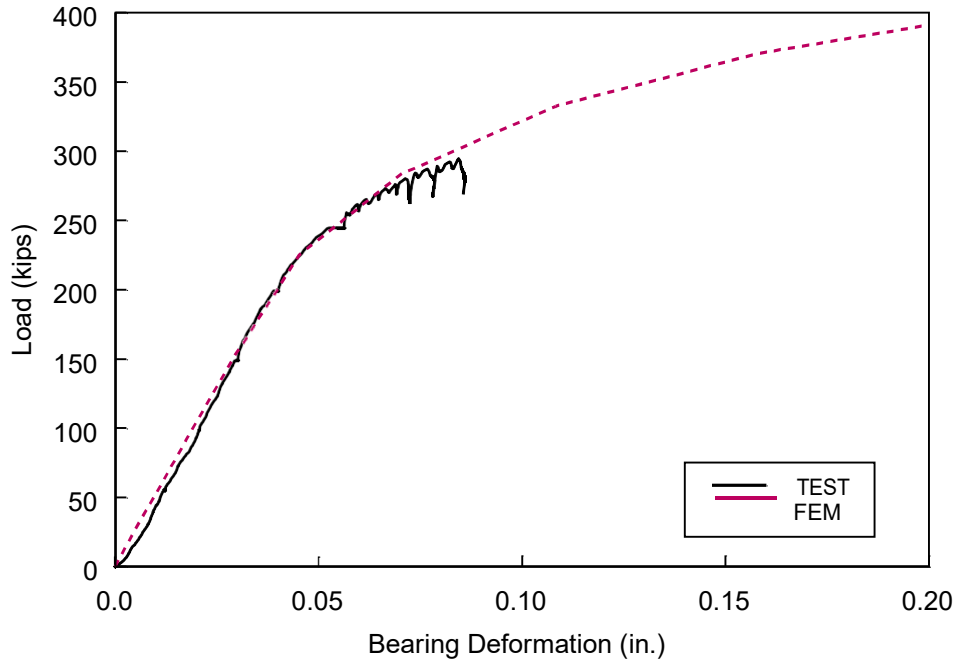


(b) Test



(c) FEM

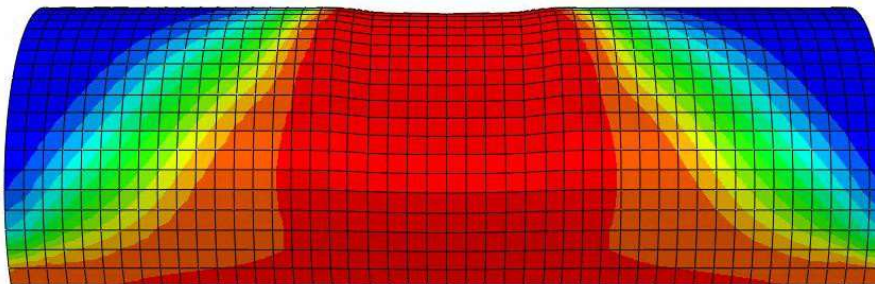
Figure 4.16 FEM Correlation of Specimen E3



(a) Global Response

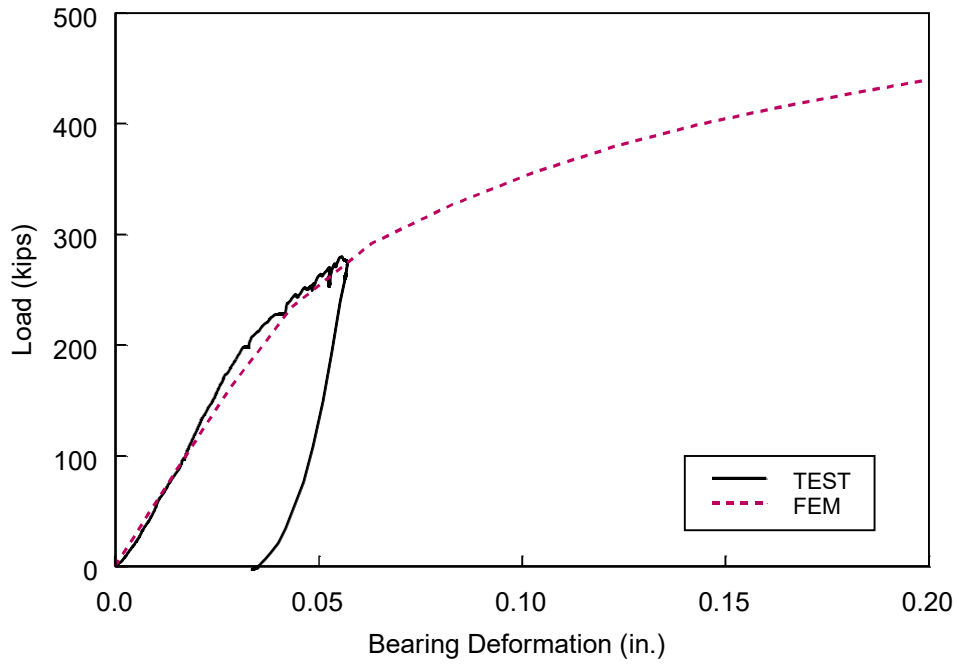


(b) Test



(c) FEM

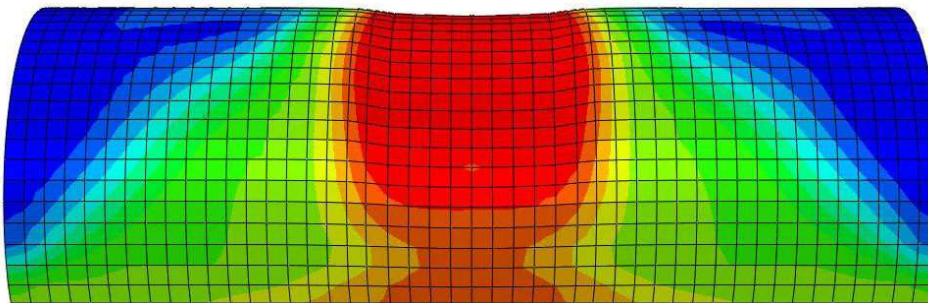
Figure 4.17 FEM Correlation of Specimen F1



(a) Global Response



(b) Test



(c) FEM

Figure 4.18 FEM Correlation of Specimen F2

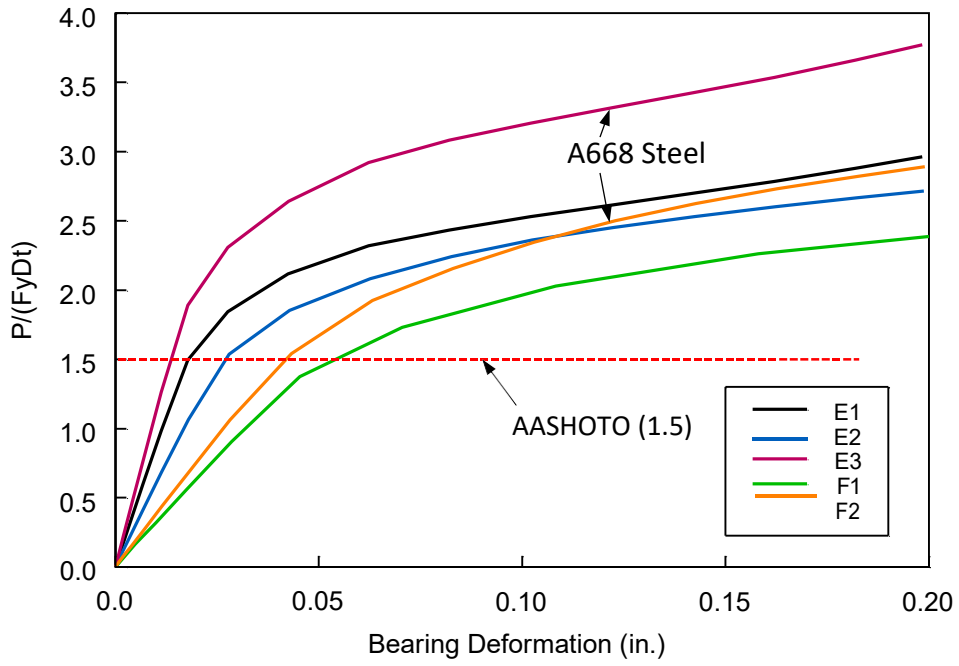


Figure 4.19 FEA Simulated Pin Bearing Responses

5 SUMMARY AND CONCLUSIONS

5.1 Pin Capacity of Combined Flexure and Shear

Based on test results of twelve 2-in. diameter steel pins with two steel grades (A108 Grade 1018 and A668 Class F) and finite element analyses of pins with diameters of 1 in, 2 in. and 4 in., the following conclusions can be made.

- (1) The current AASHTO design practice that treats the pin as a beam and the capacity that is expressed in the form of a moment-shear interaction does not reflect the actual behavior. Both testing and finite element analyses showed that the actual capacity is significantly higher than that predicted by the AASHTO Specifications. (see Figure 2.45).
- (2) The pin ultimate capacity is a function of two nondimensional length parameters (α and β in Figure 2.57) and the material strength. It is proposed that Eq. (2.20) be used to predict the ultimate shear strength of the pin. Based on the available test data, this equation is valid for α ranging from 0.31 and 1.75 and β ranging from 0.31 to 1.01.
- (3) For serviceability considerations, it is proposed that Eq. (2.26) be used to compute the pin shear capacity. This equation is established from test data that limits the flexural tensile strain at midspan to 95% of the yield strain.

5.2 Bearing Capacity of Pin Plates

Four pairs of tension plate assemblies, with two nominally identical specimens in each pair, were tested to failure (see Table 3.1 for the test matrix and Figure 3.2 for the test assembly). Both A36 steel and A572 Gr. 50 steels were included in the test program. Based on the results, the following conclusions can be made.

- (1) Since all eight specimens failed in net section rupture at the pin hole (Figure 3.22), the ultimate strengths obtained from testing represent the lower-bound strength of bearing capacity of the pin plates. Testing showed that the actual bearing resistance of the plate was at least 1.83 to 2.08 times that [Eq. (3.4)] specified in the AASHTO Specifications [see Table 3.6 and Figure 3.24(a)].
- (2) Including a 1.5 multiplier like that used to calculate the bearing resistance of the pin [Eq. (3.1)] will partially remove the conservatism [see Figure 3.24(a)]. To further

reduce the level of conservatism, the proposed Eq.(3.14) is shown to correlate well the test results [see the last column in Table 3.6 and Figure 3.24(b)].

- (3) AASHTO Specifications do not provide a service bearing resistance for pin plates. When such limit state is needed, it is proposed that Eq. (3.12) be used.

5.3 Pin Bearing Capacity

Five pin specimens were tested to evaluate the adequacy of the pin bearing strength provision in the AASHTO Specifications (see Table 4.1 for the test matrix and Figure 4.1 for the test assembly). Three parameters (thickness of loading plate, steel grade of steel, and pin diameter) were considered in this test program. Based on these results, the following conclusions can be made.

- (1) The pin bearing resistance [Eq. (3.1)] in the AASHTO Specifications underestimates the bearing strength of the pin by a large margin (at least in a range between 1.2 and 1.7 as shown in Figure 4.10).
- (2) The bearing deformation is affected by the loading plate thickness and pin diameter.

REFERENCES

- AASHTO. (2020). *LRFD Bridge Design Specifications*, 9th ed., American Association of State Highway Officials, Washington, D.C.
- ABAQUS. (2011). *ABAQUS Standard User's Manual, Version 6.11*, Dassault Systèmes. Providence, RI.
- AISC (2016). Specification for Structural Steel Buildings, *ANSI/AISC 360-16*, American Institute of Steel Construction, Chicago, IL.
- Bresler, B., Lin, T.Y., and Scalzi, J.B. (1968). *Design of Steel Structures*, John Wiley & Sons, Inc.
- Bridge, R.Q., Sukkar T., Hayward, I.G., and van Ommen, M. (2001). "Behaviour and Design of Structural Steel Pins," *Steel and Composite Structures*, 1(1), 97-110.
- CEN (2005). "Design of Steel Structures," *EN 1993-1-8*. European Committee for Standardization, Brussels.
- CSA (2014). "Design of Steel Structures," *S16-14*. Mississauga, ON, Canadian Standards Association.
- Drucker, D.C. (1956). "The Effect of Shear on the Plastic Bending of Beams," *Journal of Applied Mechanics*, ASME, Vol. 23, No. 4, 509-514.
- Hodge, P.G., Jr. (1957). "Interaction Curves for Shear and Bending of Plastic Beams," *Journal of Applied Mechanics*, ASME, V. 24, No. 3, 453-456.
- Kulicki, J.M. (1983). "Load Factor Design Applied to Truss Members in Design of Greater New Orleans Bridge No. 2," *Transportation Research Record*, No. 903 Chicago, IL., 22-26.
- Montgomery, J., Higgins, C., and Liu, J. (2018). "Capacities of Pin and Hanger Assemblies, Phase 1," *Final Report to Caltrans*, School of Civil and Construction Engineering, Oregon State University, Corvallis, OR.